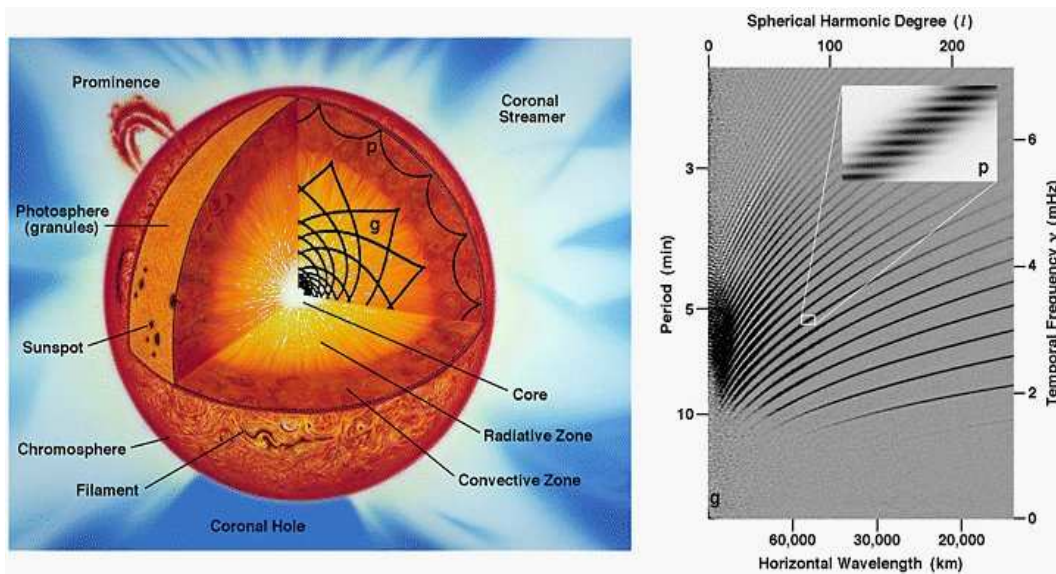


Lecture Notes for FY3451 Astrophysics II

M. Kachelrieß



M. Kachelrieß
Institutt for fysikk
NTNU, Trondheim
Norway
email: Michael.Kachelriess@ntnu.no

Watch out for errors, most was written late in the evening.
Corrections, feedback and any suggestions always welcome!

Copyright © M. Kachelrieß 2021.
Last up-date November 1, 2024

Contents

1. Overview	7
2. Radiation and its interaction with matter	9
2.1. Radiation	9
2.2. Radiation transfer	13
2.3. Interactions of radiation with matter	16
2.4. Thermodynamic equilibrium	19
2.5. Equations of state	21
2.6. Stellar atmospheres	24
Problems	24
3. Equations of stellar structure	25
3.1. Mass continuity and hydrostatic equilibrium	25
3.2. Virial theorem	27
3.3. Energy transport	30
3.4. Thermal equilibrium and energy conservation	34
3.5. Time scales	34
4. Stellar models	36
4.1. Hertzsprung-Russel diagram	36
4.2. Eddington luminosity and convective instability	36
4.3. Eddington or standard model	37
4.4. Main sequence	45
4.5. Realistic models	46
4.6. Stability of stars	48
Problems	48
5. Nuclear processes in stars	49
5.1. *** Fundamental interactions ***	50
5.2. Main nuclear burning reactions	51
5.2.1. Thermonuclear reactions and Gamov peak	51
5.2.2. Hydrogen burning: pp-chains and CNO-cycle	55
5.2.3. Later phases	55
5.3. *** Solar neutrinos ***	56
5.4. Neutron-capture nucleosynthesis	60
5.5. Cooling by neutrino emission	60
Problems	60
6. *** Stars as labs for particle physics ***	62
6.1. Stellar evolution limits for particle physics	62
6.2. Homologous analysis	63

6.3. Globular cluster limits	64
Problems	64
7. Interstellar medium and star formation	66
7.1. Interstellar medium	66
7.1.1. Interstellar dust	66
7.1.2. Interstellar gas	69
7.2. Fluid dynamics	72
7.2.1. Perfect fluid equations	72
7.2.2. Revisiting the equations of stellar structure	74
7.2.3. *** Jeans instability and shocks ***	74
7.2.4. Hydrodynamic turbulence	77
7.3. ***Star formation***	81
7.3.1. Collaps and fragmentation of gas clouds	81
7.3.2. Protostars	83
Problems	84
8. Accretion, winds, interacting binaries	85
8.1. Spherical accretion	85
8.2. Accretion disks	87
8.3. ***Winds***	88
8.4. *** Interacting binaries ***	89
8.5. *** Gravitational wave emission and binary mergers ***	90
8.6. Tidal disruption events	94
Problems	94
9. *** Elements of general relativity and applications ***	96
9.1. Basic properties of gravitation	96
9.2. Schwarzschild metric	98
9.3. Gravitational lensing	101
9.4. Gravitational radiation	106
9.5. Astrophysical black holes	108
9.6. Thermodynamics and evaporation of black holes	110
10. White dwarfs and neutron stars	113
10.1. Chandrashekar mass	113
10.2. White dwarfs	114
10.2.1. Chandrashekar’s theory for WDs	114
10.2.2. White dwarfs cooling	116
10.3. Neutron stars	116
10.3.1. *** TOV equation ***	117
10.4. Pulsars	118
10.5. Pulsar Wind Nebula	120
Problems	120
11. Supernovae, supernova remnants, GRBs	121
11.1. Type Ia supernovae	121

11.2. Core collapse supernovae	123
11.3. Supernova remnants	125
11.4. Gamma-ray bursts	127
11.4.1. Relativistic effects	128
12. Cosmic rays and acceleration	133
12.1. Acceleration of cosmic rays	133
12.1.1. Bell's approach	133
12.1.2. ***Fluid approach***	135
12.1.3. Other acceleration mechanisms	137
12.2. *** Sources of cosmic rays ***	138
12.2.1. Galactic cosmic rays	142
13. Non-thermal radiation	143
13.1. Electrodynamic processes	143
13.1.1. Synchrotron radiation	143
13.1.2. Compton scattering	147
13.2. Hadronic processes	148
13.A. ***Reaction rates and cross sections***	152
14. *** Milky Way and normal galaxies ***	155
14.1. Milky Way	155
14.1.1. Evolution of star cluster	156
14.1.2. Rotation curve of the Milkyway	160
14.1.3. Black hole at the Galactic center	162
14.2. Normal Galaxies	163
14.2.1. Hubble sequence	163
14.2.2. Dark matter in galaxies	163
14.2.3. Tully-Fisher relation	167
14.2.4. Galactic evolution	167
15. Active galaxies	169
15.1. ***Mini cosmology – redshift and distances***	169
15.2. Observations and zoology	169
15.3. Nucleus of active galaxies	171
15.4. Diffuse spectra of high-energy particles	175
16. Dark matter	178
16.1. Thermal relic particles	178
16.1.1. Freeze-out of thermal relic particles	178
16.1.2. Hot dark matter	180
16.1.3. Cold dark matter	180
16.1.4. WIMP detection	181
16.2. Axion-like particles	184
16.3. Primordial black holes	184
A. Some formulae	186
A.1. Mathematical formulae	186

A.2. Abbreviations:	186
A.3. Physical constants and measurements	187
A.4. Astronomical constants and measurements	187
A.5. Other useful quantities	187
A.6. Properties of main-sequence stars	187

1. Overview

- **warning: parts of this script are still very preliminary!**
- paragraphs with stars are not used

Units

cgs vs. SI units, units for electromagnetism

we use often as energy unit keV, MeV or GeV; also used for temperatures.

Distances

Relatively nearby stars are seen at slightly different positions on the celestial sphere (i.e. the background of stars that are “infinitely” far away) as the Earth moves around the Sun. Half of this angular difference is called the parallax angle or simply the parallax p . From Fig. 1.1, one can relate the mean distance AU of the Earth to the Sun, the parallax p and the distance d to the star by

$$\tan p = \frac{\text{AU}}{d}. \quad (1.1)$$

With $\tan p \approx p$ for $p \ll 1$, one has $d \propto 1/p$. Because of this simple and for observations important relation, a new length unit is introduced: The parsec is defined to be the distance from the Earth to a star that has a parallax of one arcsecond¹. Thus

$$d[\text{pc}] = \frac{1}{p[\text{''}]} \quad (1.2)$$

i.e. a star with a parallax angle of n arcseconds has a distance of $1/n$ parsecs. Since one arcsecond is the fraction $1/(360 \times 60 \times 60) = 1/129600$ of 2π , a parsec corresponds to 206 265 AU.

To express finally the unit pc in a known unit like cm, we have to determine first the Earth-Sun distance, the astronomical unit AU. As first step one measures the distance d to an inner planet at the time of its greatest elongation (i.e. the largest angular distance ϑ between the Sun and the planet). Nowadays, one uses a radar signal to Venus. Then $\text{AU} = d/\cos \vartheta$, cf. the right panel of Fig. 1.1, and one finds $1\text{AU} = 1.496 \times 10^{13}$ cm. As result, one determines one parsec as $1 \text{ pc} = 206,265 \text{ AU} = 3.086 \times 10^{18} \text{ cm} = 3.26 \text{ lyr}$.

¹A degree, i.e. the $1/360$ part of a circle is divided into 60 arcminutes and 60×60 arcseconds, $360^\circ = 360 \times 60' = 360 \times 60 \times 60''$.

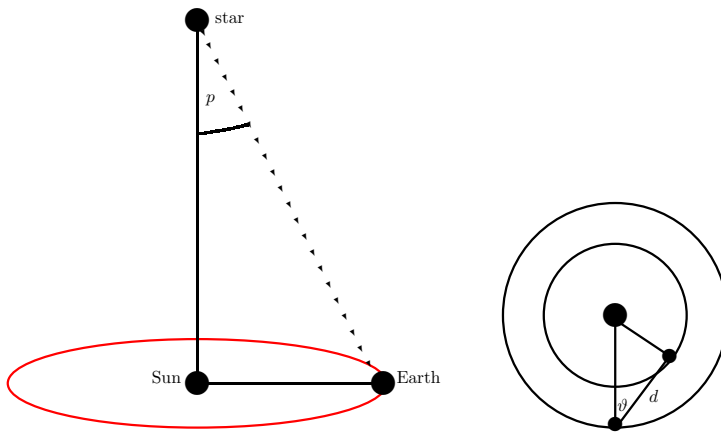


Figure 1.1.: Measurement of the trigonometric parallax. Left: The apparent movement of a nearby star during a year: Half of this angular difference is called the parallax angle or simply the parallax p . Right: Indirect determination of the Earth-Sun distance.

2. Radiation and its interaction with matter

The overwhelming part of the information astronomers gather from the universe is extracted observing electromagnetic radiation. Connecting the observed radiation with the emitted one by, e.g., a stellar surface, and in turn with the radiation produced in the interior of a star requires to study how radiation is produced and transferred. Many systems of interest are close to thermal equilibrium, and thus thermal blackbody radiation is of prime interest to us. Fig. 2.2 compares the spectrum of the Sun with the one of a blackbody: While strong deviations from a blackbody spectrum due to emission and absorption lines are visible, the two spectra agree *on average* rather well.

2.1. Radiation

Number and energy density The spectral number density n_ν of photons, i.e. the number of photons per volume and frequency interval, in thermal black-body radiation is given by

$$n_\nu = \frac{dN}{dV d\nu} = \frac{8\pi\nu^2}{c^3} \frac{1}{\exp(\frac{h\nu}{kT}) - 1}. \quad (2.1)$$

Using $E = h\nu$ for the energy of a photon, the spectral energy density follows as $u_\nu = h\nu n_\nu$ or

$$u_\nu = \frac{dE}{dV d\nu} = \frac{8\pi\nu^2}{c^3} \frac{h\nu}{\exp(\frac{h\nu}{kT}) - 1}. \quad (2.2)$$

The first factor on the RHS has the dimension of [time]/[length]³, while the second factor has the dimension of an energy. In cgs units, $[u_\nu] = \text{erg cm}^{-3} \text{ Hz}^{-1}$, i.e. the dimension corresponds to an energy density per frequency interval as required.

Remark 2.1: Equilibrium distribution functions:

The expressions for the number and energy density of blackbody radiation are special cases for the distribution function of ideal gases in equilibrium. In general, the distribution function $f(\mathbf{x}, \mathbf{p})$ in phase space gives the average occupation number of a cell in phase space with volume h^3 ,

$$dN = \frac{g}{h^3} f(\mathbf{x}, \mathbf{p}) d^3x d^3p \quad (2.3)$$

of a system with N particles and g spin degrees of freedom. Often the system is uniform, and we consider only the distribution function $f(\mathbf{p})$ in momentum space. In statistical physics, one shows that the distribution function $f(p)$ of a free gas of fermions or bosons in *kinetic equilibrium* equals

$$f(p) = \frac{1}{\exp[\beta(E - \mu)] \pm 1}, \quad (2.4)$$

where $\beta = 1/kT$ is the inverse temperature, $E = \sqrt{c^4 m^2 + (cp)^2}$, μ the chemical potential, and $+1$ refers to fermions and -1 to bosons, respectively.

2. Radiation and its interaction with matter

We can compare this expression to the number density of blackbody photons, Eq. (2.1),

$$n_\nu d\nu = \frac{2}{h^3} \frac{4\pi h^3 \nu^2 d\nu}{c^3} \frac{1}{\exp(\frac{h\nu}{kT}) - 1}. \quad (2.5)$$

With $p = h\nu/c$ and $n_\nu d\nu = n_p dp$, we see that the second factor equals the volume element in momentum space, $4\pi h^3 \nu^2 d\nu/c^3 = 4\pi p^2 dp$. Thus photons are massless bosons, $E = c|p|$, with two spin degrees of freedom. Their chemical potential is zero, since the photon number is not conserved.

Intensity and energy flux We define the (specific) intensity I_ν of radiation as the amount of energy per frequency interval $d\nu$ and solid angle $d\Omega$ crossing per time interval dt the area $dA_\perp = dA \cos \vartheta$ perpendicular to $d\Omega$, (cf. with the left panel of Fig. 2.1),

$$I_\nu = \frac{dE}{d\nu d\Omega dA_\perp dt}. \quad (2.6)$$

The intensity is a useful quantity, because as we see later, it is constant along a light-ray if no photons are absorbed or emitted.

A light ray traverses an infinitesimal box with volume $dV = dAdl$ in the time $dt = dl/(c \cos \vartheta)$, cf. with the right panel of Fig. 2.1. Hence the spectral energy density u_ν of photons can be connected to the intensity as

$$u_\nu = \frac{dE}{dV d\nu} = \frac{dE}{c \cos \vartheta dt dA d\nu} = \frac{1}{c} \int d\Omega I_\nu. \quad (2.7)$$

In thermal black-body radiation, photons are isotropically distributed, and we can replace the integral over solid angles by 4π ,

$$u_\nu = \frac{I_\nu}{c} \int d\Omega = \frac{4\pi}{c} I_\nu. \quad (2.8)$$

The intensity I_ν of blackbody radiation is therefore

$$I_\nu = \frac{c}{4\pi} u_\nu = \frac{2h\nu^3}{c^2} \frac{1}{\exp(\frac{h\nu}{kT}) - 1} \equiv B_\nu, \quad (2.9)$$

where B_ν denotes the so-called Kirchhoff-Planck (or simply Planck) distribution found by Planck empirically 1900.

The (spectral) energy flux \mathcal{F}_ν from one hemisphere through a planar detector is

$$\mathcal{F}_\nu = \frac{dE}{dA dt d\nu} = \int d\Omega I_\nu \cos \vartheta = \quad (2.10a)$$

$$= I_\nu \int_0^{2\pi} d\phi \int_0^{\pi/2} d\vartheta \sin \vartheta \cos \vartheta = 2\pi I_\nu \frac{1}{2} \int_0^{\pi/2} d\vartheta \sin 2\vartheta = \pi I_\nu, \quad (2.10b)$$

where we have assumed in the second line that the intensity is isotropic.

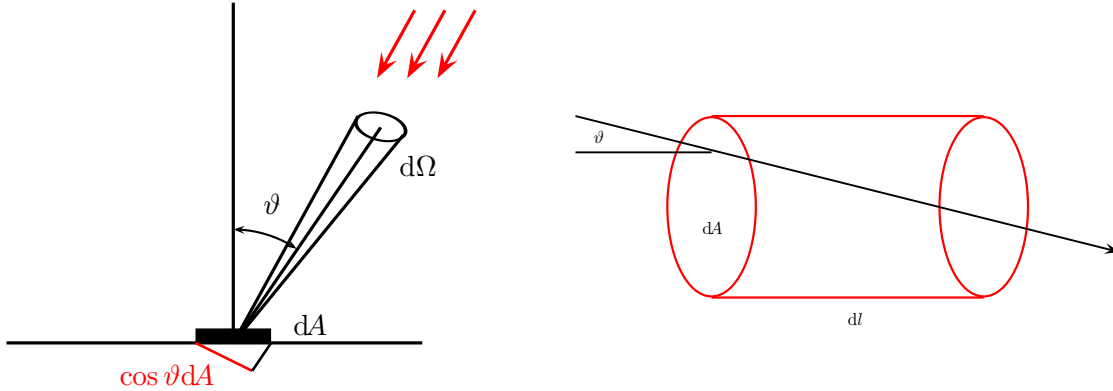


Figure 2.1.: Left: A detector with surface element dA measuring radiation coming from a direction with zenith angle ϑ . Right: Connection between the contained energy density u and the intensity I of radiation crossing the volume $dV = dA dl$.

Stefan-Boltzmann law and luminosity The Stefan-Boltzmann law determines the energy flux \mathcal{F} of blackbody radiation at temperature T . We can derive this relation integrating \mathcal{F}_ν over frequencies,

$$\mathcal{F} = \pi \int_0^\infty d\nu B_\nu = \frac{2\pi}{c^2 h^3} (kT)^4 \int_0^\infty \frac{x^3 dx}{e^x - 1} = \sigma T^4. \quad (2.11)$$

Here, we substituted first $x = h\nu/(kT)$, used then¹ $\int_0^\infty \frac{x^3 dx}{e^x - 1} = \pi^4/15$ and introduced finally the Stefan-Boltzmann constant,

$$\sigma = \frac{2\pi^5 k^4}{15c^2 h^3} = 5.670 \times 10^{-5} \frac{\text{erg}}{\text{cm}^2 \text{K}^4 \text{s}}. \quad (2.12)$$

If the Stefan-Boltzmann law is used to define the temperature of a body that is only approximately in thermal equilibrium, this temperature is called the effective temperature T_{eff} . A comparison of the spectra of the Sun and a blackbody with temperature $T = 5777 \text{ K}$ is shown in Fig. 2.2: In particular at small wave-lengths, absorption and emission lines lead to quite strong deviations from a blackbody spectrum.

The total luminosity $L = dE/dt$ of a star, i.e. the energy emitted per time, is given by the product of its surface $A = 4\pi R^2$ and the radiation σT^4 emitted per area and time,

$$L = 4\pi R^2 \sigma T^4. \quad (2.13)$$

Since the energy flux \mathcal{F} was defined as $\mathcal{F} = dE/(dA dt) = L/A$, we recover the inverse-square law for the energy flux at the distance $r > R$ outside of the star,

$$\mathcal{F} = \frac{L}{4\pi r^2}. \quad (2.14)$$

The validity of the inverse-square law $\mathcal{F}(r) \propto 1/r^2$ relies on the assumptions that no radiation is absorbed and that relativistic effects can be neglected. The later condition requires in particular that the relative velocity of observer and source is small compared to the velocity of light.

¹A list of useful integrals is given in Table A.1.

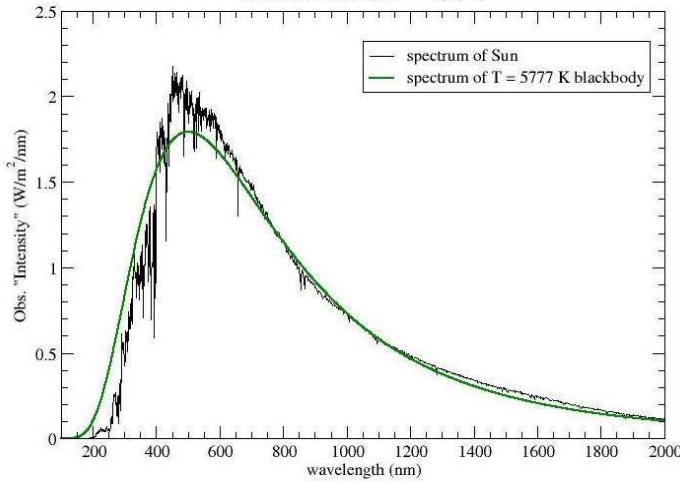


Figure 2.2.: Comparison of the spectra of the Sun and a blackbody.

Example 2.1: Calculate the mean energy of the photons in thermal black-body radiation at temperature T .

The number density of black-body photons follows with $x = h\nu/(kT)$ as

$$n = \int_0^\infty d\nu n_\nu = \frac{8\pi}{c^3} \int_0^\infty d\nu \frac{\nu^2}{\exp(\frac{h\nu}{kT}) - 1} = \frac{8\pi}{c^3} (kT/h)^3 \int_0^\infty dx \frac{x^2}{e^x - 1} = \frac{2\zeta(3)}{\pi^2} \left(\frac{kT}{hc}\right)^3,$$

while their energy density u of photons is

$$u = \frac{4\pi}{c} \int_0^\infty d\nu B_\nu = aT^4, \quad (2.15)$$

where we introduced the radiation constant a . Comparing with Eqs. (2.11) and (2.12) shows that $a = 4\sigma/c$. Thus mean energy of the photons in thermal black-body radiation is

$$\langle E \rangle = \langle h\nu \rangle = \frac{u}{n} = \frac{\pi^4}{30\zeta(3)} kT \approx 2.701kT.$$

Example 2.2: Luminosity and effective temperature of the Sun.

The energy flux received from the Sun at the distance of the Earth, $d = 1$ AU, is equal to $\mathcal{F} = 1365$ W/m². (This energy flux is also called ‘‘Solar Constant.’’) The solar luminosity L_\odot follows then as

$$L_\odot = 4\pi d^2 \mathcal{F} = 4 \times 10^{33} \text{erg/s}$$

and serves as a convenient unit in stellar astrophysics. The Stefan-Boltzmann law can then be used to define with $R_\odot \simeq 7 \times 10^{10}$ cm the effective temperature of the Sun, $T_{\text{eff}}(\text{Sun}) \equiv T_\odot \simeq 5780$ K.

Our main example in this section has been thermal blackbody radiation. However, it is useful to keep in mind that general relations like (2.7) hold for any kind of radiation, while other relations like (2.8) hold for any kind of isotropic radiation. Note also the difference between thermal blackbody radiation and blackbody radiation. In the latter case, the energy distribution of photons is proportional to a Planck distribution, but in general it is neither isotropic nor properly normalised. An example are photons from the Sun observed at Earth.

2.2. Radiation transfer

If radiation passes through matter, energy may be added or subtracted through the absorption and emission of photons. In addition, scattering may change the direction of photons. In this section, we neglect the latter effect and can thus use an one-dimensional picture.

Let us start by idealizing atoms as black discs of radius R . Then any photon hitting the disc with area πR^2 is absorbed. In other words, the cross section σ for the absorption of a photon by a single atom is $\sigma = \pi R^2$. Consider now a cylinder of length l and area A , filled with N atoms. Their number density n is $n = N/(Al)$. Let us assume first for simplicity that $N\sigma \ll A$, i.e. the atoms do not overlap and are uniformly distributed. Then the fraction τ of incoming radiation absorbed in the cylinder is simply

$$\frac{N\sigma}{A} = n l \sigma \equiv \tau \quad (2.16)$$

and defines the optical depth $\tau \equiv n l \sigma$. Our assumption $N\sigma \ll A$ corresponds to $\tau \ll 1$, an “optical thin” or transparent source in contrast to an “optical thick” source with $\tau \gg 1$. In general, matter is distributed inhomogeneously and we have to calculate how much radiation is absorbed passing the infinitesimal distance dl ,

$$dI = -I d\tau = -I n \sigma dl. \quad (2.17)$$

Dividing by I and integrating gives

$$\int_{I_0}^I \frac{dI'}{I'} = - \int_0^l dl' n \sigma = - \int_0^{\tau(l)} d\tau' = -\tau \quad \Rightarrow \quad \ln \frac{I}{I_0} = -\tau \quad (2.18)$$

and finally

$$I = I_0 \exp(-\tau) \quad \text{or} \quad I(l) = I_0 \exp\left(- \int dl n \sigma\right). \quad (2.19)$$

For small τ , the expansion of the exponential reproduces our old result: From $I_0 \exp(-\tau) \approx I_0(1 - \tau + \dots)$, one sees that the intensity is reduced by $I_0\tau$, i.e. the fraction of absorbed particles is given by τ . If $n\sigma$ does not depend on the distance l , the optical depth τ is simply obtained by multiplying $n\sigma$ with the path length l , as in our original definition (2.16). In general, however, $n\sigma$ has to be integrated along the path length l . The equation (2.19) can be seen as definition and measurement prescription for the cross section σ .

Photons can not only be absorbed, but have to be also reemitted by atoms. For instance, an atom can absorb a photon exciting one of its electrons to a level $N' > N$, de-exciting then in several steps emitting several photons of lower energy. Hence, we should add a source term which accounts for these emission processes to the previous equation. Moreover, both absorption and emission depend on the frequency ν of the photon, and we should consider therefore the evolution of the spectral intensity I_ν . Then the differential equation becomes

$$\frac{dI_\nu}{dl} = -n\sigma_\nu I_\nu + j_\nu, \quad (2.20)$$

where the emission coefficient j_ν accounts, e.g., for de-excitation of atoms. The emission coefficient has the unit $[j_\nu] = \text{erg}/(\text{cm}^3 \text{sr})$, i.e. it gives the power emitted per volume and

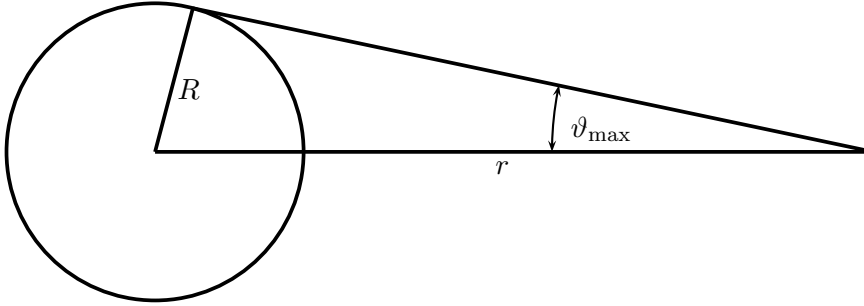


Figure 2.3.: Flux from a sphere with uniform brightness.

solid angle. Alternatively, one can rewrite this equation using as evolution variable the optical depth as

$$\frac{dI_\nu}{d\tau_\nu} = -I_\nu + S_\nu, \quad (2.21)$$

where we introduced also the source term $S_\nu \equiv j_\nu/(n\sigma_\nu)$.

Example 2.3: In empty space, both the absorption and the source terms are zero. Thus the intensity is constant along any ray of radiation,

$$\frac{dI}{dl} = 0. \quad (2.22)$$

How is this result compatible with the inverse-square law? The received flux in a detector from a source with size R at distance r is proportional to $1/r^2$, since the solid-angle extended by the source decreases as $1/r^2$. If the source is extended, its surface brightness B is constant. If the source is point-like (in practise smaller than the resolution of a telescope), it becomes dimmer. More explicitly, it is

$$\mathcal{F} = \int d\Omega I \cos \vartheta = B \int_0^{2\pi} d\phi \int_0^{\vartheta_{\max}} d\vartheta \sin \vartheta \cos \vartheta = \pi B (1 - \cos^2 \vartheta_{\max}) = \pi B \sin^2 \vartheta_{\max}. \quad (2.23)$$

From Fig. 2.3, we see that $\sin \vartheta_{\max} = R/r$ holds. Thus it follows $\mathcal{F} = \pi B (R/r)^2$. Hence the intensity is constant along a light-ray, $I = B$ – it is the decreases of the solid angle extended by the source that leads to the inverse-square law.

Example 2.4: A beam of light with intensity I_0 enters a gas layer with constant absorption α and source function S . Derive $I(l)$ and sketch $I(l)$ as function of $\tau = \alpha l$ for $S = 2I_0$ and $S = I_0/2$. We have solved already Eq. (2.20) for $S = 0$, where we obtained $I(l) = I_0 \exp(-\alpha l)$ with $\alpha \equiv n\sigma$ as absorption coefficient per length. The general solution for $S \neq 0$ is obtained by “variation of constants”, i.e. we replace I_0 by the unknown function $f(l)$. Inserting

$$\frac{dI}{dl} = \frac{df}{dl} \exp(-\alpha l) - \alpha f \exp(-\alpha l)$$

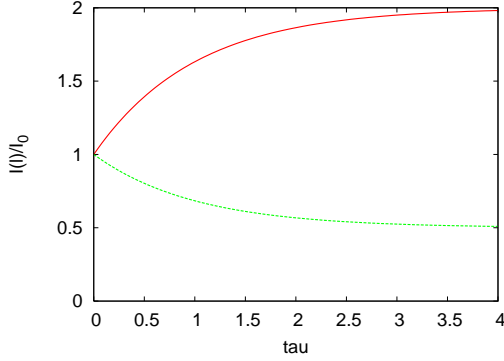


Figure 2.4.: The intensity I as function of the optical depth $\tau = \alpha l$ for $S = 2I_0$ and $S = 0.5I_0$.

into (2.20) gives

$$\frac{df}{dl} = \alpha S \exp(\alpha l)$$

or

$$f(l) = \alpha S \int dl \exp(\alpha l) = S \exp(\alpha l) + c.$$

The integration constant c has to be chosen such that $I(0) = I_0$, $c = I_0 - S$. Hence the solution is

$$I(l) = I_0 \exp(-\alpha l) + S[1 - \exp(-\alpha l)]. \quad (2.24)$$

Figure 2.4 shows how the intensity $I(l)$ of the photon beam reaches asymptotically the value S of the source function. If $I_0 < S$, more photons are replaced by the gas than absorbed and $I(l)$ approaches S from below for $\tau \rightarrow \infty$. The typical distance for a change of I is τ .

Emission from thin and thick sources Using τ as evolution variable,

$$\frac{dI_\nu}{d\tau_\nu} = -I_\nu + S_\nu, \quad (2.25)$$

multiplying by e^{τ_ν} and applying the product rule “inversely”, we obtain

$$\frac{d}{d\tau_\nu} (I_\nu e^{\tau_\nu}) = S_\nu e^{\tau_\nu}. \quad (2.26)$$

Integrating this equation, we find as general solution of the radiation transfer equation

$$I_\nu(\tau_\nu) = I_\nu(0)e^{-\tau_\nu} + \int_0^{\tau_\nu} d\tau'_\nu e^{-(\tau_\nu - \tau'_\nu)} S_\nu(\tau'_\nu). \quad (2.27)$$

Thus the intensity I_ν at τ_ν is the sum of the initial intensity diminished by absorption and the integrated source term. The latter is also diminished by absorption, however only by the material between the emission point and the observer.

If the matter is homogeneous, i.e. S_ν is constant along τ_ν , we can perform the integral and obtain again Eq. (2.24). Consider now a homogeneous object with no sources behind it. Then we can set $I_\nu(0) = 0$, and obtain

$$I_\nu = S_\nu[1 - \exp(-\tau_\nu)]. \quad (2.28)$$

For an optical thin source, $\tau_\nu \ll 1$, of size L , it is $I_\nu = S_\nu \tau_\nu$ or

$$I_\nu = j_\nu L. \quad (2.29)$$

Thus the spectrum emitted by a thin source is determined by its emission coefficient j_ν . This coefficient is strongly peaked at the energy difference between atomic or molecular bound states, and thus a thin source emits radiation mainly in emission lines. In contrast, for an optical thick source, $\tau_\nu \gg 1$, it is

$$I_\nu = S_\nu. \quad (2.30)$$

Thus the spectrum emitted by a thick source is determined by its source function S_ν . For a source in thermodynamic equilibrium, the source function equals the Planck distribution, $S_\nu = B_\nu$. [Thus $B_\nu = S_\nu = j_\nu / (n\sigma_\nu)$, which is Kirchhoff's law.] Finally, consider a thin layer of cool, diffuse gas in front of a thick source. The absorption coefficient of gas in the thin layer peaks at energies corresponding to the energy difference of atomic gas levels. As a result the blackbody spectrum emitted by the thick sources will contain absorption lines.

The observed light from stars is emitted from a thin layer, the stellar atmosphere, where the optical depth decreases from $\tau_\nu \simeq \text{few}$ to zero. We expect therefore the stellar spectra to resemble blackbody spectra, with emission lines superimposed. In addition, the temperature gradient leads to absorption lines.

2.3. Interactions of radiation with matter

A cross section is determined by strength and the range of an interaction, i.e. how black and how big the disk πR^2 is.

Compton wave-length $\lambda = \hbar / (m_e c)$, the classical electron radius $r_0 = \alpha \lambda$ the Bohr radius $r_1 = \lambda / \alpha$ in the.

The interactions of photons with

charged particles are typically proportional to the square of the Bohr radius² $r_1 = \hbar^2 / (m_e \alpha)$ in the case of bound electrons, and of the classical electron radius $r_0 = \alpha / m_e$ for scattering of photons on free electrons. Since these cross sections scale as $1/m^2$, the contribution of free protons and ions to the interaction rates can be neglected relative to the one electrons.

In stellar astrophysics, the opacity $\kappa = \sigma / m$, i.e. the cross section per mass of a certain material, is usually used together with the density ρ , such that the optical depth is $d\tau = n\sigma dr = \rho \kappa dr$.

Opacity The four most important contributions to the opacity, starting from processes important at the highest temperatures, are

1. scattering on free electrons;
2. free-free absorption: a free electron scatters in the Coulomb field of an ion and absorbs a photon; thus this process is the inverse of Bremsstrahlung;
3. bound-free absorption: a photon is absorbed and one electron is released;

²Sommerfeld's fine-structure constant α is a dimensionless number and has thus in all unit systems the same value, $\alpha \simeq 1/137$.

4. bound-bound absorption: a photon is absorbed and one electron performs a transition to an excited state.
5. absorption on negative hydrogen ion H^- : the single electron of an hydrogen atom does not screen the positive charge of the proton completely. As a result, an additional electron can be bound with binding energy 0.75 eV. This is the most important absorption process of blackbody photons at low temperatures, as in the atmosphere of the Sun.

The cross section for the scattering of photons on free electrons in the Thomson regime is energy independent. Its contribution to the opacity is given by

$$\rho\kappa_{\text{es}} = n_e\sigma_{\text{Th}} = n_e\frac{8\pi}{3}\left(\frac{\alpha}{m_e c^2}\right)^2 \quad (2.31)$$

or numerically

$$\kappa_{\text{es}} = 0.21(1 + X)\text{cm}^2/\text{g} \quad (2.32)$$

for fully ionized matter. Here, n_e denotes the number density of free electrons and X the mass fraction of hydrogen. The factor $1 + X$ takes into account that hydrogen has approximately twice as many electrons per mass than heavier elements.

The opacity coefficients due to absorption on atoms and ions cannot be measured for conditions typical for stellar interiors, and have to be determined theoretically. While the opacity due to the absorption of photons by hydrogen and hydrogen-like ions in non-degenerate matter can be calculated analytically, the Schrödinger equation must be solved approximately for two or more electron states. The results of these rather complex calculations are tabulated; simple approximate formulae are used to parametrise them as

$$\kappa = \kappa_0\rho^a T^b. \quad (2.33)$$

Kramer's law is an approximation for free-free absorption,

$$\kappa_{\text{ff}} = C\rho T^{-7/2}, \quad (2.34)$$

where C is a constant depending on chemical composition. This approximation breaks down at low and high frequencies. A sketch of the opacity as function of temperature is shown in Fig. 2.5.

Diffusion and random walks What is the fate of a photon created in the center of the Sun? If we estimate its mean free-path $\ell = 1/(n\sigma)$ by assuming that most of hydrogen in the Sun is ionized, and thus the mean density of free electron is $n_e = \rho_{\odot}/m_H \simeq 8.44 \times 10^{23}/\text{cm}^3$, and cross section $\sigma = \sigma_{\text{Th}} \simeq 6 \times 10^{-25}\text{cm}^2$, then $\ell \simeq 2\text{cm}$. In each scattering process, the photon is approximately isotropically emitted: Thus the path of a photon from the center of the Sun to the surface is not a straight-forward travel, but resembles a random-walk. The time a photon needs to travel the distance R_{\odot} can be estimated in two ways:

After N steps \mathbf{l}_i of the same size $|\mathbf{l}_i| = \ell$ a photon that started at zero is at the position $\mathbf{d} = \sum_{i=1}^N \mathbf{l}_i$. The scalar product of \mathbf{d} with itself is

$$\mathbf{d} \cdot \mathbf{d} = \sum_{i=1}^N \sum_{j=1}^N \mathbf{l}_i \cdot \mathbf{l}_j \quad (2.35)$$

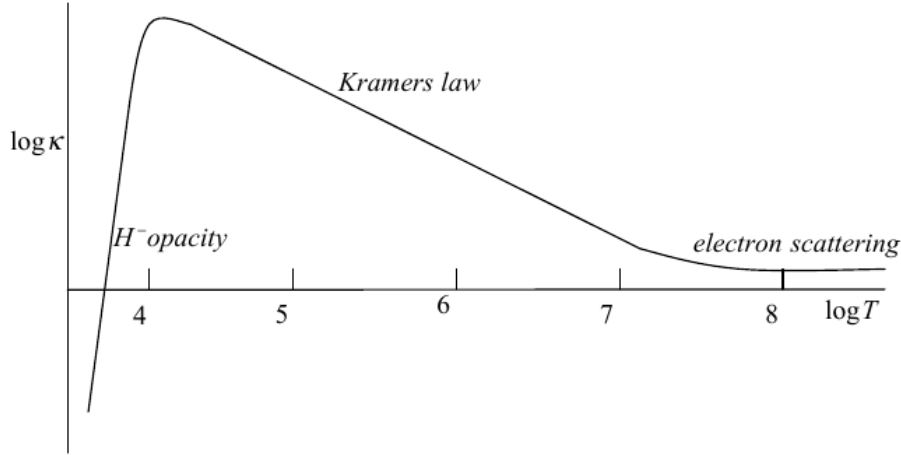


Figure 2.5.: Sketch of the opacity as function of temperature.

and splitting the sum into the diagonal and the off-diagonal terms, we obtain

$$d^2 = Nl^2 + 2l^2 \sum_{i=1}^N \sum_{j<i}^N \cos \vartheta_{ij} \approx Nl^2. \quad (2.36)$$

By assumption, the angles ϑ_{ij} between \mathbf{l}_i and \mathbf{l}_j are chosen randomly and thus the off-diagonal terms cancel against each other.

More formally, one can argue like this: The probability $p(m, n)$ to end after n steps of unit size at the distance $d = m$ is given in the Table as

m	-3	-2	-1	0	1	2	3
$n = 0$				1			
$n = 1$			1/2		1/2		
$n = 2$		1/4		1/2		1/4	
$n = 3$	1/8		3/8		3/8		1/8

The denominator of $p(m, n)$ is the sum of all possible paths, 2^n . The numerator is the sum of all paths ending at distance m after n steps; each entry in the table is given by the sum of the entries to the left and right in the line above and thus equal to the binomial coefficient (remember Pascal's triangle). Thus

$$p(m, n) = 2^{-n} \binom{n}{m}.$$

Since $p(m, n) = p(-m, n)$, the average distance is zero. A more useful quantity is the root mean square deviation $d = \langle k^2 \rangle^{1/2}$,

$$d = \left(\frac{\sum_k k^2 p(k, n)}{2^n} \right)^{1/2} = n^{1/2}$$

If the step size is L , then $d = n^{1/2}L$.

Diffusion equation The continuity equation for the number density n and its current \mathbf{j} ,

$$\nabla \cdot \mathbf{j} + \frac{\partial n}{\partial t} = 0, \quad (2.37)$$

leads together with Fick's law for an isotropic medium,

$$\mathbf{j} = -D\nabla n, \quad (2.38)$$

to the diffusion equation

$$\frac{\partial n}{\partial t} - \nabla \cdot (D\nabla n) = Q. \quad (2.39)$$

Note that the diffusion equation can be transformed for a diffusion coefficient D that is independent on \mathbf{x} into the free Schrödinger equation substituting $D \leftrightarrow \hbar^2/(2m)$ and $t \leftrightarrow -it$. Hence we can borrow the free propagator for a non-relativistic particle as Green function $G(r)$ for the diffusion equation with $D = \text{const.}$ and obtain with the mentioned substitutions,

$$G(r) = \frac{1}{(4\pi Dt)^{3/2}} \exp[-r^2/(4Dt)]. \quad (2.40)$$

Thus the mean distance traveled outward is $\propto \sqrt{Dt}$, as in a random walk with $\langle r^2 \rangle \sim Nl_0^2$. Connecting the two pictures, we obtain $D \sim Nl_0^2/t \sim vl_0$ with $v = Nl_0/t$. Therefore, the diffusion coefficient D can be estimated as the product of the photon velocity $v = c$ and its mean free path l_0 . A more precise analysis gives $D = l_0v/3$, where the factor three reflects the number of spatial dimensions.

2.4. Thermodynamic equilibrium

Local thermodynamic equilibrium A star is producing energy in its center which is transported outside. As a result, the temperature in a star decreases with radial distance. A system where the temperature depends on position (i.e., the radius of a star) cannot be in thermal equilibrium. However, the mean free path for interactions (which are responsible for establishing equilibrium) is small compared to the scale of temperature variation in a star. Therefore, we can use the concept of local thermodynamic equilibrium (LTE): We can use the equilibrium expressions like 2.54, replacing the uniform temperature T by $T(r)$. Departure from local thermodynamic equilibrium are typically small and have to be included only when they are crucial, e.g. in radiation transport.

For instance, in a stellar atmosphere, we can estimate deviations from isotropy as

$$\delta = \frac{I_{\max} - I_{\min}}{I_{\max} + I_{\min}} \simeq \frac{3\mathcal{F}}{cu} \quad (2.41)$$

Since the flux of radiation is $\mathcal{F} = \sigma T_{\text{eff}}^4$ and the energy density $u = aT^4 = 4\sigma/cT^4$, it follows

$$\delta \simeq \frac{3}{4} \left(\frac{T_{\text{eff}}}{T} \right)^4. \quad (2.42)$$

At the surface, $T \simeq T_{\text{eff}}$, and the anisotropy is maximal. Going deeper in the star, T increases and the anisotropy decreases fast.

Equilibrium distribution functions The expressions for the number and energy density of blackbody radiation are special cases for the distribution function of ideal gases in equilibrium. In general, the distribution function $f(\mathbf{x}, \mathbf{p})$ in phase space gives the average occupation number of a cell in phase space with volume h^3 ,

$$N = \frac{g}{h^3} \int d^3x d^3p f(\mathbf{x}, \mathbf{p}), \quad (2.43)$$

of a system with N particles with g spin degrees of freedom. Often the system is uniform, and we consider only the distribution function $f(\mathbf{p})$ in momentum space. In statistical physics, one shows that the distribution function $f(p)$ of a free gas of fermions or bosons in *kinetic equilibrium* is

$$f(p) = \frac{1}{\exp[\beta(E - \mu)] \pm 1} \quad (2.44)$$

where $\beta = 1/kT$ is the inverse temperature, $E = \sqrt{c^4m^2 + (cp)^2}$, μ the chemical potential, and $+1$ refers to fermions and -1 to bosons, respectively.

We can compare this expression to the number density of blackbody photons, Eq. (2.1),

$$n_\nu d\nu = \frac{2}{h^3} \frac{4\pi h^3 \nu^2 d\nu}{c^3} \frac{1}{\exp(\frac{h\nu}{kT}) - 1}. \quad (2.45)$$

With $p = h\nu/c$ and $n_\nu d\nu = n_p dp$, we see that the second factor equals the volume element in momentum space, $4\pi h^3 \nu^2 d\nu / c^3 = 4\pi p^2 dp$. Thus photons are bosons with two spin degrees of freedom. Their chemical potential is zero, since the photon number is not conserved.

Boltzmann statistics In the classical limit (large T , dilute gas), we can set $\exp[\beta(E - \mu)] \pm 1 \simeq \exp[\beta(E - \mu)]$, obtaining the Boltzmann statistics. Then the population n_i of the state i with energy E_i and degeneracy g_i is given by a Boltzmann distribution, with

$$n_i = \mathcal{Z}^{-1} g_i \exp(-E_i/kT), \quad (2.46)$$

where \mathcal{Z} is a normalization constant. Excitations with energy $E \gg kT$ are exponentially suppressed.

***** Saha equation ***** The binding energy of hydrogen is $B = m_p + m_e - m_H = 13.6$ eV. Thus the particles are non-relativistic and their number density is

$$n_i = g_i \left(\frac{m_i T}{2\pi} \right)^{3/2} \exp[-\beta(m_i - \mu_i)]. \quad (2.47)$$

If the reaction $p + e^- \leftrightarrow H + \gamma$ is in chemical equilibrium, then $\mu_p + \mu_e = \mu_H$. Thus we can replace μ_H first by μ_e and μ_p . The latter are then re-expressed by n_e and n_p ,

$$\exp(\beta\mu_H) = \exp[\beta(\mu_p + \mu_e)] = \frac{g_H}{g_p g_e} n_p n_e \left(\frac{2\pi}{m_e T} \right)^{3/2} \exp[\beta(m_p + m_e - m_H)]. \quad (2.48)$$

Here we set in the pre-factor $m_p \approx m_H$ and kept the exact masses only in the exponential. Inserting this expression for $\exp(\beta\mu_H)$ together with the definition of the binding energy B , $B_H = m_p + m_e - m_H$, we obtain

$$n_H = \frac{g_H}{g_p g_e} n_p n_e \left(\frac{2\pi}{m_e T} \right)^{3/2} \exp(B/T). \quad (2.49)$$

Define the fractional equilibrium ionization X_e^{eq} as $X_e^{\text{eq}} = n_e/n_b$ with $n_b = n_p + n_H$, then charge neutrality $n_e = n_p$ implies $n_e = n_p = Xn_B$ and $n_H = (1 - X)n_b$.

With $g_e = g_p = 2$, $g_H = 4$ and $n_b = \eta n_\gamma$ ($n_\gamma = \frac{2\zeta(3)}{\pi^2} gT^3$), we obtain the so-called ‘‘Saha equation’’ for the fractional equilibrium ionization

$$\frac{1 - X_e^{\text{eq}}}{(X_e^{\text{eq}})^2} = \frac{n_b n_H}{n_e n_p} = \frac{4\sqrt{2}\zeta(3)}{\sqrt{\pi}} \left(\frac{T}{m_e}\right)^{3/2} \eta \exp(B/T). \quad (2.50)$$

Maxwell velocity distribution The two most important cases in astrophysics are a classical, non-relativistic gas of atoms and a gas of photons. In the first case, we can derive the momentum distribution noting that the states describing a free particle are labelled by the continuous three-momentum \mathbf{p} . Thus the sum over discrete quantum numbers in the Boltzmann factor is replaced by an integration over the momenta d^3p and the volume d^3x occupied by the system,

$$\sum_i \exp(-E/kT) \rightarrow V \int \frac{d^3p}{(2\pi)^3} \exp\left(-\frac{mv^2}{2kT}\right) = \frac{V}{(2\pi)^3} \int_0^\infty \exp\left(-\frac{mv^2}{2kT}\right) 4\pi m^3 v^2 dv. \quad (2.51)$$

If the particles have a distribution n_p of momenta with

$$N = V \int_0^\infty dp n_p = V \int_0^\infty dv n_v, \quad (2.52)$$

If we compare the RHS with Eq. (2.56) we see that we need only to normalize correctly n_v . The integral can be evaluated by substituting $\alpha = m/(2kT)$ and noting that

$$-\frac{\partial}{\partial \alpha} \left\{ \int_{-\infty}^\infty dx \exp(-\alpha x^2) \right\} = \int_{-\infty}^\infty dx x^2 \exp(-\alpha x^2) = -\frac{\partial}{\partial \alpha} \sqrt{\frac{\pi}{\alpha}} = \frac{1}{2\alpha} \sqrt{\frac{\pi}{\alpha}}. \quad (2.53)$$

Multiplying the integrand with $4(\alpha/\pi)^{3/2}$, we obtain the Maxwell-Boltzmann distribution of velocities for a classical gas,

$$n_v dv = n \left(\frac{m}{2\pi kT}\right)^{3/2} \exp\left(-\frac{mv^2}{2kT}\right) 4\pi v^2 dv. \quad (2.54)$$

2.5. Equations of state

The pressure in a star is the sum of the pressure of gas and of radiation. The former can be split further into the contribution of ions and of electrons. In practically all circumstances, the ions behave in good approximation as a ideal gas, and thus

Pressure integral A (relativistic or non-relativistic) particle in a box of volume L^3 collides per time interval $\Delta t = 2L/v_x$ once with one of the two yz -sides of the box, if the x component of its velocity is v_x . Thereby it exerts the force $F_x = \Delta p_x/\Delta t = p_x v_x/L$. The pressure produced by N particles is then $P = F/A = N p_x v_x/(LA) = n p_x v_x$ or for an isotropic velocity distribution with $\langle v^2 \rangle = \langle v_x^2 \rangle + \langle v_y^2 \rangle + \langle v_z^2 \rangle = 3\langle v_x^2 \rangle$

$$P = \frac{1}{3} n v p. \quad (2.55)$$

If the particles have a distribution n_p of momenta with

$$N = V \int_0^\infty dp n_p = V \int_0^\infty dv n_v, \quad (2.56)$$

then we obtain instead of Eq. (2.55) the so-called pressure integral

$$P = \frac{1}{3} \int_0^\infty dp n_p vp. \quad (2.57)$$

Although the derivation assumed classical trajectories of the particles, the result holds for any kind of non-interacting particles, in particular also if quantum effects are important, cf. with exercise 3.

Pressure of an ideal gas Because of $n_p dp = n_v dv$, we can insert now n_v into the pressure integral (2.57),

$$P = \frac{1}{3} \int_0^\infty dv n_v vp = n \left(\frac{\alpha}{\pi}\right)^{2/3} \int_0^\infty dx x^4 \exp(-\alpha x^2) = nkT. \quad (2.58)$$

The integral $\int dx x^4 \exp(-\alpha x^2)$ has been calculated with the same method, but now differentiating twice the Gaussian integral with respect to α . Since we use generally the mass density ρ instead of the particle number density n , it is more convenient to introduce the gas constant $\mathcal{R} = k/m_H$ and the mean atomic weight μ defined by $n = \rho/(\mu m_H)$. Then the ideal gas law becomes

$$\boxed{P = nkT = \mathcal{R}\rho T/\mu.} \quad (2.59)$$

The mean atomic weight μ depends on the composition of the star. Often, one distinguishes only between hydrogen, helium and heavier elements (calling them “metals”) with mass fraction X , Y and Z , respectively. Then the mean atomic weight μ_I of ions is given by

$$\frac{1}{\mu_I} \simeq X + \frac{Y}{4} + \frac{1 - X - Y}{\langle A \rangle} \quad (2.60)$$

where $\langle A \rangle$ is the average mass number of the heavy elements. For the Sun, these mass fractions are $X \simeq 0.707$, $Y \simeq 0.274$, while $\langle A \rangle \simeq 20$. Thus the mean atomic weight of ions is $\mu_I \simeq 1.29$.

Free electrons contribute additionally to the pressure. If they can be described as an ideal gas, their contribution to the pressure is $P_e = n_e kT$, where n_e is the number density of free electrons. Defining $1/\mu_e$ as the number of free electrons per nucleon, it is $n_e = \rho/(\mu_e m_H)$. Approximately,

$$\frac{1}{\mu_e} = X + \frac{1}{2}Y + (1 - X - Y)\langle A/Z \rangle \simeq \frac{1}{2}(1 + X) \quad (2.61)$$

since $\langle A/Z \rangle \simeq 1/2$. For the Sun, $\mu_e \simeq 1.17$.

Finally, we can combine these contributions to obtain the total gas pressure

$$P_{\text{gas}} = P_I + P_e = \frac{\mathcal{R}}{\mu} \rho T \quad (2.62)$$

with

$$\frac{1}{\mu} = \frac{1}{\mu_I} + \frac{1}{\mu_e} \quad (2.63)$$

and $\mu \simeq 0.61$ for the Sun.

Degenerate fermion gas We consider a non-interacting fermion gas in the limit of complete degeneration. Then we can neglect the temperature and the Fermi-Dirac distribution function becomes a step function. Thus all levels up-to the Fermi momentum p_F are filled, and the number density of a species with two spin degrees of freedom is

$$n = \frac{2}{h^3} \int_0^{p_F} 4\pi p^2 dp = \frac{8\pi}{3h^3} p_F^3 = \frac{1}{3\pi^2 \lambda^3} x^3 \quad (2.64)$$

with $x \equiv p_F/(mc)$ and $\lambda = \hbar/(mc)$. The pressure integral becomes with $v = p/E$

$$P = \frac{1}{3} \int_0^\infty dv n_v v p = \frac{1}{3} \frac{2}{h^3} \int_0^{p_F} dp 4\pi p^2 \frac{(cp)^2}{\sqrt{(pc)^2 + m^2 c^4}} = \quad (2.65)$$

$$= \frac{8\pi m^4 c^5}{3h^3} \int_0^x dx' \frac{x'^4}{\sqrt{1+x'^2}} = \frac{mc^2}{\lambda^3} \phi(x), \quad (2.66)$$

where

$$\phi(x) = \frac{1}{8\pi^2} \left[x\sqrt{1+x^2}(2x^2-3) + 3 \operatorname{arcsinh}(x) \right] \quad (2.67a)$$

$$= \frac{1}{8\pi^2} \left[x\sqrt{1+x^2}(2x^2-3) + 3 \ln[x + \sqrt{1+x^2}] \right] = \frac{1}{8\pi^2} f(x). \quad (2.67b)$$

Example 2.5: The integral can be evaluated substituting $\sinh \vartheta = p/mc$ and $\sinh \vartheta_F = p_F/mc$,

$$\int_0^x dx' \frac{x'^4}{\sqrt{1+x'^2}} = \int_0^{\vartheta_F} d\vartheta \sinh^4 \vartheta = \frac{3}{8} \vartheta_F - \frac{3}{16} \sinh 2\vartheta_F + \frac{1}{4} \sinh^3 \vartheta_F \cosh \vartheta_F = f(x)$$

This function has as limiting cases

$$\phi(x) \simeq \begin{cases} \frac{1}{15\pi^2} (x^5 - \frac{5}{14}x^7 + \dots) & \text{for } x \ll 1, \\ \frac{1}{12\pi^2} (x^4 - x^2 + \dots) & \text{for } x \gg 1. \end{cases} \quad (2.68)$$

Let us first consider the case of degenerate electrons in a star. Then we should set $m = m_e$ in the expression for P . The density of the star is however dominated by the contribution of ions. Then with the mean molecular weight per electron μ_e , it follows

$$\rho = \mu_e m_N n_e. \quad (2.69)$$

Both in the non-relativistic, $x \ll 1$, and ultra-relativistic limit, $x \gg 1$, the equation of state has a polytropic form: In the non-relativistic limit, $x \ll 1$ and $\phi(x) \simeq x^5/(15\pi^2)$, it follows

$$P = \frac{(3\pi^2)^{2/3} \hbar^2}{5 m_e} \left(\frac{\rho}{\mu_e m_p} \right)^{5/3} = K_{5/3} \rho^{5/3}, \quad (2.70)$$

while the relativistic limit, $x \gg 1$ and $\phi(x) \simeq x^4/(12\pi^2)$, the pressure is given by

$$P = \frac{(3\pi^2)^{1/3} \hbar c}{4} \left(\frac{\rho}{\mu_e m_p} \right)^{4/3} = K_{4/3} \rho^{4/3}. \quad (2.71)$$

In the case of degenerate nucleons, the same expressions hold replacing m_e with m_N . Since the fermion mass enters in the denominator, the nucleons become degenerate at higher densities. [Criteria for the star: compare classical gas and degenerate pressure.]

Pressure of radiation The second important example is the pressure P_{rad} of radiation, i.e. the pressure of a photon gas. With $p = h\nu/c$ and $n_\nu d\nu = n_p dp$ it follows

$$P_{\text{rad}} = \frac{1}{3} \int_0^\infty d\nu n_\nu h\nu. \quad (2.72)$$

Noting that the spectral energy density u_ν and the intensity B_ν of a thermal photon gas are connected by $u_\nu d\nu = 4\pi/c B_\nu d\nu$, it follows

$$P_{\text{rad}} = \frac{aT^4}{3} = \frac{u_{\text{rad}}}{3}. \quad (2.73)$$

The relation $P = u/3$ holds for all relativistic particles.

2.6. Stellar atmospheres

We have found in Eq. (2.30) the general solution for the one-dimensional radiation transfer equation. Apart from the outermost layer of a star, it is $\tau \gg 1$, and we can thus approximate $S_\nu \simeq B_\nu$. But even in the stellar interior, the radiation transfer problem is non-trivial since the local temperature $T(r)$ determining the source function $S_\nu \simeq B_\nu$ depends itself on how the energy produced in the core of the star is transported outside.

In the case of stellar atmospheres, the problem becomes even more complex since the approximation $S_\nu \simeq B_\nu$ is not valid anymore and the source function has to be calculated from the energy spectra of elements.

Problems

2.1 Equilibrium temperature of the Earth. Derive the equilibrium temperature of the Earth assuming a.) that it absorbs 60% of the incoming Solar radiation, b.) adding now a layer that is completely transparent to visible light received from the Sun but absorbs all infrared radiation emitted by the surface of the Earth.

for the outer layer of a star that both the source function and the opacity change as a power-law, $\kappa = \kappa_0(r_0/r)^3$ (density) and $S(r) = S_0(r_0/r)$ (T).

2.3 Pressure. Show that the relation (2.57) for the pressure of non-interacting particles holds also for a quantum gas.

2.2 Model atmosphere. Consider as a simple model

3. Equations of stellar structure

We determine in this section the equations of stellar structure assuming a spherically symmetric, static star. This requires that rotation, magnetic fields, and other effects that break rotational symmetry have only a minor influence on the star. Since stellar evolution proceeds on very large time scales, it is sufficient to consider a static star at a fixed time, i.e. for a given chemical composition. Moreover, we assume LTE. Finally, we neglect general relativistic effects which are negligible for all stars satisfying $R \gg R_S = 2GM/c^2$.

3.1. Mass continuity and hydrostatic equilibrium

We denote by $M(r)$ the mass enclosed inside a sphere with radius r and density $\rho(r)$,

$$M(r) = 4\pi \int_0^r dr' r'^2 \rho(r'), \quad (3.1)$$

or in differential form

$$\boxed{\frac{dM(r)}{dr} = 4\pi r^2 \rho(r)}. \quad (3.2)$$

Although almost trivial, this relation constitutes the first (“the continuity equation”) of the equations needed to describe the structure and evolution of stars. An important application of the continuity equation is to express physical quantities not as function of the radius r but of the enclosed mass $M(r)$. This facilitates e.g. the numerical computation of the stellar properties as function of time, because the mass of a star remains nearly constant during its evolution, while the stellar radius can change considerably. Moreover, one wants usually to construct a stellar model for a prescribed mass M , with the stellar radius R as the outcome of the model. Often, a change of variable from r to $M(r)$ is also convenient in analytical calculations.

As an example for the usefulness of this variable transformation, we calculate the total gravitational energy U_{pot} of a spherical star. According to Gauß’ law, only the enclosed mass $M(r)$ contributes to the gravitational field at the distance r . Finding the total gravitational energy of a spherical star amounts therefore to integrating $dU_{\text{pot}} = -GM(r)dM(r)/r$, or

$$U_{\text{pot}}(R) = -G \int_0^R \frac{M(r)dM(r)}{r}. \quad (3.3)$$

Without further assumption on the density distribution $\rho(r)$, we cannot proceed. For simplicity, we assume a uniform density, obtaining

$$U_{\text{pot}}(R) = -G \frac{(4\pi\rho)^2}{3} \int_0^R dr r^4 = -\frac{3}{5} \frac{GM^2}{R}. \quad (3.4)$$

In Ex. X, we consider as two more realistic cases an exponential and power-law profile. For not too extreme choices, the results differs only by a factor of few. Thus for order-of-magnitude estimates, the use of a simple uniform density profile is adequate.

3. Equations of stellar structure

Example 3.1: The density profile of a.) the Sun can be approximated in the range $0.15R_\odot \lesssim r \lesssim 0.65R_\odot$ by $\rho(r) = \rho_0 \exp(-r/r_0)$ with $r_0 = R_\odot/10.54$, b.) of massive stars by a power-law $\rho(r) = \rho_0(R/r)^\alpha$ with $\alpha \sim 3$. Find the potential energy as function of M and R in these cases.

A radial-symmetric mass distribution $M(r)$ produces according Gauß' law the same gravitational acceleration, as if it would be concentrated at the center $r = 0$. Therefore the gravitational acceleration $g(r)$ produced by $M(r)$ is

$$g(r) = -\frac{GM(r)}{r^2}. \quad (3.5)$$

If the star is in equilibrium, this acceleration has to be balanced by a pressure gradient from the center of the star to its surface. Pressure is defined as force per area, $P = F/A$, and thus a pressure change along r to $r + dr$ corresponds to an increment

$$dF = -\underbrace{A}_{\text{force}} dP = \underbrace{\rho(r)A}_{\text{mass}} dr \underbrace{a(r)}_{\text{acceleration}} \quad (3.6)$$

of the force F produced by the pressure gradient dP . For increasing r , the resulting force dF is positive and therefore directed outward, if the pressure P decreases outwards, $dP < 0$. Hydrostatic equilibrium, $g(r) = -a(r)$, requires

$$\boxed{\frac{dP}{dr} = \rho(r)g(r) = -\frac{GM(r)\rho(r)}{r^2}}. \quad (3.7)$$

If the pressure gradient and gravity do not balance each other, the layer at position r is accelerated,

$$a_{\text{tot}}(r) = -\frac{GM(r)}{r^2} - \frac{1}{\rho(r)} \frac{dP}{dr}. \quad (3.8)$$

In general, we need an equation of state, $P = P(\rho, T, Y_i)$, that connects the pressure P with the density ρ , the (not yet) known temperature T and the chemical composition Y_i of the star. Thus we need additional equations which describe the energy generation and transport in the star.

For an estimate of the central pressure $P_c = P(0)$ of a star in hydrostatic equilibrium, we integrate (3.7) and obtain with $P(R) \approx 0$,

$$P_c = -\int_0^R \frac{dP}{dr} dr = G \int_0^M dM \frac{M}{4\pi r^4}, \quad (3.9)$$

where we used again the continuity equation to substitute $dr = dM/(4\pi r^2\rho)$ by dM . If we replace furthermore r by the stellar radius $R \geq r$, we obtain a lower limit for the central pressure,

$$P_c = G \int_0^M dM \frac{M}{4\pi r^4} > G \int_0^M dM \frac{M}{4\pi R^4} = \frac{GM^2}{8\pi R^4}. \quad (3.10)$$

Inserting values for the Sun, it follows

$$P_c > \frac{GM^2}{8\pi R^4} = 4 \times 10^8 \text{bar} \left(\frac{M}{M_\odot}\right)^2 \left(\frac{R_\odot}{R}\right)^4. \quad (3.11)$$

An alternative way to derive an estimate for the central pressure is to convert the differential equation (3.7) into a finite difference equation. With $dP = P_c - P(R) = P_c$ and $dr = -R$, it follows

$$P_c \sim \frac{3GM^2}{4\pi R^4}. \quad (3.12)$$

The value obtained integrating the hydrostatic equation using the ‘‘Solar Standard Model’’ is $P_c = 2.48 \times 10^{11}$ bar, i.e. a factor 500 larger.

The continuity and hydrostatic equations are two first-order differential equations for $M(r)$ and $P(r)$. If the pressure would be only a function of the density, $P = P(\rho)$, the two equations could be solved. This special case results in the Lane-Emden equation, which we will discuss later. In general, however, the E.o.S. depends also on temperature. As a result, we need two more equations describing the generation and transport of energy in a star. Before we discuss these additional two equation, we derive the virial theorem for stars.

3.2. Virial theorem

Classical gas The virial theorem is an important link between the (gravitational) potential energy and the internal (kinetic) energy of any system in equilibrium. In order to derive it for the special case of a star, we multiply both sides of the hydrostatic equilibrium equation (3.7) with $4\pi r^3$ and integrate over r ,

$$\int_0^R dr 4\pi r^3 P' = - \int_0^R dr 4\pi r^3 \frac{GM(r)\rho}{r^2}. \quad (3.13)$$

Next we insert $dM(r) = 4\pi r^2 \rho dr$ on the RHS and integrate partially the LHS,

$$[4\pi r^3 P]_0^R - 3 \int_0^R dr 4\pi r^2 P = - \int_0^M dM \frac{GM(r)}{r}. \quad (3.14)$$

The RHS is the gravitational potential energy U_{pot} of the star. Using the boundary conditions $V(0) = 0$ and $P(R) = 0$, we see that the first term of the LHS vanishes. We can rewrite the remaining second term of the LHS as

$$\boxed{-3 \int_0^M dm \frac{P}{\rho} = U_{\text{pot}}.} \quad (3.15)$$

This is the general form of the virial theorem for a star. For the special case of an ideal gas, $P = nkT = \frac{2}{3}dU_{\text{kin}}/dV$, and thus $P/\rho = \frac{2}{3}dU_{\text{kin}}/dm$, we obtain

$$\boxed{-2U_{\text{kin}} = U_{\text{pot}}.} \quad (3.16)$$

Hence the average energy of a single atom or molecule of the gas is $\langle E_{\text{kin}} \rangle = -\frac{1}{2}\langle E_{\text{pot}} \rangle$. This is the same result as for a free hydrogen atom, indicating that only the shape not the strength of the potential $V(r) \propto r^{-\alpha}$ determines the ratio of kinetic and potential energy.

Example 3.2: Estimate the central temperature of the Sun with the virial theorem. The Sun consists mainly of (ionized) hydrogen. Thus we can estimate the average gravitational potential energy of a single particle inside the Sun as

$$\langle E_{\text{grav}} \rangle \sim -\frac{GM_{\odot}m_p}{R_{\odot}} \approx -3.2\text{keV}/c^2.$$

For a thermal velocity distribution of a Maxwell-Boltzmann gas we obtain

$$\langle E_{\text{kin}} \rangle = \frac{3}{2}kT = -\frac{1}{2}\langle E_{\text{grav}} \rangle \approx 1.6\text{keV}/c^2.$$

Hence our estimate for the central temperature of the Sun is $T_c \approx 1.1\text{keV}/c^2 \approx 1.2 \times 10^7\text{K}$ – compared to $T_c \sim 1.3\text{keV}/c^2$ in the so-called Solar Standard Model.

Adiabatic expansion Processes without exchange of heat with the surrounding medium are called adiabatic. Since the thermalization time in stars is typically much larger than the time scales we are interested in, many processes in stars are adiabatic. The first law of thermodynamics, $\delta U = \delta Q - P\delta V$, applied to a mass element dm implies then with $\delta Q = 0$ and $U = udm$ that

$$\delta(udm) + P\delta\left(\frac{dV}{dm}dm\right) = \delta udm + P\delta\left(\frac{1}{\rho}\right)dm = 0. \quad (3.17)$$

Here, we denoted the variations of quantities due the the adiabatic process by δ , in order to distinguish them from the ordinary differentials. Moreover, we used mass conservation, $\delta dm = 0$. Dividing by dm and setting $\delta \rightarrow d$, it follows

$$du + Pd\left(\frac{1}{\rho}\right) = 0. \quad (3.18)$$

(Note also that in this paragraph u denotes the internal energy per mass, not per volume.) If the specific energy u is proportional to P/ρ , i.e.

$$u = n\frac{P}{\rho}, \quad (3.19)$$

then differentiation leads to

$$nPd\left(\frac{1}{\rho}\right) + n\frac{1}{\rho}dP + Pd\left(\frac{1}{\rho}\right) = -(n+1)P\frac{d\rho}{\rho^2} + n\left(\frac{1}{\rho}\right)dP = 0 \quad (3.20)$$

or

$$\frac{dP}{P} = \frac{n+1}{n}\frac{d\rho}{\rho}. \quad (3.21)$$

Integrating this relation, we can express the pressure as function of the density,

$$P = K\rho^{(n+1)/n} = K\rho^{\gamma}. \quad (3.22)$$

where we introduced also the adiabatic exponent $\gamma = (n+1)/n$.

General polytrope We want to generalize the virial theorem to a gas with an equation of state given by $P(r) = K\rho(r)^\gamma$, where K is independent of the radius r . Solutions with such an equation of state that satisfy the equation of hydrostatic equilibrium are called polytropes. Although the defining equation $P(r) = K\rho(r)^\gamma$ of a polytrope is formally equal to the condition of adiabatic changes, Eq. (3.22), the meaning of the two relations is different: The latter describes the adiabatic change of a fluid element at the same point, while the former constrains the variation of $P(r)$ and $\rho(r)$ as function of the radial distance r .

We have already seen some important examples for polytropes. First, the E.o.S. of a degenerate fermion gas in its limiting cases has the polytropic form $P = K\rho^\gamma$, with $\gamma = 5/3$ in the non-relativistic and $\gamma = 4/3$ in the ultra-relativistic limit, respectively. Another example is an isothermal, ideal gas with $P = \mathcal{R}\rho T_0/\mu \equiv K\rho$, $K = \mathcal{R}T_0/\mu$ and $\gamma = 1$ or $n = \infty$. Note the difference between the reasons for having a polytropic relation in a star: In one case, the E.o.S. has a polytropic form $P(r) = K\rho(r)^\gamma$ with K fixed and given by natural constants as for a degenerate fermion gas. In the other case, the E.o.S. depends on the temperature T , but an additional condition allows one to obtain a constant K ; in this case, K is arbitrary and can vary from star to star.

In order to derive the virial theorem for a general polytrope, we have to express the kinetic energy density as function of the pressure and the adiabatic index γ . Combining $dP/P = \gamma d\rho/\rho$ and $d\rho/\rho = -dV/V$, we obtain

$$VdP = -\gamma PdV. \quad (3.23)$$

Next we add PdV to both sides,

$$d(VP) = VdP + PdV = -(\gamma - 1)PdV, \quad (3.24)$$

and rewrite both sides as total differentials,

$$d\left(\frac{VP}{\gamma - 1}\right) = -PdV = dU_{\text{kin}}, \quad (3.25)$$

which can be integrated. Hence the pressure and the (kinetic) energy density are connected by

$$P = (\gamma - 1)\frac{U_{\text{kin}}}{V}. \quad (3.26)$$

We can use this expression to define an ‘‘adiabatic index’’ even for the case when the star is not a polytrope. In the case of an ideal gas with average temperature T , it is $U_{\text{kin}}/V = 3nkT/2$ and $P = nkT$, and the adiabatic index follows as $\gamma = 5/3$, while for radiation, $U_{\text{kin}}/V = aT^4$ and $P = aT^4/3$, and thus $\gamma = 4/3$.

The relation $P = (\gamma - 1)U_{\text{kin}}/V$ allows us to re-express the LHS of Eq. (3.14) as

$$-3(\gamma - 1)U_{\text{kin}} = U_{\text{pot}}. \quad (3.27)$$

A star can be only stable, if its total energy $U_{\text{tot}} = U_{\text{kin}} + U_{\text{pot}}$ is smaller than zero,

$$U_{\text{tot}} = (4 - 3\gamma)U_{\text{kin}} = \frac{3\gamma - 4}{3\gamma - 3}U_{\text{pot}} < 0. \quad (3.28)$$

For $\gamma = 5/3$, we obtain back our old result for an ideal gas. A star with $\gamma = 4/3$ has zero energy and marks the border of matter that can become gravitationally bound: Adding an

arbitrary small amount of energy would disrupt such a star, while subtraction would lead to its collapse. Important examples for matter with $\gamma = 4/3$ are all free relativistic particles, i.e. not only photons but also relativistic electrons and nucleons.

Stars with $\gamma > 4/3$, or more generally all gravitationally bound systems, have surprising thermodynamic properties: Consider e.g. the heat capacity of such a system using for concreteness the EoS of an ideal gas, $C_V = \partial U_{\text{tot}}/\partial T = (4 - 3\gamma)\partial U_{\text{kin}}/\partial T = -\partial U_{\text{kin}}/\partial T = -\frac{3}{2}Nk$: Losing energy, the star becomes hotter.

Since $U_{\text{pot}} = -\alpha GM^2/R$, a contracting star becomes hotter.

3.3. Energy transport

We can distinguish three different mechanisms for the transport of energy: i) radiative energy transfer, i.e. energy transport by photons, ii) conduction, i.e. the transport of heat by the Brownian motion of electrons or atoms, and iii) convection, i.e. macroscopic matter flows. Conduction plays a prominent role as energy transport only for dense systems, and is therefore only relevant in the dense, final stages of stellar evolution.

Radiative energy transport For the energy flux \mathcal{F} emitted per area and time by an layer of the star at radius r and temperature T , a transport equation similar to Eq. (2.20) for the intensity I holds,

$$d\mathcal{F} = -\sigma n\mathcal{F}dr = -\kappa\rho\mathcal{F}dr. \quad (3.29)$$

Here we introduced also the opacity $\kappa = \sigma/m$ being the cross section per mass of a certain material. Absorption of radiation leads also to a transfer of momentum to the medium. Since the momentum of photons is $p = E/c$ and $\mathcal{F} = E/(At)$, a slab of matter absorbs the momentum \mathcal{F}/c per area and time. According to Newton's second law, $F = dp/dt$, the momentum change has to be equal to the net force applied to the layer. This force is simply the difference in radiation pressure dP_{rad} times the area. Thus

$$\frac{1}{c} d\mathcal{F} = \frac{dp}{dA dt} = dP_{\text{rad}} \quad (3.30)$$

and

$$\mathcal{F} = -\frac{1}{\kappa\rho} \frac{d\mathcal{F}}{dr} = -\frac{c}{\kappa\rho} \frac{dP_{\text{rad}}}{dr}. \quad (3.31)$$

The pressure of radiation is $P_{\text{rad}} = aT^4/3$ and hence we can connect the energy flux \mathcal{F} , the interaction probability $\kappa\rho dr$ and the resulting temperature gradient dT/dr as

$$\mathcal{F} = -\frac{c}{3\kappa\rho} \frac{d(aT^4)}{dr} = -\frac{4acT^3}{3\kappa\rho} \frac{dT}{dr}. \quad (3.32)$$

Comparing this equation to Fick's law (2.38), we see the similarity to usual diffusion: A temperature gradient leads to an energy flux towards cooler regions.

This elegant derivation given originally by Eddington hides one complication: The interaction rate of matter with photons and thus the opacity depends on the photon frequency. Hence Eq. (3.31) should be written in differential form,

$$\mathcal{F}_\nu = -\frac{c}{\kappa_\nu\rho} \frac{dP_{\text{rad},\nu}}{dr}. \quad (3.33)$$

If we now require that integrating this equation reproduces Eq. (3.31),

$$\mathcal{F} = \int_0^\infty d\nu \mathcal{F}_\nu = -\frac{c}{\rho} \int_0^\infty d\nu \frac{1}{\kappa_\nu} \frac{dP_{\text{rad},\nu}}{dr} \stackrel{!}{=} -\frac{c}{\langle \kappa \rangle \rho} \frac{dP_{\text{rad}}}{dr}, \quad (3.34)$$

then we can use this relation as definition for the average opacity $\langle \kappa \rangle$,

$$\frac{1}{\langle \kappa \rangle} = \frac{\int d\nu \frac{1}{\kappa_\nu} \frac{dP_{\text{rad},\nu}}{dr}}{\int d\nu \frac{dP_{\text{rad},\nu}}{dr}}. \quad (3.35)$$

Since $P_{\text{rad},\nu} = 4\pi/(3c)B_\nu$, cf. with Eqs. (2.73) and (2.8), it its

$$\frac{dP_{\text{rad},\nu}}{dr} = \frac{4\pi}{3c} \frac{\partial B_\nu}{\partial T} \frac{dT}{dr} \quad (3.36)$$

where we used also the chain rule. Thus we can rewrite the average (3.35) as

$$\frac{1}{\langle \kappa \rangle} = \frac{\int d\nu \frac{1}{\kappa_\nu} \frac{\partial B_\nu}{\partial T}}{\int d\nu \frac{\partial B_\nu}{\partial T}}, \quad (3.37)$$

where the temperature gradients canceled. The average opacity $\langle \kappa \rangle$ defined by Eq. (3.37) is called the Rosseland mean opacity, after Svein Rosseland who introduced it in 1925.

Finally, we can connect the luminosity $L(r)$ of a shell at radius r and temperature T with the temperature gradient dT/dr as

$$\boxed{L(r) = 4\pi r^2 \mathcal{F}(r) = -\frac{16\pi r^2}{3\langle \kappa \rangle \rho} acT^3 \frac{dT}{dr}}. \quad (3.38)$$

Convection Convection is a cyclic mass motion carrying energy outwards, if the temperature gradient becomes too large (or $L > L_{\text{Edd}}$ as discussed later) – a phenomenon familiar to everybody from water close to the boiling point. In the shadowed regions of Fig. 3.1 convection is important for Main Sequence stars of various masses. In the case of the Sun, convection takes places in its outer layer, $M(r) > 0.98M_\odot$.

We want to set up a simple criterion when convection sets in. To do so we ask what happens to a small volume element of gas with initial parameters T, P and ρ , if it moves outward to a new position with the parameters $T + dT, P + dP$ and $\rho + d\rho$, cf. Fig. 3.2. The gas bubble will expand until it reaches the same pressure as the environment, thereby changing its temperature to $T + \delta T$ and its density to $\rho + \delta\rho$. The fate of the bubble depends on its new density $\rho + \delta\rho$: If the density of the bubble decreases faster than the unperturbed density of the star, $\delta\rho < d\rho$ (< 0), it will continue to move upward and turbulent motion will set in. Hence we use as criterion for the absence of convection

$$\frac{\delta\rho}{\rho} > \frac{d\rho}{\rho}. \quad (3.39)$$

Remark 3.0: In the case of power-law dependencies, it is often convinient to consider logarithmic derivatives $df/f = d(\ln(f))$: If, e.g., $f = ab^\gamma$, with γ a constant, then $df/f = da/a + \gamma db/b$.

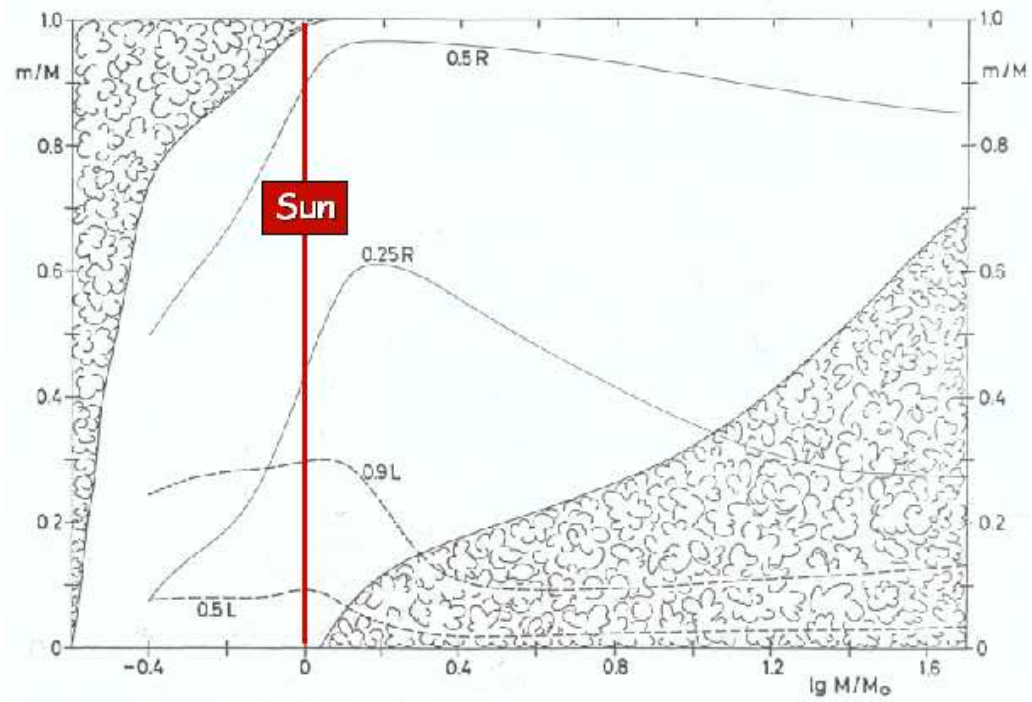


Figure 3.1.: In the shadowed regions convection is important for Main Sequence stars, the x axis labels the total mass of the stars, $x = \log(M/M_\odot)$, while the y axis labels the position in the star, $y = M(r)/M$.

We evaluate the RHS taking the logarithmic derivative of the ideal gas law, $\rho \propto P/T$, or

$$\frac{d\rho}{\rho} = \frac{dP}{P} - \frac{dT}{T}. \quad (3.40)$$

For the LHS, we assume that the bubble expands adiabatically. Taking the logarithmic derivative of $P = K\rho^\gamma$, we find

$$\frac{\delta\rho}{\rho} = \frac{1}{\gamma} \frac{\delta P}{P}. \quad (3.41)$$

Combining the two expressions and using $\delta P = dP$, we obtain

$$\frac{dT}{T} > \left(1 - \frac{1}{\gamma}\right) \frac{dP}{P}. \quad (3.42)$$

We can rewrite this as an condition on the temperature and pressure gradients,

$$\frac{dT}{dr} > \frac{\gamma - 1}{\gamma} \frac{T}{P} \frac{dP}{dr}, \quad (3.43)$$

for the absence of convection. Since both gradients are negative, it is less confusing to use absolute values and to revert the inequality sign,

$$\left| \frac{dT}{dr} \right| < \frac{\gamma - 1}{\gamma} \frac{T}{P} \left| \frac{dP}{dr} \right|. \quad (3.44)$$

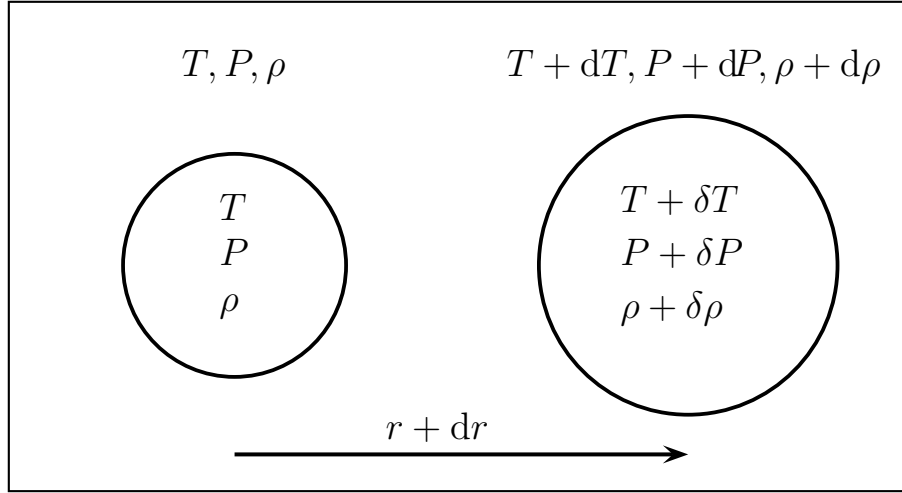


Figure 3.2.: A gas bubble displaced by the distance dr will adjust its internal properties from T, P, ρ to $T + \delta T, P + \delta P, \rho + \delta \rho$, while the star changes to $T + dT, P + dP, \rho + d\rho$.

In this form, the condition for convection is called the Schwarzschild criterion.

Convection happens in stars for two reasons: First, for a given energy flux \mathcal{F} the temperature gradient $|dT/dr|$ due to radiation can become too large, if the opacity κ is too large. Since the opacity increases with decreasing temperature (down to $\simeq 10^4$ K), the outer cool layer of stars like the Sun are convective. Second, the energy flux $\mathcal{F} \propto L(r)/r^2$ of luminous stars can become close to the center too large. Both effects are visible in Fig. 3.1 where the convective region in the outer part of low-mass stars and in the inner part of high-mass stars is visible.

How does one determine the actual temperature gradient dT/dr , if convection sets in a certain layer of a star? Since convection transports energy very effectively, it is a good approximation to assume that convection drives the temperature gradient close to the value given using an equality in the Schwarzschild criterion, Eq. (3.44). For an ideal gas, $\gamma = 5/3$, this implies that $dT/dr \simeq 2/5 T/P dP/dr$ should be used in Eq. (3.38).

Convection corresponds to an adiabatic transport of energy. We expect therefore that a fully convective star can be approximated by a polytrope. Rewriting Eq. (3.42) as

$$d \ln T \simeq \left(1 - \frac{1}{\gamma}\right) d \ln P \simeq \frac{2}{5} d \ln P \quad (3.45)$$

we see that the temperature varies as $T \propto P^{2/5}$ through the star. For an ideal gas with homogeneous composition, $\mu = \text{const.}$, it is $T \propto P/\rho$. Since the pressure is dominated by radiation, $P \propto T^4$ and thus $P \propto \rho^{4/3}$. Thus a fully convective star can be approximated as a polytrope with polytropic index $n = 3$.

3.4. Thermal equilibrium and energy conservation

Local thermal equilibrium and energy conservation require that the energy density ε produced per time and mass by all possible processes corresponds to an increase of the luminosity L ,

$$\boxed{\frac{dL}{dr} = 4\pi r^2 \varepsilon \rho}. \quad (3.46)$$

The energy production rate per time and mass unit, $\varepsilon = dE/(dtdm)$, consists of three terms,

$$\varepsilon = \varepsilon_{\text{grav}} + \varepsilon_{\text{nuc}} - \varepsilon_{\nu}, \quad (3.47)$$

where ε_{nuc} accounts for the energy production by nuclear processes and ε_{ν} for the energy carried away by neutrinos. Both effects will be discussed in the next chapter in more detail. The term $\varepsilon_{\text{grav}}$ is the only one that can be both positive (contraction) or negative (expansion of the star) and is therefore crucial for the stability of a star.

3.5. Time scales

Characteristic time-scales We have assumed that the stellar structure equations allow for static solutions. In order to understand the limitations of this assumption, we can consider characteristic time-scales for changes in a star, if external parameters are changed. We can estimate the characteristic time-scale τ for the change \dot{f} of the quantity f calculating $\tau^{-1} = \dot{f}/f$.

We can estimate the dynamical time-scale, i.e. the typical time for changes induced if the equilibrium between gravitational force and pressure is changed, by the time-scale of gravitational collapse (or free-fall) of a star: Using $R \sim 1/2gt^2$ and $g = GM/R^2$ it follows $\tau_{\text{ff}} \sim 1/\sqrt{G\rho}$. Numerically,

$$\tau_{\text{ff}} \approx 10^3 \text{ s} \left(\frac{R}{R_{\odot}} \right)^{3/2} \left(\frac{M}{M} \right)^{1/2} \quad (3.48)$$

This is a very short time-scale. If a star cannot restore dynamical equilibrium, the process should be visible as the collapse or explosion of the star; in particular, these time-scale should characterize supernova explosions.

The thermal time-scale is the typical time for changes in the internal energy due to the emission of radiation. Using the virial theorem, $U \approx GM^2/R$ and setting $\dot{U} \approx L$, it is $\tau_{\text{th}} = U/L \approx GM^2/(RL)$, Numerically,

$$\tau_{\text{th}} \approx 10^{15} \text{ s} \left(\frac{R_{\odot}}{R} \right) \left(\frac{L_{\odot}}{L} \right) \left(\frac{M}{M_{\odot}} \right)^2. \quad (3.49)$$

Although much larger than the dynamical time-scale, it is still small compared to the life-time of a star. If a stars evolves keeping hydrostatic and thermal equilibrium, its total energy is conserved. The virial theorem implies that the thermal and potential energy are separately conserved. Thus if, e.g., the center of a star contracts, the envelope has to expand to keep the potential energy constant.

Finally, we consider the nuclear (or in general energy production) time-scale. If processes convert the fraction f of the rest energy Mc^2 into energy, then $\tau_{\text{en}} = fMc^2/L$, Numerically,

$$\tau_{\text{en}} \approx 5 \times 10^{20} \text{ s } f \left(\frac{L_{\odot}}{L} \right) \left(\frac{M}{M_{\odot}} \right) \quad (3.50)$$

For nuclear processes, $f \sim 20 \text{ MeV}/4 \text{ GeV} \simeq 5 \times 10^{-3}$. Thus nuclear processes can supply the energy output of stars, even if only a fraction of material participates in the fusion process. In contrast, chemical processes release typically only tens of eV, are thus a factor 10^{-6} less effective.

4. Stellar models

4.1. Hertzsprung-Russel diagram

Between 1905 and 1913, Hertzsprung and Russel examined the distribution of stellar luminosities for different spectral classes. The latter quantity characterizes the surface temperature T , and since the luminosity is proportional to T^4 and the stellar surface $\propto R^2$, one expects a wide distribution in this diagram. As shown in Fig. 4.1, this is not the case and stars appear only in well-defined regions of the Hertzsprung-Russel (HR) diagram. Thus arbitrary combinations of T and L , and thus of R and L are not allowed.

Most stars are found in a narrow band from the left-upper to the right-lower corner, the so-called main sequence. Stars of the main sequence of the same temperature have approximately the same luminosity and thus also radius. This correlation has to be explained by any theory of stellar astrophysics. Moreover, the mass range of stars covers only approximately three orders of magnitude, much smaller than the mass range of gas clouds which might potentially collapse to proto-stars.

Apart from the main sequence, there are two other star populations. Above the main sequence, there are the giant and super giant stars: They are more luminous for the same temperature as main sequence stars, hence their radius has to be larger. Much below the main sequence stars (10 magnitudes fainter) and with roughly white spectral color, there are the so called white dwarf stars.

4.2. Eddington luminosity and convective instability

Our first aim in this section is to derive an upper limit on the luminosity of any stable object. We divide first Eqs. (3.31) and (3.7) and obtain

$$\frac{dP_{\text{rad}}}{dP} = \frac{\kappa L(r)}{4\pi cGM(r)}. \quad (4.1)$$

Since the total pressure P is the sum of radiation and gas pressure, $P = P_{\text{rad}} + P_{\text{gas}}$, and both decrease outwards, it follows that dP_{rad} and dP_{gas} have the same sign. Hence, $dP_{\text{rad}} < dP$ and

$$L(r) < \frac{4\pi cGM(r)}{\kappa}. \quad (4.2)$$

This bound relies on Eq. (3.31), i.e. it assumes that the energy is transported only by radiation, and is therefore not valid in zones of the star with convection. However, for $r = R$, energy transport should be purely radiative if the star is stable. As noted by Eddington, Eq. (4.2) represents therefore a critical luminosity,

$$L < L_{\text{Edd}} = \frac{4\pi cGM}{\kappa} = 3.2 \times 10^4 \frac{M}{M_{\odot}} \frac{\kappa_{\text{es}}}{\kappa} L_{\odot}. \quad (4.3)$$

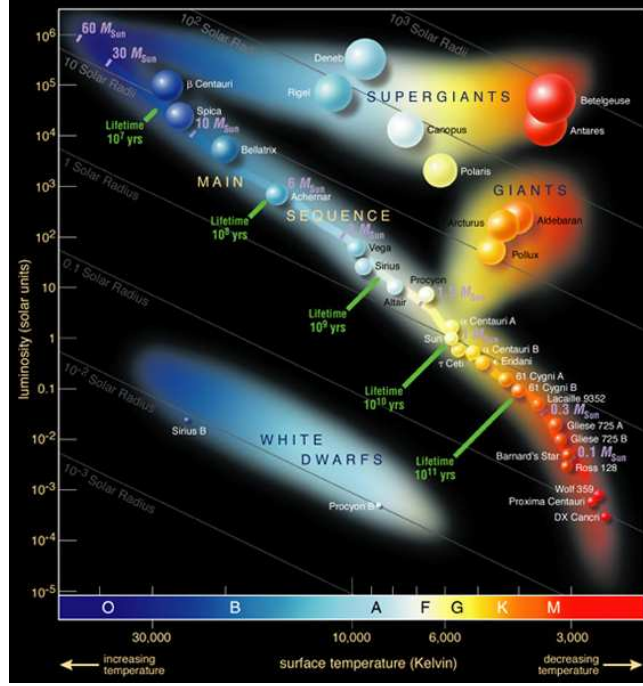


Figure 4.1.: A Hertzsprung-Russell diagram. The position of a star along the main-sequence defines uniquely all important stellar parameters: Mass, radius, temperature, lifetime.

If this luminosity is exceeded, the star ejects its outer layers in a stellar wind. To obtain the numerical estimate, we inserted the opacity κ_{es} for Thomson scattering on free electrons in the last step.

Next we consider what happens if for $r < R$ the condition (4.2) is violated. We rewrite first the energy transport equation as equation for dP_{rad}/dr ,

$$\frac{dP_{\text{rad}}}{dr} = -\frac{\kappa\rho}{c} \frac{L(r)}{4\pi r^2}. \quad (4.4)$$

Then we solve the hydrostatic equilibrium equation,

$$\frac{dP}{dr} = -\frac{GM(r)\rho}{r^2}, \quad (4.5)$$

with $P = P_{\text{gas}} + P_{\text{rad}}$ for dP_{gas}/dr ,

$$\frac{dP_{\text{gas}}}{dr} = \frac{dP}{dr} - \frac{dP_{\text{rad}}}{dr} = -\frac{GM(r)\rho}{r^2} + \frac{\kappa\rho}{c} \frac{L(r)}{4\pi r^2} = -\frac{GM(r)\rho}{r^2} \left(1 - \frac{\kappa L(r)}{4\pi c GM(r)}\right). \quad (4.6)$$

Thus for $L > L_{\text{Ed}}$, the expression in the parenthesis changes sign and the gas pressure increases outwards: The stratification of the gas layers becomes unstable and convection starts.

4.3. Eddington or standard model

An important test for any model for stellar structure consists in deriving the mass-luminosity relation it predicts and comparing it to observations. Apart from solving numerically realistic

stellar models, one can gain some insight solving simplified analytical models. Historically important models are stellar models described by a polytropic equation of state that lead to the Lane-Emden equation. These are still useful approximations for white dwarf stars and main-sequence stars with a large convective zone.

Let us define

$$\eta(r) \frac{L}{M} = \frac{L(r)}{M(r)} \quad (4.7)$$

and insert it into Eq. (4.1),

$$\frac{dP_{\text{rad}}}{dP} = \frac{\kappa\eta}{4\pi cG} \frac{L}{M}. \quad (4.8)$$

At the surface, $\eta = 1$ by definition. In general, κ increases for small r , while η decreases ($L(r) \approx \text{const.}$ and $M(r) \rightarrow 0$ for $r \rightarrow 0$). To proceed, Eddington made the assumption that the product $\kappa\eta$ is approximately independent from the radius r , $\kappa\eta \equiv \kappa_s = \text{const.}$ Then we can integrate Eq. (4.8) immediately,

$$P_{\text{rad}} = \frac{\kappa_s L}{4\pi cGM} P. \quad (4.9)$$

Defining β as the fraction the gas contributes to the total pressure, $P_{\text{rad}} = (1 - \beta)P$ and $P_{\text{gas}} = \beta P$, we have

$$\frac{P_{\text{rad}}}{1 - \beta} = P = \frac{P_{\text{gas}}}{\beta}. \quad (4.10)$$

Assuming an ideal gas law, $P_{\text{gas}} = \mathcal{R}\rho T/\mu$, and inserting $P_{\text{rad}} = aT^4/3$, we have

$$\frac{aT^4}{3(1 - \beta)} = \frac{\mathcal{R}}{\beta\mu} \rho T. \quad (4.11)$$

Now we can express the temperature as function of the density,

$$T = \left(\frac{3\mathcal{R}(1 - \beta)}{a\beta\mu} \right)^{1/3} \rho^{1/3}. \quad (4.12)$$

The total equation of state, $P = P_{\text{gas}}/\beta = (\mathcal{R}\rho/\beta\mu)T$, is therefore

$$P = \underbrace{\left(\frac{3\mathcal{R}^4(1 - \beta)}{a\beta^4\mu^4} \right)^{1/3}}_K \rho^{4/3}, \quad (4.13)$$

where the factor K is independent of the radius r . Thus the Eddington approximation leads to a polytrope with index $\gamma = 4/3$ or $n = 3$. We have already seen that main-sequence stars whose energy is transported by convection can be approximated by such a polytrope. In the next section, we will discuss therefore polytropes for general n .

Lane-Emden equation For a polytrope, the continuity and the hydrostatic equation decouple from the other equations of stellar structure. We want to combine now these two first order differential equation into one of second order. Thus we multiply the hydrostatic equation by r^2/ρ and differentiate it then with respect to r ,

$$\frac{d}{dr} \left(\frac{r^2}{\rho} \frac{dP}{dr} \right) = -G \frac{dM(r)}{dr} = -4\pi Gr^2 \rho(r), \quad (4.14)$$

where we inserted the continuity equation in the last step. Using also the equation of state with $P = K\rho^\gamma$, we obtain

$$\frac{(n+1)}{n} \frac{K}{4\pi G r^2} \frac{d}{dr} \left(\frac{r^2}{\rho^{\frac{n-1}{n}}} \frac{d\rho}{dr} \right) = -\rho(r). \quad (4.15)$$

In order to solve this equation, we need two boundary conditions: One of them, $\rho(R) = 0$, is obvious, another one, $d\rho/dr(r=0) = 0$, follows from $dP/dr(0) = 0$. It is convenient to go over to a new dimensionless variable $\vartheta \in [0 : 1]$ defining $\rho = \rho_c \vartheta^n$ with ρ_c as central density. Then

$$\underbrace{\frac{(n+1)K}{4\pi G \rho_c^{\frac{n-1}{n}}}}_{\alpha^2} \frac{1}{r^2} \frac{d}{dr} \left(r^2 \frac{d\vartheta}{dr} \right) = -\vartheta^n. \quad (4.16)$$

Since ϑ is dimensionless, the parameter α has the dimension of a length. Hence we can use α to make the variable r dimensionless, $r = \alpha\xi$, obtaining finally

$$\frac{1}{\xi^2} \frac{d}{d\xi} \left(\xi^2 \frac{d\vartheta}{d\xi} \right) = -\vartheta^n. \quad (4.17)$$

This second order differential equation was studied already a century ago by Lane and Emden. The boundary conditions are now $\vartheta(0) = 1$ such that at the centre $\xi = 0$ of the star $\rho(0) = \rho_c$ is satisfied. Moreover, $dP/dr(0) = 0$ implies $d\vartheta/d\xi(0) = 0$.

Apart from the cases $n = 0, 1, 5$, and ∞ , the Lane-Emden equation has to be solved numerically. For $n < 5$, the solutions $\vartheta(\xi)$ decrease monotonically and become zero at a finite value $\vartheta(\xi_0) = 0$, corresponding to the stellar radius $R = \alpha\xi_0 = \alpha R_n$. The smaller n , the more concentrated is the mass at the center, cf. Fig. 4.2. For $n \geq 5$, the solutions $\vartheta(\xi)$ have no zero and cannot represent a star.

Mass-radius relation All physical quantities characterising a polytrope are determined by ρ_c , n and K . Similar to the radius $R = \alpha R_n$, they can be expressed by numerical constants obtained by solving the Lane-Emden equation. For the particular case of the mass of a polytrope, we express first ρ by ϑ ,

$$M = 4\pi \int_0^R dr r^2 \rho = 4\pi \alpha^3 \rho_c \int_0^{\xi_0} d\xi \xi^2 \vartheta^n. \quad (4.18)$$

Then we replace ϑ^n using the Lane-Emden equation,

$$M = -4\pi \alpha^3 \rho_c \int_0^{\xi_0} d\xi \frac{d}{d\xi} \left(\xi^2 \frac{d\vartheta}{d\xi} \right) = -4\pi \alpha^3 \rho_c \xi_0^2 \left. \frac{d\vartheta}{d\xi} \right|_{\xi_0} \equiv 4\pi \alpha^3 \rho_c M_n. \quad (4.19)$$

In order to obtain a relation between the mass and the radius, we have to eliminate the variables α and ρ_c . We use first the definition of α to express ρ_c as

$$\rho_c = \left[\frac{(n+1)K}{4\pi G \alpha^2} \right]^{\frac{n}{n-1}} = \left[\frac{(n+1)K}{4\pi G} \right]^{\frac{n}{n-1}} \left(\frac{R_n}{R} \right)^{2n/(n-1)}. \quad (4.20)$$

Inserting the definition of α and ρ_c into (10.19), we find

$$\left(\frac{GM}{M_n} \right)^{n-1} \left(\frac{R}{R_n} \right)^{3-n} = \frac{[(n+1)K]^n}{4\pi G}. \quad (4.21)$$

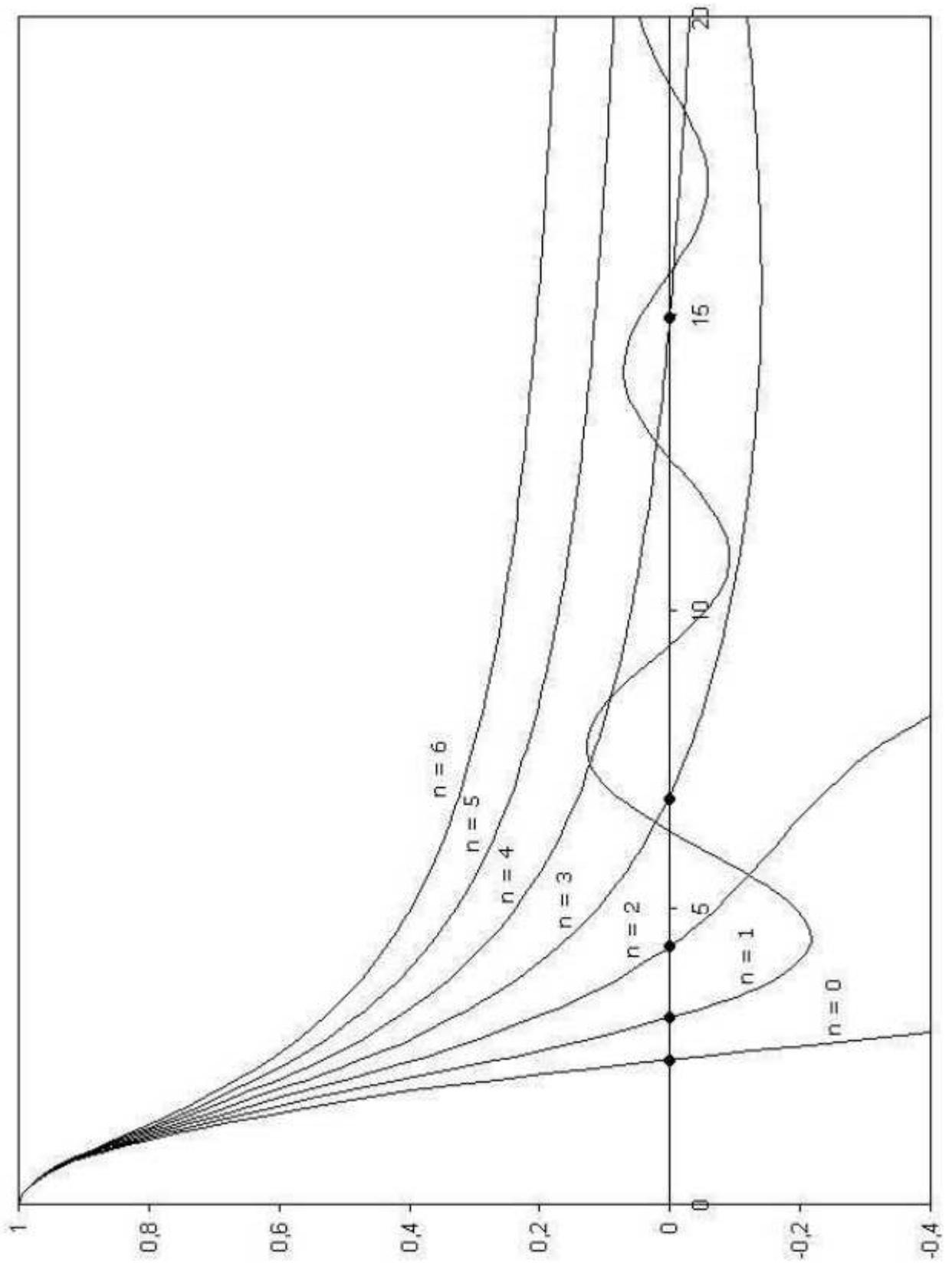


Figure 4.2.: Solutions of the Lane-Emden equation.



Figure 4.3.: Enclosed mass in the SSM (red), $n = 3$ polytrope (blue), and for a linear density law (black).

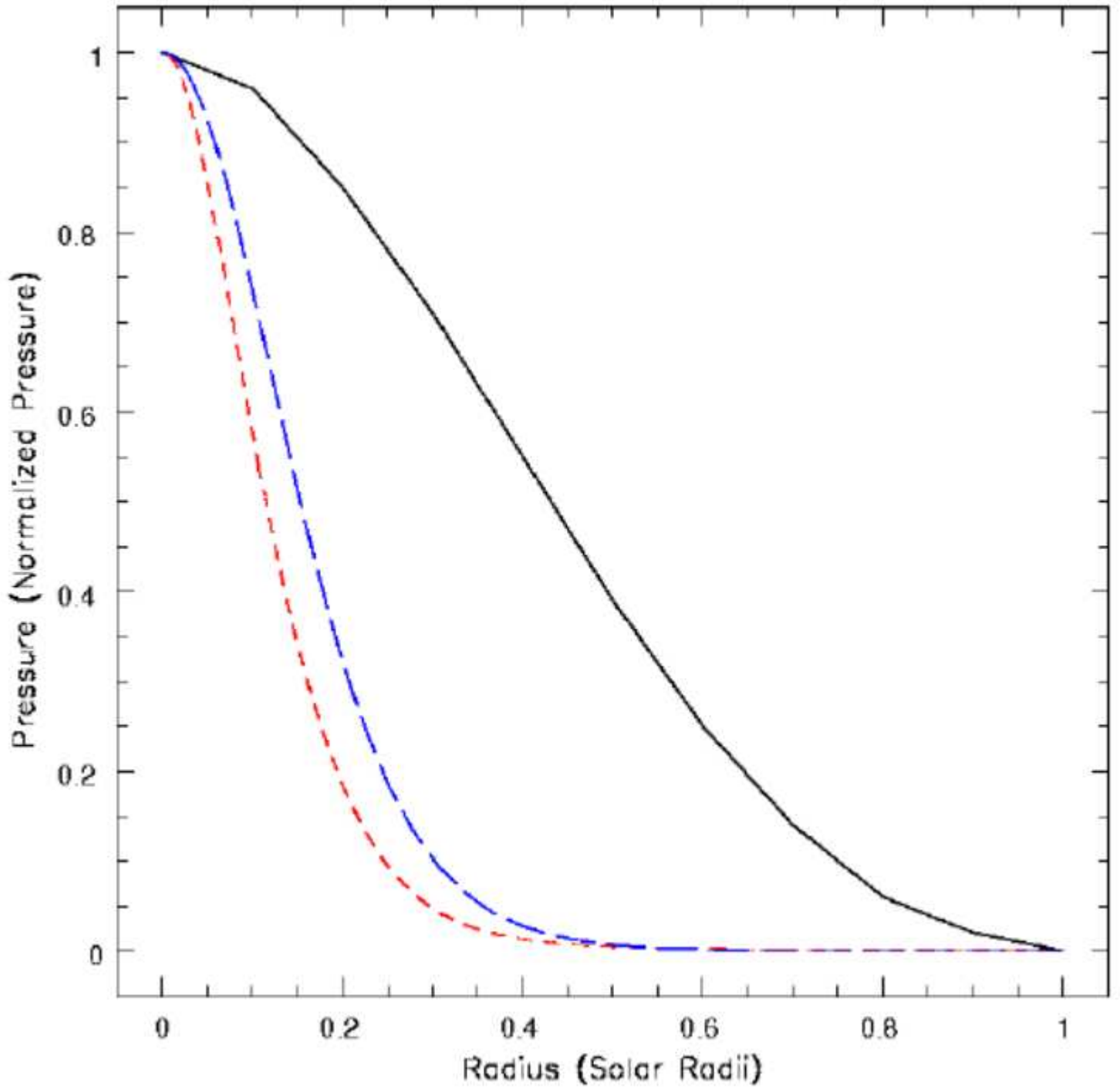


Figure 4.4.: Pressure in the SSM and $n = 3$ polytrope.

Table 4.1.: Numerical constants from the integration of the Lane-Emden equation.

n	$R_n = \xi_0$	$M_n = -\xi_0^2 (d\vartheta/d\xi)_{\xi_0}$	$D_n = \rho_c/\bar{\rho}$	B_n
1	3.14	3.14	3.29	0.233
1.5	3.65	2.71	6.00	0.206
2	4.35	2.41	11.4	0.185
2.5	5.36	2.19	23.4	0.170
3	6.90	2.02	54.2	0.157
3.5	9.54	1.89	153	0.145
4	15.0	1.80	622	
4.5	31.8	1.74	6189	
5	∞	1.73	∞	

For the case of interest, $n = 3$, the mass is independent of the radius and determined solely by the numerical value of K ,

$$M = 4\pi M_3 \left(\frac{K}{\pi G} \right)^{3/2}, \quad (4.22)$$

where $M_3 \simeq 2.02$. Inserting K from Eq. (4.13) for the Eddington model gives¹

$$M \propto \frac{(1 - \beta)^{1/2}}{\mu^2 \beta^2}. \quad (4.23)$$

Squaring and inserting the numerical values of the constants, we obtain ‘‘Eddington’s quartic equation’’,

$$1 - \beta = 0.003 \left(\frac{M}{M_\odot} \right)^2 \mu^4 \beta^4. \quad (4.24)$$

Its solution is shown in Fig. 4.5.

What can one learn about the structure and evolution of stars from this result?

- Remembering the meaning of $\beta = P_{\text{gas}}/P$, we recognize that the limit $\beta \rightarrow 0$ leads to a free gas of photons, while $\beta \rightarrow 1$ corresponds to a ‘‘primordial’’, cold cloud of gas. Stars exist only in the small range of $\mu^2 M$ where β has an intermediate value.
- Inserting

$$L = \frac{4\pi cGM}{\kappa_s} (1 - \beta) \quad (4.25)$$

into Eq. (4.24), we obtain

$$\frac{L}{L_\odot} = \frac{4\pi cGM_\odot}{\kappa_s L_\odot} \mu^4 \beta^4 \left(\frac{M}{M_\odot} \right)^3, \quad (4.26)$$

close to a power-law with exponent 3 and observations of main-sequence stars!

- The variation in μ can explain scatter in L - M plot.

¹In keeping β^4 on the RHS, we neglect a term $L/L_{\text{Edd}} \ll 1$.

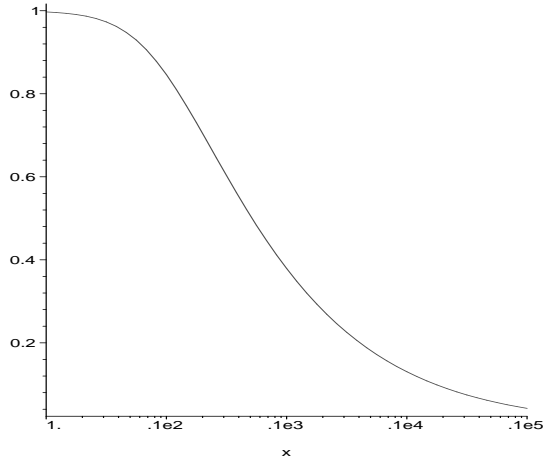


Figure 4.5.: The solution β of Eddington's quartic equation as function of $x = \mu^2 M / M_\odot$.

- For stars of given composition (fixed μ), β decreases as M increases. Thus, radiation pressure is more important in massive stars.
- Nuclear reaction cause a gradual increase of μ and therefore an decrease of β . Thus, radiation pressure becomes more important when stars become older. In late stages, stars may eject part of their envelope (stellar winds).

Example 4.1: Express the central pressure as function of the central density and the stellar mass:

Solving the mass-radius relation for K and inserting it into $P_c = K \rho_c^{1+1/n}$ gives

$$P_c = \frac{(4\pi G)^{1/n}}{n+1} \left(\frac{GM}{M_n} \right)^{\frac{n-1}{n}} \left(\frac{R}{R_n} \right)^{\frac{3-n}{n}} \rho_c^{\frac{n+1}{n}}. \quad (4.27)$$

We have still to express R/R_n as function of M and R ,

$$\rho_c = \frac{M}{\frac{4\pi}{3} R^3} \frac{\xi_0^3}{3M_n} \equiv \bar{\rho} D_n. \quad (4.28)$$

In the last step, we inserted the average density $\bar{\rho}$ and defined also

$$D_n = \frac{\rho_c}{\bar{\rho}} = \frac{\xi_0^3}{3M_n} = - \left[\frac{3}{\xi_0} \frac{d\vartheta}{d\xi} \Big|_{\xi_0} \right]^{-1}. \quad (4.29)$$

Combining everything, it follows

$$P_c = (4\pi)^{1/3} B_n G M^{2/3} \rho_c^{4/3} \quad (4.30)$$

where B_n is a numerical factor. Note that the relation $P_c \propto \rho_c^{4/3}$ is independent of the polytropic index n . Moreover, the factor B_n varies only slowly with n , cf. with table 4.1, making this relation almost universal.

Chandrasekhar mass Another application of the mass-radius relation for $n = 3$ are stars where the pressure is dominated by relativistic fermions. In this case, K from Eq. (2.71) is determined solely by natural constants, the fermion mass m and the chemical composition, i.e. μ . Substituting K from Eq. (2.71) results in

$$M_{\text{Ch}} = 4\pi M_3 \left(\frac{K}{\pi G} \right)^{3/2} = \frac{\sqrt{1.5} M_3}{4\pi} \left(\frac{hc}{G m_p^{4/3}} \right)^{3/2} \frac{1}{\mu_e^2} \simeq 5.83 \mu_e^{-2} M_\odot \quad (4.31)$$

4.4. Main sequence

We sketch how one can use dimensional analysis to learn something about the stellar structure equations without actually solving them. First, we introduce the dimensionless variable $x = M(r)/M$, and replace then the functions $f(M(r))$ by dimensionless functions $f(x)$ of x , defining

$$r = f_1(x) R_*, \quad P = f_2(x) P_*, \dots \quad (4.32)$$

Thus the starred quantities, R_*, P_*, \dots , carry the dimension of the original functions. We only consider the hydrostatic equilibrium equation as an example for this procedure: Introducing x and P_* leads to

$$\frac{P_*}{M} \frac{df_2}{dx} = - \frac{GMx}{4\pi f_1^4 R_*^4}. \quad (4.33)$$

The unknown P_* has to be proportional to GM^2/R_*^4 . Choosing the proportionality constant as one, we obtain

$$\frac{df_2}{dx} = - \frac{x}{4\pi f_1^4}, \quad P_* = GM^2/R_*^4 \quad (4.34)$$

and similar for f_2, \dots, f_5 . We have now separated the problem into a set of dimensionless nonlinear differential equations defined on $0 < x < 1$, which are independent of M , and a set of algebraic equations depending on the stellar mass M . The important conclusion is that the profile of all physical quantities as function of x is the same for any value of M , differing only by constant factors. Solving then the algebraic equations involving the starred quantities, we can obtain how physical quantities depend on the stellar mass M . Using $P_* = GM^2/R_*^4$ and $\rho_* = M/R_*^3$ in $T_* = \mu P_*/(\mathcal{R}\rho_*)$, it follows

$$T_* = \frac{\mu GM}{\mathcal{R} R_*} \quad (4.35)$$

and finally

$$L_* \propto M^3. \quad (4.36)$$

Thus the luminosity at a given x in stars with the different mass scales as the cube of their mass ratios. In particular, for $x = 1$, we obtain $L \propto M^3$.

Similar relations can be obtained for the radius and the density. In particular, one can derive the slope of the MS as

$$\log L = 5.6 \log T_{\text{eff}} + \text{const.} \quad (4.37)$$

for $n = 4$ (pp chain) and

$$\log L = 8.4 \log T_{\text{eff}} + \text{const.} \quad (4.38)$$

for $n = 16$ (CNO cycle).

4.5. Realistic models

Summary of equations The equations describing a spherical star in equilibrium consists of the four first-order differential equations, 10.25,3.7, 3.38 3.46,

$$\frac{dM(r)}{dr} = 4\pi r^2 \rho(r), \quad \frac{dP}{dr} = -\frac{GM(r)\rho(r)}{r^2}, \quad (4.39a)$$

$$\frac{dT}{dr} = -\frac{3L(r)\langle\kappa\rangle\rho}{16\pi r^2 acT^3}, \quad \frac{dL}{dr} = 4\pi r^2 \varepsilon\rho. \quad (4.39b)$$

In the case of convection, the temperature gradient has to be replaced by the limiting value of the Schwarzschild criteria. Moreover, these equations contain three “material functions” which have to be known as external input: the equation of state $P = P(T, \rho, Y_i)$, the opacity $\kappa = \kappa(T, \rho, Y_i)$ and the nuclear energy production rate $\varepsilon_{\text{nuc}}(T, \rho, Y_i)$. In addition, the initial nuclear composition of a star has to be specified.

These equations describe a star for a given chemical composition at a given time. Nuclear reactions will change the composition, causing thereby the solution of the star.

For any realistic composition of a star, these quantities are complicated functions of the parameters T, ρ, Y_i , preventing thereby analytical solutions except for the simplest toy models. Thus one has to rely on numerical solutions.

Numerical methods Thus we have four (non-linear) first-order differential equations for the four functions r, P, T and L_r seen as functions of $M(r)$. In order to specify completely the solution, we have to add four boundary conditions. The natural choice of boundary conditions for these equations are a mixture of conditions at the center and the outer layer of the star: At the center of the star, the boundary conditions $r = M(0) = L(r) = 0$ have to be imposed, while the central values of the temperature and pressure have to be determined. The two boundary conditions at the surface are more complicated²: One can use the Stefan-Boltzmann law to fix $L(R)$ and set $P(R) = 0$.

The equations of stellar structure were first solved using a computer in 1956. Such a set of coupled differential equations with boundary conditions both at the center and the surface of the star can be solved by a trial-and-error method: Starting with an initial guess for the derivatives $df/dr(0)$ and $df/dr(R)$, one integrates the equations both from $r = R$ inside and from $r = 0$ outside. As initial guess one can use e.g. analytical solutions to the Lane-Emden equation. In general, the two trial solutions will not meet, but the mismatch can be used to improve the initial guess for the derivatives $df/dr(0)$ and $df/dr(R)$. In an iterative process, one can thus obtain an arbitrary precise solution. The most commonly used method, a specific application of the relaxation method, to solve this two-boundary problem was suggested by Louis Henyey.

In these models one starts with an initial nuclear composition, evolves the model in time and updating the changes due to nuclear reactions.

Voigt-Russell theorem If a set of n first-order differential equations with n boundary conditions has a solution, it is a unique. Voigt and Russell conjectured that the same holds

²More accurately, the effective temperature and thus the luminosity via the Stefan-Boltzmann law is defined at the position of the photosphere $\tau = 2/3$. Therefore, one should integrate with $d\tau = -\kappa_R \rho dr$ the hydrostatic equilibrium equation $dP/d\tau = g/\kappa_R$ up to the position of the photosphere $\tau = 2/3$, obtaining there $P = 2g/3\langle\kappa\rangle$.

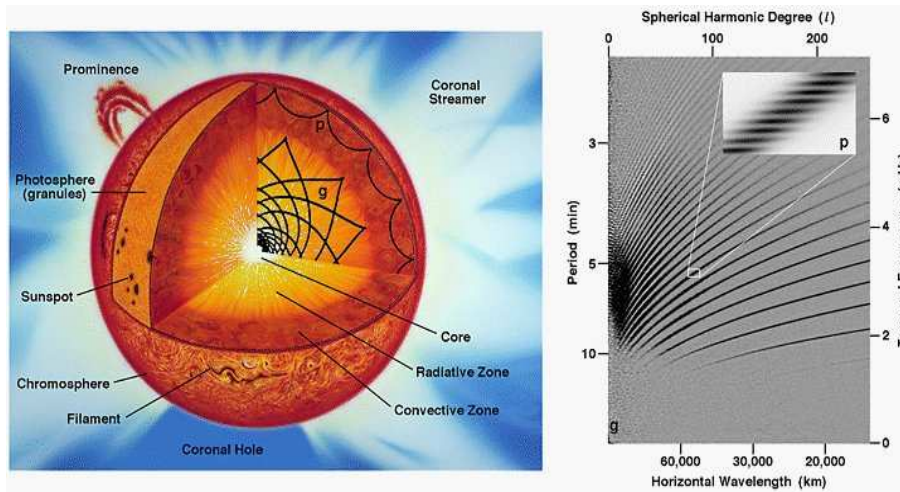


Figure 4.6.: Schematic picture of the Sun and different oscillation modes (left) together with the measured oscillation frequencies (right).

also for the stellar structure equations, i.e. that their solution for a given mass and chemical composition is unique. However, the full set of the stellar structure equations are the four differential equations supplemented by the three material equations. But the E.o.S. can be a multi-valued function: For instance, the source of pressure for a polytrope with $n = 3$ can be either radiation, leading to a MS star, the degeneracy of electrons (leading to WD) or of neutrons (leading to a NS). Thus the stellar structure equations are only locally unique.

Solar Standard model and helioseismology A “standard solar model” uses the i) conservation laws together with ii) an equation of state, iii) energy production by fusion processes and iv) energy transport equation to evolve the Sun in small time-step from some initial conditions to its age of 4.5×10^9 yr. (Age estimated from meteorites.) Agreement with present-day luminosity and radius is enforced by tuning unknown pre-solar helium abundance and a technical parameter determining convection.

The structural changes in the Sun, as it evolves, are caused by the nuclear reactions occurring in the central regions of the Sun. The transmutation of four hydrogen atoms into one helium reduces the number density of particles in the central regions which decreases the pressure. The pressure decrease does not actually occur because the surrounding layers respond to the force imbalance by contracting in the central regions. Half of the gravitational energy released from the contraction goes to raising the temperature of the central regions (the other half, according to the Virial Theorem, is radiated away). The increased temperature, by the ideal gas law, increases the pressure of this region and restores the balance between the pressure and gravitational forces. The larger mean molecular weight increases the luminosity of the star, and the rate of nuclear reactions. Also, while the central layers contract, the outer regions expand, in a sense, compensating for the steepening temperature gradients in the central regions. Therefore, as the Sun evolves from the zero age both its luminosity and radius increase.

The solar standard model can be tested by helioseismology: Inside the Sun, pressure waves with periods between 2 min and 1 h have been observed by Doppler shifts of spectral lines

4. Stellar models

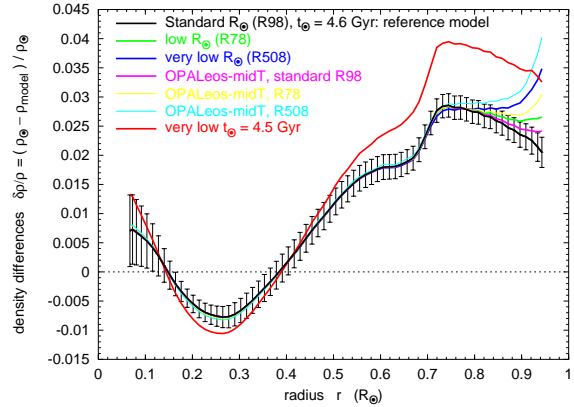
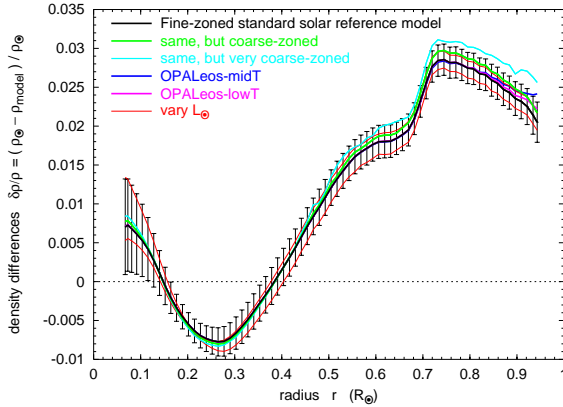


Figure 4.7.: Relative density difference between the solar standard model or its variations and the deduced values from helioseismology as function of the solar radius.

Figure 4.8.: Comparison of the enclosed mass $M(r)$ for the $n = 3$ and Solar Standard Model.

on the solar surface. (Amplitude is a few meters: solar surface rising and falling a few meters every few minutes!) The oscillation pattern depends on the sound speed in the solar interior and allows therefore to test predictions of the solar standard model in the interior.

4.6. Stability of stars

Stability conditions

Variable stars – Period-luminosity relation of Cepheids

Problems

4.1 *Schwarzschild vs. Eddington* Show that the condition $L > L_{\text{Edd}}$ agrees with the Schwarzschild criterion for $P_{\text{rad}}/P \rightarrow 1$.

can be expressed as $M_{\text{P1}}^3/m_N^2 = (M_{\text{P1}}/m_N)^2 m_N \simeq 30M_{\odot}$. Thus stars are massive, because the ratio $M_{\text{P1}} \gg m_N$ is large.

4.2 *Stellar mass* Show that the ratio $(K/G)^{3/2}$

5. Nuclear processes in stars

Eddington suggested first hydrogen-helium fusion in 1920 as the primary source of stellar energy. Quantum tunneling as a necessary ingredient was discovered by Hund in 1926, Fermi formulated the first theory of weak interactions in 1933.

Nuclear fusion The total mass $m(Z, N)$ of a nuclei with Z protons and N neutrons is because of its binding energy E_b somewhat reduced compared to its constituent mass,

$$E_b/c^2 = Zm_H + Nm_n - m(Z, N). \quad (5.1)$$

Measured values of the binding energy per nucleon E_b/A as function of nucleon number $A = Z + N$ are shown in Fig. 5.1. In Tab. 5.1, the masses of ${}^4\text{He}$ and its constituent nucleons are compared.

- The binding energy per nucleon E_b/A has its maximum at $A \sim 56$, i.e. iron ${}^{56}\text{Fe}$ is the most stable element.
- Energy can be released by fusing two light nuclei or 'breaking' a heavy one.
- While E_b/A is a rather smooth function of A for $A > 20$, there several peaks visible for small A : ${}^4\text{He}$, ${}^{12}\text{C}$, ${}^{14}\text{N}$, ${}^{20}\text{Ne}$, and ${}^{16}\text{O}$ are energetically much more favourable than their neighbouring elements. The bound states of nucleons in nuclei have a similar shell structure as electrons in atoms. Nuclei with filled shells are especially stable, as noble gases are especially stable atoms.
- constance of E_b/A for $A \gtrsim 50$ leads to liquid-drop model (Bethe-Weizsäcker),

$$E_b = aA - bA^{2/3} - E_C - E_{\text{sym}} \quad (5.2)$$

- Thus the fusion of four protons to ${}^4\text{He}$ releases 26.2 MeV energy, a factor 10^7 more than in our estimate for chemical reactions. Converting a solar mass into helium releases $M_\odot/(4m_p) \times 26.2 \text{ MeV} \approx 1.25 \times 10^{52} \text{ erg}$ and thus around 5% of the Sun have been already converted into helium.
- As shown by the failure of using fusion for the energy production on Earth and the longevity of stars fusion is a non-trivial process.

	n	p	2p+2n	${}^4\text{He}$
m/u	1.0090	1.0081	4.0342	4.0039

Table 5.1.: The masses of nucleons and ${}^4\text{He}$ in atomic mass units u.

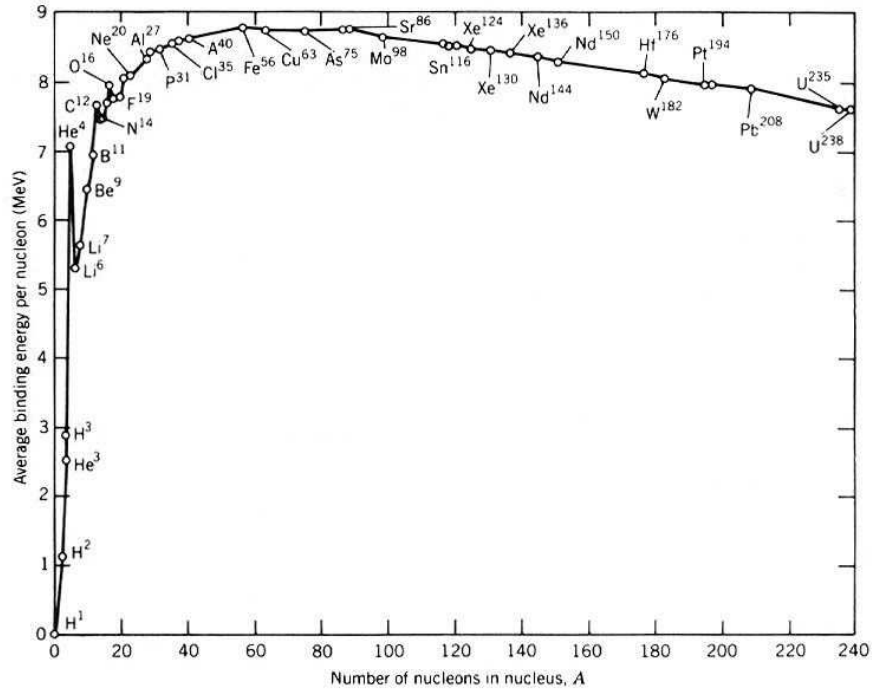


Figure 5.1.: The binding energy per nucleon E_b/A as function of the nucleon number A .

- All four interactions are involved in the energy release by nuclear fusion: The strong interaction leads to the binding of nucleons in nuclei, the Coulomb repulsion has to be overcome to combine them, and the weak interactions convert half of the protons into neutrons. Finally, gravitation is responsible for the confinement of matter, first heating up the proto-star to the required “start temperature” for fusion processes and serving then as a heat regulator.

5.1. *** Fundamental interactions ***

Bosons and forces We know four fundamental forces in nature, that are all transmitted by the exchange of bosons, i.e. particles with integer spin. Two of them are the gravitational and electromagnetic force we have already encountered. These two forces fall-off like $1/r^2$ and are important on macroscopic scales. By contrast, the weak and the strong force are exponentially suppressed beyond a distance which corresponds to the Compton wavelength $\lambda = h/(mc)$ of the particle that carries this force. A comparison of some properties of the four fundamental forces is given in Table 5.2.

A specific property of strong interactions is the confinement of the strong charge (“colour”): We do not observe the fundamental carriers of the strong force (massless “gluons”) but colourless bound-states (pions, kaons, ...). This force is somewhat similar to the van-der-Waals force between neutral atoms.

The first line shows the force law characterising the different interactions. The strength of an interactions depends both on how strong the charges or couplings are and how long its

interaction	gravitation	electromagnetic	weak	strong
force	$G_N m_p^2 / r^2$	e^2 / r^2	$G_F E^2 e^{-r/\lambda_W} / r^2$	$\alpha_s e^{-r\lambda_\pi} / r^2$
coupling	$G_N = (\hbar c) / M_{\text{Pl}}^2$	$\alpha_{\text{em}} = e^2 / (\hbar c) \approx 1/137$	$G_F = \sqrt{2} g^2 / (8 M_W^2)$	$\alpha_s = g_s^2 / (\hbar c) \approx 1$
range	∞	∞	$\lambda_W = \hbar / (M_W c)$	$\lambda_\pi = \hbar / (M_\pi c)$
particle	graviton	photon	W and Z-boson	pions
mass	0	0	80 and 91 GeV	140 MeV
cross section	$[E / (m_{\text{Pl}} c^2)]^2 \lambda_{\text{Pl}}^2$	$\alpha_{\text{em}}^2 \lambda_e^2$	$[E / (m_W c^2)] \lambda_W^2$	λ_π^2
decay process			$\mu^- \rightarrow e^+ + \bar{\nu}_e + \nu_\mu$	$\rho \rightarrow 2\pi$
decay time			$\tau \sim 10^{-6} \text{s}$	$\tau \sim 10^{-22} \text{s}$

Table 5.2.: Some properties of the four fundamental forces.

range λ of the exchange particles is. In a simple analogy, one can imagine the cross section for a specific reaction as a grey disc: Its area is given by $\pi\lambda^2$ and its greyness depends on the magnitude of the coupling constant. The typical size given in the sixth line should be considered as indicative.

Fermions and the family structure Fermions carry half-integer spin and obey the Pauli principle, a principle that is crucial for the stability of matter. Protons and neutrons differ from electrons and neutrinos in that they have also strong interactions.

The discovery of the muon happened accidentally in 1936-1937. The realization that it is an exact copy of an electron having only a different mass came as a real surprise. Nowadays we know that there exist three different “families” or “flavors” of fermions, – but still not why three. For instance, the electron has additionally to the muon with $m_\mu = 207 m_e$ an even heavier copy, the tau with $m_\tau = 3480 m_e$. In the same way, three different neutrinos exist. They are called ν_e , ν_μ and ν_τ , depending on if they are generated together with an electron, muon or tau.

ch. lepton	e^-	μ^-	τ^-
neutrinos	ν_e	ν_μ	ν_τ
hadrons	n,p

5.2. Main nuclear burning reactions

5.2.1. Thermonuclear reactions and Gamov peak

Coulomb barrier-classically Nuclear forces are strong but of short range. The simplest model for the forces between two nuclei is therefore an attractive square potential well (Topf?) with radius equal to the size of the nuclei plus the Coulomb force dominating outside over the strong force. Thus a nuclei should have classically the energy $V \approx Z_1 Z_2 e^2 / r_N$ to cross the “Coulomb barrier” and to reach another nucleus of size r_N . For a thermal plasma of particles with reduced mass μ and charges $Z_i e$, this condition reads

$$\frac{1}{2} \mu \langle v^2 \rangle = \frac{3}{2} kT = \frac{Z_1 Z_2 e^2}{r}. \quad (5.3)$$

Specifically, we obtain for protons with $Z_1 = Z_2 = 1$ and size $r_N \approx 10^{-15}$ m that the temperature should be above

$$T \gtrsim \frac{2e^2}{3kr_0} \approx 10^{10} \text{ K}. \quad (5.4)$$

On the other hand, we have estimated the central temperature of the Sun as $T_c \approx 10^7$ K. Hence we should expect that only the tiny fraction of protons with $v^2 \gtrsim 1000 \langle v^2 \rangle$ is able to cross the Coulomb barrier.

Gamov factor and tunneling Quantum mechanically, tunneling through the Coulomb barrier is possible. The wave-function of a particle with $E - V < 0$ is non-zero, but exponentially suppressed. In order to avoid a too strong suppression, we require that $\lambda = h/p \approx r_N$,

$$\frac{h^2}{2\mu\lambda^2} = \frac{Z_1 Z_2 e^2}{\lambda}. \quad (5.5)$$

Inserting $\lambda = h^2/(2Z_1 Z_2 e^2 \mu)$ for r_N in Eq. (5.4) gives

$$T \gtrsim \frac{4Z_1^2 Z_2^2 e^4 \mu}{3h^2 k} \approx Z_1^2 Z_2^2 \times 10^7 \text{ K}. \quad (5.6)$$

Hence we expect that quantum effects lead only to a marginal suppression of fusion rates of light nuclei.

Next we want to make this statement more precise: We can estimate the tunneling probability using the WKB approximation as

$$P_0 \propto \exp \left(-2 \int_R^{r_0} dr \sqrt{\frac{2m}{\hbar^2} [V(r) - E]} \right) \equiv \exp(-I). \quad (5.7)$$

Here R is the range of the nuclear force, i.e. the point where the strong force becomes equal to the Coulomb force, and $r_0 = 2\mu Z_1 Z_2 e^2 / (\hbar k)^2$ is the classical turning point, $V(r_0) = E = (\hbar k)^2 / (2m)$, for a particle with energy E and wave-vector k at infinity. The suppression is smallest for s-wave scattering, when the centrifugal barrier in the potential V is absent. Then

$$I = 2k \int_R^{r_0} dr \sqrt{\frac{r_0}{r} - 1} \quad (5.8)$$

and substituting $\xi = (r/r_0)^{1/2}$, we obtain

$$I = 4kr_0 \int_{\sqrt{R/r_0}}^1 d\xi \sqrt{1 - \xi^2}. \quad (5.9)$$

We now rewrite the integral first as $\int_0^1 - \int_0^{\sqrt{R/r_0}}$. Then we use that $R \ll r_0$ to expand then the second term,

$$I = 4kr_0 \left\{ \int_0^1 d\xi \sqrt{1 - \xi^2} - \int_0^{\sqrt{R/r_0}} d\xi \left(1 - \frac{1}{2}\xi^2 + \dots \right) \right\} = 4kr_0 \left\{ \frac{\pi}{4} - \sqrt{R/r_0} + \dots \right\} \quad (5.10)$$

Luckily, the leading term does not depend on poorly known details of nuclear physics like the range R of the nuclear potential. Neglecting the subleading terms, we can write

$$I = \frac{\pi Z_1 Z_2 e^2}{\hbar} \sqrt{\frac{2\mu}{E}} \equiv B/\sqrt{E} \quad (5.11)$$

Reaction rates We are interested in the average reaction rate R , i.e. the number of reactions per time and volume, when both the projectile and target have a velocity distribution $f(v)dv$. Then

$$R = n_1 n_2 \int d^3 v_1 d^3 v_2 f(v_1, m_1) f(v_2, m_2) \sigma(E) v_{\text{rel}}. \quad (5.12)$$

The nuclei are non-relativistic and follow the Maxwell-Boltzmann distribution,

$$f(m, v) dv = \left(\frac{m}{2\pi kT} \right)^{3/2} \exp\left(-\frac{mv^2}{2kT}\right) 4\pi v^2 dv \propto e^{-E/kT} E^{1/2} dE. \quad (5.13)$$

Introducing relative and the center-of-mass velocities, one can show that

$$R = n_1 n_2 \int d^3 v_{\text{rel}} f(v_{\text{rel}}, \mu) \sigma(E) v_{\text{rel}}. \quad (5.14)$$

where μ is the reduced mass.

Example 5.1: Derive Eq. (5.14) for the reaction rate.

The product of the two Maxwell-Boltzmann distribution is given by

$$f_1 f_2 = \frac{(m_1 m_2)^{3/2}}{(2\pi kT)^3} \exp\left(-\frac{m_1 v_1^2 + m_2 v_2^2}{2kT}\right).$$

We introduce the relative velocity $\mathbf{v}_{\text{rel}} = \mathbf{v}_2 - \mathbf{v}_1$ and the cms velocity $\mathbf{V} = \frac{m_1 \mathbf{v}_1 + m_2 \mathbf{v}_2}{m_1 + m_2}$. Solving the second for \mathbf{v}_1 and inserting $\mathbf{v}_2 = \mathbf{v}_{\text{rel}} + \mathbf{v}_1$, it follows

$$\mathbf{v}_1 = \mathbf{V} - \frac{m_2 \mathbf{v}_{\text{rel}}}{m_1 + m_2}.$$

In the same way, we find

$$\mathbf{v}_2 = \mathbf{V} + \frac{m_1 \mathbf{v}_{\text{rel}}}{m_1 + m_2}.$$

Thus the kinetic energy becomes

$$\frac{1}{2}(m_1 v_1^2 + m_2 v_2^2) = \frac{1}{2}(m_1 + m_2)V^2 + \frac{1}{2}\mu v_{\text{rel}}^2.$$

Using also $m_1 m_2 = (m_1 + m_2)\mu$ for the prefactor, it is

$$f_1 f_2 = \frac{(m_1 + m_2)^{3/2}}{(2\pi kT)^{3/2}} \exp\left(-\frac{(m_1 + m_2)V^2}{2kT}\right) \frac{\mu^{3/2}}{(2\pi kT)^{3/2}} \exp\left(-\frac{\mu v_{\text{rel}}^2}{2kT}\right).$$

Finally we have to calculate the Jacobian J for the transformation $d^3 v_1 d^3 v_2 = J d^3 v_{\text{rel}} d^3 V$. This six-dimensional determinant can be decomposed into the product of three two-dimensional determinants of the type

$$J_x = \begin{vmatrix} \frac{\partial v_{1,x}}{\partial V_x} & \frac{\partial v_{1,x}}{\partial v_{\text{rel},x}} \\ \frac{\partial v_{2,x}}{\partial V_x} & \frac{\partial v_{2,x}}{\partial v_{\text{rel},x}} \end{vmatrix} = \begin{vmatrix} 1 & \frac{-m_2}{m_1 + m_2} \\ 1 & \frac{m_1}{m_1 + m_2} \end{vmatrix} = 1.$$

Similarly, the other two Jacobians are one. Separating the two integrals appropriately,

$$\int d^3 V \left[\left(\frac{m_1 + m_2}{2\pi kT} \right)^{3/2} \exp\left(-\frac{(m_1 + m_2)V^2}{2kT}\right) \right] \int d^3 v_{\text{rel}} \left(\frac{\mu}{2\pi kT} \right)^{3/2} \exp\left(-\frac{\mu v_{\text{rel}}^2}{2kT}\right) \sigma v_{\text{rel}}$$

we see that the first integral corresponds simply to the normalization condition for a Maxwell-Boltzmann distribution and is therefore equal to one.

Cross section for strong interactions are of geometrical nature, $\sigma(E) \approx \pi\lambda^2$ with $\lambda = h/p$ as the Compton wavelength of the nuclei. Thus it follows $\sigma(E) \propto 1/E$. Then the rate is

$$R = n_1 n_2 \langle \sigma v \rangle \propto \int dE \sigma(E) E e^{-b/E^{1/2}} e^{-E/kT} = \int dE S(E) e^{-b/E^{1/2}} e^{-E/kT}. \quad (5.15)$$

In the last step we introduced the so-called S -factor $S(E) = E\sigma(E)$ of the reaction. If the cross-section behaves indeed as $\sigma(E) \propto 1/E$, then $S(E)$ is a slowly varying function. The remainder of the integrand is sharply peaked (“Gamov peak”) in the region around 10 keV.

Example 5.2: Gamov peak.

Rates of fusion reactions in stars are proportional to $f(E) = e^{-b/E^{1/2}} e^{-E/kT}$ with $b = \pi\mu^{1/2} Z_1 Z_2 e^2 / (\sqrt{2}\epsilon_0 h)$ (SI units). Show that the maximum of this function (“Gamov peak”) is at $E_{\max} = (bkT/2)^{2/3}$ and find the numerical value for the Sun (hydrogen burning, $T = 10^7$ K). We find the only extremum of $f(E)$ by solving $f'(E_{\max}) = 0$ or

$$\left(\frac{1}{kT} - \frac{1}{2} b E_{\max}^{-3/2} \right) f(E_{\max}) = 0.$$

Solving for E_{\max} gives $E_{\max} = (bkT/2)^{2/3}$. With $\mu = m_p/2$ and $\alpha = e^2/(4\pi\epsilon_0\hbar c) \approx 1/137$ we can express b as $b = \pi\alpha(m_p c^2)^{1/2}$, while $T = 10^7$ K ≈ 0.86 keV/k. Hence the Gamov peak is at

$$E_{\max} = \left(\frac{\pi}{137} \times (0.94 \times 10^6)^{1/2} \times 0.86 \right)^{2/3} \text{ keV} \approx 7 \text{ keV}.$$

Using the more precise value $T = 1.57 \times 10^7$ K reproduces the literature value 9.6 keV.

Plasma and screening effects The calculation of cross sections is performed for the scattering of particles in vacuum, while the presence of a surrounding plasma is taken into account only via the (thermal) distribution functions in the rates. This oversimplistic approach neglects several effects: For instance, the electric charge of nucleus is screened in plasma since the surrounding positive and negative charges redistribute slightly. As a result, the Coulomb potential will be changed into a Yukawa potential with finite range,

$$V(r) = \frac{Ze e^{-r/\lambda_D}}{r} \quad (5.16)$$

where λ_D is the Debye radius. Expanding the exponential, it follows

$$V(r) = \frac{Ze}{r} - \frac{Ze}{\lambda_D} \quad (5.17)$$

Thus the Coulomb barrier of a nucleus is reduced by the “screening potential” Ze/λ_D in a plasma. The typical size of this effect is 10–50%.

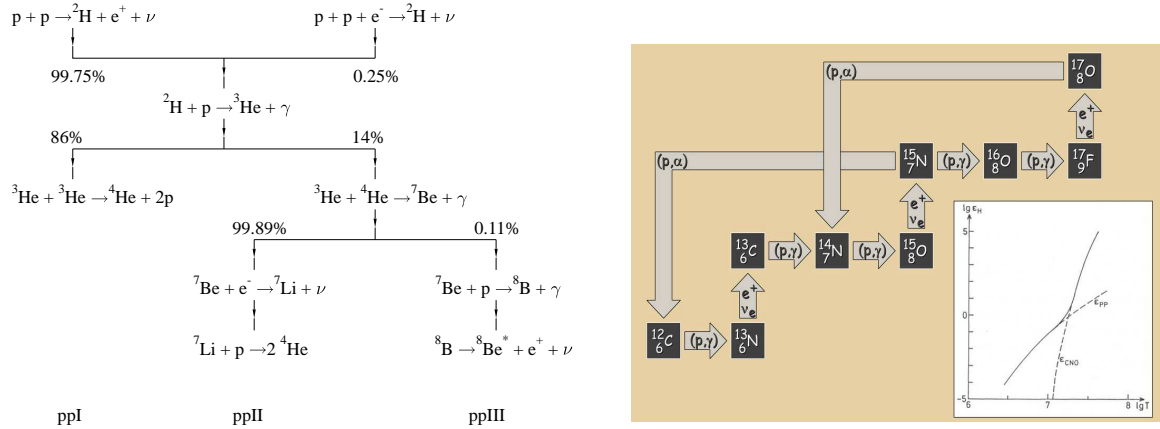


Figure 5.2.: Left: proton-proton chains Right: CNO cycle.

5.2.2. Hydrogen burning: pp-chains and CNO-cycle

The pp-chains are shown in detail in the left panel of Fig. 5.2. Its main chain uses three steps:

Step 1: $p + p \rightarrow d + e^+ + \nu_e$

Step 2: $p + d \rightarrow \text{}^3\text{He} + \gamma$

Step 2: $\text{}^3\text{He} + \text{}^3\text{He} \rightarrow \text{}^4\text{He} + p + p$

The CNO-cycle is shown in detail in the right panel of Fig. 5.2. The small inset compares the temperature dependence of the pp-chain and the CNO-cycle: For solar temperatures, the contribution of the pp-chains to the solar energy production is four order of magnitudes more important than the CNO-cycle.

5.2.3. Later phases

The increasing Coulomb barrier for heavier nuclei means that the fusion of heavier nuclei requires higher and higher temperatures. Since the temperatures decreases outwards, the different fusion phases – hydrogen, helium, carbon, ... burning – proceed in different shells, leading to onion-like structure of a massive star. Moreover, the fraction of the core participating in fusion becomes smaller in each new burning phase, cf. Fig. 5.3.

- Hydrogen burning $4p + 2e^- \rightarrow \text{}^4\text{He} + 2\nu_e$
 - proceeds by pp chains and CNO cycle
 - no heavier elements formed because no stable isotopes with mass number $A = 8$
 - neutrinos from $p \rightarrow n$ conversion
 - typical temperature 10^7 K (~ 1 keV)
- Helium burning $4\text{}^4\text{He} + 4\text{}^4\text{He} + 4\text{}^4\text{He} \leftrightarrow \text{}^8\text{Be} + 4\text{}^4\text{He} \rightarrow \text{}^{12}\text{C}$
 - triple alpha reaction builds up Be with concentration $\sim 10^{-9}$
 - $\text{}^{12}\text{C} + \text{}^4\text{He} \rightarrow \text{}^{16}\text{O}$
 - $\text{}^{16}\text{O} + \text{}^4\text{He} \rightarrow \text{}^{20}\text{Ne}$
 - typical temperature 10^8 K (~ 10 keV)
- Carbon burning
 - many reactions like $\text{}^{12}\text{C} + \text{}^{12}\text{C} \rightarrow \text{}^{20}\text{Ne} + \text{}^4\text{He}$ etc.
 - typical temperature 10^9 K (~ 100 keV)







Burning Phase	Dominant Process	T_c [keV]	ρ_c [g/cm ³]	L_γ [$10^4 L_{\text{sun}}$]		Duration [years]
					L_ν/L_γ	
 Hydrogen	H → He	3	5.9	2.1	-	1.2×10^7
 Helium	He → C, O	14	1.3×10^3	6.0	1.7×10^{-5}	1.3×10^6
 Carbon	C → Ne, Mg	53	1.7×10^5	8.6	1.0	6.3×10^3
 Neon	Ne → O, Mg	110	1.6×10^7	9.6	1.8×10^3	7.0
 Oxygen	O → Si	160	9.7×10^7	9.6	2.1×10^4	1.7
 Silicon	Si → Fe, Ni	270	2.3×10^8	9.6	9.2×10^5	6 days

 Figure 5.3.: Burning Phases of a $15 M_\odot$ Star.

Burning phase	process	kT_c/keV	$\rho_c/\text{g/cm}^3$	$L_\gamma/10^4 L_\odot$	L_ν/L_γ	duration/yr
hydrogen	H→He	3	5.9	2.1	0	1.2×10^7
helium	He→C,O	14	1.3×10^3	6.0	1.7×10^{-5}	1.3×10^6

 Table 5.3.: Burning phases with the dominant fusion processes, core parameters and luminosity of a $15 M_\odot$ star.

Carbon and oxygen burning many reactions like $^{12}\text{C}+^{12}\text{C} \rightarrow ^{20}\text{Ne}+^4\text{He}$ etc. typical temperature 10^9 K (~ 100 keV)

Silicon burning The large Coulomb barrier of silicon nuclei prevents the fusion of two silicon nuclei into iron. Instead, at temperature above the oxygen burnig, the energy of photons is sufficiently large to photo-disintegrate nuclei: For instance, the reaction $^{16}\text{O} + \alpha \leftrightarrow ^{20}\text{Ne} + \gamma$ produces neon around 10^9 K, but reverse direction at higher temperature. As a result, silicon photodesintegrate and forms together with lighter nuclei a mixture of nuclei with $A = 28 - 60$ close to nuclear statistical equilibrium, with reactions like $^{28}\text{Si}(\alpha, \gamma)^{32}\text{S}(\alpha, \gamma)^{36}\text{Ar}(\alpha, \gamma)^{40}\text{Ca}(\alpha, \gamma)^{44}\text{Ti}(\alpha, \gamma)^{48}\text{Cr}(\alpha, \gamma)^{52}\text{Fe}(\alpha, \gamma)^{56}\text{Ni}$. Being close but not in real equilibrium, a small net production of the iron group elements Fe, Mn, Co and Ni occurs over time.

5.3. *** Solar neutrinos ***

Solar neutrinos flux From $L_\odot = 4 \times 10^{33} \text{erg/s} = 2 \times 10^{39} \text{MeV/s}$ and the energy release of 26.2 MeV per reaction, the minimal number of neutrinos produced in the Sun per time is

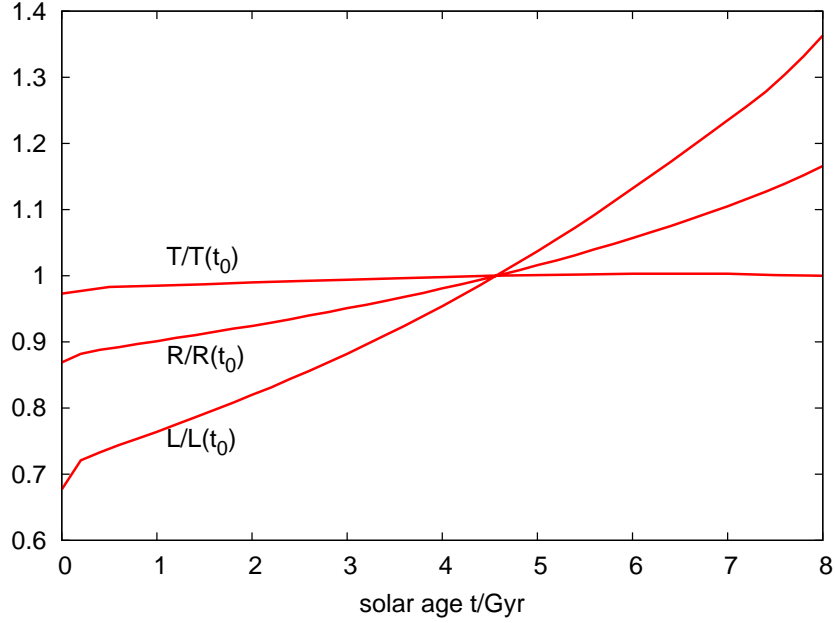


Figure 5.4.: The change of the Solar surface temperature, radius and luminosity as function of time.

$\dot{N}_\nu = 2 \times 10^{38}/\text{s}$. This rate does not include the neutrinos produced in the side-reactions of the pp chain, their relative fluxes are shown in Fig. 5.5. As we have seen, photons perform a random-walk, diffusing outward from the center. Neutrinos have much smaller interactions,

$$\sigma_{\nu e e} = 10^{-43} \text{cm}^2 \frac{E_\nu}{\text{MeV}} \quad (5.18)$$

and thus they can escape from the Sun: The interaction depth for a neutrino in the Sun is approximately

$$\tau = \sigma_{\nu e e} n_e R_\odot = 10^{-9}. \quad (5.19)$$

At Earth this corresponds to the flux of

$$\phi_\nu = \frac{\dot{N}_\nu}{4\pi D^2} = 7 \times 10^{10} \frac{1}{\text{cm}^2 \text{s}}. \quad (5.20)$$

(or directly via $\phi_\nu = 2S/(26.2 \text{MeV})$ with Solar constant.)

Weak interactions in the Sun produce always electron neutrinos, i.e. $p \rightarrow n + e^+ + \nu_e$, but not $p \rightarrow n + \mu^+ + \nu_\mu$ or $p \rightarrow n + \tau^+ + \nu_\tau$, because the energy released in nuclear reaction and the temperature is too small to produce a μ or τ . Similarly, only ν_e neutrinos are detected in radiochemical reactions via “inverse beta-decay”, while all type of neutrinos can be detected in elastic scattering on electrons.

Solar neutrino experiments Radiochemical experiments detect neutrinos by “inverse beta-decay” in suitable nuclei. The historically first isotope used was chlorine, $\nu_e + {}^{37}\text{Cl} \rightarrow {}^{37}\text{Ar} + e^-$, i.e. changing a neutron inside a ${}^{37}\text{Cl}$ nuclei into a proton, thereby converting it into a ${}^{37}\text{Ar}$.

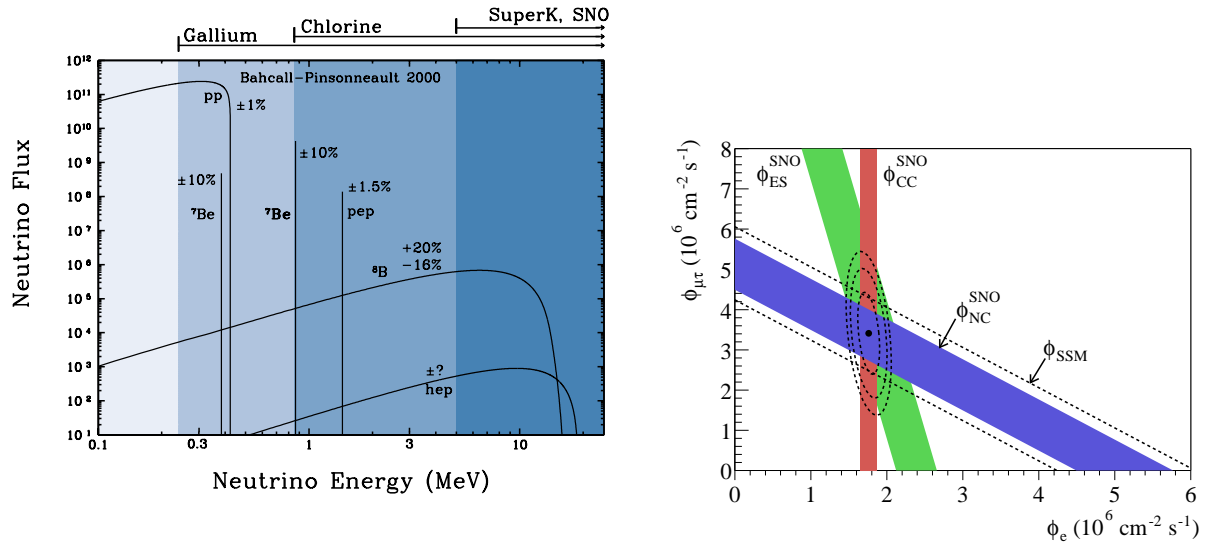


Figure 5.5.: Left: The solar standard model predicts the neutrino flux and thus also the number of events that should be measured. Right: Results of the SNO experiment.

The disadvantage of this reaction is its high energy threshold, $E_\nu \geq 0.814\text{MeV}$, only sensitive to 9% of all solar neutrinos.

The experiment consists of 615 tons of C_2Cl_4 solutions in a mine 1500 m underground. After exposure of a 2,3 months, a few Ar atoms are produced. They are chemically extracted and counted by their subsequent decays with a halftime of 35 days. Starting from the first data in 1968, a deficit appeared relative to the theoretically expected flux: only 30% of predicted event number is measured! This deficit was dubbed “solar neutrino problem.” Finding the solution to this problem required more than 30 years of intensive experimental and theoretical work.

Starting from 1991, two Gallium experiments $\nu_e + {}^{71}\text{Ga} \rightarrow {}^{71}\text{Ge} + e^-$ with threshold $E_\nu \geq 233\text{keV}$ took data. They found 55% of the expected neutrino flux, corresponding to 9 atoms of ${}^{71}\text{Ge}$ in 30 tons of solution containing 12 tons ${}^{71}\text{Ga}$, after three weeks of run time.

What are plausible solutions to the solar neutrino problem?

- Experiments might be wrong: difficult chemistry, no calibration of Ar cross section,...
- Nuclear physics: cross sections measured at higher energies are extrapolated to the Gamov peak
- Our model of the Sun: crucial T_c
- Particle physics: does a ν_e survive the travel to the Earth?

As latter experiments showed conclusively, the latter reason is the correct one: An energy-dependent fraction of electron neutrinos is transformed (“neutrino oscillations”) into a combination of muon and tau neutrinos. The red band in the right panel of Fig. ?? shows the flux of ν_e , measured in the SNO experiment by inverse-beta decay reactions. This flux is just 36% of the expected flux from the solar standard model. However, the experiment was able to measure also the flux of ν_μ and ν_τ . Summing all three up, one obtains the value predicted by the solar standard model. Hence neutrinos oscillate, changing their flavor.

***** Solar neutrino oscillations ***** Neutrino oscillations can be understood as a simple application of a two-level system in quantum mechanics. If such a system is described by a Hamiltonian H with eigenstates $|n\rangle$ and eigenvalues E_n ,

$$H|n\rangle = E_n|n\rangle, \quad (5.21)$$

then the time-evolution of the energy eigenstates $|n\rangle$ is given by

$$|n(t')\rangle = |n(t)\rangle e^{-iE_n(t'-t)/\hbar}. \quad (5.22)$$

An arbitrary (normalized) state $|\alpha(t)\rangle$ is connected by a unitary transformation U with the eigenstates $|n\rangle$, as $|\alpha\rangle = U_{\alpha n}|n(t)\rangle$. Thus the time evolution of this state is given by

$$|\alpha(t')\rangle = \sum_n U_{\alpha n}|n(t)\rangle e^{-iE_n(t'-t)/\hbar}. \quad (5.23)$$

The probability to measure the eigenvalue n will depend in general on time.

By definition we call the flavour of a neutrino according to the produced charged leptons in weak interaction, ν_α with $\alpha = \{e, \mu, \tau\}$. These states are eigenstates of the Hamiltonian H_{wk} of weak interactions. However, they are not necessary eigenstates of the Hamiltonian H_{mass} which generates neutrino masses. The eigenstates of this Hamiltonian are called the mass eigenstates ν_i with mass m_i . In order to describe the propagation of particles, we should use states with a definite mass, i.e. we should express the state ν_α produced in weak interactions as a superposition of mass eigenstates ν_i .

The time-evolution of the weak eigenstate $\nu_e(t)$ follows thus as

$$|\nu_e(t)\rangle = \sum_n U_{en}|n\rangle e^{-iE_n t/\hbar} = \cos\vartheta|\nu_1\rangle e^{-iE_1 t/\hbar} + \sin\vartheta|\nu_2\rangle e^{-iE_2 t/\hbar}, \quad (5.24)$$

where we set $|n\rangle \equiv |\nu_n\rangle$. Moreover, we used that the unitarity condition $UU^\dagger = UU^{-1} = 1$ can be satisfied for a two-level system by a rotation matrix,

$$U = \begin{pmatrix} \cos\vartheta & \sin\vartheta \\ -\sin\vartheta & \cos\vartheta \end{pmatrix}. \quad (5.25)$$

Thus the probability to measure the flavour α will depend in general ($\vartheta \neq 0$) on time.

The survival probability $P_{\nu_e \rightarrow \nu_e}$ of an ν_e is

$$P_{\nu_e \rightarrow \nu_e}(t) = |\langle \nu_e(t) | \nu_e(0) \rangle|^2 = 1 - \sin^2[(E_2 - E_1)t/2] \sin^2(2\vartheta). \quad (5.26)$$

For ultrarelativistic neutrinos, $E_i = (c^4 m_i^2 + c^2 p^2)^{1/2} \simeq p^2 + m_i^2 c^3 / (2p)$. Replacing also the travel time t by the distance L , we find

$$P_{\nu_e \rightarrow \nu_e}(L) = 1 - \sin^2 \left[\frac{\Delta m^2 c^3}{4\hbar E} L \right] \sin^2(2\vartheta). \quad (5.27)$$

with the mass squared difference of the two neutrino states $\Delta m^2 \equiv m_2^2 - m_1^2$.

The two-neutrino survival probability depends on the vacuum oscillation length

$$l_{\text{osc}} = 4\pi \frac{E}{\Delta m^2} \approx 2.5 \text{ m} \left(\frac{E}{\text{MeV}} \right) \left(\frac{\text{eV}^2}{\Delta m^2} \right)$$

that in turn depends the mixing angle ϑ and mass squared difference of the two neutrino states. However, the oscillation length is not sensitive to the absolute mass scale of the neutrino masses.

What is the Δm^2 accessible to solar neutrino experiments? (AU= 1.5×10^{13} cm)

$$\pi d/l_{\text{osc}} \sim 0.3 - 0.5 \quad \Rightarrow \quad \Delta m^2 \sim 10^{-12} \text{ eV}^2$$

If the solar neutrino problem would be explained by vacuum oscillations, then $P_{\nu_e \rightarrow \nu_e}$ would depend rather strongly on E , and experiments measuring different energy range should see this dependence. However, the relative simple picture describing neutrino oscillations in vacuum has to be refined for neutrinos propagating in a medium like the Sun. In particular, medium effects (or the so-called MSW effect) can lead to neutrino conversion probabilities close to one even for small neutrino mixing angles.

5.4. Neutron-capture nucleosynthesis

s-process and r-process nucleosynthesis We discussed how fusion processes in the most massive stars can produce elements up to the iron group, $A \sim 56$. How and where are the heavier elements, from copper to uranium, produced? The answer to this question has not been completely settled yet, but is based most likely on the following basic idea: The main obstacle for the fusion of heavy elements, the Coulomb barrier, can be circumvented if neutrons scatter with nuclei. Thus in a neutron rich environment, the processes



can produce heavier nuclei. If A is too large, i.e. the nuclei is too far from the valley of stability $A \sim Z$, it will decay by beta-decay,



If the half-time for beta-decay is slower than the time for absorbing an additional neutron, nucleosynthesis is said to proceed by the slow or s-process. The opposite case is called rapid or r-process nucleosynthesis. Which of the two processes dominates depends on the flux of available neutrons: The neutron rich environment of a core-collapse SN or a merger of neutron stars were suggested as possible sites of r-process nucleosynthesis, while the s-process happens during the normal stellar evolution of massive stars.

5.5. Cooling by neutrino emission

The emission of neutrinos in the pp chain and CNO cycle withdraws only a small fraction of the total energy released per reaction. As a result, these losses shorten the life of a MS star only slightly compared to its lifetime without such losses. In contrast, thermal energy can be removed from the hot cores of evolved stars independently of thermonuclear reactions by neutrino emission. The three most important processes are electron-positron pair annihilation into neutrino pairs $e^+ + e^- \rightarrow \nu_x + \bar{\nu}_x$, the plasma neutrino process $\gamma \rightarrow \nu_x + \bar{\nu}_x$ and the photoneutrino process $\gamma + e^- \rightarrow e^- + \nu_x + \bar{\nu}_x$.

Problems

5.1 Derive ...

6. *** Stars as labs for particle physics ***

6.1. Stellar evolution limits for particle physics

Stability A main-sequence star evolves very slowly, being stable against small perturbations around its equilibrium configuration. Its main pressure source is thermal movement of electrons/ions, $P \propto (\rho/\mu)T$.

Its stability is closely connected to the fact that a gravitationally bound system has negative heat capacity, i.e. a star heats up by emitting energy: The total energy of a star is continuously reduced by the emission of radiation. If the star is close to equilibrium, then the virial theorem $U = -U_{\text{pot}}/2$ implies that the star contracts. At the same time the average kinetic energy and thus the temperature increases, since only half of the lost energy is radiated away.

The steep energy dependence of nuclear reaction rates counteracts this tendency to shrink: A small contraction leads to an higher energy output and therefore to an increased temperature and finally to an expansion. Thus the stability of a main-sequence stars depends on both the negative heat capacity of a gravitationally bound system and the and the energy dependence of nuclear reaction rates.

Impact of new particles Novel particles may affect stars in two ways. They can act as an additional energy-loss mechanism ε_x ,

$$\frac{dL(r)}{dr} = 4\pi r^2(\varepsilon_{\text{nuc}} + \varepsilon_{\text{grav}} - \varepsilon_\nu - \varepsilon_x)\rho \quad (6.1)$$

in particular when these particles are weakly interacting. In the opposite case, they contribute to the transfer of energy,

$$L(r) = \frac{4\pi r^2}{3\kappa\rho} \frac{d(aT^4)}{dr}, \quad (6.2)$$

where the total opacity consists of

$$\kappa^{-1} = \kappa_\gamma^{-1} + \kappa_c^{-1} + \kappa_x^{-1}. \quad (6.3)$$

The radiative opacity κ_γ is defined by $\langle\lambda_\gamma\rangle = 1/(\kappa_\gamma\rho)$, where $\langle\lambda_\gamma\rangle$ is the mean free path of a photon, while κ_c is the electron conduction and κ_x denotes the additional energy transfer by scatterings between the novel particles and normal matter.

Applying this to the final stages of stellar evolution, WDs or NSs, with $\varepsilon_{\text{nuc}} = 0$, is trivial. On the other hand, for a star with $\varepsilon_{\text{nuc}} > 0$ we have to take into account that the star adjusts itself to the new energy losses.

Particles are produced effectively in stars only if $m \lesssim T$. Thus we can expect that stellar limits are useful for light particles like neutrinos (with non-standard properties), axions or similar particles.

6.2. Homologous analysis

Assume that the contraction due to the novel energy losses is uniform or *homologous*: the distance between any two points shall change in the same way as the radius of the star. Thus, if the new radius is $R' = yR$ with $y < 1$, then any point r inside the star is mapped into $r' = yr$. The mass inside r' equals to the mass inside r , $m'(r') = m(r)$, and the chemical composition is unchanged. The density transforms as $\rho'(r') = y^{-3}\rho(r)$ and from Eq. (3.7) the pressure scales as

$$P'(r') = y^{-4}P(r) \quad (6.4)$$

If the EoS is the one of an ideal gas, $P \propto (\rho/\mu)T$, and $\mu'(r') = \mu(r)$ by the uniformity assumption, the temperature scales as $T'(r') = y^{-1}T(r)$.

For an homologous star, the energy generation rate and the opacity have the following general form,

$$\varepsilon \propto \rho^n T^m \quad \kappa \propto \rho^s T^p \quad (6.5)$$

with n, m, s, p free constants. Let's use "Kramer's law" $\kappa \propto \rho T^{-3.5}$. (Then $\kappa' \propto y^{-3}y^{3.5} \propto y^{0.5}$.)

Then the energy flux scales ($L \propto rT^4/(\kappa\rho)$ scales as $L' \propto yy^{-4}/(y^{-3}y^{0.5})$) as

$$L'(r') = y^{-1/2}L(r) \quad (6.6)$$

In general, one can ignore $\varepsilon_{\text{grav}}$ and ε_{ν} and for simplicity we assume that ε_x depends in the same way on T and ρ as $\varepsilon_x \propto \varepsilon_{\text{nuc}} \propto \rho^n T^m$ with $n = 1$ and $m = 3 - 5$. Then

$$\varepsilon = (1 - \delta_x)\varepsilon_{\text{nuc}} \quad (6.7)$$

where δ_x the relative contribution of the new particles. From

$$\frac{dL(r)}{dr} = 4\pi r^2(\varepsilon_{\text{nuc}} + \varepsilon_{\text{grav}} - \varepsilon_{\nu} - \varepsilon_x)\rho \quad (6.8)$$

we have

$$L'(r') = (1 - \delta_x)y^{-(3+m)}L(r). \quad (6.9)$$

Comparing Eq. (6.6) and (6.9), we obtain the dependence of y as function of δ_x ,

$$y = (1 - \delta_x)^{2/(5+2m)}. \quad (6.10)$$

Inserting this expression into the homologous relations, $R' = yR$, etc., and linearising them for $\delta_x \ll 1$, it follows

$$\frac{\delta R}{R} = y - 1 = \frac{-2\delta_x}{2m + 5}, \quad \frac{\delta T}{T} = \frac{2\delta_x}{2m + 5}, \quad \frac{\delta L}{L} = \frac{\delta_x}{2m + 5}. \quad (6.11)$$

Hence a star contracts, heats up and becomes more luminous.

Even when the new energy losses are relatively large, the stellar structure is not changed much: For instance $\delta_x = 0.5$ results in a moderate 8% change of radius and temperature. Hence the main effect is an increased consumption of nuclear fuel and a decrease in the duration of the hydrogen-burning phase,

$$\delta\tau/\tau \approx -\delta_x. \quad (6.12)$$

Since the Sun is already more than half through its main-sequence evolution, the conservative bound $\delta_x < 0.5$ follows.

Since the solar standard model contains two free parameter, the initial helium abundance Y_0 and a parameter describing the importance of convection, one cannot use directly the measured values of R_\odot and of T_\odot to constrain δ_x . The range of value of Y_0 is however restricted by BBN, $Y_0 \geq 0.23$.

6.3. Globular cluster limits

Globular clusters consists typically of 10^4 – 10^6 stars within a diameter of $D \sim 20$ – 100 pc. The globular clusters in our galaxy form a spherical distribution with center around 10kpc away.

HR diagrams for clusters

- Make HR diagram for stars of one cluster using apparent magnitude (and normally color-index instead of T or spectral classes)
- shift it up/down so that MS is in correct position \Rightarrow distance modulus $m - M$, the difference between the apparent and absolute magnitudes. Thus $d/\text{pc} = 10^{(m-M+5)/5}$.
- generally a cluster HR diagram has a turn-off point above which no MS stars are found:
 - thus more luminous stars that are hotter and have a shorter life-time are missing
 - evolved already into WD/NS
 - stars in a cluster were formed at the same time of the same material, thus turn-off point fixes the cluster age
 - age of oldest globular cluster, $t \sim 12$ Gyr, gives lower limit to age of the universe.
- after MS, stars evolve to RG and then to HB
- use relative number of RG and HB stars to limit additional energy losses

Problems

6.1 Derive...

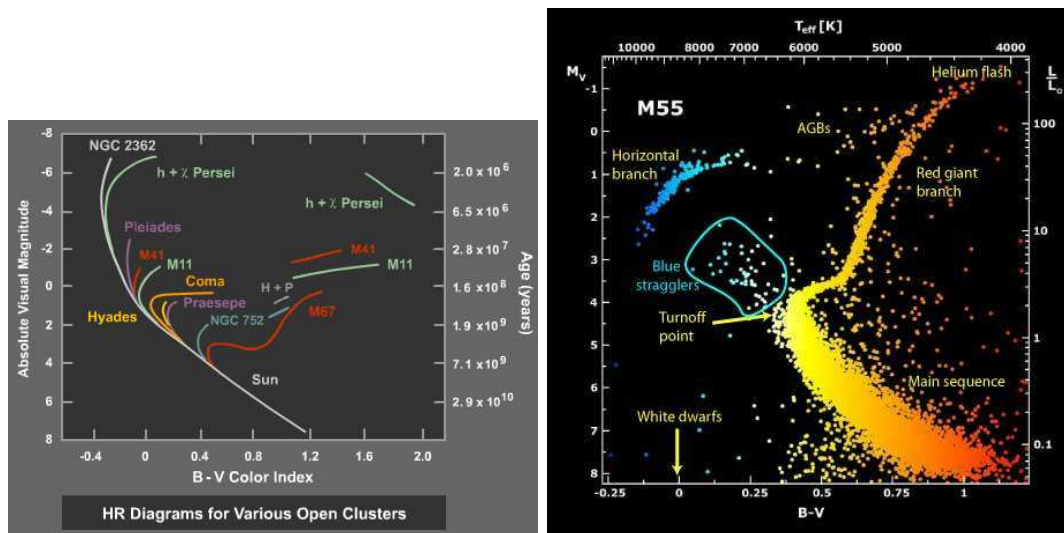


Figure 6.1.: HR diagrams for open and globular clusters.

7. Interstellar medium and star formation

The interstellar matter accounts for 10-15% of the total mass of the Galactic disk. It tends to concentrate near the Galactic plane and along the spiral arms, while being very inhomogeneously distributed at small scales. Roughly half the interstellar mass is confined to discrete clouds occupying only 1-2% of the interstellar volume.

7.1. Interstellar medium

The distance of the Sun to the nearest star is of order few pc, while the solar system up to Neptune extends over ~ 30 AU. If we take these distances as characteristic for the Galactic disk, then the volume dominated by stellar systems encompasses only a fraction of order 10^{-13} . The remainder is however not just empty space: The disk is filled with the interstellar medium (ISM) which is a rather heterogeneous mixture of several components. Apart from dust that is noted mainly by extinction or obscuration of other objects, it is dominated by hydrogen either in form of molecules (H_2), atoms (HI) or ions (HII). Moreover, the interstellar space is filled with magnetic fields and energetic particles called cosmic rays. All components of the ISM are interacting not only with each other but also with stars: Dense regions of the ISM are the birthplaces of stars, which in turn influences via ionizing photons, stellar winds and finally shock waves from supernova explosions the ISM.

A plot of typical temperatures of the ISM versus density is shown in Fig. ?? together with lines of constant pressure. One can observe that the ISM consists of various phases which are clearly separated. If this phases are in equilibrium, they should have the same pressure and thus be aligned along lines of constant pressure which are shown as the dashed lines. The expectation of equal pressure holds for most of the phases, with HII clouds as the clearest exception.

7.1.1. Interstellar dust

While dust contributes only a small mass fraction to the ISM, it efficiently absorbs and scatters photons with wavelengths in the visible and ultraviolet range. Therefore dust becomes visible by its blocking effect of star light. The combined effect of scattering and absorption of light, mainly by dust grains, is called extinction. Clearly, extinction may affects the properties like the luminosity or the distance of a star or galaxy that we deduce from its observed spectra. Surprisingly, this possibility has been ignored until the 1930s by astronomers.

R.J. Trümpler found the first clear evidence for extinction by dust examining cluster of stars in our galaxy. He plotted the angular diameter D of these star clusters versus their distance r . For the derivation of their distance he assumed the validity of the inverse-square law, $\mathcal{F} \propto 1/r^2$. The derived distribution $n(D/r, r)$ of the number of star clusters should not depend on r , but he found a systematic increase of the linear size D/r of clusters with distance. There are only two interpretations possible: i) The Sun is at a special place in the

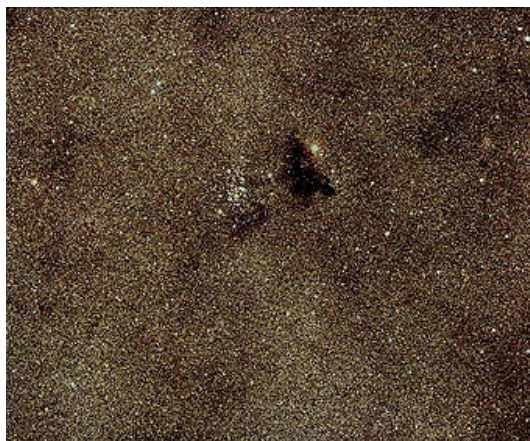


Figure 7.1.: A dark cloud, Barnard 86, is silhouetted against a starry background.

galaxy where the size of star clusters has a minimum. ii) Some light is absorbed and thus the energy flux decreases faster than $1/r^2$.

If the dust between us and the source leads to the optical depth τ , then the observed intensities with (I) and without (I_0) absorption are connected by $I = I_0 \exp(-\tau)$. We can relate the optical depth τ to the extinction A measured in magnitudes via

$$A \equiv m_0 - m = 2.5 \log(I_0/I) \quad (7.1)$$

or

$$A = 2.5 \log(\exp(-\tau)) = 2.5\tau \log(e) \approx 1.09\tau. \quad (7.2)$$

Thus the extinction A equals approximately the optical depth. The extinction due to interstellar medium depends strongly on the direction of the line of sight: Towards the center of the Milky Way, extinction of visible light reaches 30 magnitudes. Thus only $\exp(-A/1.09) \simeq 10^{-12}$ photons pass the Galactic center. As a result, we have no information about extragalactic objects towards these directions in the visible light. Excluding the Galactic center region, the extinction is on average two magnitudes per kpc.

If the spectral type and distance of a star is known, then the extinction between us and the star can be determined: The spectral type determines the absolute magnitude M , while the apparent magnitude m is observed directly. Then

$$m = M + 5 \log(r/(10\text{pc})) + A, \quad (7.3)$$

and we can find A for known m , M and r . On the other hand, distance measurements using spectroscopic parallaxes or standard candles like Cepheids or supernovae of type Ia are affected by extinction. Such distance measurements require an independent estimate of the amount of extinction between us and the object considered.

Reddening and extinction curves The scattering cross section of light on a dust grain of radius R is wave-length dependent. In general, light with shorter wavelengths is more efficiently scattered. Since more blue than red light is scattered, interstellar dust leads to a reddening of the spectra of stars and galaxies.

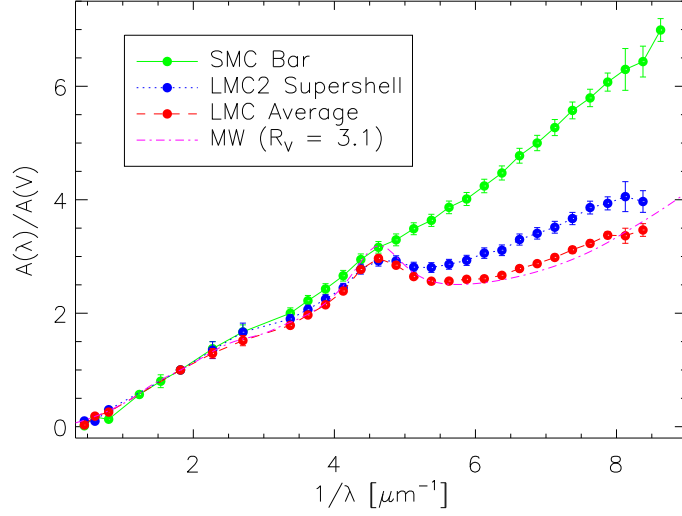


Figure 7.2.: The normalized extinction curve $A(\lambda)/A(V)$ for the average Milky Way, the bar of the Small Magellanic Cloud and two positions of the Large Magellanic Cloud as function of the inverse wave-length. From Ref. [11].

More precisely, one can roughly distinguish three scattering regimes in classical electrodynamics,

$$\lambda \ll R : \sigma \sim \pi R^2, \quad \text{geometrical scattering,} \quad (7.4)$$

$$\lambda \sim R : \sigma \propto \lambda^{-1}, \quad \text{Mie scattering,} \quad (7.5)$$

$$\lambda \gg R : \sigma \propto \lambda^{-4}, \quad \text{Rayleigh scattering.} \quad (7.6)$$

Measuring extinction at different wave-lengths allows astronomers to determine the properties of interstellar dust. One finds roughly $A \propto 1/\lambda$, thus the typical size of dust grains is comparable to the wave-length of visible light. If the wave-length dependence of extinction for “typical dust” is known, the absolute value of the extinction in the spectrum of a certain source can be estimated by observing it at different wave-lengths.

Figure 7.2 shows extinction curves for an average line-of-sight of the Milky Way and towards two smaller nearby galaxies, the Large and the Small Magellanic Clouds (LMC, SMC). The curves show the extinction $A(\lambda)$ normalised to the one of visible light, $A(V)$, as function of the inverse wave-length in order to display the behavior for large frequencies better. While the three curves agree quite well for wave-lengths larger than 2500 \AA , there are clear differences in the UV. These differences may be explained by the varying degree of star-formation in these galaxies which in turn influences the amount and properties of dust in the ISM. Below 2500 \AA , one finds roughly $A \propto 1/\lambda$, thus the typical size of dust grains is comparable to the wave-length of visible light.

Polarization Light passing dust clouds becomes polarized and the degree of its polarization is found to be proportional to the extinction. Using classical electrodynamics one can show that this requires a non-spherical shape of dust grains. Since the polarization builds up scattering on different dust grains, the dust grains have to be moreover partially aligned. The

most likely explanation for the observed polarization is that dust grains have a magnetic moment and become aligned by magnetic fields.

Composition and sources The absorption features visible in the IR of extinction curves correspond to vibrational transitions of silicates and ice, while extinction features in the UV can be connected to the presence of carbon. This leads to the idea that dust grains are mainly “dirty ice balls” containing some graphite. The composition suggests that dust originates from massive stars: In their red giant phase they lose part of their envelope; silicon and carbon condense cooling down, and a layer of hydrogen is bound around the silicon and graphite core.

7.1.2. Interstellar gas

HI gas and the 21cm line Interstellar gas was first detected by its absorption of background light. Since gas clouds are much cooler than the surface of stars, their absorption lines are narrower and have smaller excitation energies, making them thereby distinguishable from stellar absorption lines.

One expects that gas clouds consist mainly of hydrogen. Since they are cool, hydrogen is in the ground state. Therefore the main absorption feature is the Lyman- α line that is in the UV and thus not observable with a ground telescope. Instead, early studies concentrated on absorption lines of simple molecules like CH and CN and of atoms like Ca and So.

Nowadays, one observes gas clouds mainly with radio observations of the 21cm line of hydrogen. This wavelength corresponds to the temperature $T = ch/k\lambda \simeq 0.07\text{ K}$ and can thus be excited even in cool clouds. The 21cm line is caused by transitions between the two hyperfine levels of the hydrogen 1s ground state. The ground state of hydrogen can be occupied by an electron with spin up or down. These two states have the same energy, apart from a small correction due to the interaction of the electron spin with the spin of the proton. The 21cm emission line corresponds to a flip of the electron spin from parallel to anti-parallel to the spin of the proton.

The 21cm emission line is an extremely useful tool to study gas clouds in our and nearby galaxies. Since their movement can be measured using the Doppler effect, they serve as tracers for the velocity distribution of matter in galaxies. Radio observations are not hampered by dust, and thus one can observe gas clouds close to the Galactic center and beyond, regions that are obscured to optical observations. The Zeeman effect allows one to measure magnetic fields in the clouds and thereby to trace the Galactic magnetic field. In summary, these studies conclude that gas clouds fill $\sim 5\%$ of the galaxy; they have an average density $n_H \sim (1 - 10)\text{ cm}^{-3}$.

One can employ also the distribution of dust as a tracer for gas, using that the extinction due to dust is proportional to the hydrogen column density as [8]

$$N_H = 2.87 \times 10^{21} \text{ cm}^{-2} A_V/\text{mag}. \quad (7.7)$$

Since the extinction and the parallaxes of about five million stars within few kiloparsecs around the Sun are known, the local gas distribution can be reconstructed from these measurements. As an example, the surface gas density in a 720 pc^2 square around the Sun is shown in Fig. 7.3: Several

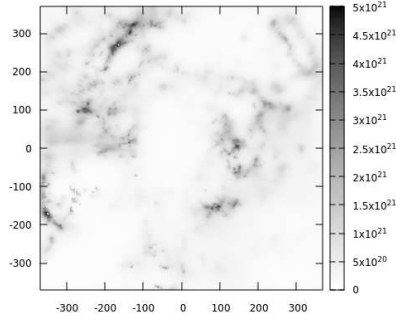


Figure 7.3.: The gas surface density

HII regions and the Strömgen sphere Some of the most spectacular objects of the Milky Way visible already in small telescopes are irregular regions of gas called diffuse nebula like the xxx shown in Fig. ???. All these nebula are found in the plane of the Milky Way. Apart from their emission in the optical band, they emit both a continuum and line spectrum in the radio range. While the latter originates from transitions between very high energy levels of hydrogen and helium, the former is produced by accelerated free electrons. Thus these regions should be hot and contain a source of ionizing photons. Since all these nebulae are associated with OB stars, we can assume that the UV photons with energy $E > I_H = 13.6 \text{ eV}$ emitted by these very hot stars ionize the hydrogen atoms in the nebula. If the nebula is stationary, ionization and recombination reactions $\text{H} + \gamma \leftrightarrow \text{p} + \text{e}^-$ should balance each other.

The recombination rate \mathcal{R}_{rec} per volume and time,

$$\mathcal{R}_{\text{rec}} = \frac{dN_{\text{rec}}}{dVdt} = n_e n_p \langle \sigma_{\text{rec}} v \rangle = x^2 n^2 \alpha(T) \quad (7.8)$$

is given by the product of the proton and electron densities, $n_p n_e$, and the thermally averaged recombination cross section $\langle \sigma_{\text{rec}} v \rangle$. For a pure hydrogen cloud, the number of free electrons equals the one of free protons, $n_e = n_p$. If we denote with $n = n_H + n_p$ the total number density of hydrogen atoms and free protons, then it is $n_e = n_p = xn$ with x as the fraction of ionized hydrogen. The recombination rate $\alpha(T) \equiv \langle \sigma_{\text{rec}} v \rangle$ of hydrogen can be approximated as

$$\alpha(T) \simeq 3 \times 10^{-14} \left(\frac{T_e}{10^4 \text{K}} \right)^{-1/2} \text{ cm}^3/\text{s}. \quad (7.9)$$

Finally, we have to consider the ionization rate per volume and time,

$$\mathcal{R}_{\text{ion}} = \frac{dN_{\text{ion}}}{dVdt} = cn_\gamma (1-x)n\sigma_{\text{ion}}, \quad (7.10)$$

where the photo-ionization cross section scales as

$$\sigma_{\text{ion}}(\nu) \simeq \sigma_0 \left(\frac{\nu}{\nu_0} \right)^{-3} \quad (7.11)$$

above the ionisation threshold $\nu > \nu_I$ with $\sigma_0(\nu) \approx 6.3 \times 10^{-18} \text{ cm}^2$. Since most photons able to ionize hydrogen come from the exponentially suppressed Wien tail of the Planck spectrum,

we can approximate $\sigma_{\text{ion}} \simeq \sigma_0$. The number density of ionizing photons at the distance r from the star scales as

$$n_\gamma = \frac{\dot{N}_\gamma}{4\pi r^2 c}. \quad (7.12)$$

Since the recombination rate of hydrogen typically is much smaller than the ionization rate, a sphere with almost completely ionized hydrogen forms around the star, with a sharp transition to zero ionisation outside. We can estimate the size of this HII region, assuming it to be spherically symmetric. The radius of this sphere is called Strömgen radius. In steady-state conditions, the number of recombinations inside the Strömgen sphere must equal the number of ionizations, $\mathcal{R}_{\text{ion}} = R_{\text{rec}}$. The former is in turn equal to the rate \dot{N}_γ of emitted ionizing photons,

$$\dot{N}_\gamma = \frac{4\pi}{3} R_*^3 \mathcal{R}_{\text{rec}}. \quad (7.13)$$

Example 7.1: Find the rate \dot{N}_γ of photons with energy $h\nu > I_H$ emitted by an O5 star. We use $T = 35.000 \text{ K}$ and $R = x$. The number \dot{N}_γ of photons emitted per time for an O5 star is

$$\dot{N}_\gamma = 4\pi R^2 \pi \int_{\nu_*}^{\infty} d\nu \frac{B_\nu}{h\nu} = \frac{8\pi}{c^3} \left(\frac{kT}{h} \right)^3 \int_{x_*}^{\infty} dx \frac{x^2}{e^x - 1} \approx 5.1 \times 10^{48} \text{ s}^{-1}$$

with $x_* = h\nu_*/(kT) \approx 4.51$ for an O5 star. This corresponds to a fraction of 14% of ionizing photons.

Thus

$$\dot{N}_\gamma = \frac{4\pi}{3} R_*^3 \mathcal{R}_{\text{rec}} = \frac{4\pi}{3} R_*^3 \alpha(T) x^2 n_0^2 \quad (7.14)$$

With the approximation of a sharp boundary, we can set $x \sim 1$ and obtain

$$R_* = \left(\frac{3\dot{N}_\gamma}{4\pi\alpha n^2} \right)^{1/3}. \quad (7.15)$$

For a density $n \sim 10^4/\text{cm}^3$, the radius of the Strömgen sphere around an O5 star is around 0.2 pc.

Finally, we want to justify our assumption of a sharp boundary for the Strömgen sphere. If the nebula is stationary, the ionization and recombination rates are equal,

$$c \frac{\dot{N}_\gamma}{4\pi r^2 c} (1-x)n\sigma_{\text{ion}} = x^2 n^2 \alpha. \quad (7.16)$$

This is a quadratic equation, $x^2 + Bx + C = 0$, for the ionisation fraction $x(r)$ at each point r which is controlled by the ratio of the ionization and recombination rates,

$$B = \frac{\dot{N}_\gamma \sigma_{\text{ion}}}{4\pi r^2 \alpha n}. \quad (7.17)$$

Solving $x(r = R_*/2)$ for the values of our example gives $B \simeq 10^5 \gg 1$, or $1-x \simeq 10^{-5}$. Thus the ionization fraction inside R_* is indeed close to one and decreases then sharply.

Three-phase model McKee & Ostriker 1977

7.2. Fluid dynamics

The perhaps simplest definition of a fluid is that of a substance that can flow. Thus the word fluid encompasses gases and liquids, but excludes solids where the positions of the atoms form a fixed lattice. This implies that we can model practically all astrophysical systems as a fluid, apart from few exceptions as white dwarf and neutron stars.

7.2.1. Perfect fluid equations

Introduction For the description of fluids we introduce the concept of a “fluid element:” This is a volume V which on one hand is large enough that the number N of contained particles is macroscopic, $N = nV \gg 1$. On the other hand, it is small enough that macroscopic quantities as, e.g., the particle density n do not vary within V . This requires strong enough interaction to smooth out all quantities of interest within a fluid element.

We will derive in this section the equations describing the evolution of an *perfect* or ideal fluid. These are fluids which move without internal friction, i.e. the momentum of two neighboring fluid elements with different velocities is not influenced by their differential motion. Processes which interchange momentum between two neighboring fluid elements are called viscous and are assumed to be negligible in the case of a perfect fluid. This assumption holds in many astrophysical systems, important exceptions are, e.g., accretion disks which we will discuss later.

In many astrophysical applications, the density ρ of the fluid is so small that the fluid speed u is larger than the sound speed $c_s \propto \rho^{(\gamma-1)/2}$. For instance, hydrogen clouds in the interstellar medium (ISM) have typical densities of $n_H \sim 1/\text{cm}^3$ and temperatures in the range $10^3 - 10^4$ K, leading to sound speeds of order 10 km/s. A flow with speed $u > c_s$ is called supersonic, with Mach number $\mathcal{M} \equiv u/c_s > 1$. Supersonic motion leads to the development of shocks, where otherwise smooth variables as e.g. the density ρ are discontinuous. Therefore we can not use the simplification that the fluid is incompressible, an assumption made in most application of fluid dynamics on Earth.

For the description of a fluid two choices of coordinates are common. In the Lagrangian formulation, one uses coordinates comoving with the fluid, while the Eulerian formulation employs coordinates of a fixed inertial system. To find the connection between these two descriptions, we consider the change of an arbitrary quantity $f(\mathbf{x}, t)$ during the time dt as the fluid element moves from \mathbf{x} to $\mathbf{x} + d\mathbf{x}$,

$$df = f(\mathbf{x} + d\mathbf{x}, t + dt) - f(\mathbf{x}, t) = f(\mathbf{x}, t + dt) - f(\mathbf{x}, t) + f(\mathbf{x} + d\mathbf{x}, t + dt) - f(\mathbf{x}, t + dt). \quad (7.18)$$

In the second step we added $f(\mathbf{x}, t + dt) - f(\mathbf{x}, t + dt)$ on the RHS which allows us to split the total change df into a part along dt and a part along $d\mathbf{x}$,

$$df = \frac{\partial f(\mathbf{x}, t)}{\partial t} dt + d\mathbf{x} \cdot \nabla f(\mathbf{x}, t + dt). \quad (7.19)$$

Taylor expanding the second term around t , neglecting the second order term $d\mathbf{x}dt$ and then dividing by dt we obtain

$$\frac{df}{dt} = \frac{\partial f}{\partial t} + \mathbf{u} \cdot \nabla f, \quad (7.20)$$

where we introduced also the fluid velocity $\mathbf{u} = d\mathbf{x}/dt$. Thus the change of the quantity f within a fixed fluid element consists of the change at a fixed coordinate, $\partial f/\partial t$, and the change due to the movement of the fluid element, $\mathbf{u} \cdot \nabla f$. To make the distinction clearer, we denote this total (or convective) derivative with

$$\frac{\mathcal{D}}{\mathcal{D}t} \equiv \frac{\partial}{\partial t} + \mathbf{u} \cdot \nabla. \quad (7.21)$$

Note that our use of the enclosed mass $M(r)$ as replacement of the radial distance r in the equations for stellar structure is an example for the usefulness of the Lagrangian formulation.

Continuity equation In non-relativistic fluid mechanics, the mass is a conserved quantity. Hence a continuity equation similar to the one for charge conservation in electrodynamics holds: The change of the mass contained in a volume V is equal to the flow through its boundary ∂V , or in differential (Eulerian) form,

$$\frac{\partial \rho}{\partial t} + \nabla \cdot (\rho \mathbf{u}) = 0. \quad (7.22)$$

Expressing ∂t by $\mathcal{D}t$, we use Eq. (7.20) and the identity $\nabla \cdot (\rho \mathbf{u}) = \rho \nabla \cdot \mathbf{u} + \mathbf{u} \cdot \nabla \rho$ to obtain the Lagrangian form of the continuity equation,

$$\frac{\mathcal{D}\rho}{\mathcal{D}t} + \rho \nabla \cdot \mathbf{u} = 0. \quad (7.23)$$

Even in the case of a conserved quantity like the mass or the proton number, the continuity equation may be modified by adding a source term $Q(\mathbf{x}, t)$ on the RHS: For instance, the injection of protons by a star, eg. in a stellar wind, at the position \mathbf{x}_0 could be modeled by adding a source term $Q(\mathbf{x}, t) = q(t)\delta(\mathbf{x} - \mathbf{x}_0)$ to the RHS of this equation.

Momentum equation The equation expressing momentum conservation is straight-forward in the Lagrangian form,

$$\rho \frac{\mathcal{D}\mathbf{u}}{\mathcal{D}t} = \mathbf{f} = -\nabla P - \rho \nabla \Phi. \quad (7.24)$$

Thus the change $\rho \mathcal{D}\mathbf{u}/\mathcal{D}t$ of the momentum density of a fluid element equals the sum of the force density due to a pressure gradient $-\nabla P$ and other applied external force densities, as e.g., a gravitational force density $-\rho \nabla \Phi$. Going over to the Eulerian form, we have to sum the change at a fixed coordinate, $\partial_t \mathbf{u}$, and the change due to the movement of the fluid element on the LHS,

$$\rho \frac{\partial \mathbf{u}}{\partial t} + \rho (\mathbf{u} \cdot \nabla) \mathbf{u} = \mathbf{f} = -\nabla P - \rho \nabla \Phi. \quad (7.25)$$

Remark 7.1: The Euler equation (7.25) with zero external forces \mathbf{f}_{ex} is equivalent to the conservation law $\partial_i \sigma_{ij} = 0$ for a perfect fluid, where the stress tensor for an ideal fluid is given by $\sigma^{ij} = \rho u^i u^j + P \delta^{ij}$.

Energy equation We apply the first law of thermodynamics, $dU = dQ - PdV$, to a fluid element. Then we find as energy equation

$$\frac{DU}{Dt} = Q - P \frac{DV}{Dt}, \quad (7.26)$$

with $U = U/\rho$ as the internal energy per mass, $V = 1/\rho$ as the specific volume and Q as external power per mass.

7.2.2. Revisiting the equations of stellar structure

7.2.3. *** Jeans instability and shocks ***

Jeans instability The perfect fluid equations cannot be solved in general, because the Euler equation is a non-linear differential equation. In contrast to linear equations as the Maxwell equations, no general theory exists from which solutions for prescribed initial conditions can be derived.

One way to gain some understanding is to employ perturbation theory. Following Jeans, we consider now small perturbations x_1 around a static background, $\rho_0 = \text{const.}$, $P_0 = \text{const.}$ and $u_0 = 0$. Restricting us to small perturbations, $x_1 \ll x_0$, allows us to neglect all quantities quadratic in the perturbations. Sound waves propagate in most circumstances adiabatically, i.e. without production of entropy, $dS = 0$. Thus changes in P and ρ are connected via

$$P = P_0 + \left(\frac{\partial P}{\partial \rho} \right)_S d\rho + \left(\frac{\partial P}{\partial S} \right)_P dS \simeq P_0 + c_s^2 d\rho. \quad (7.27)$$

We will see below that c_s is the sound speed in the background medium. Inserting $x = x_0 + x_1$ into the fluid equations and neglecting quadratic terms gives

$$\partial_t \rho_1 + \rho_0 \nabla \cdot \mathbf{u}_1 = 0, \quad (7.28a)$$

$$\Delta \Phi_1 = 4\pi G \rho_1, \quad (7.28b)$$

$$\partial_t \mathbf{u}_1 + \frac{c_s^2}{\rho_0} \nabla \rho_1 + \nabla \Phi_1 = 0, \quad (7.28c)$$

where we used also

$$\nabla_i P = \frac{\partial \rho_1}{\partial x_i} \frac{\partial}{\partial \rho_1} P_1 = c_s^2 \nabla_i \rho_1. \quad (7.29)$$

These three equations can be combined into one second-order differential equation for ρ_1 . We multiply first Eq. (7.28c) by ρ_0 and apply ∇ on it,

$$c_s^2 \Delta \rho_1 = -\rho_0 (\partial_t \nabla \cdot \mathbf{u}_1 + \Delta \Phi_1). \quad (7.30)$$

Then we insert Eq. (7.28b) for $\Delta \Phi_1$ and Eq. (7.28a) for $\nabla \cdot \mathbf{u}_1$, and obtain a linear inhomogeneous wave equation,

$$\partial_t^2 \rho_1 - \underbrace{c_s^2 \Delta \rho_1}_{\text{pressure}} = \underbrace{4\pi G \rho_0 \rho_1}_{\text{grav. force}}, \quad (7.31)$$

Inserting plane waves $\rho_1 \propto e^{-i(\omega t - \mathbf{k} \cdot \mathbf{x})}$ into this equation, we obtain as their dispersion relation

$$\omega^2 = c_s^2 k^2 - 4\pi G \rho_0. \quad (7.32)$$

This confirms that $c_s = (\partial P/\partial \rho)^{1/2}$ is the sound speed. The dispersion relation (7.32) becomes zero for

$$k_J = \left(\frac{4\pi G \rho_0}{c_s^2} \right)^{1/2}. \quad (7.33)$$

This wave number is called the Jeans wave number and marks the border between oscillating ($k > k_J$) and exponentially growing or decaying modes ($k < k_J$). The former are equivalent to acoustic oscillations or sound waves, while the growing mode corresponds to the gravitational collapse of the system. Defining the Jeans mass as the total mass M_J contained within a sphere of radius $R_J = \lambda_J/2 = \pi/k_J$, we obtain as the minimal mass which can collapse

$$M_J = \frac{4\pi}{3} \left(\frac{\pi}{k_J} \right)^3 \rho_0 = \frac{\pi^{5/2}}{6} \frac{c_s^3}{G^{3/2} \rho_0^{1/2}}. \quad (7.34)$$

Recalling the time-scale of gravitational collapse, $\tau_{\text{ff}} \sim (G\rho_0)^{-1/2}$, suggests another intuitive interpretation of the Jeans criterion: It compares the time-scale of gravitational collapse $\tau_{\text{ff}} \sim (G\rho_0)^{-1/2}$ with the one pressure can react, $\tau_p \sim R/v_s$. For $\tau_{\text{ff}} \ll \tau_p$, or $R \gg v_s/(G\rho_0)^{1/2}$, gravitational collapse occurs.

For a mono-atomic gas, the equation of state is $P = K\rho^\gamma$ with $\gamma = 5/3$. Thus, the sound speed is $c_s = (\gamma P/\rho)^{1/2}$ and if an adiabatic compression with density $\rho_2 = \varepsilon\rho_1$ propagates, then $c_s \propto \varepsilon^{(\gamma-1)/2}$. Hence the sound speed increases for a compression, the dense region overruns uncompressed regions and becomes even denser: As a result, a discontinuity develops in some hydrodynamical variables like the density. Such a discontinuity is called a shock.

*****Shocks***** Since a shock is characterized by discontinuities, we need to derive the relation between the pre- and post-shock values of these variables. In order to derive this connection, we will consider the simplest case of an one-dimensional, steady shock in its rest frame and assume that magnetic or gravitational fields can be neglected. Then the continuity equation for mass, $\partial_t \rho + \nabla \cdot (\rho \mathbf{v}) = 0$, becomes simply

$$\frac{d}{dx} (\rho v) = 0. \quad (7.35)$$

The Euler equation simplifies using the same assumptions and taking into account Eq. (7.35) to

$$\frac{d}{dx} (P + \rho v^2) = 0. \quad (7.36)$$

Additionally to the conservation laws for mass (7.35) and momentum (7.36) we need the conservation law for energy,

$$\frac{\partial}{\partial t} \left(\frac{\rho v^2}{2} + \rho U + \rho \Phi \right) + \nabla \cdot \left[\rho \mathbf{v} \left(\frac{v^2}{2} + U + \frac{P}{\rho} + \Phi \right) \right] = 0. \quad (7.37)$$

Here, the first bracket accounts for the change of kinetic, internal and potential energy with time which has to be balanced by the energy flux through the boundary of the considered volume. Specializing again to the case of an one-dimensional, stationary flow with $\Phi = 0$ gives

$$\frac{d}{dx} \left(\frac{\rho v^3}{2} + (U + P)v \right) = 0. \quad (7.38)$$

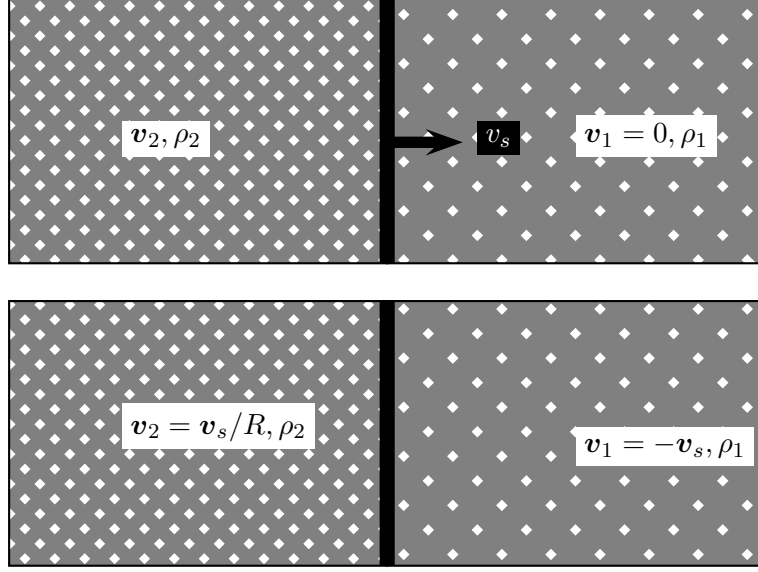


Figure 7.4.: Conditions on the down-stream (left) and the up-stream (right) side of a shock in the lab system (top) and in the shock rest frame with $v_1 = -v_s$ (bottom).

Integrating these equations over the discontinuity of the shock results in the ‘‘Rankine-Hugoniot’’ jump conditions,

$$[\rho v]_1^2 = 0, \quad (7.39a)$$

$$[P + \rho v^2]_1^2 = 0, \quad (7.39b)$$

$$\left[\frac{\rho v^2}{2} + \frac{\gamma}{\gamma - 1} P \right]_1^2 = 0, \quad (7.39c)$$

where we used also $U = P/(\gamma - 1)$. Since we assumed a steady flow, these jump conditions have to be evaluated in the shock rest frame, cf. Fig 7.4 – otherwise time-derivatives should be included.

From Eq. (7.39a) we see that the ratio of densities and velocities behaves inverse to each other. We define the compression ratio R as

$$R \equiv \frac{\rho_2}{\rho_1} = \frac{v_1}{v_2}. \quad (7.40)$$

Inserting first $\rho_2 = (v_1/v_2)\rho_1$ into (7.39b) gives $P_2 = P_1 + \rho_1 v_1(v_1 - v_2)$. We could use these two expressions to eliminate ρ_2 and P_2 from Eq. (7.39c), obtaining a quadratic equation for the ratio v_2/v_1 . Alternatively, we solve Eq. (7.39b) using (7.40) for the velocities,

$$v_1^2 = \left(\frac{P_2 - P_1}{\rho_2 - \rho_1} \right) R, \quad (7.41a)$$

$$v_2^2 = \left(\frac{P_2 - P_1}{\rho_2 - \rho_1} \right) / R. \quad (7.41b)$$

Reordering the resulting equation according to powers of v_2 ,

$$\left(\frac{\gamma + 1}{\gamma - 1} \right) v_2^2 + \frac{2\gamma}{\gamma - 1} \left(\frac{P_1 + \rho_1 v_1^2}{\rho_1 v_1} \right) v_2 + v_1^2 \frac{2\gamma}{\gamma - 1} \frac{P_1}{\rho_1} = 0, \quad (7.42)$$

replacing P_1 by the sound speed and dividing by v_1^2 , we obtain finally a quadratic equation for the ratio $t = v_2/v_1$,

$$\left(\frac{\gamma+1}{\gamma-1}\right)t^2 + \frac{2\gamma}{\gamma-1}\left(\frac{c_1^2}{v_1^2} + \gamma\right)t + \left(1 + \frac{2}{\gamma-1}\frac{c_1^2}{v_1^2}\right) = 0. \quad (7.43)$$

Now we recognize v_1/c_1 as the Mach number \mathcal{M} . Since we are interested in fast flows, $v_1 \gg c_1$, we can neglect the two $1/\mathcal{M}^2$ terms and obtain as approximate solutions

$$t = 1 \quad \text{or} \quad v_1 = v_2, \quad (7.44a)$$

$$t = \frac{\gamma-1}{\gamma+1} \equiv R \quad \text{or} \quad Rv_2 = v_1. \quad (7.44b)$$

The first solution is obviously trivial, while the second one is the strong shock solution. The compression ratio R indicates how strong the density and the velocity in the up- and down stream regions differ. Since we are using as reference frame the shock frame, we have $v_s = v_1$ and thus for $\gamma = 5/3$ the compression ratio is universal, $R = 4$, in the limit $\mathcal{M} \gg 1$,

$$v_2 = v_s/R = v_s/4, \quad (7.45a)$$

$$\rho_2 = R\rho_1 = 4\rho_1, \quad (7.45b)$$

$$P_2 = 3\rho_1 v_s^2/4. \quad (7.45c)$$

Hence no matter how strong a supersonic shock is, it can compress a mono-atomic gas only by a factor four. The same factor relates the velocity of the shock and of the matter after the passage of the shock.

We will later see that shocks are efficient accelerators of charged particles. Moreover, the universal ratio of the up- and down-stream velocities for any strong shock will lead to an universal slope of the energy spectrum of accelerated particles.

7.2.4. Hydrodynamic turbulence

Viscosity and turbulence In the previous sections, we considered perfect fluids which are a useful idealization of real fluids in the limit when friction can be neglected. Allowing for a small amount of friction, the new phenomenon of turbulence can appear. We can use the familiar concept of the flow of a fluid through a pipe to illustrate this. In the case of a perfect fluid, such a flow is always laminar. This means that the velocity field $\mathbf{u}(\mathbf{x})$ shown in the left panel of Fig. 7.5 is a smooth function and, since there is no friction, the velocity does not depend on the distance to the boundary of the pipe. Since no energy is dissipated, the flow is stationary. If we consider instead the flow of a real fluid through a pipe, we have to distinguish the two regimes sketched in the two other panels of Fig. 7.5: For small enough velocities, the flow is also for a viscous fluid laminar. The velocity field $\mathbf{u}(\mathbf{x})$ is again smooth, but increases continuously from zero at the boundary of the pipe to its maximal value at the center. Above a certain critical value of the velocity, we enter a new regime and the flow becomes turbulent: Time-dependent eddies of various sizes form and the velocity field $\mathbf{u}(\mathbf{x}, t)$ has to be split into a regular, average and a chaotic, turbulent component,

$$\mathbf{u}(\mathbf{x}, t) = \langle \mathbf{u}(\mathbf{x}) \rangle + \delta \mathbf{u}(\mathbf{x}, t). \quad (7.46)$$

Here, the average $\langle \cdot \rangle$ is formally an ensemble average over many realisations of the same experiment. In astrophysics and cosmology, such an ensemble average has to be replaced

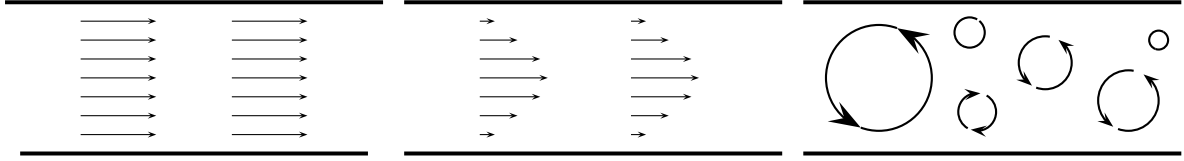


Figure 7.5.: Flow of a fluid through a pipe: The velocity field $\mathbf{u}(\mathbf{x})$ for a perfect fluid (left), for a laminar flow (middle) and the turbulent (right) component $\delta\mathbf{u}(\mathbf{x})$ of a viscous fluid.

by an average over, e.g., different regions on the sky which are statistically independent and subject to similar physical conditions.

Although the hydrodynamic equations are deterministic, the prediction of the turbulent component $\delta\mathbf{u}(\mathbf{x}, t)$ is in practise impossible, since it would require the precise knowledge of the initial and boundary conditions. However, in general, we do not want to know the time development of the flow $\mathbf{u}(\mathbf{x}, t)$ for a specific set of initial conditions. Instead, we are interested in its generic properties, e.g, how large the fluctuations $\langle\delta\mathbf{u}^2\rangle$ are and how their energy is distributed over the different length scales ℓ .

In order to address such questions, it is useful to express the turbulent velocity field $\delta\mathbf{u}(\mathbf{x})$ by its Fourier modes

$$\delta\mathbf{u}(\mathbf{k}) = \int d^3x \delta\mathbf{u}(\mathbf{x})e^{-i\mathbf{k}\mathbf{x}}. \quad (7.47)$$

Since we separated the ordered motion, such a random field $\delta\mathbf{u}$ satisfies $\langle\delta\mathbf{u}(\mathbf{x})\rangle = 0$. The energy density¹ ε of the velocity fluctuations is given by

$$\varepsilon = \frac{\rho}{2} \int \frac{d^3k}{(2\pi)^3} |\delta\mathbf{u}(\mathbf{k})|^2 \simeq \frac{\rho}{4\pi^2} \int dk k^2 |\delta\mathbf{u}(k)|^2 \equiv \int dk w(k) = \int \frac{dk}{k} kw(k). \quad (7.48)$$

Here, we assumed in the second step that the fluctuations are isotropic, $\delta\mathbf{u}(\mathbf{k}) = \delta\mathbf{u}(k)$, and in the third we introduced the spectral energy density $w(k)$. More convenient is often the logarithmic spectral energy density $kw(k)$, which has the unit of an energy density, and can thus compared directly with ε . Note that $|\delta\mathbf{u}(\mathbf{k})|$ has not the meaning of the typical velocity u_λ of fluctuations with scale $\lambda = 2\pi/k$: $\mathbf{u}(\mathbf{k})$ as the Fourier transform of $\mathbf{u}(\mathbf{x})$ has not even the unit of a velocity. We can estimate the typical velocity by comparing u_λ^2 to the logarithmic spectral energy density,

$$kw(k) \simeq \frac{\rho}{2} u_\lambda^2. \quad (7.49)$$

Alternatively, we can define

$$u_\lambda^2 = \frac{2}{\rho} \frac{d[kw(k)]}{d \ln(k)}. \quad (7.50)$$

In the case of a power law, $w(k) = Ck^\alpha$, the two definitions agree except for a numerical factor and we will use below the simpler version (7.49).

Next we want to find the physical quantity which determines the transition between a laminar and a turbulent flow. Our problem of a flowing fluid in a pipe contains three characteristic

¹Note that many authors do not include the density ρ into the definition of ε .

quantities: the fluid velocity u , the radius R of the pipe and a constant ν characterising the friction of the fluid. First, we determine the physical dimension of the quantity ν , called the (kinematic) viscosity of a fluid. Friction is caused by the relative velocity of neighbouring fluid elements; thus the stress tensor σ_{ij} of a viscous fluid should contain in addition to $u_i u_j$ terms with velocity gradients $\partial_i u_j$. Adding a term like $\nu[\partial_i \partial_i u_j + \dots]$ to the Euler equation, we find that the dimension of the constant ν is $[\nu] = \text{cm}^2/\text{s}$. Out of the three characteristic quantities u , L and ν , we can form one dimensionless quantity, the Reynolds number

$$\mathcal{R}_e = \frac{uL}{\nu}. \quad (7.51)$$

Experimentally, it is found that flows in systems with the same Reynolds number behave similarly. In particular, turbulence sets in above $\mathcal{R}_e = uL/\nu \sim 3000$. Thus turbulence appears in fast flows over large scales in media with small viscosity ν . This is typically the case in astrophysics, and thus many astrophysical flows are turbulent. Note also that the limit $\nu \rightarrow 0$, which corresponds formally to the transition to a perfect fluid, leads to strong turbulence.

Kolmogorov scaling We want to determine the spectral energy density $w(k)$ of the turbulent velocity fluctuations of a fluid in the stationary limit. To sustain a turbulent flow a persistent source of energy supply is required, because turbulence dissipates as the kinetic energy of the unordered motion $\delta \mathbf{u}$ is converted into heat by friction. Such sources are, e.g., stellar winds, supernova shocks or the differential rotation of the Milky Way. They inject energy into the interstellar medium on scales of tens of parsecs. Friction which is caused by the diffusion of molecules or atoms becomes effective only on much smaller length scales. Thus there is a large separation between the injection scale L_{\max} and the dissipation scale L_{\min} . On intermediate scales $L_{\min} \ll \ell \ll L_{\max}$, the so-called inertial range, the energy cascades from larger to smaller scales as large eddies break into smaller ones. We can understand the formation of smaller and smaller eddies by considering the action of $u_i \partial_i u_j$ on a one-dimensional Fourier mode $u = u_0 \sin(kx)$,

$$u \partial_x u = u_0^2 k \sin(kx) \cos(kx) \propto \sin(2kx). \quad (7.52)$$

Thus the non-linear term in the Euler equation shifts kinetic energy to larger and larger wave-numbers. This process does not dissipate energy—as it is present already in the perfect fluid equations—and thus we can use energy conservation to describe the cascading of the turbulent motion from the injection scale L_{\max} to the dissipation scale L_{\min} .

The question how the energy is distributed over the different length scales ℓ was addressed successfully first by Kolmogorov in 1941. He made two hypotheses: First, he assumed that at scales $\ell \ll L_{\max}$ the turbulent motion is statistically isotropic. Although the injection process depends on the specific geometry, eddies of scale $\ell \ll L_{\max}$ have lost the memory of the initial conditions. Second, Kolmogorov suggested that for $\mathcal{R}_e \gg 1$, the cascade is universal and uniquely determined by the kinematic viscosity ν and the rate of energy dissipation $\dot{\epsilon}$. In the stationary case, $\dot{\epsilon}$ has to equal the injected power density. Starting then at the injection scale, the injected power density is

$$\dot{\epsilon} = \langle \mathbf{u} \cdot \mathbf{f}_{\text{ex}} \rangle \simeq \left. \frac{\rho u_\ell^2}{2\tau_\ell} \right|_{\ell=L_{\max}} \quad (7.53)$$

with \mathbf{f}_{ex} as the external force density. At each scale in the inertial range, where dissipation can be neglected and thus energy conservation applies, the energy transferred at the scale ℓ

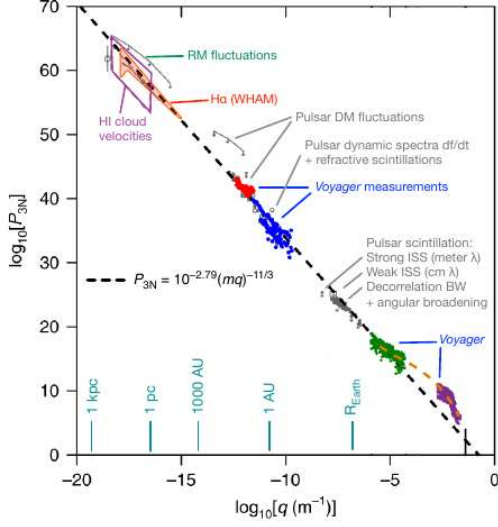


Figure 7.6.: Observations of the power-spectrum of velocity fluctuations in the Milky Way, from Ref. [1]. Right: Schematic power spectrum $w(k)$ between....

to smaller scales equals the total power $\dot{\epsilon}$ injected at the initial scale L_{\max} ,

$$\dot{\epsilon} \simeq \frac{\rho u_\ell^2}{2\tau_\ell}. \quad (7.54)$$

Here, τ_ℓ denotes the cascade time at the scale ℓ which, by dimensional reasons, equals $\tau_\ell \simeq \ell/u_\ell$. Solving now for u_ℓ gives $u_\ell \simeq (2\dot{\epsilon}\ell/\rho)^{1/3}$. The kinetic energy density $w(k)$ follows then as

$$w(k) = \frac{\rho u_k^2}{2k} = (2\pi^2 \rho \dot{\epsilon}^2)^{1/3} k^{-5/3}. \quad (7.55)$$

This is the famous $w(k) \propto k^{-5/3}$ behaviour of the power-spectrum for Kolmogorov turbulence. In the left panel of Fig. 7.6, we show measurements of the power-spectrum of velocity fluctuations of electrons in the Milky Way: These fluctuations follow over nearly 20 decades the $k^{-5/3}$ scaling law suggested by Kolmogorov. Moreover, the normalisation of the velocity fluctuations is in the whole range the same. This suggests that all energy is injected at the largest scales, 10 pc–100 pc.

Remark 7.2: Viscosity: Let us return to the stress tensor of a fluid. In the case of a perfect fluid,

$$\sigma_{ij} = \rho u_i u_j + \delta_{ij} P, \quad (7.56)$$

the stress tensor does not contain velocity gradients $\partial_i u_j$. In order to incorporate friction, we should add a new contribution $\tilde{\sigma}_{ij}$ containing all possible terms constructed out of the velocity u_i and its gradients $\partial_i u_j$. In order to find the most general symmetric tensor of rank two containing these terms, we consider how such a tensor transforms under rotations: The tensor $\tilde{\sigma}_{ij}$ can be split into two irreducible components, a symmetric traceless tensor

$$\partial_i u_j + \partial_j u_i - \frac{2}{3} \delta_{ij} \partial_k u_k, \quad (7.57)$$

and a trace part

$$\delta_{ij} \partial_k u_k. \quad (7.58)$$

The former transforms as a tensor under rotations, the latter as a scalar. A viscous fluid is therefore characterised by two additional material constants, and we define

$$\tilde{\sigma}_{ij} = \eta \left[\partial_i u_j + \partial_j u_i - \frac{2}{3} \delta_{ij} \partial_k u_k \right] + \xi \delta_{ij} \partial_k u_k, \quad (7.59)$$

where η and ξ are called the shear and the bulk viscosity, respectively. We can understand their meaning recalling that any vector field can be decomposed into a rotation and divergence free part. In the case of the velocity, this decomposition corresponds to a splitting into bulk and rotational or shear motion,

$$\mathbf{u} = \nabla s + \nabla \times \mathbf{r}. \quad (7.60)$$

Inserting $\nabla \times \mathbf{r}$ into $\tilde{\sigma}_{ij}$, we see that rotational motion does not contribute to the bulk viscosity. Rotational motion, i.e. the formation of eddies, is however typical for most fluids which are thus characterised by $\eta \gg \xi$. In particular, ξ vanishes for the important cases of a mono-atomic ideal gas or a photon gas. Neglecting thus the bulk viscosity ξ , the Euler equation for the momentum becomes

$$\frac{\partial \mathbf{u}}{\partial t} + (\mathbf{u} \cdot \nabla) \mathbf{u} = -\frac{1}{\rho} \nabla P - \nabla \Phi + \frac{\eta}{\rho} \left[\Delta \mathbf{u} + \frac{1}{3} \nabla (\nabla \cdot \mathbf{u}) \right]. \quad (7.61)$$

Thus we can identify the quotient η/ρ with the kinematic viscosity, $\nu \equiv \eta/\rho$, which we introduced in our intuitive discussion of the viscous term in the fluid equations.

7.3. ***Star formation***

7.3.1. Collaps and fragmentation of gas clouds

Embedded isothermal sphere We have seen that perturbations in the uniform ISM with an enclosed mass larger than the Jeans mass will collapse. Let us consider now as a more realistic example the case of an isothermal sphere embedded in a medium of uniform pressure P_s . The density structure of the isothermal sphere can be obtained from the Lane-Emden equation, cutting of the solution such that the surface pressure equals the external pressure, $P(R) \equiv P_0 = P_s$. For the outer medium, we assume that the E.o.S. of an ideal gas holds.

We can derive the main characteristics for the evolution of the system applying the virial theorem. The internal energy of the isothermal sphere is $U_{\text{kin}} = c_v M T$, while its gravitational energy is $U_{\text{pot}} = \alpha G M^2 / R$, where α is a numerical factor of order one which could be determined by integrating the Lane-Emden equation. Keeping in the virial theorem (3.14) for an ideal gas the surface pressure term,

$$2U_{\text{kin}} + U_{\text{pot}} = 4\pi R^3 P_0, \quad (7.62)$$

and solving for the surface pressure gives

$$P_0 = \frac{c_v M T}{2\pi R^3} - \frac{\alpha G M^2}{4\pi R^4}. \quad (7.63)$$

The first term is proportional to the mean density, M/R^3 , and tries to expand the sphere. The second one due to gravity tries to compress the sphere. How does P_0 changes as function of R ? For $R \rightarrow 0$, P_0 is negative. Increasing R , it changes sign and approaches zero from above for $R \rightarrow \infty$. The maximum of P_0 at R_{max} follows from solving dP_0/dR as

$$R_{\text{max}} = \frac{4\alpha}{9} \frac{G\mu M}{RT}. \quad (7.64)$$

Suppose now that the sphere is in equilibrium with the surrounding gas. For $R < R_{\max}$, the surface pressure decreases with decreasing R . For a small compression, $P < P_0$, and thus the sphere will shrink further and thus collapse. In contrast, for $R > R_{\max}$, the pressure will increase, and the sphere is driven back to the equilibrium radius. Thus we have rederived the Jeans criteria, with

$$R_{\max} = \frac{4\alpha}{9} \frac{G\mu M}{\mathcal{R}T} \quad (7.65)$$

playing the role of the Jeans radius.

For the corresponding Jeans mass we find

$$M_J = \frac{4\pi}{3} \bar{\rho} R_{\max}^3 = \frac{27\sqrt{3}}{16\sqrt{\pi}} \left(\frac{\mathcal{R}T}{\alpha G\mu} \right)^{3/2} \bar{\rho}^{-1/2}. \quad (7.66)$$

Neglecting the numerical prefactor, we can express this as

$$M_J = \left(\frac{\pi\mathcal{R}}{G\mu} \right)^{3/2} T^{3/2} \rho^{-1/2} = 1.2 \times 10^5 M_{\odot} \left(\frac{T}{100\text{K}} \right)^{3/2} \left(\frac{\rho}{10^{-24}\text{g/cm}^3} \right)^{-1/2} \mu^{-3/2} \quad (7.67)$$

For typical values in interstellar clouds of neutral hydrogen, $T = 100\text{ K}$, $\rho = 10^{-24}\text{ g/cm}^3$, and $\mu = 1$, it follows $M_J \sim 10^5 M_{\odot}$. Thus the Jeans mass is much larger than the one of even the most massive stars, corresponding instead to the typical mass of stellar clusters.

Finally, we have to justify our assumption of an isothermal collapse. The free-fall time-scale is of order 10^8 yr , what is much larger than the thermalisation time-scale $\tau_{\text{th}} \sim 100\text{ yr}$. Thus our assumption of an isothermal sphere is well justified.

Fragmentation and minimum mass Since the Jeans mass of a collapsing cloud is for typical conditions in the ISM much larger than stellar masses, an additional fragmentation of the collapsing clouds has to happen. A condition for fragmentation is that the Jeans mass decreases during the collapse. In the case of isothermal collapse, $M_J \propto \rho^{-1/2}$, this condition is indeed satisfied. In contrast, in the case of adiabatic collapse of an mono-atomic ideal gas, $d \ln T / d \ln P = 2/5$ or $T \propto P^{2/5}$. Applying the ideal gas law, $P \propto \rho T$, it follows $T \propto (\rho T)^{2/5}$ or $T^{3/5} \propto \rho^{2/5}$ and thus $T \propto \rho^{2/3}$. Hence the Jeans mass $M_J \propto c_s^3 \rho^{-1/2} \propto T^{3/2} / \rho^{-1/2} \propto \rho^{1/2}$ grows during an adiabatic collapse. We have seen that initially the free-fall time-scale is larger than the thermal time-scale. Thus the collapse proceeds initially isothermally and the cloud can fragment. As a rough criteria for the stop of the fragmentation process we can use $\tau_{\text{ff}} \simeq \tau_{\text{th}}$, i.e. the transition to an adiabatic collapse.

A simple estimate for the limiting mass of the fragmentation process was put forward by Rees. The total energy to be radiated away during the time $(G\rho)^{-1/2}$ of the collapse is half the gravitational potential energy, $\simeq GM^2/R$. The total energy $E = -(3/10)GM^2/R$ changes in time as

$$\frac{\Delta E}{\Delta t} \simeq \frac{GM^2}{R^2} (G\rho)^{1/2} \simeq \frac{G^{3/2} M^{5/2}}{R^{5/2}} \quad (7.68)$$

The cloud cannot radiate more energy than a blackbody at the same temperature, $L = 4\pi R^2 \sigma T^4$. An isothermal collapse requires $\Delta E / \Delta t \gg L$, and the transition to an adiabatic collapse will occur around $\Delta E / \Delta t \simeq L$ or

$$M_{\min}^5 = \frac{64\pi^3}{3} \frac{\sigma^2 T^8 R^9}{G^3} \quad (7.69)$$

Identifying M_{\min} with M_J at the end of the fragmentation process, we obtain

$$M_{\min} \simeq 0.02 M_{\odot} \frac{(T/\text{K})^{1/4}}{f^{1/2}} \quad (7.70)$$

For a numerical estimate, we assume that the deviation from isothermal collapse are sufficiently large at $f = 0.1$ to stop the fragmentation process. Setting also $T = 1000$ K, we find that the minimal masses of the fragments are of the order of $0.1\text{--}1 M_{\odot}$.

Open problems Our simple estimates agree both with the observation that most stars are formed in stellar clusters, with typical cluster masses and the lower limit of stellar masses around $0.1 M_{\odot}$. Our simple one-dimensional model neglects however the effect of rotation and magnetic fields. Both tend to counteract gravitational collapse. Moreover, a one-dimensional model cannot capture the effect of turbulence. Thus more realistic calculations of star formation have to rely on numerical simulations.

It should be clear that the real process of star formation is much more complicated than our 1d estimates. In particular, angular momentum conservation and magnetic flux conservation may obstruct collapse, leading to accretion disks, while turbulence cannot be included in a 1d picture.

7.3.2. Protostars

Let us apply once again the virial theorem for the evolution of a collapsing cloud. The total energy $E = -\alpha GM^2/R$ of a collapsing cloud changes in time as

$$\frac{dE}{dt} = \alpha \frac{GM^2}{R^2} \frac{dR}{dt} \quad (7.71)$$

or

$$-\frac{1}{E} \frac{dE}{dt} = \frac{1}{R} \frac{dR}{dt}. \quad (7.72)$$

Thus the relative decrease of the radius is directly connected to the relative energy release of the cloud: If energy cannot be emitted efficiently, the collapse is slowed down. The isothermal evolution considered in the previous section stops when the energy released cannot be radiated fast enough away. Two alternative processes able to absorb the released gravitational potential energy are the dissociation of H_2 (using 4.5 eV per molecule) and the ionisation of H atoms. Thus the formation of a proto-star can be divided into two stages: Initially, the cloud consists of molecular and atomic hydrogen plus atomic helium. Half of the energy deliberated by the collapse is transferred into the internal energy of the proto-star. In the beginning, the energy is not used to heat the gas, but for its ionization. Only after that, the proto-star heats up and its pressure increases, slowing-down the collapse. Let us now estimate the temperature and the size of a $1M_{\odot}$ cloud after the first stage. If we assume that all released energy is used for the dissociation and ionisation then

$$U_{\text{pot}} = - \left(\frac{1}{2} n_H E_{\text{dis}} + n_H E_{\text{ion}} \right) \quad (7.73)$$

Using then $U_{\text{pot}}/2 = U_{\text{kin}} = 3/2 n_H kT$, the temperature follows as $T \simeq 40.000$ K, while the radius of the cloud is 0.7 AU. Thus the cloud is around $100 R_{\odot}$

Example 7.2: For a $1M_{\odot}$ proto-star with an initial radius $R = 500R_{\odot}$, find the free-fall time $\tau \approx (G\rho)^{1/2}$, the energy released and the average luminosity in the last 100 years of collapse. We use our standard approximation of a spherically symmetric and homogeneous gas cloud,

$$E = \frac{3}{10} \frac{GM^2}{R} \approx 2 \times 10^{45} \text{erg}.$$

The average luminosity is $\langle L \rangle = \Delta E / \Delta t$, or

$$L = \frac{2 \times 10^{45} \text{erg}}{100 \times \pi 10^7 \text{s}} \approx 7 \times 10^{35} \text{erg/s} \approx 170L_{\odot}.$$

Once the luminosity reached typical stellar luminosities, the cloud is called proto-star. For increasing density, the interior becomes more and more opaque to radiation, and finally only the surface can radiate. The central temperature is rising until fusion processes start. At same point, the pressure gradient is large enough to stop the collapse and a stable main sequence star is born.

Regions of star formation

Problems

7.1 Strömgren sphere. a.) Solve the steady state condition $R_{\text{ion}} = R_{\text{rec}}$ for arbitrary x . b.) Show that the decrease in photon flux n_{γ} close to R_{*} is much faster than the geometrical $1/r^2$ suppression.

7.2 Stress tensor. a.) Show that the Euler equation (7.25) with zero external forces \mathbf{f}_{ex} is equivalent to the conservation law $\partial_i \sigma_{ij} = 0$ for a perfect fluid.

8. Accretion, winds, interacting binaries

In this section we will discuss two important situations where accretion plays a role. In the first one, mass flows on a compact object, which may be either a star, a stellar black hole or a supermassive black hole at the center of a galaxy, releasing thereby gravitational potential energy. This mechanism is thought to be the mechanism underlying some of the most energetic events observed in the Universe. The opposite case, a wind, corresponds to a mass out-flow from a massive star (or a galaxy) is an important energy input into the ISM, as well as structuring it. Finally, we discuss interacting binary which are binary star so close that their evolution is influenced by mass flows from one to the other star.

[1]

8.1. Spherical accretion

We start by considering spherically symmetric accretion where gas follows radially in towards a point mass M . This requires that the non-radial velocities are negligible what should be an adequate assumption for sufficiently large distances. The continuity equation becomes then in the stationary case

$$\nabla \cdot (\rho \mathbf{u}) = \frac{1}{r^2} \frac{d}{dr} (r^2 \rho u) = 0 \quad (8.1)$$

with $\mathbf{u} = u \mathbf{e}_r$. Thus $r^2 \rho u = \text{const.}$ and hence the mass flow \dot{M} through a shell at radius r is independent of r ,

$$\dot{M} = 4\pi r^2 \rho u. \quad (8.2)$$

The Euler equation expresses the momentum change of a fluid element due to the pressure gradient and the gravitational force,

$$u \frac{du}{dr} = -\frac{1}{\rho} \frac{dP}{dr} - \frac{GM}{r^2}. \quad (8.3)$$

We want to combine this equation and $r^2 \rho u = \text{const.}$ into a single differential equation for $u(r)$. Using the definition of the sound speed $c_s^2 = dP/d\rho$, we rewrite the first term on the RHS as

$$\frac{1}{\rho} \frac{dP}{dr} = \frac{1}{\rho} \frac{dP}{d\rho} \frac{d\rho}{dr} = c_s^2 \frac{d \ln \rho}{dr}. \quad (8.4)$$

Expressing also $u' \equiv du/dr$ as a logarithmic derivative, Eq. (8.3) becomes

$$u^2 \frac{d \ln u}{dr} = -c_s^2 \frac{d \ln \rho}{dr} - \frac{GM}{r^2}. \quad (8.5)$$

Next we perform the differentiation in $(r^2 \rho u)' = 0$,

$$\frac{2}{r} + \frac{\rho'}{\rho} + \frac{u'}{u} = 0, \quad (8.6)$$

or

$$\frac{d \ln \rho}{dr} = -\frac{2}{r} - \frac{d \ln u}{dr}. \quad (8.7)$$

Now we can eliminate $d \ln \rho/dr$ and obtain

$$u^2 \frac{d \ln u}{dr} = -c_s^2 \left(-\frac{2}{r} - \frac{d \ln u}{dr} \right) - \frac{GM}{r^2} \quad (8.8)$$

and finally

$$(u^2 - c_s^2) \frac{d \ln u}{dr} = \frac{2c_s^2}{r} \left(1 - \frac{GM}{2c_s^2 r} \right). \quad (8.9)$$

It is clear that the radius

$$r_s = \frac{GM}{2c_s^2} \quad (8.10)$$

has a special meaning: Since at $r = r_s$ the RHS vanishes, the fluid velocity u becomes at $r = r_s$ either equal to the sound speed c_s or has there an extremum. Physically, we have to require that the fluid speed u is a monotonic function of the radius r : Either v increases monotonically for increasing r , corresponding to an outflow of mass appropriate for modeling a stellar wind, or u decreases monotonically in the case of accretion. Thus at $r = r_s$ the fluid speed equals the sound speed, and r_s is therefore called “the sonic point.” The condition $u(r_s) = c_s$ means that only one value of \dot{M} is consistent (for given external parameters as M, ρ_∞) with a stationary flow. This is similar to the familiar situation of a bound system in quantum mechanics where the normalization condition imposed on the wave functions allows only discrete values for the energy of the system.

Bondi accretion To proceed we have to specify the equation of state of the gas. We will consider the simplest case of accretion of an isothermal gas that is called Bondi accretion.

For a given temperature of the infalling gas, we know the sound speed c_s and thus r_s . Then the mass inflow \dot{M} is determined via Eq. (8.2). However, in general we want to connect \dot{M} to the measured density at large distances, ρ_∞ . We obtain the relation between ρ_∞ and ρ_s integrating (8.5),

$$\frac{u^2}{2} \Big|_{r_s}^r = -c_s^2 \ln \rho \Big|_{r_s}^r + \frac{GM}{r} \Big|_{r_s}^r \quad (8.11)$$

or with $c_s^2 = \frac{GM}{2r_s}$

$$u^2 = 2c_s^2 \left[\ln \frac{\rho_s}{\rho} - \frac{3}{2} \right] + \frac{2GM}{r}. \quad (8.12)$$

For $r \rightarrow 0$, the velocity is given by $u^2 \rightarrow 2GM/r$, i.e. the gas is in free fall. From the opposite limit, $r \rightarrow \infty$, we find with $u \rightarrow 0$ first $\ln \rho_s/\rho_\infty = 3/2$ and then $\rho_s = \rho_\infty e^{3/2} \approx 4.48\rho_\infty$.

Example 8.3: Find the mass collected by a star with mass $M = M_\odot$ surrounded by a hydrogen cloud with temperature $T = 200$ K and density $n_H = 1 \text{ cm}^{-3}$.

With $r_s = GM_\odot/2c_s^2 \approx 4 \times 10^{11} \text{ cm}$ we obtain

$$\dot{M} = 4\pi r_s^2 \rho_s c_s \sim 3 \times 10^{21} \text{ g/yr}.$$

Thus such a star accretes only 1% of its mass during the age of the universe. One may conclude that accretion cannot be the main responsible for star formation. We will see later that gravita-

tional collapse drives the formation of star (and all other bound system up to super clusters).

8.2. Accretion disks

Accretion disks are naturally formed when angular momentum conservation forces infalling gas into a two-dimensional pancake-like structure. If such a disk is dense enough, viscous processes (i.e. friction between fluid elements with different velocity) can consume angular momentum and heat the disk up.

Consider a mass element dM falling from a Keplerian orbit at $r + dr$ to r due to viscous interactions. Half of the gain in potential energy is used to increase the kinetic energy of the mass element, while the other half is radiated away and heats up the environment,

$$dE_{\text{heat}} = \frac{1}{2} \left(\frac{GMdM}{r} - \frac{GMdM}{r + dr} \right). \quad (8.13)$$

Assuming that the accretion is stationary, the produced heat equals the emitted radiation. Thus the luminosity of the accretion disk emitted by the shell at radius r is given by

$$dL = \frac{dE_{\text{heat}}}{dt} = 2(2\pi r)dr\sigma T^4 = \frac{1}{2} \frac{GM\dot{M}}{r} [1 - (1 - dr/r + \dots)] = \frac{1}{2} \frac{GM\dot{M}dr}{r^2}, \quad (8.14)$$

where we used the Stefan-Boltzmann law and the factor two accounts for the “top” and “bottom” side of the disk. The temperature profile follows as

$$T(r) = \left(\frac{GM\dot{M}}{8\pi\sigma r^3} \right)^{1/4} \propto r^{-3/4}. \quad (8.15)$$

Example: Estimate the maximal temperature of the accretion disk, the peak wave-length and the luminosity of the emitted blackbody radiation for the case of i) a neutron star, ii) a white dwarf star, and iii) supermassive black hole.

The total luminosity can be obtained integrating Eq. (8.14) from the inner to the outer edge of the disc,

$$L_{\text{tot}} = \frac{1}{2}GM\dot{M} \int_{r_{\text{in}}}^{r_{\text{out}}} \frac{dr}{r^2} = \frac{1}{2}GM\dot{M} \left(\frac{1}{r_{\text{in}}} - \frac{1}{r_{\text{out}}} \right) \approx \frac{1}{2} \frac{GM\dot{M}}{r_{\text{in}}} \quad \text{for } r_{\text{in}} \ll r_{\text{out}}. \quad (8.16)$$

In order to estimate the maximal efficiency of accretion, we compare L_{tot} with the total rest mass of the accreted material, $\dot{M}c^2$. Expressing r_{in} by the Schwarzschild radius, $r_{\text{in}} = xR_s = 2xGM/c^2$, we see that the efficiency is of order $\eta = L_{\text{tot}}/(\dot{M}c^2) = 1/(4x)$. Hence the efficiency to release energy by accretion can be very large, if the disk extends close to the last stable circular orbit of the black hole. Our estimate neither takes into account general relativistic effects nor how much energy is transferred by viscous effects into heat and how much energy is swalled by the black hole. Numerical studies of the accretion process show that the efficiency is strongly correlated to the ratio of mass inflow and the Eddington luminosity, $\dot{M}c^2/L_{\text{Edd}}$: For $\dot{M}c^2$ close to L_{Edd} , the efficiency can reach $\sim 10\%$, while the efficiency decreases to $\sim 10^{-4}$ for $\dot{M}c^2 \ll L_{\text{Edd}}$.

A more accurate expression of the temperature profile of an accretion disk is

$$T(r) = \left(\frac{3GM\dot{M}}{8\pi\sigma r^3} \right)^{1/4} \left(1 - \sqrt{\frac{R_{\text{in}}}{r}} \right)^{1/4} \quad (8.17)$$

We can obtain the spectral distribution of the emitted photon energies by integrating over the radial distribution,

$$L_\nu = 2\pi \int_{r_{\text{in}}}^{r_{\text{out}}} dr r (\pi B_\nu) \propto \nu^3 \int_{r_{\text{in}}}^{r_{\text{out}}} \frac{dr r}{\exp[h\nu/(kT)] - 1}. \quad (8.18)$$

Substituting $x = h\nu r^{3/4}/k$, it follows

$$L_\nu \propto \nu^{1/3} \int_{x_{\text{in}}}^{x_{\text{out}}} dx \frac{x^{5/3}}{e^x - 1}. \quad (8.19)$$

Hence the spectral luminosity is $L_\nu \propto \nu^{1/3}$ in the frequency range where the integral is dominated by intermediate r values, $r_{\text{in}} \ll r \ll r_{\text{out}}$. At low frequency, the spectral luminosity is dominated by the Rayleigh-Jeans tail of the outer edge of the disk, $L_\nu \propto \nu^2$, while for frequencies above $kT(r_{\text{in}})/h$ the spectrum is exponentially suppressed.

8.3. ***Winds***

Stellar winds In the case of stellar winds, we have to account in addition to the gas pressure for the pressure of radiation. Thus while both the mass continuity equation and the Euler equation remain the same, we have to use $P = P_{\text{gas}} + P_{\text{rad}}$ in the latter,

$$u \frac{du}{dr} = -\frac{1}{\rho} \frac{dP}{dr} - \frac{GM}{r^2}. \quad (8.20)$$

For the gradient of the radiation pressure, we re-use our results from section 3.3, Eq. (3.31),

$$\frac{dP_{\text{rad}}}{dr} = -\frac{\kappa\rho}{c} \mathcal{F} = -\frac{\kappa\rho}{c} \frac{L}{4\pi r^2}. \quad (8.21)$$

Inserting into the Euler equation, we find

$$u \frac{du}{dr} = -\frac{1}{\rho} \frac{dP_{\text{gas}}}{dr} - \frac{GM}{r^2} \left(1 - \frac{\kappa\rho}{c} \frac{L}{4\pi GM} \right) = -\frac{1}{\rho} \frac{dP_{\text{gas}}}{dr} - \frac{GM}{r^2} \left(1 - \frac{L}{L_{\text{Edd}}} \right). \quad (8.22)$$

As expected, the radiation pressure balances for $L = L_{\text{Edd}}$ the gravitational force. Thus we expect outflows and stellar winds for $L > L_{\text{Edd}}$. Compared to the case of accretion, one more variable, \mathcal{F} or L , enters the equation. Therefore we need in addition equations for energy conservation and transport. For the energy transport, we can re-use our result from section 3.3. For energy conservation, we use the first law of thermodynamics in Eulerian form 7.26, setting energy generation term Q to zero and assuming spherical symmetry,

Galactic winds Milky Way, starburst galaxies

8.4. *** Interacting binaries ***

50%–80% of all stars are gravitationally bound in multiple star systems, most of them in binary systems.

For instance, 50 binaries, 14 triple and three systems with four stars were known up to a distance of 10 pc from the Sun in the year 1980. For solar-type stars, the ratio of single:double:triple:quadruple stars is 45:46:8:1. On the other hand, most dwarf stars that are more difficult to detect are isolated stars.

Interacting binaries are divided into detached binaries, semi-detached binaries and contact binaries. In the first case neither of the stars fills its Roche lobe, while in the second case one of the two stars fills its Roche lobe completely. In the last case, the atmospheres of the two stars overlap and form a single peanut-like object.

Roche lobes We consider a binary system in a corotating coordinate system, i.e. the one where the two stars are at rest. For simplicity, we assume that the stars move on circular orbits. Additionally to the gravitational force from the two stars, a test particle will feel in this rotating system a centrifugal force (and, if it is moving, also a Coriolis force.)

The equipotential lines for a binary system are in the plan of the orbit

$$\Phi = -G \left(\frac{M_1}{r_1} + \frac{M_2}{r_2} \right) - \frac{1}{2} \omega^2 r^2, \quad (8.23)$$

where r_i is the distance from the test particle to the mass M_i and r to the center of mass, respectively, while ω is the rotation velocity. The potential Φ goes to $-\infty$ for $r_{1/2} \rightarrow 0$ and $r \rightarrow \infty$. Therefore it has five extrema, three along the line connecting the two stars and two forming equilateral triangles. These extrema are called Lagrangian points, L1, . . . , L5, ordered according $\Phi(L1) < \dots < \Phi(L5)$.

From Kepler's law,

$$\omega^2 = \frac{G(M_1 + M_2)}{a^3}. \quad (8.24)$$

In Fig. 8.1, we show the resulting equipotential lines for two stars with mass ratio $M_1/M_2 = 5$. Since the effective force is perpendicular to the equipotential surface, $\mathbf{F} = -m\nabla\Phi$, hydrostatic equilibrium means that equipotential surfaces are also surfaces of constant density of a star. Hence stars in close binary systems can become strongly deformed and, if they fill the Roche lobe, a mass flow to the companion star results.

Evolution of interacting binaries We consider the evolution of a close binary system. For simplicity, we assume that the two stars move on circular orbits. Thus their angular momentum L is

$$L = \left(\frac{Ga}{m_1 + m_2} \right)^{1/2} m_1 m_2. \quad (8.25)$$

Taking the logarithmic derivative of this expression, accounting for angular momentum and mass conservation gives

$$\frac{dL}{L} = \frac{dm_1}{m_1} + \frac{dm_2}{m_2} + \frac{da}{2a} = 0. \quad (8.26)$$

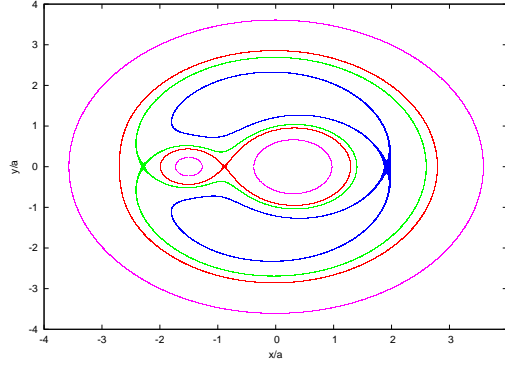


Figure 8.1.: Equipotential surfaces in units of $G(M_1 + M_2)/a$ for two stars with mass ratio $M_1/M_2 = 5$; The (inner) red figure-of-eight corresponds to the Roche lobe, Lagrange point L1 at the “crossing”, Lagrange point L2 and L3..., and maxima L4 and L5 at...

Mass conservation $m_1 + m_2 = \text{const.}$ implies also $dm_1 = -dm_2$ and dividing also by dt , we obtain as connection between mass flows \dot{m}_i and the change of the orbital radius

$$\frac{\dot{a}}{a} = 2 \frac{\dot{m}_2}{m_2} \left(\frac{m_2}{m_1} - 1 \right). \quad (8.27)$$

Not that the change of $|\dot{a}/a|$ increases, the more the masses of the binary system differ. Let us label the stars such that we have a mass flow from star 1 to 2, $\dot{m}_2 > 0$. Then the distance a increases if $m_2 > m_1$, and decreases if $m_2 < m_1$. Hence if mass flows from the heavier to the lighter star, their separation decreases. As a result, the Roche radius is reduced and accretion enhanced, leading to further shrinkage of the orbit. This positive feedback leads fast to a common-envelope system where

8.5. *** Gravitational wave emission and binary mergers ***

Gravitational wave luminosity Maxwell’s theory replaced the instantaneous Coulomb interaction law by the interaction of charges with electromagnetic fields that carry energy and momentum. In particular, we used in Sec. ?? that an accelerated system of electric charges emits electromagnetic dipole radiation with luminosity

$$L_{\text{em}} = \frac{2}{3c^3} |\ddot{\mathbf{d}}|^2, \quad (8.28)$$

where the dipole moment of a collection of N charges at positions \mathbf{x}_i is $\mathbf{d} = \sum_{i=1}^N q_i \mathbf{x}_i$.

Einstein’s general theory of relativity predicts in an analogous way the existence of gravitational waves, which one can imagine as ripples in space-time that carry away energy and momentum with the speed of light. Since q^2 and GmM have the same dimension, one might guess that for the emission of gravitational radiation the replacement $q^2 \rightarrow GmM$ in the dipole formula should give qualitatively the correct result. But since $\sum m_i \dot{\mathbf{x}}_i = \mathbf{p}_{\text{tot}} = \text{const.}$, momentum conservation implies that the change in the dipole moment of a mass distribution is zero. Therefore gravitational radiation contains no dipole contribution and the first

non-zero term in the multipole expansion of gravitational wave emission is the quadrupole term,

$$Q_{ij} = \sum_{k=1}^N m^{(k)} (x_i x_j - \frac{1}{3} \delta_{ij} r^2). \quad (8.29)$$

The resulting luminosity emitted into gravitational waves is given by

$$L_{\text{gr}} = \frac{G}{5c^5} \sum_{i,j} |\ddot{Q}_{ij}|^2. \quad (8.30)$$

Example 8.4: a.) Show that q^2 and GmM have the same dimension. Derive b.) $L_{\text{em}} \propto d^2/c^3$ and $L_{\text{gr}} \propto GQ^2/c^5$ using dimensional analysis.

a. We start inverting the definition of Sommerfeld's fine structure constant, $e^2 = \hbar c \alpha$. Thus the dimension of the electric charge squared is $[e^2] = \text{erg} \times \text{cm}$. Setting $[e^2]$ equal to the dimension of $[GmM] = \text{g cm}^3/\text{s}^2$ and using $\text{erg} = \text{g cm}^2/\text{s}^2$ shows that the statement is indeed correct.

b. In the case of electromagnetic dipole radiation, we use again $[e^2] = \text{erg} \times \text{cm}$, while the definition (9.31) implies $[\ddot{Q}] = \text{g cm}^2/\text{s}^3$. Then we compare

$$[L_{\text{em}}] = \frac{\text{erg}}{\text{s}} \stackrel{!}{=} \frac{\text{s}^3}{\text{cm}^3} \times \text{erg} \times \text{cm} \times \frac{\text{cm}^2}{\text{s}^4} = \frac{\text{erg}}{\text{s}},$$

which agrees with the definition of luminosity as energy/time. In the same way, we can show that the luminosity of gravitational quadrupole radiation is proportional to c^a with $a = -5$: The unique solution for a from

$$[L_{\text{gr}}] = \frac{\text{erg}}{\text{s}} = \frac{\text{g cm}^2}{\text{s}^3} \stackrel{!}{=} \frac{\text{cm}^3}{\text{g s}^2} \times \frac{\text{cm}^a}{\text{s}^a} \times \frac{\text{g}^2 \text{cm}^4}{\text{s}^6}$$

is $a = -5$.

Evolution of binary systems The emission of gravitational radiation is negligible for most systems where Newtonian gravity is a good approximation. One of the rare examples where general relativistic effects can become important are close binary systems of compact stars. Let us estimate the change in the orbital period for such a binary system. We start recalling that the energy of binary system with total mass $M = m_1 + m_2$ and separation a is given by (cf. with ??)

$$E = \frac{1}{2} \mu \omega^2 a^2 - \frac{G\mu M}{a} = -\frac{G\mu M}{2a}. \quad (8.31)$$

For simplicity, we assume in the following circular orbits. Evaluating then the tensor of inertia (9.31) for a binary and inserting the result into (9.32) gives (cf. problem)

$$L_{\text{gw}} = \frac{32 G^4 \mu^2 M^3}{5 a^5}. \quad (8.32)$$

Time evolution of a merger Let us now discuss qualitatively the time evolution of a close binary system. Equating the change of the energy of the binary system and the gravitational wave luminosity, it is

$$-\frac{dE}{dt} = L_{\text{gw}} = \frac{32 G^4 \mu^2 M^3}{5 a^5}. \quad (8.33)$$

Next we can relate the relative changes per time in the orbital period P , the separation a and the energy E using $E \propto 1/a$ and $P \propto a^{3/2}$ as

$$\frac{\dot{E}}{E} = -\frac{\dot{a}}{a} = -\frac{2\dot{P}}{3P}. \quad (8.34)$$

Solving first for the change in the period,

$$\dot{P} = \frac{3 L_{\text{gw}}}{2 E} P = -\frac{96 G^3 \mu M^2}{5 a^4} P, \quad (8.35)$$

and eliminating then a gives

$$\dot{P} = -\frac{96}{5} (2\pi)^8 G^{5/3} \mu M^{2/3} P^{-5/3}. \quad (8.36)$$

Thus the orbital period decreases due to the emission of gravitational waves.

Hulse-Taylor pulsar The first example for a close binary systems of compact stars was found 1974 by Hulse and Taylor who discovered a pulsar in a binary system via the Doppler-shift of its radio pulses. The extreme precision of the periodicity of the pulsar signal makes such binary systems to an ideal laboratory to test various effect of special and general relativity:

- The pulsar's orbital speed changes by a factor of four during its orbit and allows us to test the usual (special relativistic) Doppler effect.
- At the same time, the gravitational field alternately strengthens at periastron and weakens at apastron, leading to a periodic gravitational redshift of the pulse.
- The small size of the orbit leads to a precession of the Perihelion by $4.2^\circ/\text{yr}$.
- The system emits gravitational waves and loses thereby energy. As a result the orbit of the binary shrinks by $4\text{mm}/\text{yr}$.

Let us now compare the observed change in the orbit of the binary with the prediction of general relativity. The binary system consists of a pulsar with mass $m_1 = 1.44M_\odot$ and a companion with mass $m_2 = 1.34M_\odot$. Their orbital period is $P = 7\text{h}40\text{min}$ on an orbit with rather strong eccentricity, $e = 0.617$. In this case, the emission of gravitational radiation is strongly enhanced compared to an circular orbit,

$$\dot{P}(e) = \dot{P}(0) \frac{1 + \frac{73}{24}e^2 + \frac{37}{96}e^4}{(1 - e^2)^{7/2}} \simeq -2.4 \times 10^{-12} \quad (8.37)$$

This results is in excellent agreement with the prediction of general relativity, cf. Fig. ??.

Coalescence of binaries Let us now discuss the (final stage) in the time evolution of a close binary system. Combining (9.35) and (9.36), we obtain

$$\dot{a} = \frac{2\dot{P}}{3P}a = -\frac{64 G^3 \mu M^2}{3 a^3}. \quad (8.38)$$

Separating variables and integrating, we find

$$a^4 = \frac{256}{5} G^3 \mu M^2 (t - t_c). \quad (8.39)$$

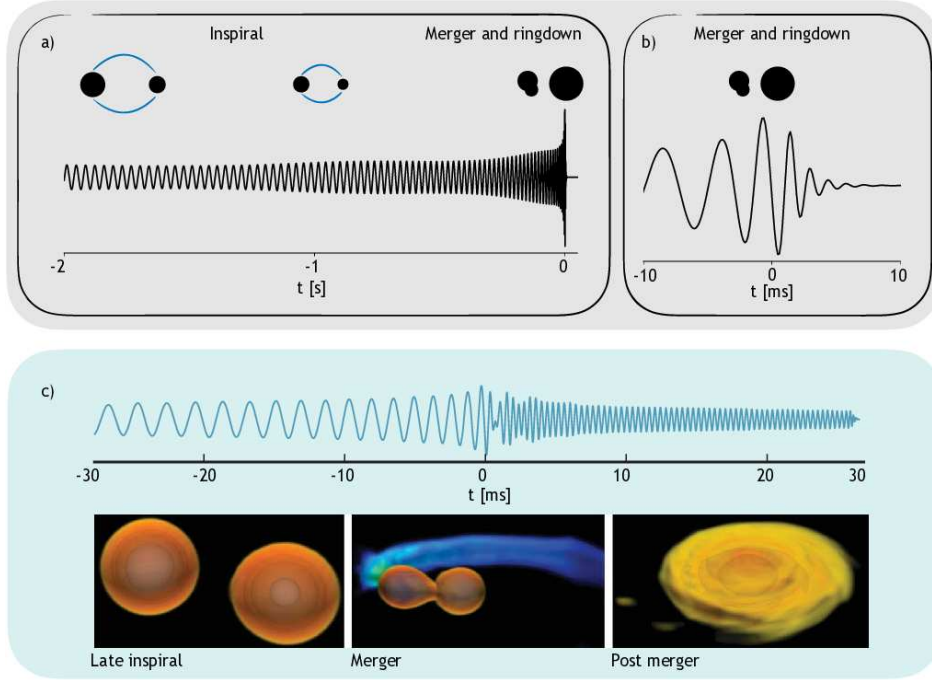


Figure 8.2.: Typical waveforms for the merger of black hole (upper) and neutrons star (lower panel) binaries.

Here, t_c denotes the (theoretical) coalescence time for point-like stars. With the initial condition $a(t = 0) = a_0$, it follows

$$a(t) = a_0 \left(1 - \frac{t}{t_c}\right)^{1/4} \quad (8.40)$$

and

$$t_c = \frac{5}{256} \frac{a_0^4}{G^3 \mu M^2}. \quad (8.41)$$

In the lectures Gravitation and Cosmology, you can learn that the amplitude of the GW is inverse proportional to the separation a of the binary system, Moreover, the emitted gravitational wave is monochromatic, with frequency twice the orbital frequency of the binaries,

$$\nu_{\text{GW}} = \frac{2\omega}{2\pi} = \frac{2}{P} = \frac{(GM)^{1/2}}{\pi a^{3/2}} = \nu_0 \left(1 - \frac{t}{t_c}\right)^{-3/8}. \quad (8.42)$$

Thus, the amplitude $h(t)$ of the gravitational wave signal increases with time as

$$h(t) \propto \frac{1}{a} \propto (t - t_c)^{-1/4}. \quad (8.43)$$

Expressed as function of the frequency ν_{GW} , the amplitude becomes

$$h(t) = \frac{4G\mu M}{a} = 4G\mu M \frac{\omega^{2/3}}{(GM)^{1/3}} \equiv 4\pi^{2/3} G^{2/3} \mathcal{M}^{5/3} \nu_{\text{GW}}^{2/3}. \quad (8.44)$$

In the last step, we introduced the chirp mass,

$$\mathcal{M} \equiv \mu^{3/5} M^{2/5} = \frac{(m_1 m_2)^{3/5}}{(m_1 + m_2)^{1/5}}, \quad (8.45)$$

which is the combination of the masses m_1 and m_2 easiest to extract from the gravitational wave signal. Both the amplitude and the phase evolution of the gravitational wave signal provide information on the chirp mass \mathcal{M} .

A typical wave-form of the merger of a black hole binary is shown in the upper panel of Fig. 8.2. It consists of the waves emitted during the inspiral (“the chirp”), the merger, and the ring-down. In this last phase, oscillations of the BH formed during the merger are damped by the emission of GWs and decay exponentially, leading to standard Kerr BH. The frequencies and the damping times of the eigenmodes of a BH can be calculated, and thus the ring-down provides additional opportunities to test GR. The lower panel of Fig. 8.2 shows a typical wave-form of a neutron star merger: When tidal interactions start to deform the neutron stars, the gravitational wave signal is not monochromatic anymore and the structure of the stars has to be accounted for.

8.6. Tidal disruption events

At the center of most galaxies, a supermassive black hole (SMBH) with mass $\gtrsim 10^5 \mathcal{M}_\odot$ is thought to reside, surrounded by a nuclear star cluster or bulge [?]. Stars in such dense environments undergo two-body scattering with other stars, which sometimes takes them on nearly elliptical orbits close to the SMBH. If the pericenter distance is so small that the stellar self-gravity is smaller than the tidal forces exerted by the SMBH, it is tidally disrupted. The processes following the disruption may generate a burst of radiation luminous enough to outshine entire host galaxies. Such events are called tidal disruption events (TDEs).

Problems

8.3 .. Derive

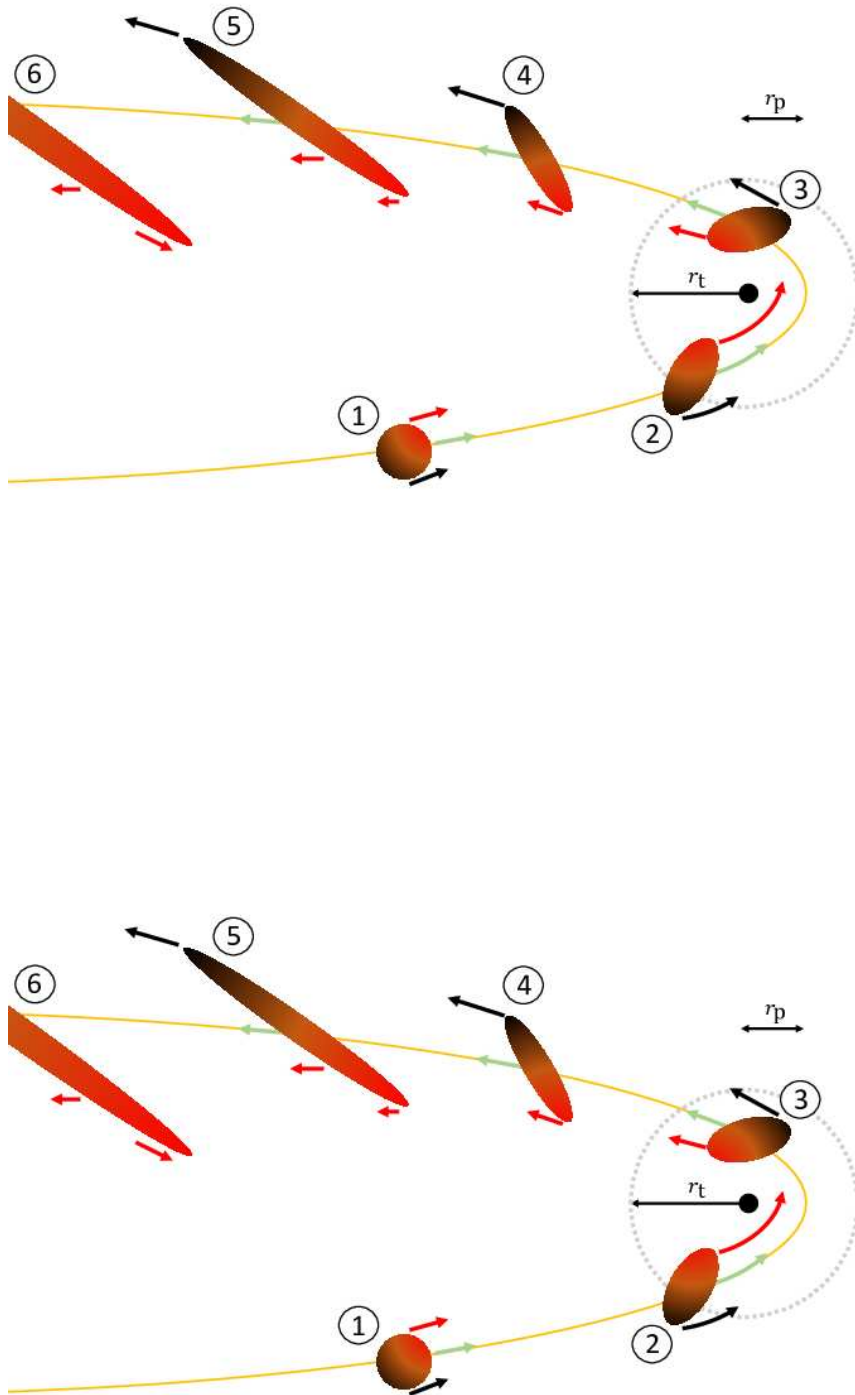


Figure 8.3.: A schematic diagram showing a disruption event of a star. The *top* panel depicts successive moments of the disruption from the initial approach of the star (1) on a parabolic orbit (counterclockwise) with pericenter distance $r_p < r_t$ around a

9. *** Elements of general relativity and applications ***

an appetizer for those interested...

A relativistic theory of gravity is required for the description of either very strong or very extended gravitational fields. More precisely, a non-relativistic description of gravity is sufficient, if the Newtonian gravitational potential is small compared to the squared speed of light, $|\Phi/c^2| \ll 1$, and the considered distances and velocities are so small that retardation effects can be neglected, $v \ll c$. The first successful example of a relativistic theory of gravity was general relativity developed by Einstein between 1907 and 1915. This theory has passed all experimental tests until present.

In astrophysics, we expect to need a relativistic theory of gravity as Einstein's theory of general relativity in two cases: First for the description of compact object as neutron stars or black holes where $|\Phi| = GM/r$ approaches c^2 close to the compact object. Second for the universe on the largest scales where retardation effects become important and the approximation of an instantaneous interactions fails. A self-consistent introduction into Einstein's theory of general relativity requires to develop a considerable mathematical framework. Fortunately, the salient features of relativistic gravity close to stars and in cosmology can be understood without the need to employ the full formalism of general relativity—if one is willing to accept an heuristic derivation of our initial equations.

9.1. Basic properties of gravitation

We start by reviewing three basic properties of gravitation.

- 1.) The idea underlying the equivalence principle emerged in the 16th century, when among others Galileo Galilei found experimentally that the acceleration g of a test mass in a gravitational field is universal. Because of this universality, the gravitating mass $m_g = F/g$ and the inertial mass $m_i = F/a$ are identical in classical mechanics, a fact that puzzled already Newton. While $m_i = m_g$ can be achieved for one material by a convenient choice of units, there should be in general deviations for test bodies with differing compositions.

Knowing more forces, this puzzle becomes even stronger: Contrast the acceleration of a particle in a gravitational field to the one in a Coulomb field. In the latter case, two independent properties of the particle, namely its charge q determining the strength of the electric force acting on it and its mass m_i , i.e. the inertia of the particle, are needed as input in the equation of motion. In the case of gravity, the “gravitational charge” m_g coincides with the inertial mass m_i .

The equivalence of gravitating and inertial masses has been tested already by Newton

and Bessel, comparing the period P of pendula using different materials,

$$P = 2\pi \sqrt{\frac{m_i l}{m_g g}}, \quad (9.1)$$

but finding no measurable differences. The first precision experiment giving an upper limit on deviations from the equivalence principle was performed by Loránd Eötvös in 1908 using a torsion balance. Current limits for departures from universal gravitational attraction for different materials are $|\Delta g_i/g| < 10^{-12}$.

- 2.) Newton's gravitational law postulates as the latter Coulomb law an instantaneous interaction. Such an interaction is in contradiction to special relativity. Thus, as interactions of currents with electromagnetic fields replace the Coulomb law, a corresponding description should be found for gravity. Moreover, the equivalence of mass and energy found in special relativity requires that not only mass but all forms of energy should couple to gravity: Imagine a particle-antiparticle pair falling down a gravitational potential well, gaining energy and finally annihilating into two photons moving the gravitational potential well outwards. If the two photons would not lose energy climbing up the gravitational potential well, a perpetuum mobile could be constructed. If all forms of energy act as sources of gravity, then the gravitational field itself is gravitating. Thus the theory is non-linear and its mathematical structure is much more complicated than the one of electrodynamics.
- 3.) Gravity can be switched-off locally, just by cutting the rope of an elevator: Inside a freely falling elevator, one does not feel any gravitational effects except for tidal forces. The latter arise if the gravitational field is non-uniform and tries to stretch the elevator. Inside a sufficiently small freely falling system, also tidal effects play no role. This allows us to perform experiments like the growing of crystals in "zero-gravity" on the International Space Station which is orbiting only at an altitude of 300 km.

Motivated by 2.), Einstein used 1.), the principle of equivalence, and 3.) to derive general relativity, a theory that describes the effect of gravity as a deformation of the space-time known from special relativity.

In general relativity, the gravitational force of Newton's theory that accelerates particles in an Euclidean space is replaced by a curved space-time in which particles move force-free along geodesic lines. In particular, photons move still as in special relativity along curves satisfying $ds^2 = 0$, while all effects of gravity are now encoded in the form of the line-element ds . Thus all information about the geometry of a space-time is contained in the metric $g_{\mu\nu}$ in front of the infinitesimal displacements dx^i ,

$$ds^2 = \sum_{\mu, \nu=0}^3 g_{\mu\nu} dx^\mu dx^\nu. \quad (9.2)$$

Switching on a gravitational field, the metric $g_{\mu\nu}$ introduced in Chap. ?? cannot be transformed by a coordinate change into the form $g_{\mu\nu} = \text{diag}(1, -1, -1, -1)$. Einstein's field equation tells us how space-time is curved by matter and at the same time how matter moves in a curved space-time. We will circumvent the use of this equation, using symmetry arguments and the known non-relativistic limit to guess the correct form of $g_{\mu\nu}$.

9.2. Schwarzschild metric

The mathematical structure of Einstein's theory is much more complicated than the one of Newton's, and therefore no analytical solution to the two-body problem is known. Instead, we are looking first for the effect of a finite point-mass on the surrounding space-time and consider then the motion of a test particle or light-ray in this space-time. Using the field equations of general relativity, we would have to determine first the metric $g_{\mu\nu}(x)$ (or equivalently the line-element ds) of the space-time for the given mass distribution and then find its geodesics. We use instead the following heuristic derivation of the space-time around a (non-rotating) point mass as short-cut.

Heuristic derivation Consider a space ship moving freely without using its rocket propellers in the gravitational field of a radial-symmetric mass distribution with total mass M . Since the space ship is freely falling, no effects of gravity are felt inside and the space-time coordinates from $r = \infty$ should remain valid in the space ship. Let us call these coordinates K_∞ with x_∞ (parallel to the movement of the space ship), y_∞, z_∞ (transverse) and t_∞ . The space ship has the velocity v at the distance r from the mass M , measured in the coordinate system $K = (r, \phi, \vartheta, t)$ in which the mass M at $r = 0$ is at rest.

We assume that special relativity can be used for the transformation between the coordinate systems K and K_∞ which are moving with the relative velocity $v = \beta c$ as long as the gravitational field is weak. We shall see shortly what "weak" means in this context. For the moment, we presume that the effects of gravity are small as long as the velocity v of the space ship that was at rest at $r = \infty$ is still small compared to the velocity of light, $v \ll c$. Applying then the usual rules for a Lorentz transformation between two inertial frames, we obtain

$$dt_\infty = dt\sqrt{1 - \beta^2}, \quad dy_\infty = r d\vartheta \quad (9.3a)$$

$$dx_\infty = \frac{dr}{\sqrt{1 - \beta^2}}, \quad dz_\infty = r \sin \vartheta d\phi. \quad (9.3b)$$

Thus the line-element of special relativity, i.e. the infinitesimal distance between two space-time events in Minkowski space,

$$ds^2 = c^2 dt_\infty^2 - dx_\infty^2 - dy_\infty^2 - dz_\infty^2, \quad (9.4)$$

becomes

$$ds^2 = (1 - \beta^2)c^2 dt^2 - \frac{dr^2}{1 - \beta^2} - r^2(d\vartheta^2 + \sin^2 \vartheta d\phi^2). \quad (9.5)$$

Here, $d\vartheta^2 + \sin^2 \vartheta d\phi^2$ is the usual expression for the angular variables in spherical coordinates, while the time and radial distance are modified by the prefactor $(1 - \beta^2)^{\pm 1}$. Next, we want to relate this factor to the quantities M and r . Consider the energy of the space ship with rest mass m ,

$$(\gamma - 1)mc^2 - \frac{G\gamma mM}{r} = 0, \quad (9.6)$$

where the first term is its kinetic energy and the second the Newtonian expression for its potential energy. According to 2.), we made here the crucial assumption that gravity couples

not only to the mass m of the space ship but to its total energy γmc^2 . Dividing by γmc^2 gives

$$\left(1 - \frac{1}{\gamma}\right) - \frac{GM}{rc^2} = 0. \quad (9.7)$$

The quantity $R_g \equiv GM/c^2$ has the dimension of a length and is numerically given by

$$R_g \equiv \frac{GM}{c^2} \simeq 1.5 \text{ km} \frac{M}{M_\odot}. \quad (9.8)$$

Because R_g contains both the natural constants G and c , it combines gravity and special relativity. Therefore we expect that this length determines the distance from the mass M where deviations from the Newtonian prediction become large. Remembering the definition $\gamma = 1/\sqrt{1 - \beta^2}$, we have

$$\sqrt{1 - \beta^2} = 1 - \frac{R_g}{r} \quad (9.9)$$

or

$$1 - \beta^2 = 1 - \frac{2R_g}{r} + \frac{R_g^2}{r^2} \simeq 1 - \frac{2R_g}{r}. \quad (9.10)$$

In the last step, we neglected the term $(R_g/r)^2$, since we attempt only an approximation valid for large distances $r \gg R_g$, where gravity is still weak. Inserting this expression into Eq. (9.5), we obtain the metric describing the gravitational field produced by the mass M ,

$$ds^2 = \left(1 - \frac{2R_g}{r}\right) c^2 dt^2 - \left(1 - \frac{2R_g}{r}\right)^{-1} dr^2 - r^2(d\vartheta^2 + \sin^2 \vartheta d\phi^2). \quad (9.11)$$

Somewhat surprisingly, our approximation agrees with the exact result found by Karl Schwarzschild 1916 for the line-element describing the space-time outside a radial-symmetric, non-rotating mass distribution with total mass M .

Correction to the gravitational potential The Schwarzschild metric (9.11) does not depend on time and the metric is therefore static. Moreover, the only dependence on the angular variables ϑ and ϕ is contained in $d\vartheta^2 + \sin^2 \vartheta d\phi^2$, which is the usual rotation-invariant surface element $d\Omega$ of a two-dimensional sphere. Thus the motion of a test particle around a point mass conserves also in general relativity energy and angular momentum. Using these two conserved quantities, one can solve the equation of motion for a test particle in the Schwarzschild metric. One finds that its energy can be, as in the Newtonian case, divided into kinetic and potential energy. The radial movement of a test particle corresponds to the one in an effective potential

$$\Phi_{\text{eff}} = -\frac{GM}{r} + \frac{l^2}{2r^2} - \frac{GMl^2}{c^2 r^3} = \Phi_0 - \frac{GMl^2}{c^2 r^3} \quad (9.12)$$

with $\Phi = V/m$ and $l = L/m$ as the potential energy and the angular momentum per mass of the test particle, respectively. The effective potential Φ_{eff} contains apart from the Newtonian part $\Phi_0 = -GM/r + l^2/(2r^2)$ consisting of the $1/r$ potential and the centrifugal barrier $l^2/(2r^2)$ the additional term $\Phi_{\text{GR}} = GMl^2/(c^2 r^3)$. The latter vanishes in the limit of an instantaneous interaction, $c \rightarrow \infty$, bringing us back to Newtonian gravity. Less formal, this limit should correspond to small velocities, $v \ll c$. We can see this correspondance if we use

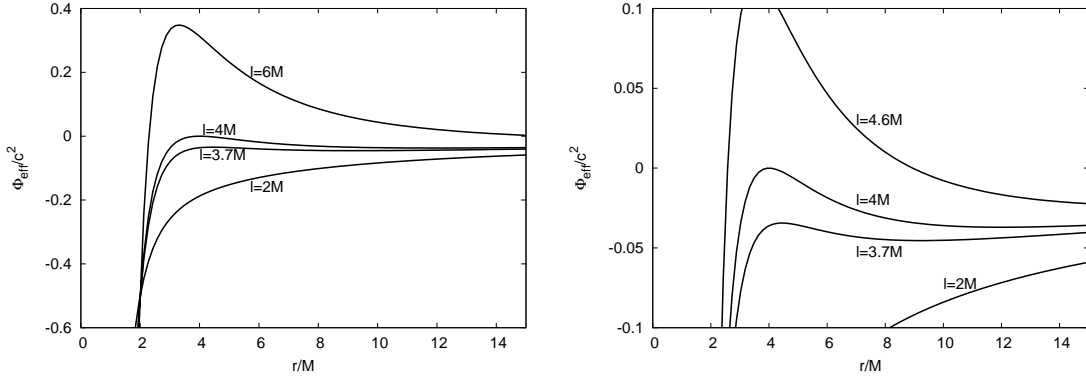


Figure 9.1.: The effective potential Φ_{eff}/c^2 for various values of l/M as function of the distance r/R_g , for two different scales. $M \rightarrow R_g$

the virial theorem, $GM/r \sim v^2$, to express r by v . Using additionally $l \sim vr$, we find as estimate for the size of the general relativistic correction

$$\Phi_{\text{GR}} = \frac{GMl^2}{c^2 r^3} \sim \frac{v^2 l^2}{c^2 r^2} \sim \frac{v^4}{c^2}.$$

Thus the correction Φ_{GR} is negligible, $\Phi_{\text{GR}}/c^2 \ll 1$, for small velocities or equivalently at large distances from the star.

The asymptotic behavior of Φ_{eff} for $r \rightarrow 0$ and $r \rightarrow \infty$ is

$$\Phi_{\text{eff}}(r \rightarrow \infty) \rightarrow -\frac{GM}{r} \quad \text{and} \quad \Phi_{\text{eff}}(r \rightarrow 0) \rightarrow -\frac{GMl^2}{c^2 r^3}, \quad (9.13)$$

while $\Phi_{\text{eff}}(2R_g) = 1/(2c^2)$ is independent of the mass M . Next we determine the extrema of Φ_{eff} by solving $d\Phi_{\text{eff}}/dr = 0$ and find

$$r_{1,2} = \frac{l^2}{2GM} \left[1 \pm \sqrt{1 - 12 \left(\frac{GM}{cl} \right)^2} \right]. \quad (9.14)$$

Hence the potential has no extrema for $l/(cR_g) > \sqrt{12}$ and is always negative, cf. with Fig. 9.1: Consequently, a particle can reach $r = 0$ for small enough but finite angular momentum, in contrast to the Newtonian case. By the same argument, there exists a last stable circular orbit at $r = 6R_g$, when the two extrema r_1 and r_2 coincide for $l/(cR_g) = \sqrt{12}$.

The existence of a *last stable orbit* has some important observational consequence. Gas flowing e.g. from a companion star to a black hole forms an accretion disk, settling into circular orbits. As the gas loses angular momentum by viscous interactions, it moves inwards and heats up until it reaches the last stable orbit at $r = 6R_g$. From there on it will spiral fast into the black hole, taking along almost all of its remaining potential energy. We will show in chapter 8.2 that the maximal temperature of the accretion disk is determined by its minimal radius and thus by the black hole mass. Measuring the temperature of accretion disks allows thus astronomers to estimate the mass of a black holes. Hence we found the important implication that an accretion disk around a Schwarzschild black hole has the minimal radius $R = 6R_g = GM/c^2$.

Perihelion precession Ellipses are solutions of the two-body problem only for a potential $V(r) \propto 1/r$. As result of the relativistic $1/r^3$ corrections to the Newtonian potential, the perihelion of ellipses describing approximately the motion of e.g. planets processes. In the solar system, this effect is largest for Mercury, where $\Delta\omega/\Delta t \approx 43''/\text{century}$ (after subtracting the much larger effects due to the precession of the equinoxes [$5029''/\text{century}$] and perturbations by other planets [$530''/\text{century}$], while the quadrupole moment of the Sun is only a minor effect [$0.0254''/\text{century}$]). The precession of Mercury's perihelion was the only known discrepancy of the planetary motions in the solar system with the predictions of Newtonian gravity at the time, when Einstein and others worked on relativistic theories of gravity.

Light deflection The factor $(1 - 2R_g/r)$ in the line-element ds will lead to the bending of light in gravitational fields. This displacement can be made visible comparing the positions of stars close to the Sun during a solar eclipse and before or after that. The measurement of the deflection of light by the Sun during the solar eclipse 1919 was the first test passed successfully by general relativity.

We shall discuss this effect in the limit of small deflections, $\alpha \ll 1$. We can view the spatial part of the Schwarzschild metric as an refractive index n ,

$$\frac{dr}{dt} = \left(1 - \frac{2R_g}{r}\right) c \stackrel{!}{=} \frac{c}{n}. \quad (9.15)$$

The space-dependence of the refractive index $n = c/v$ leads according to Hyggen's principle to the deflection of light-rays, as sketched in Fig. 9.2: Two light-rays separated by db have the velocity difference dv . If the light-rays move initially along the z axis with the impact parameter b and $b + db$ to the Sun, the resulting infinitesimal deflection is

$$d\alpha = \frac{\partial v}{\partial b} dt = \frac{\partial(n^{-1})}{\partial b} c dt = \frac{\partial(n^{-1})}{\partial b} dz. \quad (9.16)$$

Expressing r as function of b and z using Fig. 9.2, we obtain

$$n^{-1} = 1 - \frac{2R_g}{r} = 1 - \frac{2R_g}{(z^2 + b^2)^{1/2}}. \quad (9.17)$$

Thus integrating

$$d\alpha = \frac{2R_g}{(z^2 + b^2)^{3/2}} b dz, \quad (9.18)$$

we find for the deflection angle of a light-ray

$$\alpha = \int d\alpha = 2R_g \int_{-\infty}^{\infty} \frac{dz}{(z^2 + b^2)^{3/2}} = \frac{4R_g}{b}. \quad (9.19)$$

Thus the deflection angle of a light-ray is determined by the ratio of the gravitational length scale R_g and the impact parameter b . Numerically, one obtains for a light-ray grazing the surface of the Sun $\alpha = 4GM_{\odot}/(c^2 R_{\odot}) \simeq 1.75''$.

9.3. Gravitational lensing

The deflection of light in the intervening gravitational field of stars or galaxies can lead to images of astrophysical objects that are distorted in shape and magnified in apparent brightness. This phenomenon is called gravitational lensing and, depending on the strength of the lensing effect, one distinguishes three different cases of gravitational lensing:

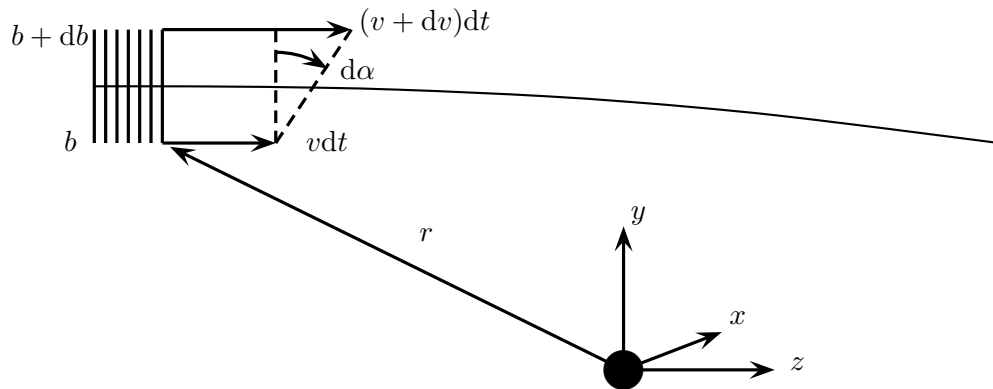


Figure 9.2.: The different velocity $v(r) = c/n(r)$ of light-rays leads according to Hyggen's principle to the deflection of light.

1. Strong lensing occurs when the lens is very massive and the source is close: In this case light can take different paths to the observer and more than one image of the source will appear, either as multiple images or deformed arcs of a source, cf. for an example Fig. 9.4. In the extreme case that a point-like source, the lens and the observer are aligned the image forms an "Einstein ring".
2. Weak Lensing: In many cases the lens is not strong enough to form multiple images or arcs. However, the source can still be distorted and its image may be both stretched and magnified. If a source class would be well known in size and shape, one could just the deformation of the source image to deduce the properties of the lens. For instance, one can examine the observed shape of elliptical galaxies for deviations from the theoretically expected probability distribution of, e.g., the ellipticity induced by gravitational lensing.
3. Microlensing: In this case the deflection angle is smaller than the resolution of the best optical telescopes and one observes therefore only the usual point-like image of the source. However, the additional light bent towards the observer leads to a brightening of the source. Thus microlensing is only observable as a transient phenomenon, when the lens crosses the axis observer-source.

Lens equation We consider the simplest case of a point-like lens with mass M , placed between the observer O and the source S as shown in Fig. 9.3. The angle β denotes the (unobservable) angle between the true position of the source and the direction to the lens, while ϑ_{\pm} are the angles between the image positions and the source. The corresponding distances D_{os} , D_{ol} , and D_{ls} are also depicted in Fig. 9.3. We keep all three distances, because we see later that $D_{os} + D_{ls} = D_{ol}$ does not hold in cosmology. Finally, the impact parameter b is as usual the smallest distance between the light-ray and the lens.

Then the lens equation in the "thin lens" ($b \ll D_i$) and weak deflection ($\alpha \ll 1$) limit follows from $\overline{AS} + \overline{SB} = \overline{AB}$ as

$$\vartheta D_{os} = \alpha D_{ls} + \beta D_{os} . \quad (9.20)$$

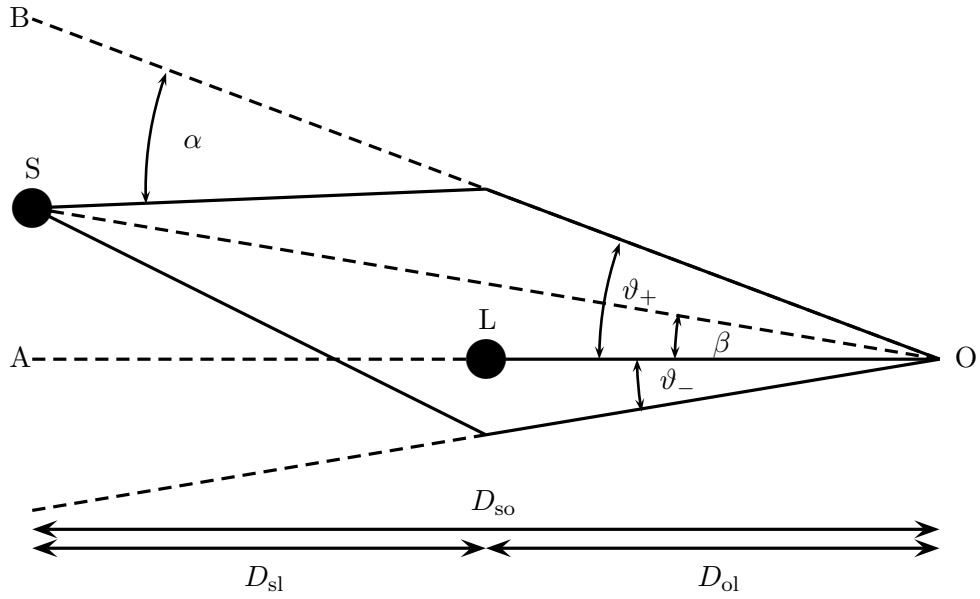


Figure 9.3.: The source S that is off-set relative the optical axis OL by the angle β appears as two images on opposite sides from OL . The two images are separated by the angles ϑ_{\pm} from the optical axis OL .

The thin lens approximation implies $\vartheta \ll 1$, and since $\beta < \vartheta$, also β is small. Solving for b and inserting the deflection angle $\alpha = 4GM/(c^2b)$ and $b = \vartheta D_{ol}$, we find first

$$\beta = \vartheta - \frac{4GM}{c^2} \frac{D_{ls}}{D_{os}D_{ol}} \frac{1}{\vartheta}. \quad (9.21)$$

Multiplying by ϑ , we obtain then a quadratic equation for ϑ ,

$$\vartheta^2 - \beta\vartheta - \vartheta_E = 0, \quad (9.22)$$

where we introduced the Einstein angle

$$\vartheta_E = \left(4R_g \frac{D_{ls}}{D_{os}D_{ol}} \right)^{1/2}. \quad (9.23)$$

The two images of the source are deflected by the angles

$$\vartheta_{\pm} = \frac{1}{2} [\beta \pm (\beta^2 + 4\vartheta_E^2)^{1/2}] \quad (9.24)$$

from the line-of-sight to the lens. If observer, lens and source are aligned, then symmetry implies that $\vartheta_+ = \vartheta_- = \vartheta_E$, i.e. the image becomes a circle with radius ϑ_E . Deviations from this perfectly symmetric situations break the circle into arcs as shown in an image of the galaxy cluster Abell 2218 in Fig. 9.4.

If we do not know the lens location, measuring the separation of the two lense images, $\vartheta_+ + \vartheta_-$, provides only an upper bound on the lens mass. For a numerical estimate of the Einstein angle in the case of a stellar object in our own galaxy, we set $M = M_{\odot}$ and $D_{ls}/D_{os} \approx 1/2$ and obtain

$$\vartheta_E = 0.64'' \times 10^{-4} \left(\frac{M}{M_{\odot}} \frac{D_{ol}}{10 \text{ kpc}} \right)^{1/2}. \quad (9.25)$$

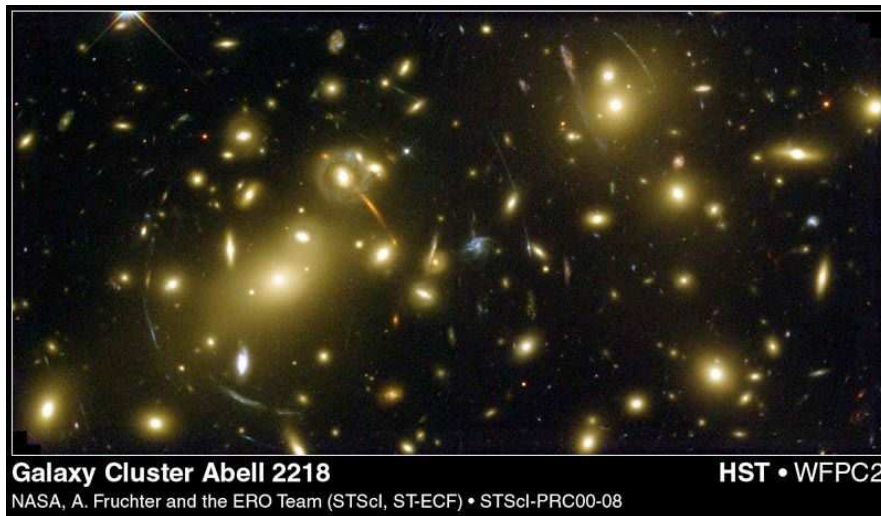


Figure 9.4.: Gravitational lensing of the galaxy cluster Abell 2218.

The numerical value of order 10^{-4} arcseconds typical for the deflection by a stellar object in our galaxy led to the name “microlensing.” Since the resolution of telescopes is of order arcsecond, lensing by Galactic objects can be only observed by the transient magnification of the source fluence to be discussed in the next section. Using instead typical values for lensing of galaxies, $M \sim 10^{10} M_{\odot}$ and $D_{ol} \sim 500$ Mpc, the expected Einstein angle increases by a factor $10^{14.5/2}$, becoming much larger than the resolution of large telescopes, cf. Fig. 9.4.

Magnification Without scattering or absorption of photons, we showed earlier that the conservation of photon number N implies that the intensity I along the trajectory of a light-ray stays constant, In particular, we found that the observed intensity I equals the surface brightness B of the source.

Gravity can affect this result in two ways: First, gravity can redshift the frequency of a photon emitted with ν_{sr} from the source, $\nu_{sr} = \nu_{obs}(1+z)$. This can be either the gravitational redshift as in Eq. (9.41) or a cosmological redshift due to the expansion of the universe (that will be discussed in Chpt. ??). Thus the intensity I_{obs} at the observed frequency ν_{obs} is the emitted intensity evaluated at $\nu_{obs}(1+z)$ and reduced by $(1+z)^3$,

$$I_{obs}(\nu_{obs}) = \frac{I(\nu_{sr})}{(1+z)^3}. \quad (9.26)$$

In both cases, this redshift depends only on the initial and the final point of the photon trajectory, not on the actual path in-between. Thus the redshift cancels if one considers the relative magnification of a source by gravitational lensing.

Second, gravitational lensing affects the solid angle the source is seen in a detector of fixed size. As a result, the apparent brightness of a source increases proportionally to the increase of the visible solid angle, if the source cannot be resolved as an extended object (cf. Sec. ??). Hence we can compute the magnification of a source by calculating the ratio of the solid angle visible without and with lensing.

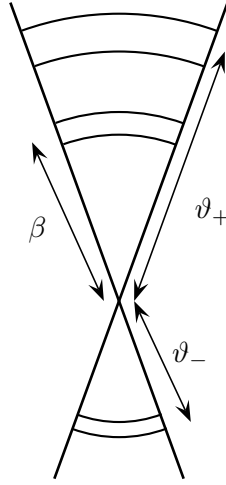


Figure 9.5.: The effect of gravitational lensing on the shape of an extended source: The surface element $2\pi\beta d\beta d\phi$ of the unlensed image at position β is transformed into the two lensed images of size $2\pi\vartheta_{\pm}d\vartheta_{\pm}d\phi$ at position ϑ_{\pm} .

In Fig. 9.5, we sketch how the two lensed images are stretched: An infinitesimal small surface element $2\pi \sin \beta d\beta d\phi \approx 2\pi\beta d\beta d\phi$ of the unlensed source becomes in the lense plane $2\pi\vartheta_{\pm}d\vartheta_{\pm}d\phi$. Thus the images are tangentially stretched by ϑ_{\pm}/β , while the radial size is changed by $d\vartheta_{\pm}/d\beta$. As a result, the magnification a_{\pm} of the source is given by

$$a_{\pm} = \frac{\vartheta_{\pm}d\vartheta_{\pm}}{\beta d\beta}. \quad (9.27)$$

Differentiating Eq. (9.24) gives

$$\frac{d\vartheta_{\pm}}{d\beta} = \frac{1}{2} \left[1 \pm \frac{\beta}{(\beta^2 + 4\vartheta_E^2)^{1/2}} \right] \quad (9.28)$$

and thus the total magnification is given by

$$a_{\text{tot}} = a_+ + a_- = \frac{x^2 + 2}{x(x^2 + 4)^{1/2}} > 1 \quad (9.29)$$

with $x = \beta/\vartheta_E$. For large separation x , the magnification a_{tot} goes to one, while the magnification diverges for $x \rightarrow 0$ as $a_{\text{tot}} \sim 1/x$: In this limit we would receive light from an infinite number of images on the Einstein circle. Physically, the approximation of a point source breaks down when $x \propto \beta$ reaches the extension of the source. Since a_{tot} is larger than one, gravitational lensing always increases the total flux observed from a lensed source, facilitating the observation of very faint objects. As compensation, the source appears slightly dimmed to all those observers who do not see the source lensed.

We shall discuss as one important applications of gravitational lensing the search for dark matter in the form of black holes or brown dwarfs in our own galaxy (Sec. 14.2.2).

9.4. Gravitational radiation

Maxwell's theory replaced the instantaneous Coulomb interaction law by the interaction of charges with electromagnetic fields that carry energy and momentum. In particular, we used in Sec. ?? that an accelerated system of electric charges emits electromagnetic dipole radiation with luminosity

$$L_{\text{em}} = \frac{2}{3c^3} |\ddot{\mathbf{d}}|^2, \quad (9.30)$$

where the dipole moment of a collection of N charges at positions \mathbf{x}_i is $\mathbf{d} = \sum_{i=1}^N q_i \mathbf{x}_i$.

Einstein's general theory of relativity predicts in an analogous way the existence of gravitational waves, which one can imagine as ripples in space-time that carry away energy and momentum with the speed of light. Since q^2 and GmM have the same dimension, one might guess that for the emission of gravitational radiation the replacement $q^2 \rightarrow GmM$ in the dipole formula should give qualitatively the correct result. But since $\sum m_i \dot{\mathbf{x}}_i = \mathbf{p}_{\text{tot}} = \text{const.}$, momentum conservation implies that the change in the dipole moment of a mass distribution is zero. Therefore gravitational radiation contains no dipole contribution and the first non-zero term in the multipole expansion of gravitational wave emission is the quadrupole term,

$$Q_{ij} = \sum_{k=1}^N m^{(k)} \left(x_i x_j - \frac{1}{3} \delta_{ij} r^2 \right). \quad (9.31)$$

The resulting luminosity emitted into gravitational waves is given by

$$L_{\text{gr}} = \frac{G}{5c^5} \sum_{i,j} |\ddot{Q}_{ij}|^2. \quad (9.32)$$

Example: a.) Show that q^2 and GmM have the same dimension. Derive b.) $L_{\text{em}} \propto d^2/c^3$ and $L_{\text{gr}} \propto GQ^2/c^5$ using dimensional analysis.

a. We start inverting the definition of Sommerfeld's fine structure constant, $e^2 = \hbar c \alpha$. Thus the dimension of the electric charge squared is $[e^2] = \text{erg} \times \text{cm}$. Setting $[e^2]$ equal to the dimension of $[GmM] = \text{g cm}^3/\text{s}^2$ and using $\text{erg} = \text{g cm}^2/\text{s}^2$ shows that the statement is indeed correct.

b. In the case of electromagnetic dipole radiation, we use again $[e^2] = \text{erg} \times \text{cm}$, while the definition (9.31) implies $[\ddot{Q}] = \text{g cm}^2/\text{s}^3$. Then we compare

$$[L_{\text{em}}] = \frac{\text{erg}}{\text{s}} \stackrel{!}{=} \frac{\text{s}^3}{\text{cm}^3} \times \text{erg} \times \text{cm} \times \frac{\text{cm}^2}{\text{s}^4} = \frac{\text{erg}}{\text{s}},$$

which agrees with the definition of luminosity as energy/time. In the same way, we can show that the luminosity of gravitational quadrupole radiation is proportional to c^a with $a = -5$: The unique solution for a from

$$[L_{\text{gr}}] = \frac{\text{erg}}{\text{s}} = \frac{\text{g cm}^2}{\text{s}^3} \stackrel{!}{=} \frac{\text{cm}^3}{\text{g s}^2} \times \frac{\text{cm}^a}{\text{s}^a} \times \frac{\text{g}^2 \text{cm}^4}{\text{s}^6}$$

is $a = -5$.

Evolution of binary systems The emission of gravitational radiation is negligible for most systems where Newtonian gravity is a good approximation. One of the rare examples where general relativistic effects can become important are close binary systems of compact stars. Let us estimate the change in the orbital period for such a binary system. We start recalling that the energy of binary system with total mass $M = m_1 + m_2$ and separation a is given by (cf. with ??)

$$E = \frac{1}{2}\mu\omega^2 a^2 - \frac{G\mu M}{a} = -\frac{G\mu M}{2a}. \quad (9.33)$$

For simplicity, we assume in the following circular orbits. Evaluating then the tensor of inertia (9.31) for a binary and inserting the result into (9.32) gives (cf. problem)

$$L_{\text{gw}} = \frac{32}{5} \frac{G^4 \mu^2 M^3}{d^5}. \quad (9.34)$$

Next we can relate the relative changes per time in the orbital period P , the separation a and the energy E using $E \propto 1/a$ and $P \propto a^{3/2}$ as

$$\frac{\dot{E}}{E} = -\frac{\dot{a}}{a} = \frac{2}{3} \frac{\dot{P}}{P}. \quad (9.35)$$

Solving first for the change in the period,

$$\dot{P} = -\frac{3}{2} \frac{L_{\text{gw}}}{E} P = \frac{96}{5} \frac{G^3 \mu M^2}{a^4} P, \quad (9.36)$$

and eliminating then a gives

$$\dot{P} = -\frac{96}{5} (2\pi)^8 G^{5/3} \mu M^{2/3} P^{-5/3}. \quad (9.37)$$

Hulse-Taylor pulsar The first example for a close binary systems of compact stars was found 1974 by Hulse and Taylor who discovered a pulsar in a binary system via the Doppler-shift of its radio pulses. The extreme precision of the periodicity of the pulsar signal makes such binary systems to an ideal laboratory to test various effect of special and general relativity:

- The pulsar's orbital speed changes by a factor of four during its orbit and allows us to test the usual (special relativistic) Doppler effect.
- At the same time, the gravitational field alternately strengthens at periastron and weakens at apastron, leading to a periodic gravitational redshift of the pulse.
- The small size of the orbit leads to a precession of the Perihelion by $4.2^\circ/\text{yr}$.
- The system emits gravitational waves and loses thereby energy. As a result the orbit of the binary shrinks by $4\text{mm}/\text{yr}$.

Let us now compare the observed change in the orbit of the binary with the prediction of general relativity. The binary system consists of a pulsar with mass $m_1 = 1.44M_\odot$ and a companion with mass $m_2 = 1.34M_\odot$. Their orbital period is $P = 7\text{h}40\text{min}$ on an orbit with rather strong eccentricity, $e = 0.617$. In this case, the emission of gravitational radiation is strongly enhanced compared to an circular orbit,

$$\dot{P}(e) = \dot{P}(0) \frac{1 + \frac{73}{24}e^2 + \frac{37}{96}e^4}{(1 - e^2)^{7/2}} \simeq -2.4 \times 10^{-12}/\text{yr}. \quad (9.38)$$

This results is in excellent agreement with the prediction of general relativity, cf. Fig. ??.

9.5. Astrophysical black holes

Gravitational redshift As in special relativity, the line-element ds determines the time and spatial distance between two space-time events. The time measured by an observer called the proper-time $d\tau$ is given by $d\tau = cds$. In particular, the time difference between two events at the same point is given by setting $dx^i = 0$ in the line-element ds^2 . If we choose two static observers at the position r and r' in the Schwarzschild metric (9.11), then we find with $dr = d\phi = d\vartheta = 0$,

$$\frac{d\tau(r)}{d\tau(r')} = \frac{\sqrt{g_{00}(r)} dt}{\sqrt{g_{00}(r')} dt} = \sqrt{\frac{g_{00}(r)}{g_{00}(r')}}. \quad (9.39)$$

The time-intervals $d\tau(r')$ and $d\tau(r)$ are different and thus the time measured by clocks at different distances r from the mass M will differ too. In particular, the time τ_∞ measured by an observer at infinity will pass faster than the time experienced by an observer in a gravitational field,

$$\tau_\infty = \frac{\tau(r)}{\sqrt{1 - 2R_g/r}} < \tau(r). \quad (9.40)$$

Since frequencies are inversely proportional to time, the frequency or energy of a photon traveling from r to r' will be affected by the gravitational field as

$$\frac{\nu(r')}{\nu(r)} = \sqrt{\frac{1 - 2R_g/r}{1 - 2R_g/r'}}. \quad (9.41)$$

Hence an observer at $r' \rightarrow \infty$ will receive photons with frequency

$$\nu_\infty = \sqrt{1 - \frac{2GM}{rc^2}} \nu(r), \quad (9.42)$$

if these photons were emitted by a source at position r with frequency $\nu(r)$: Thus the frequency of a photon is redshifted by a gravitational field, in agreement with our argument against a perpetuum mobile in 2). The size of this effect is of order Φ/c^2 , where $\Phi = -GM/r$ is the Newtonian gravitational potential. We are now in position to specify more precisely what “weak gravitational fields” means: As long as $|\Phi|/c^2 \ll 1$, the deviation of $g_{tt} = 1 - \frac{2GM}{rc^2} \approx 1 - 2\Phi(r)/c^2$ from the Minkowski value $g_{tt} = 1$ is small and Newtonian gravity is a sufficient approximation.

Schwarzschild radius What is the physical meaning of the distances $R_s \equiv 2R_g$ called Schwarzschild radius where $g_{rr} = (1 - R_s/r)^{-1}$ diverges? We see from Eq. (9.42) that R_s corresponds to a two-dimensional surface with infinite gravitational redshift: A signal emitted by a space craft flying towards $r = R_s$ appears to an observer at infinity more and more redshifted, and for $r \rightarrow R_s = 2R_g$ the signal disappears completely. This indicates that no communication with the region inside the Schwarzschild radius is possible. By the same argument, a clock located at R_s measures the proper-time $d\tau(r = R_s) = 0$, i.e. time stands still at the Schwarzschild radius! Since light-rays satisfy $ds^2 = 0$, time-like tangent vectors exist at all points of the surface $R_s \equiv 2R_g$ that are generated by light-rays, cf. Fig.xx. Moreover, we know that the trajectories of massive particles are always contained in the forward-light-cone. Performing a more detailed analysis, one can show that in the Schwarzschild metric all

trajectories crossing R_s are directed inwards. The only exception are the light-rays tangential at R_s : They are on a circular orbit, where in the Newtonian language gravitational and centrifugal force balance each other.

Such a two-dimensional surface acting as a semi-permeable membrane is called an event horizon, while an object smaller than its Schwarzschild radius is called a black hole. One expects that as soon a gravitating mass is concentrated¹ inside a radius smaller than R_s , a black hole forms and we cannot obtain any information about what is going on inside R_s .

The event horizon of stellar black holes is comparable to the size of neutron stars,

$$R_s = \frac{2GM}{c^2} \approx 3 \text{ km} \frac{M}{M_\odot}, \quad (9.43)$$

i.e. failed type II SNe lead to black holes with event horizons of order ~ 10 km. By contrast, the event horizon of supermassive black holes with masses of order $(10^6 - 10^8)M_\odot$ that are believed to be in the center of most galaxies are much more compact as other objects of the same mass. Thus a way to detect such massive black holes is to search for very large invisible masses concentrated in a small volume via their effect of surrounding stars.

Finally, we note that the coordinate system (9.11) becomes ill-defined both at $r = 0$ and $r = R_s$. Since we are allowed in general relativity to make arbitrary coordinate transformations $x = x(x')$, such coordinate singularities do not necessarily indicate a “physical singularity” where some measurable quantities diverge. From our Newtonian experience we expect that tidal forces become infinite for $r \rightarrow 0$, while they are finite at $r = R_s$. One can show that the latter singularity is indeed an artefact of badly chosen coordinates and can be eliminated by a suitably chosen coordinate transformation.

Example: Tidal forces in Newtonian theory

Approaching a black hole Light rays are characterized by $ds^2 = 0$. Choosing a light ray in radial direction with $d\phi = d\vartheta = 0$, the metric (9.11) can be rewritten as

$$\frac{dr}{dt} = \left(1 - \frac{2R_g}{r}\right) c. \quad (9.44)$$

Thus a light signal traveling towards the star, as seen from the outside, will travel slower and slower as it comes closer to the Schwarzschild radius $R_s = 2R_g$. We should stress that this behaviour does not contradict special relativity: All observers measure in the moment when the photon passes their position that the photon travels with the speed of light.

In fact, for an observer at infinity the signal will reach $r = 2R_g$ only asymptotically for $t \rightarrow \infty$: Integrating Eq. (9.44) gives

$$t = \int_{-\infty}^r \frac{dr'}{c} \left(1 - \frac{2R_g}{r'}\right)^{-1} = t' - \frac{2GM}{c} \ln(1 - 2R_g/r) \rightarrow \infty \quad \text{for } r \rightarrow 2R_g, \quad (9.45)$$

where t' is the start time at $r \rightarrow \infty$. Since the coordinate time t agrees with the proper time τ for an observer at infinity, a photon reaches the Schwarzschild radius $r = 2R_g$ only

¹Recall that in Newtonian gravity only the enclosed mass $M(r)$ contributes to the gravitational potential outside r for a spherically symmetric system. Thus, e.g., the Sun is not a black hole, since for all r the enclosed mass is $M(r) < rc^2/2G$.

asymptotically for $t \rightarrow \infty$ for such an observer. Similarly, the communication with a freely falling space ship becomes impossible as it reaches $r = R_g$: Not only the frequency of single emitted photons becomes more and more redshifted, but also the time between the emission of two photons goes to infinity.

Remark 9.2: exponential decline with typical scale $4M...$

Stellar black holes Final stage of failed SNII,

Supermassive black holes

9.6. Thermodynamics and evaporation of black holes

Black holes thermodynamics We argued that the two-dimensional surface at the Schwarzschild radius acts as a semi-permeable membrane around a black hole. Therefore, the mass of a black hole and thus also the area of its event horizon can only increase with time. The only other quantity in physics with the same property is the entropy S . This suggests a connection between a quantity characterizing the size of the black hole and its entropy. Such a relation should also exist, if we want to apply the second law of thermodynamics, $dS(t) \geq 0$, to the combined system of a black hole and its surrounding: Dropping a macroscopic body with mass m and entropy S into a black hole reduces the entropy S_{out} of the surrounding; only if the entropy S_{BH} of the black hole increases sufficiently, the total entropy $dS_{\text{BH}} + dS_{\text{out}} > 0$ can grow as required by the second law of thermodynamics.

To derive the relation between the size of the black hole and its entropy, we apply the first law of thermodynamics $dU = TdS - PdV$ to a Schwarzschild black hole. Its internal energy U is given by $U = Mc^2$, while for a static black hole it is $dV = 0$. Thus the first law of thermodynamics becomes

$$dU = dMc^2 \stackrel{!}{=} TdS. \quad (9.46)$$

Such a black hole is fully characterised by only one quantity, which we may choose e.g. as its gravitational radius R_g . Hence both the temperature T and the entropy S of a black hole should be determined solely by R_g .

A straightforward way to test this conjecture is connect by dimensional analysis the temperature T and entropy S with the mass M of the black hole and the relevant fundamental constants. A fast way to find the dimensionally correct relation between T and M is to set the potential energy U_{pot} associated to an object with gravitational radius R_g equal to its thermal energy kT . However, using $U_{\text{pot}} \sim GM^2/R_g$ gives

$$kT \propto \frac{GM^2}{R_g} = Mc^2. \quad (9.47)$$

Because of $R_g = GM/c^2$, the gravitational constant cancels on the RHS and we failed to form an energy T/k which depends on both constants characteristic for classical, relativistic gravity, G and c . The only way to form an energy containing also G is to use as additional fundamental constant Planck's constant \hbar . This indicates that we are leaving the realm of classical gravity: Ascribing a temperature to a black hole implies that quantum effects $\propto \hbar$

become important. Having \hbar at our disposal, we can set the Compton wavelength of a BH equal to its gravitational radius, $\lambda_C = \hbar/(Mc) \sim R_g$. Then we set the resulting energy $Mc^2 \sim \hbar c/R_g$ equal to its thermal energy kT ,

$$kT = \gamma_1 \frac{\hbar c}{R_g} = \gamma_1 \frac{\hbar c^3}{GM}. \quad (9.48)$$

Here γ_1 is a free numerical factor which we cannot determine by dimensional analysis.

Next we consider the entropy S . Since the entropy $S = k \ln \Omega$ counts the number of quantum states of a thermodynamical system, we know that the quantity S/k is dimensionless. Dividing the gravitational radius R_g by the Planck length $l_{\text{Pl}} = (\hbar G/c^3)^{1/2}$, we obtain another dimensionless ratio which we can associate with the entropy S . Thus dimensional analysis leads us to the conjecture

$$S = \gamma_2 k \left(\frac{c^3}{\hbar G} R_g^2 \right)^\delta = \gamma_2 k \left[\frac{c^3}{\hbar G} \left(\frac{GM}{c^2} \right)^2 \right]^\delta, \quad (9.49)$$

with a new proportionality factor γ_2 and the unknown power δ . We can derive the value of δ requiring the consistency of Eqs. (9.49) and (9.48) with the relation $dU = TdS$. Forming the differential dS ,

$$dS = \gamma_2 k \left(\frac{c^3}{\hbar G} \right)^\delta 2\delta R_g^{2\delta-1} dR_g \propto M^{2\delta-1} dM, \quad (9.50)$$

and multiplying then the expression with $T \propto 1/M$, we find

$$dU = c^2 dM = TdS \propto M^{2\delta-2} \quad (9.51)$$

or $\delta = 1$: Applying the usual laws of thermodynamics to BHs suggests thus that the BH entropy is proportional to their area, not to their volume. This result implies that the degrees of freedom of a three-dimensional gravitating system are related to the quantum states of a two-dimensional system localised on its surface. The generalisation of this result has been dubbed “holographic principle” and its investigation is today one of the most active research areas in theoretical physics. Clearly, one hopes that understanding the microscopic picture underlying the entropy of a black hole may provide new insights into the quantum theory of gravity, similar as the derivation of the blackbody formula (??) was the starting point for the development of quantum mechanics.

If this analogue is more than a formal coincidence, a black hole should behave similar as other thermodynamical systems we know. In particular, if its surrounded by a cooler medium, it should emit radiation and heat up the environment. Hawking could indeed show 1974 that a black hole in vacuum emits black-body radiation (“Hawking radiation”) with temperature

$$kT = \frac{\hbar c^3}{8\pi GM}. \quad (9.52)$$

This fixes also the proportionality factor in our formula for the entropy of a Schwarzschild black hole,

$$S = \frac{kc^3}{4\hbar G} A \quad (9.53)$$

with $A = 4\pi R_s^2$ as area of the event horizon. Introducing the Planck length squared, we can rewrite the entropy as $S = 4kA/l_{\text{Pl}}^2$. The entropy of a macroscopical black hole is extremely large, because its basic unit l_{Pl} is so small.

Evaporation of Black Holes The emission of radiation by a black hole is a quantum process, as indicated by the presence of Planck's constant \hbar in Eq. (9.52). We can understand the basic mechanism and the magnitude of the black hole temperature by considering a quantum fluctuation near its event horizon at R_s : Heisenberg's uncertainty principle allows the creation of a virtual electron-positron pair with total energy E for the time $\Delta t \lesssim \hbar/E$. This pair can become real, if the gravitational force acting on them during the time Δt can supply the energy E . More precisely, the work is done by the tidal force

$$dF = \frac{\partial F}{\partial r} dr = -\frac{GME/c^2}{2r^3} dr, \quad (9.54)$$

because the electron-positron pair is freely falling.

After the time Δt , the pair is separated by the distance $\Delta r = c\Delta t \sim c\hbar/E$. The energy gain by the tidal force is

$$F\Delta r \sim (E/c^2)GM/r^3(\Delta r)^2. \quad (9.55)$$

If we require that $F\Delta r > E$ and identify the energy E of the emitted pair with the temperature T of the black hole, we find

$$kT \sim E \lesssim \hbar(GM/r^3)^{1/2}. \quad (9.56)$$

The emission probability is maximal close to the event horizon, $r = R_s$, and thus we obtain $kT \sim E \sim \hbar c^3/(GM)$, in agreement with Hawking's result in Eq. (9.52).

10. White dwarfs and neutron stars

10.1. Chandrashekar mass

Recall the mass-radius relation (4.21) for a polytrope,

$$\left(\frac{GM}{M_n}\right)^{n-1} \left(\frac{R}{R_n}\right)^{3-n} = \frac{[(n+1)K]^n}{4\pi G}. \quad (10.1)$$

or

$$M \propto R^{(3-n)/(1-n)}. \quad (10.2)$$

There are two interesting special cases. For $n = 3$, the mass becomes independent from R . Another application of the mass-radius relation for $n = 3$ are stars where the pressure is dominated by relativistic fermions. In this case, K from Eq. (2.71) is determined solely by natural constants, the fermion mass m and the chemical composition, i.e. μ . Substituting K from Eq. (2.71) and setting $m = m_p$ results in

$$M_{\text{Ch}} = 4\pi M_3 \left(\frac{K}{\pi G}\right)^{3/2} = \frac{\sqrt{1.5}M_3}{4\pi} \left(\frac{hc}{Gm_p^{4/3}}\right)^{3/2} \frac{1}{\mu_e^2} \simeq 5.83\mu_e^{-2} M_\odot \quad (10.3)$$

In the other case, $n = 1$, the radius becomes independent of the mass M and is determined by K ,

$$R = R_1 \left(\frac{K}{2\pi G}\right)^{1/2}. \quad (10.4)$$

Between these two limiting cases, the scaling

$$R^{(3-n)} \propto 1/M^{1-n}. \quad (10.5)$$

implies that the stellar radius decreases for more massive stars.

For a non-relativistic, degenerate star $M \propto 1/R^3$, i.e. a more massive WD is more compact.

$$M = 0.7 \left(\frac{R}{10^4 \text{km}}\right) (\mu_e/2)^{-5} M_\odot \quad (10.6)$$

$$R = 0.7 \left(\frac{\rho_c}{10^4 \text{km}}\right) \mu_e/2 M_\odot \quad (10.7)$$

In the relativistic, $n = 3$, the mass becomes independent from R , as we discussed in the case of the convective MS stars. While in the latter case, the ratio of radiative and gas pressure leads to variation, here only one variable: thus a single mass Chandrasekara limit. mass-radius relation, fig. 5.2 prilanak

10.2. White dwarfs

Observations of Sirius B Sirius is with a distance of 2.6 pc the fifth closest stellar system to the Sun. Analyzing the motions of Sirius 1833–1844, F.W. Bessel concluded that it had an unseen companion, with a orbital period $P \sim 50$ yr. In 1862, A. Clark discovered this companion, Sirius B, at apastron or the time of maximal separation of the two components of the binary system. Following-up observations showed that the mass of Sirius B equals approximately the one of the Sun, $M \approx M_\odot$. Sirius B's peculiar properties were not established until the next apastron, 1915, by W.S. Adams. He noted the high temperature of Sirius B, which requires together with its small luminosity an extremely small radius and thus a large density of this star.

Example: Find the mean density of Sirius B from its apparent magnitude, $m = 8.5$, and its surface temperature $T = 25,000$ K.

We convert first the apparent into an absolute magnitude,

$$M = m - 5 \log(d/10\text{pc}) = 11.4,$$

and express then the absolute magnitude as a luminosity,

$$L = 3.02 \times 10^{28} \text{W} \times 10^{-0.4M} = 3.84 \times 10^{26} \text{W}.$$

Now we can use the Stefan-Boltzmann law and obtain

$$\frac{R}{R_\odot} = \left(\frac{L}{L_\odot}\right)^{1/2} \left(\frac{T}{T_\odot}\right)^{-2} \approx 10^{-2}.$$

Therefore the mean density of Sirius B is a factor 10^6 higher than the one of the Sun. More precisely one finds $\rho = 3 \times 10^6 \text{g/cm}^3$.

We now apply the lower limit for the central pressure of a star in hydrostatic equilibrium, Eq. (3.11), to Sirius B,

$$P_c > \frac{M^2}{8\pi R^4} = 4 \times 10^8 \text{bar} \left(\frac{M}{M_\odot}\right)^2 \left(\frac{R_\odot}{R}\right)^4 = 4 \times 10^{16} \text{bar}. \quad (10.8)$$

What would be the central temperature T_c needed, if the pressure is dominated by an ideal gas? From the ideal gas law, we find

$$T_c = \frac{P_c}{nk} \sim 10^2 T_{c,\odot} \approx 10^9 \text{K}. \quad (10.9)$$

For such a high central temperature, the temperature gradient dT/dr in Sirius B would be a factor 10^4 larger than in the Sun. This would in turn require a larger luminosity $L(r)$ and a larger energy production rate ε than in a main sequence star. The solution to this puzzle is that the main source of pressure in such compact stars is the degeneracy pressure of fermions.

10.2.1. Chandrasekar's theory for WDs

Assumptions: no radiation pressure, ideal gas pressure only important for a thin outer layer which can be neglected.

Assume that the pressure of white dwarf (WD) stars is given by completely degenerate (non-interacting) electrons. In the general case, where the relativity parameter $x = p_F/(mc)$ is neither zero or one, the E.o.S. is not a polytrope and the Lane-Emden equation has to be generalised. Chandrasekhar showed that writing the pressure and the density of degenerate electrons as function of the relativity parameter x as $P(x) = Af(x)$ and $\rho(x) = Bx^3$, one can derive

The pressure (2.67a) and the density of degenerate electrons as function of the relativity parameter $x = p_F/(mc)$ can be written as $P(x) = Af(x)$ and $\rho = Bx^3$ with

$$f(x) = 8\pi^2\phi(x) = x\sqrt{1+x^2}(2x^2/3 - 1) + 3\operatorname{arcsinh}(x). \quad (10.10)$$

Using the starting point (4.14) for the derivation of the Lane-Emden equation,

$$\frac{1}{r^2} \frac{d}{dr} \left(\frac{r^2}{\rho} \frac{dP}{dr} \right) = -G \frac{dM(r)}{dr} = -4\pi G\rho(r). \quad (10.11)$$

and inserting the pressure and density gives

$$\frac{A}{Br^2} \frac{d}{dr} \left(\frac{r^2}{x^3} \frac{df(x)}{dr} \right) = -G \frac{dM(r)}{dr} = -4\pi GBx^3. \quad (10.12)$$

The relativity parameter x is a function of radius, $x = x(r)$. Using the chain rule, we obtain

$$\frac{df(x(r))}{dr} = \frac{8x^4}{x^3} (1+x^2)^{1/2} \frac{dx}{dr} \quad (10.13)$$

or

$$\frac{1}{x^3} \frac{df}{dr} = \frac{8x}{x^3} (1+x^2)^{1/2} \frac{dx}{dr} = \frac{d(1+x^2)^{1/2}}{dr}. \quad (10.14)$$

Inserting this expression into (10.12) and setting $z^2 = 1+x^2$ results in

$$\frac{1}{r^2} \frac{d}{dr} \left(r^2 \frac{dz}{dr} \right) = -\frac{\pi GB^2}{2A} (z^2 - 1)^{3/2}. \quad (10.15)$$

Next we make this equation dimensionless: Denoting the values at $r = 0$ as $x_c \equiv x(0)$ and $z_c \equiv z(0)$, and introducing the new variables

$$r = \alpha\eta \quad \text{and} \quad z = z_c\phi$$

which satisfy.

$$\alpha^2 = \frac{2A}{\pi G} \frac{1}{(Bz_c)^2} \quad \text{and} \quad z_c^2 = x_c^2 + 1$$

it follows

$$\frac{1}{\eta^2} \frac{d}{d\eta} \left(\eta^2 \frac{d\phi}{d\eta} \right) = - \left(\phi^2 - \frac{1}{z_c^2} \right)^{3/2}. \quad (10.16)$$

We need to specify two boundary conditions for this equation: The relation $y = y_c\phi$ implies $\phi = 1$ at the center. Moreover, as for $x = 0$, the derivative of ϕ has to be zero at the center. Finally, the radius of the star is defined by $\rho(R) = 0$ and thus $x(R) = 0$. Hence $z(R) = 1$ and $\phi(\eta(R)) = z/z_c = 1/z_c$. Thus the integration starts with $\phi(0) = 1$, and $\phi'(0) = 0$ at the

center $\eta = 0$ of the star, choosing a value of z_c , until one reaches the stellar radius $R = r(\eta_1)$ when $\phi = 1/z_c$.

The stellar radius is given by $R = \alpha\eta_0$ or

$$R = \sqrt{\frac{2A}{\pi G}} \frac{1}{Bz_c} \eta_1,$$

where η_1 is defined by $\phi = 1/z_c$. As in the case of the “ordinary” Lane-Emden equation, we express first ρ by ϕ ,

$$\rho(x) = Bx^3 = B(z^2 - 1)^{3/2} = Bz_c^3 \left(\phi^2 - \frac{1}{z_c^2} \right)^{3/2}.$$

Then we replace r and ρ in

$$M = 4\pi \int_0^R dr r^2 \rho = 4\pi \alpha^3 B z_c^3 \int_0^{\phi_1} d\eta \eta^2 \left(\phi^2 - \frac{1}{z_c^2} \right)^{3/2}. \quad (10.17)$$

Then we replace $(\dots)^{3/2}$ using the generalised Lane-Emden equation,

$$M = 4\pi \alpha^3 B z_c^3 \left(-\eta^2 \frac{d\phi}{d\eta} \right) \Big|_{\eta_1} \quad (10.18)$$

In the last step, we insert the definition of α and z_c , obtaining

$$M = \frac{4\pi}{B^2} \left(\frac{2A}{\pi G} \right)^{3/2} \left(-\eta^2 \frac{d\phi}{d\eta} \right) \Big|_{\eta_1}. \quad (10.19)$$

Now we can evaluate numerically M and R for a given value of z_c , see the table 10.1 for some results.

There exist solutions between $M = 0$ and $M_{\text{Ch}} \simeq 5.84M_\odot$. The upper limit corresponds to $x = 1$ (ultra-relativistic limit), which is unstable according to the virial theorem.

How reliable are these results? Our main assumption was that interactions can be neglected. This is not true in particular for low masses: For $M \rightarrow 0$, we expect $\rho \simeq \text{const.}$ instead of $\rho \rightarrow 0$ allowing for the existence of planets—their stability is caused by electrostatic interactions between electrons and ions. In the other extreme, $M \rightarrow M_{\text{Ch}}$ implies $\rho \rightarrow \infty$ and at some point weak interactions may play a role.

10.2.2. White dwarfs cooling

10.3. Neutron stars

Cold ideal npe gas (Inverse) beta-decay leads an equilibrium distribution of neutrons, protons, and electrons in a (proto-) neutron star. The chemical potential are connected by $\mu_e + \mu_p = \mu_n + \mu_\nu$ with $\mu_\nu = 0$, since neutrinos can escape freely and thus their number density is negligible.

For a cold degenerate gas, we can neglect the temperature and the Fermi-Dirac distribution function becomes a step function. Thus all levels up-to the Fermi momentum p_F are filled, and the number density of species with two spin degrees of freedom is

$$n = \frac{2}{h^3} \int_0^{p_F} 4\pi p^2 dp = \frac{8\pi}{3h^3} p_F^3 = \frac{1}{3\pi^2 \lambda^3} x^3 \quad (10.20)$$

Table 10.1.: Numerical constants from the integration of the generalised Lane-Emden equation.

$1/z_c^2$	z_c	ξ_1	$-\eta^2 (d\phi/d\eta)_{\eta_1}$	ρ_c/μ_e	$\mu_e^2 M \text{g/cm}^3$	$\mu_e R/\text{km}$
0	∞	6.70	2.02	∞	5.84	0
0.01	9.95	5.36	1.93	9.48e8	5.60	4.17
0.02	7	4.99	1.86	3.31e8	5.41	5.50
0.05	4.36	4.46	1.71	7.98e7	4.95	7.76
0.1	3	4.07	1.52	2.59e5	4.40	10.0
0.2	2	3.73	1.24	7.70e6	3.60	13.0
0.3	1.53	3.58	1.03	3.43e6	2.99	16.0
0.5	1	3.53	0.707	9.63e5	2.04	19.5
0.8	0.5	4.04	0.309	1.21e5	0.89	28.2
1	0	∞	0	0	0	∞

with $x \equiv p_F/(mc)$ and $\lambda = \hbar/(mc)$. Since the Fermi energy equals the chemical potential, we have

$$m_e(1+x_e^2)^{1/2} + m_p(1+x_p^2)^{1/2} = m_n(1+x_n^2)^{1/2}. \quad (10.21)$$

Charge neutrality implies that $n_e = n_p$ or $m_e x_e = m_p x_p$. Thus we can eliminate x_e and find the ratio n_p/n_n . Squaring twice (10.21) and using $Q, m_e \ll m_n$, we obtain

$$\frac{n_p}{n_n} = \left(\frac{m_p x_p}{m_n x_n} \right)^3 \approx \frac{1}{8} \left\{ \frac{1 + \frac{4Q}{m_n x_n^2} + 4 \frac{Q^2 - m_e^2}{m_n^2 x_n^4}}{1 + 1/x_n^2} \right\}^{3/2}. \quad (10.22)$$

Example 10.1: a.) Derive the limiting value $n_p/n_n = 1/8$ directly.

a) For large x_n , all three species are relativistic and Eq. (10.21) becomes $m_e x_e + m_p x_p = m_n x_n$. Charge neutrality implies then immediately that

$$n_p/n_n = \left(\frac{m_p x_p}{m_n x_n} \right)^3 = (1/2)^3 = 1/8.$$

10.3.1. *** TOV equation ***

In general relativity, the hydrostatic equilibrium Eq. (3.7) becomes

$$\frac{dP}{dr} = -\frac{GM(r)\rho(r)}{r^2} \left(1 + \frac{P}{\rho c^2} \right) \left(1 + \frac{4\pi r^3 P}{Mc^2} \right) \left(1 - \frac{2GM(r)}{c^2 r} \right)^{-1} \quad (10.23)$$

with

$$M(r) = 4\pi \int_0^r dr' r'^2 \rho(r'), \quad (10.24)$$

GR effects lead to three correction terms:

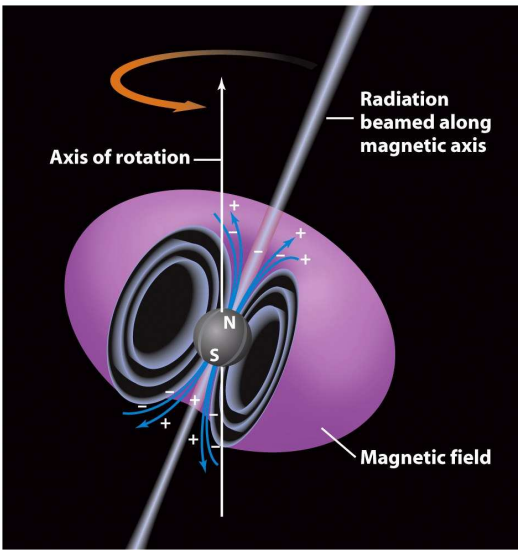
- since gravity is sourced also by pressure, the term $P/\rho c^2$ increases the density $\rho(r)$.
- moreover, the term $4\pi r^3 P/Mc^2$ increases the enclosed mass $M(r)$.
- finally, the $1/r^2$ law is modified by the third term

$$\boxed{\frac{dM(r)}{dr} = 4\pi r^2 \rho(r)}. \quad (10.25)$$

10.4. Pulsars

Generalities of compact stars White dwarf and neutron stars have in common that their radius is strongly increased with respect to a main sequence star, $R_{WD}/R_{\odot} \sim 10^{-2}$ and $R_{NS}/R_{\odot} \sim 10^{-5}$. Using two conservation laws involving the stellar radius, we can derive immediately two important properties of these compact stars:

- Conservation of angular momentum, $L = I\omega = \text{const.}$ with $I = \alpha MR^2$, implies (initially) fast rotation of a compact star: A star like the Sun, rotating once per month, $P \approx 10^6 \text{s}$, would rotate with a ms period when contracted down to 10 km in size.
- The magnetic flux, $\phi_B = BA = \text{const.}$, is a conserved quantity for an ideal conductor, where magnetic field lines are frozen in the plasma. As the core collapses, the magnetic field lines are pulled more closely together, intensifying the magnetic field by a factor $(R_{\odot}/R_{NS})^2 \sim 10^{10}$. Magnetic A stars have surface fields up to 10^4G , and the observed field strengths of white dwarfs are of the order of $B \approx (10^6 - 10^8) \text{G}$. Neutron stars can have magnetic fields up to $B \approx (10^{12} - 10^{13}) \text{G}$. In extreme cases, called magnetars, it has been speculated that the magnetic field of young neutron stars may reach up to $B \approx 10^{15} \text{G}$.



Discovery and identification of pulsars In 1967, J. Bell and A. Hewish detected an object emitting a radio signal with period $P = 1.377 \text{s}$. They called the object “Pulsar”. Already one year later, Gold argued that pulsars are rotating neutron stars. He predicted an increase of the period as pulsars, because they should lose energy via electromagnetic radiation. The slowdown of the Crab pulsar was indeed discovered in 1969.

The key observations that helped to identify pulsars with rotating neutron stars were:

1. The smallness of the observed periods, $P \sim 1 \text{ms} - 5 \text{s}$.
2. The extreme stability of the periods, $\Delta P/P = 10^{-13}$.
3. The periods increase slowly.

Additional information from later observations include that the source distribution is peaked in the Galactic

plane, implying a Galactic origin. Moreover, several pulsars like the Crab and Vela pulsars were found in remnants of type II supernovae.

Since the light travel time ct is 500 km for 1.5 ms, we can use this distance as an upper limit for the emission region (that has to be causally connected to act as good clock). This implies that a pulsar has to be a compact object and we have to choose between white dwarfs, neutron stars or black holes as possible sites for the radio emission. Possible clock mechanisms are rotation or pulsation of a single star or the orbital movement of a binary system. We now consider the different options:

Black holes are surrounded by an event horizon. Radiation is emitted by the accretion disk surrounding a black hole. However, both accretion and radiation is very irregular process, excluding the surrounding of a black holes as source of a very regular pulsed radio signal.

The shortest period for a rotating system corresponds to rotation at the break-up velocity,

$$R\omega^2 = \frac{GM}{R^2} \quad (10.26)$$

($v = \omega R$) or in terms of the mean density $\rho \sim M/R^3$

$$\omega^2 = G\rho. \quad (10.27)$$

Using as extreme value for the density of a white dwarf $\rho = 10^8 \text{g/cm}^3$ yields $P = 2\pi/\omega \gtrsim 1 \text{ s}$. This excludes rotating white dwarfs.

What about a pulsating white dwarf? The estimate $\omega^2 = G\rho$ holds also for the fundamental frequency of pulsations. Higher harmonics as explanation are excluded because a superposition of frequencies would destroy the observed periodicity. Moreover, energy losses lead generally to an increase of the period in case of oscillations. In case of a binary white dwarf systems we can replace the radius R of the star by the distance $d \gg R$ of the system. Thus the resulting periods are certainly even larger.

Finally, we consider the last option left over, neutron stars. If they are pulsating, the fundamental frequency would be with $\rho_{\text{NS}} \sim 10^6 \rho_{\text{WD}}$ typically too short, $P \sim 10^{-3} \text{ ms}$. A binary system of neutron stars is a copious emitter of gravitational waves as we will discuss in the next chapter. For such small distances as required by the ms periods, the life-time of these systems would be too short. In summary, the only remains option is a rotating neutron star.

Rotating dipole model A simple model for a pulsar is depicted in the figure above as a neutron star with a non-aligned rotation and magnetic field axes. Physically, one can model a pulsar as a rotating sphere endowed with a magnetic dipole moment. The energy of a rotating sphere is $E = 1/2 I \omega^2$ and the energy change due to a change in the rotation velocity ω is

$$\dot{E} = I\omega\dot{\omega}. \quad (10.28)$$

We can estimate the rotational kinetic energy of the Crab nebula, the remnant of a SN observed by Chinese astronomers in 1054, as $E = \frac{1}{2} I \omega^2 \approx 3 \times 10^{49} \text{ erg}$ with $I = aMR^2$ and $a \approx 2/5$ for a homogeneous sphere; its energy-loss per time is the time-derivative $\dot{E} = I\omega\dot{\omega} \approx 7 \times 10^{38} \text{ erg/s}$, with $I = 1.5 \times 10^{45} \text{ g cm}^2$ and the observed change $\dot{\omega} = 4 \times 10^{-4} \text{ yr} \omega$.

The energy loss of a rotating magnetic dipole due to the emission of electromagnetic radiation is

$$\dot{E} = -\frac{B^2 R^6 \omega^4 \sin^2 \alpha}{6c^3}, \quad (10.29)$$

where α denotes the angle between rotation and dipole axis. If the energy is lost as electromagnetic dipole radiation, then

$$\dot{E} = -\frac{B^2 R^6 \omega^4 \sin^2 \alpha}{6c^3} \quad (10.30)$$

where α denotes the angle between rotation and dipole axis, and we obtain an estimate for Crab's magnetic field, $B \approx 7 \times 10^{12}$ G for $\sin \alpha = 1$. Thus pulsars have indeed extremely strong magnetic fields that, if they are fast rotating, may accelerate particles to high energies.

If we define as time-scale τ characterizing the slow-down of a pulsar,

$$\tau = -\frac{\omega}{\dot{\omega}} = -\frac{I\omega^2}{\dot{E}} = \frac{6Ic^3}{B^2 R^6 \omega^2 \sin^2 \alpha}, \quad (10.31)$$

then we can compare the estimated life-time, e.g. of the Crab nebula, $\tau \sim 1243$ yr with its true age, $1972-1054 = 918$ yr, obtaining reasonable agreement. Also, the derived energy output $\dot{E} \sim 6 \times 10^{38}$ erg is comparable to one derived from observations.

Using pulsars as tool

- Dispersion measure and Galactic electron density:

The velocity v of electromagnetic waves in a medium is different from c , $n = v/c \neq 1$. The refractive index n is a function of the wave-length λ and thus there is a dispersion between the arrival times of a pulse at different wave-lengths,

$$\Delta t = \frac{L}{c}(n(\lambda_1) - n(\lambda_2)). \quad (10.32)$$

The deviation of the refractive index n from one is proportional to the number density of electrons, $\Delta n \propto n_e$. (Since n_e is not constant, one should integrate along the line of sight.) Thus the time-delay Δt measures the integrated number density of electron along the line of sight to a pulsar. This was used originally as a check that pulsars are indeed Galactic objects. If the distance to a specific pulsar is known, one can use the method as a tool to measure the electron density n_e in the Galaxy.

- The Faraday effect is used as measure for the Galactic magnetic field.
- Binary systems of pulsars have been used as test for the emission of gravitational waves as predicted by general relativity, as we will discuss in the next chapter.

10.5. Pulsar Wind Nebula

Problems

10.1 Rotating dipole model. A star with radius R and a magnetic dipole field of strength B_p at its pole emits electromagnetic radiation at a rate $\dot{E} = -2/(3c^3)|\dot{\mathbf{m}}|^2$, where the dipole moment is $|\mathbf{m}| = B_p R^3/2$. Estimate for the Crab pul-

sar ($M = 1.4M_\odot$, $R = 12$ km, $P = 0.0331$ s, $\dot{P}/P = 4 \times 10^{-4} \text{yr}^{-1}$) its rotational kinetic energy, its energy loss due to dipole radiation, its age and the value of its magnetic field strength B_p .

11. Supernovae, supernova remnants, GRBs

Novae and supernovae were characterized empirically according to their luminosity and their spectral lines. Novae show a smaller luminosity increase than supernovae with peak luminosities between 10 and 10^6 times their average luminosity. They are recursive events with periods in the range $P \sim 1 \text{ h} - 10^5 \text{ yr}$. By contrast, supernovae are singular events. Supernovae are further divided into type II and type I, depending on the presence of Balmer lines in their spectrum, respectively. cf. with the left panel of Fig. 11.1.

The main observational facts are:

- Type Ia are associated with old stellar populations, while type Ib, Ic and II are associated with young stellar populations.
- No stellar remnant is found in case of type Ia SNe, while in the other cases a neutron star or black hole is formed.
- The spectra in Fig. 11.3 show at early times such large Doppler broadening that single spectral lines are not visible. From this one deduces expansion velocities of $(2 - 10) \times 1000 \text{ km/s}$, with those of type Ia at the upper end of the range.
- The light curves of type Ia are brighter at peak, with total energy close to $E_{\text{light}} \simeq 10^{49} \text{ erg}$. All light curves show an exponential decay on scales of 100 days, cf. with the right panel of Fig. 11.1.

From the first two points one concludes that type Ia SNe are associated with white dwarfs, while the other types are connected to the final stage of massive stars.

11.1. Type Ia supernovae

The physical interpretation of novae and supernovae does not follow precisely this division: Novae and a subset of all type I supernovae called type Ia are variations of accreting binary systems in which energy is generated via thermonuclear reactions. In the case of a nova, the accreted material starts the CNO cycle in a thin layer on the stellar surface when the pressure is large enough, expelling the outermost shell of the star, but not destroying the star. In a type Ia SN, a white dwarf is driven by accretion beyond M_{Ch} and explodes. Alternatively, two white dwarfs in a binary system merge.

From numerical simulations, one finds the following picture

- For $M \rightarrow 1.44 M_{\odot}$, carbon in a white dwarf core starts to fuse into Ni, Co, and lighter elements like Si, Mg. The burning expands outwards from the core, synthesizing lighter elements such as Si, Ca.
- If the burning front reaches around $0.7R$, the pressure of the outer layers is not sufficient to confine the burning process. The white dwarf star explodes.
- If flame travels supersonically (a detonation), then the temperatures are high enough to burn the entire star to Ni. If the flame travels instead subsonically (a deflagration),

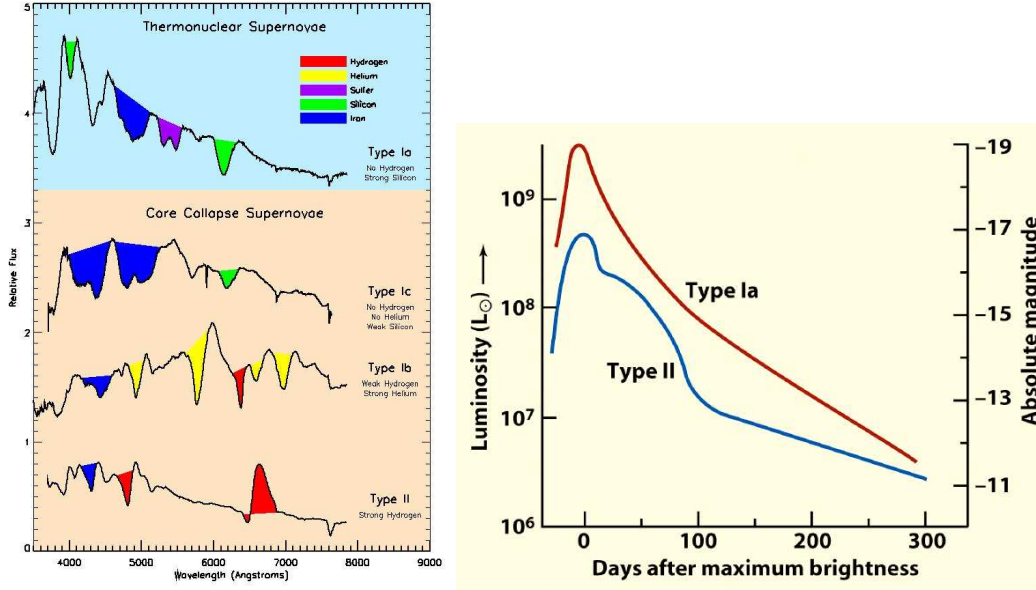


Figure 11.1.: Left: Characteristic spectra of different SN types. Right: Light curve as function of time for type Ia and type II SNe

then the star can pre-expand and burn at lower densities and temperatures. In this case also intermediate elements as Si and Ca are formed.

Observations are best reproduced if $0.8M_{\odot}$ Ni is produced, while the remaining $0.4M_{\odot}$ are converted into lighter elements. This suggests that the ignition starts as a deflagration which then turns into a detonation.

Light curves Let us first assume that after the explosion practically all energy is stored in radiation, $E = uV = aT^4V$. If the radiation contained in the volume $V = 4\pi R^3/3$ expands adiabatically, $dU = -PdV$, it follows

$$R^3 du = -3(1+w)uR^2 dR, \quad (11.1)$$

where we used also $P = wu$ with $w = 1/3$ for radiation. Separating variables and integrating, it follows $u \propto R^{-3(1+w)} = R^{-4}$. Thus the energy in radiation scales as

$$E = uV \propto 1/R \quad (11.2)$$

If the shock moves with $v_{\text{sh}} \simeq 7000 \text{ km/s}$, then the radius is after 10 days around $10^6 R_{WD}$. Thus even starting with 10^{51} erg, after 10 days not enough energy would be left to power the light curve.

The resolution is that the necessary energy is released by radioactive decays:

- $^{56}\text{Ni} \rightarrow ^{56}\text{Co} + e^+ + \nu_e$ with $\tau_{1/2} = 6.1$ days and $q = 3.0 \times 10^{16} \text{ erg/gm}$
- $^{56}\text{Co} \rightarrow ^{56}\text{Fe} + e^+ + \nu_e$ with $\tau_{1/2} = 77.1$ days and $q = 6.4 \times 10^{16} \text{ erg/gm}$

Hence 0.6 solar masses of radioactive Ni and Co can provide 1.1×10^{50} erg at late times after adiabatic expansion is essentially over.

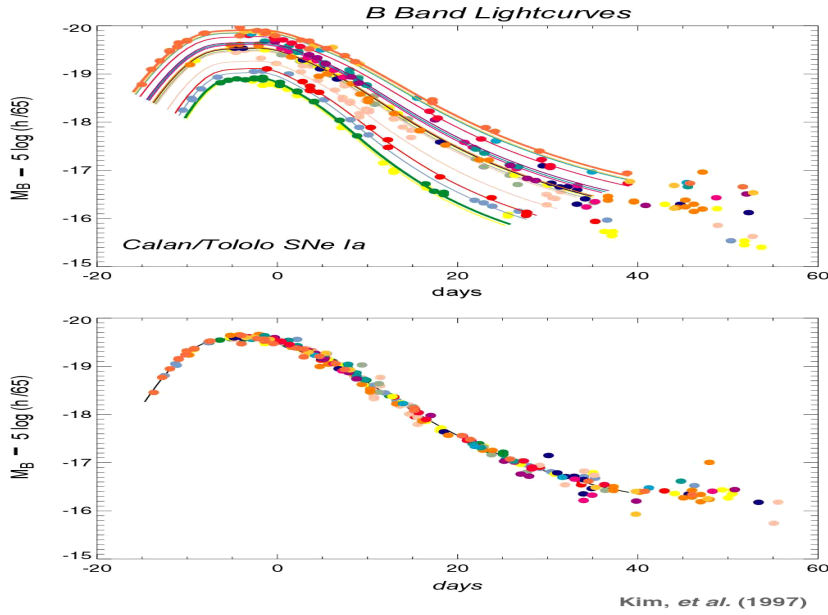


Figure 11.2.: Lightcurves of type Ia supernovae; top observed ones, bottom after rescaling.

SNIa as standard candles Since the white dwarf stars explode crossing the Chandrasekhar limit, $M \gtrsim 1.4M_{\odot}$, the released total energy should vary not to much. Thus one may wonder if they are possible standard candles? This requires that the spread in luminosity, $L = dE/dt$, is not big. As the upper panel of Fig. 11.2, shows more luminous supernovae evolve slower. If this effect is taken into account, as done in the lower panel, the peak luminosity of type Ia SNe varies only by 10%. They can be therefore used as standard candles. Since they are extremely bright, they allow to test the geometry of spacetime at large distances.

11.2. Core collapse supernovae

In addition to type II, core collapse supernovae comprise supernovae showing little or no hydrogen (denoted type Ib and Ic, respectively). The latter are explosions of massive stars that lost some or most of their outer envelopes. How they lose their mass is unclear, but it likely involves binary interaction.

Minimal mass for collapse The large temperature gradient in the center of massive stars leads to convection, mixing the chemical elements in the core. Thus a homogenous core, surrounded by an onion-like shells.

We approximate the exact E.o.S. as the sum of two terms, an ideal gas term and one of a degenerate electrons,

$$\frac{P}{\rho} \simeq \frac{Y_e k T}{m_B} + K_{\gamma} Y_e^{\gamma} \rho^{\gamma-1} \quad (11.3)$$

with electron fraction $Y_e = n_e/n_B$ and $\gamma = 4/3$ (rel.) or $5/3$ (nr). We can use the hydrostatic equilibrium equation to estimate

$$\frac{P_c}{\rho_c} \simeq \frac{GM}{R} \approx CM^{2/3} \rho_c^{1/3} \quad (11.4)$$

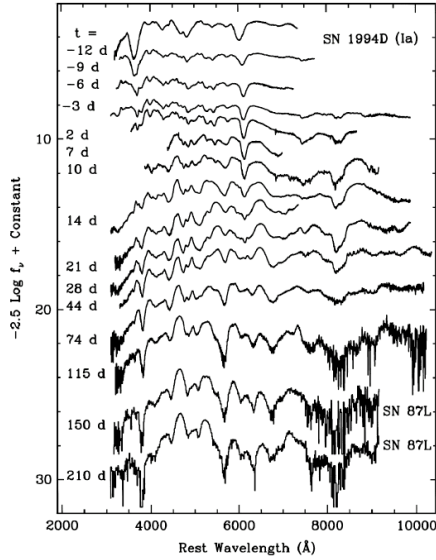


Figure 11.3.: Spectra of type Ia supernovae at different times.

Combining the two equations, we can eliminate the central pressure,

$$\frac{Y_e k T_c}{m_B} \simeq C M^{2/3} \rho_c^{1/3} - K_\gamma Y_e^\gamma \rho_c^{\gamma-1} \quad (11.5)$$

obtaining a relation for the central temperature T_c as the star contracts. For massive stars, the first term dominates and $T_c \propto M^{2/3} \rho_c^{1/3}$. Thus as the core contracts, the central density and temperature increase and as a result heavier and heavier nuclei can ignite. By contrast, the central temperature decreases for small enough M as the star contracts: The temperature of low-mass stars passes through a maximum as they contract and when their pressure is dominated by degenerate electrons they will cool.

We estimate the critical density ρ_0 that separates the two behavior equating the two terms in Eq. (11.5),

$$\rho_0 = \left(\frac{C G M^{2/3}}{K_\gamma Y_e^\gamma} \right)^{\frac{1}{\gamma-4/3}}. \quad (11.6)$$

The border-line between evolution to a WD and core collapse is around $M \gtrsim (6 - 8)M_\odot$.

Onset of collapse Type II or core collapse supernovae occur at the end of the fusion process in very massive stars, $M \gtrsim (5 - 8)M_\odot$. In the last possible fusion reaction, an α particle is added to ^{24}Cr . Inserting into Eq. (5.4) for the reduced mass $\mu = 4 \times 52 / (4 + 52)m_N$ and $Z_1^2 Z_2^2 = (2 \times 24)^2$, we find that iron burning requires temperatures in the MeV range. Thus electrons are relativistic, and photons can produce electron-positron pairs that in turn can produce neutrinos, $\gamma\gamma \leftrightarrow e^+e^- \rightarrow \bar{\nu}\nu$. The latter can escape from the core, leading to efficient cooling to $T \sim m_e \sim 0.5 \text{ MeV}$.

Very massive stars have an onion-like structure with a degenerate iron core. When the iron core reaches the Chandasekhar limit, $M_c \sim 1.4M_\odot$, the self-gravity becomes too strong and the core collapses. Photo-disintegration destroys the heavy nuclei, e.g. via $\gamma + {}^{56}\text{Fe} \rightarrow$

$13\ ^4\text{He} + 4n - 124.4\text{ MeV}$, and removes the thermal energy necessary to provide pressure support. Hence the star contracts further, increasing the central temperature until thermal photons even dissociate helium, $\gamma +\ ^4\text{He} \rightarrow 2p + 2n - 28.3\text{ MeV}$.

As the density increases during the collapse of the core, free electrons are forced together with protons to form neutrons via inverse beta decay, $e^- + p \rightarrow n + \nu_e$. A proto-neutron star is formed. Neutrons are stable, since the Fermi momentum of electrons is larger than the maximal momentum of an electron emitted in beta decay, $p \approx \sqrt{Q^2 - m_e^2} \approx 1.2\text{ MeV}$, where $Q = m_n - m_p$. When core density reaches nuclear density, the equation of state stiffens suddenly and the infalling material is “reflected”. If the supernova is successful, a neutron star is left over. Otherwise a black hole is formed.

Energy budget The released gravitational binding energy,

$$\Delta E = \left[-\frac{3GM^2}{5R} \right]_{\text{NS}} \sim 3 \times 10^{53} \text{ erg} \left(\frac{15\text{ km}}{R} \right) \left(\frac{M_{\text{NS}}}{1.4M_{\odot}} \right)^2 \quad (11.7)$$

is much larger than what is needed for the explosion or the light-curve. The photo-disintegration and inverse beta decay requires 7%, the binding energy of envelope 2%, kinetic energy 0.3% and the light curve 0.3%. The rest is carried away by neutrinos. It is thus clear that the treatment of neutrinos and their transport is crucial for a correct modelling of the explosion mechanism of a core-collapse SN.

Example 11.1: Neutrinos from supernova SN1987A.

The proto-neutron formed during the core collapse of a massive star emits copiously neutrinos. Its mass is $\approx 1.4M_{\odot}$, and its radius $\approx 15\text{ km}$. Estimate the total (gravitational potential) energy E_b released. Apply the virial theorem to a nucleon N at the surface of the proto-neutron star and estimate its kinetic energy E_N . Estimate the number N_{ν} of neutrinos emitted and the duration of the neutrino signal (random walk) using $E_{\nu} = E_N$, $E_b = N_{\nu}E_{\nu}$ and $\sigma_{\nu} = 10^{-43}\text{ cm}^2(E_{\nu}/\text{MeV})^2$. For the case of SN1987A in the Large Magellanic Cloud at a distance of 50 kpc, how many neutrinos were observed (using the same σ_{ν}) in a detector with 10^{32} protons?

The gravitational energy released by the collapse is $E_b \approx 3GM^2/(5R) \approx 2.1 \times 10^{53}\text{ erg}$. The mean kinetic energy E_N of a nucleon is $E_N = E_{\text{pot}}/2 \approx Gm_N M/(2R) \approx 1 \times 10^{-4}\text{ erg}$ or 64 MeV. The number of emitted neutrinos follows as $N_{\nu} = E_b/E_N \approx 2 \times 10^{57}$.

The number of steps in a random walk with step size ℓ_{int} needed to reach the distance R is $N = R^2/\ell_{\text{int}}^2$. Hence the duration τ of the neutrino signal is $\tau \approx N\ell_{\text{int}}/c = R^2/(c\ell_{\text{int}})$. The step size ℓ_{int} is found as $\ell_{\text{int}} = 1/(n\sigma) \approx 1\text{ m}$ for $E_{\nu} = 30\text{ MeV}$ and $n \approx 10^{38}/\text{cm}^3$. Thus $\tau \approx 1\text{ s}$.

The neutrino flux at Earth is $\phi_{\nu} = N_{\nu}/(4\pi D^2)$ with $D = 50\text{ kpc}$. The event number N_{ev} in a detector with N_p targets each with cross section σ is $N_{\text{ev}} = N_p\sigma\phi_{\nu} \approx 54$. However, from all 2×3 neutrino types, only $\bar{\nu}_e$ have the quoted large cross section with protons. Thus $N_{\text{ev}}(\bar{\nu}_e) \approx N_{\text{ev}}/6$. Our simplified picture agrees roughly with reality: From SN1987A 11-12 and 8 neutrino events with energies 20 – 40 MeV during $\sim 10\text{ s}$ were observed in the two water Cherenkov detectors operating at that time.

11.3. Supernova remnants

A supernova explosion acts as a point-like injection of kinetic energy $E = Mv^2/2$ into the interstellar medium (ISM). After a few months, when the light-curve of a SN faded away,

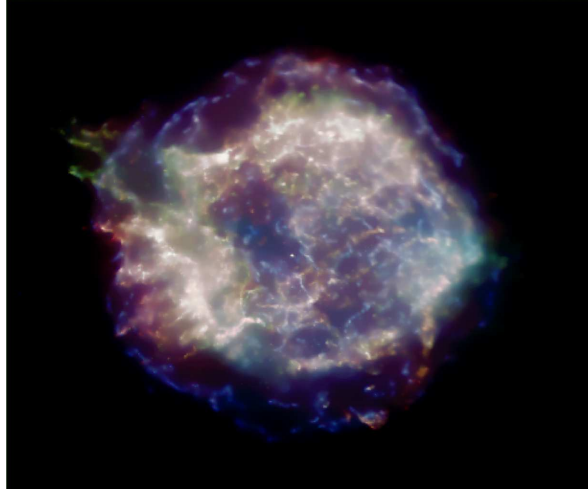


Figure 11.4.: SNR Cas A

a supernova remnant becomes visible as the blastwave of the explosion crosses the ISM. A famous example for a SNR is the remnant of the SN CasA shown in Fig. 11.4.

We make the simplistic assumption that the ISM around the SN has constant density ρ_0 and pressure P_0 . The word explosion implies that the velocity of the ejected material is much larger than the thermal velocities of the ISM, $E/M \gg P_0/\rho_0$. Our assumption of a point-like injection of energy into a uniform medium implies that the shock wave will be spherical symmetric, and we can specify the time-evolution implicitly by the shock radius $R_{\text{sh}}(t)$.

The evolution of a SNR can be split into several phases: In phase I, the shock has swept out less mass from the ISM than its own mass. With $P_0 = \rho_0 v^2/3$ and $E = Mv_{\text{sh}}^2/2$ it follows $\rho_0 \ll M/R^3$. Hence the shock expands freely, $R_{\text{sh}} \propto t$. In phase III, the injected energy became smaller than the internal energy of the ISM inside the shock, $E \ll P_0 R^3$. In the intermediate phase II, the shock radius satisfies the inequality

$$(M/\rho_0)^{1/3} \ll R \ll (E/P_0)^{1/3}. \quad (11.8)$$

Hence, the dynamics in this phase is determined only by the injected mechanical energy E and the original density ρ_0 of the surrounding ISM, while we can neglect the variables M and P_0 . Using only the former two quantities, we cannot form a combination $E^\alpha \rho_0^\beta$ with the dimension of a length or time. This means that the problem does not contain a typical time- or length-scale¹ and therefore the solution has to be *self-similar*. This implies that any quantity $X(r, t)$ factorises as $X(r, t) = g(t)f(\xi)$ with $\xi = r/\lambda$: Thus the spatial dependence of any physical quantity varies as function of time only by the normalisation.

Sedov-Taylor solution We consider now the time-evolution of the shock in phase II, which is often called the Sedov-Taylor phase.

If R_{sh} denotes the position of the shock, then dimensional analysis shows that

$$R_{\text{sh}}(t) = \alpha \left(\frac{Et^2}{\rho} \right)^{1/5}, \quad (11.9)$$

¹Contrast this to stellar physics, where M, R and G can be combined into the free-falling time $\tau_{\text{ff}} \approx (G\rho)^{-1/2}$.

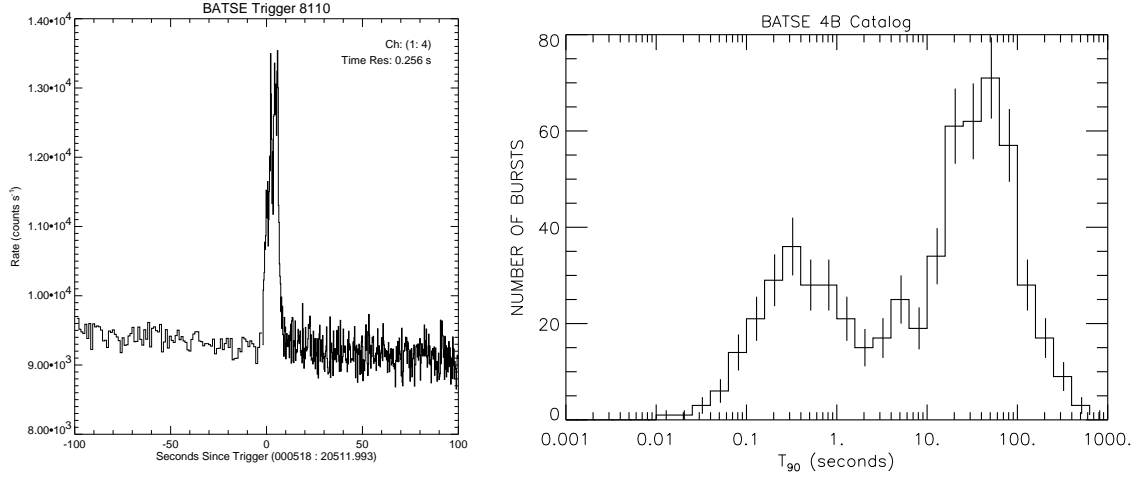


Figure 11.5.: Left: Light curve of GRB000518. Right: Durations of GRBs in the 4B catalogue; the duration parameter used is T_{90} , which is the time over which a burst emits from 5% of its total measured counts to 95%.

where α is dimensionless constant that depends on the EoS of the ISM (with $\alpha \simeq 1.21$ for a mono-atomic gas).

The shock velocity follows differentiating R_{sh} as

$$v_{\text{sh}}(t) = \dot{R}_{\text{sh}}(t) = \frac{2\alpha}{5} \left(\frac{E}{\rho t^3} \right)^{1/5} = \frac{2}{5} \frac{R_{\text{sh}}}{t}. \quad (11.10)$$

11.4. Gamma-ray bursts

Gamma Ray Bursts were first observed as flushes of gamma-rays in the MeV range by the Vela satellites in the late 1960s. Their light curves are extremely diverse, with large variations from event to event. Depending on their duration that varies from fraction of a second to many minutes, they are divided into two sub-varieties: The distribution of the observed duration show a clear bimodality, suggesting the existence of two separate populations: a "short" population with an average duration of about 0.3 seconds and a "long" population with an average duration of about 30 seconds.

Two basic observations are:

- Compactness: time variability $\delta t \sim 10 \text{ ms} \Rightarrow$ source $R < c\delta t \sim 3000 \text{ km}$
- Energy budget (with the fluence F as the time-integrated flux)

$$E_{\text{iso}} = 4\pi D^2 F \approx 10^{41} \text{ erg} \left(\frac{D}{3\text{kpc}} \right)^2 \left(\frac{F}{10^{-4} \text{ erg/cm}^2} \right)$$

The large energy output required was interpreted for long time in favor of a Galactic origin of GRBs, as e.g. glitches in the crust of neutron stars. This interpretation was challenged when the BATSE detector on board NASA's Compton Gamma-Ray Observatory started to detect from 1991 on a large numbers of GRBs, with an isotropic distribution on the sky (cf. left panel of Fig. 11.6), pointing therefore to an extragalactic origin.

The confirmation came in 1997 when the satellite BeppoSAX detected the gamma-ray burst GRB 970508. This event was localized within four hours of its discovery, allowing observations much sooner than any previous burst. The spectrum of the object revealed a redshift of $z = 0.835$, corresponding to a (luminosity) distance of 5400 Mpc. The largest redshift of a GRB found is $z = 9.4$, corresponding to an age of the universe of 500 Myr at the explosion.

The distance and time-variability poses two major problems: First, the energy released in photons can be up to $\text{few} \times 10^{54}$ erg, i.e. much larger than the total energy released in a type II SN. Second, the photon density in such a object should be so high that GeV photons produce e^+e^- pairs and cannot escape. The presence of e^+e^- pairs (and thus of temperatures in the MeV range) is however suggested, as they are effective radiator of high-energy photons. We can estimate the density of photons from the observed luminosity and the time-variability as

$$\tau_\gamma = \sigma_{\text{pair}} n_b R \simeq \frac{\sigma_{\text{Th}} L_{\text{iso}}}{m_e c^3 R} \quad (11.11)$$

$$= 10^{13} \left(\frac{L_{\text{iso}}}{10^{52} \text{erg/s}} \right) \left(\frac{\delta t}{10 \text{ms}} \right)^{-1}. \quad (11.12)$$

Here, we used $L = 4\pi R^2 \mathcal{F}$, $\mathcal{F} = \pi I$, $u = 4\pi/cI$ and $n = u/\langle \varepsilon \rangle$ with $\langle \varepsilon \rangle = m_e c^2$ as typical energy of the photons as well as the approximation $\sigma_{\text{pair}} \approx \sigma_{\text{Th}}$. Thus the optical depth is extremely high, and photons above the pair-creation threshold should be absorbed.

Both problems are avoided if the source (“fireball”) of these photons moves with relativistic velocities, as we will discuss next.

11.4.1. Relativistic effects

An important relativistic effect is the beaming of emitted radiation into the forward direction. As a result, the intensity of a relativistic source (e.g. a GRB or the hot spot of a radio galaxy) moving towards us can be increased by a large factor, 10^3 – 10^6 , compared to isotropic emission.

Doppler effect We recall first how the frequency of photon emitted by a moving source changes. We consider now how the wave-vector of a photon ($\omega/c, \mathbf{k}$) transforms under a Lorentz transformation,

$$\frac{\omega'}{c} = \frac{\frac{\omega}{c} - \frac{V}{c} k_x}{[1 - (V/c)^2]^{1/2}} \quad (11.13)$$

Setting $k_x = k \cos \alpha = \frac{\omega}{c} \cos \alpha$, where α the angle between the wave vector/propagation direction and the direction of movement of the source, we obtain the relativistic Doppler formula

$$\delta \equiv \frac{\omega}{\omega'} = \frac{[1 - (V/c)^2]^{1/2}}{1 - (V/c) \cos \alpha} = \frac{[1 - \beta^2]^{1/2}}{1 - \beta \cos \alpha} = [\gamma(1 - \beta \cos \alpha)]^{-1}. \quad (11.14)$$

Aberration and beaming Classical aberration was discovered 1725 by James Bradley: He discovered and later explained an apparent motion² of celestial objects caused by the finite

²This motion depends on the velocity of the observer perpendicular to the line-of-sight to the star, but is independent of the distance to the star. The deviation induced by classical aberration is much larger than the parallax we discussed already.

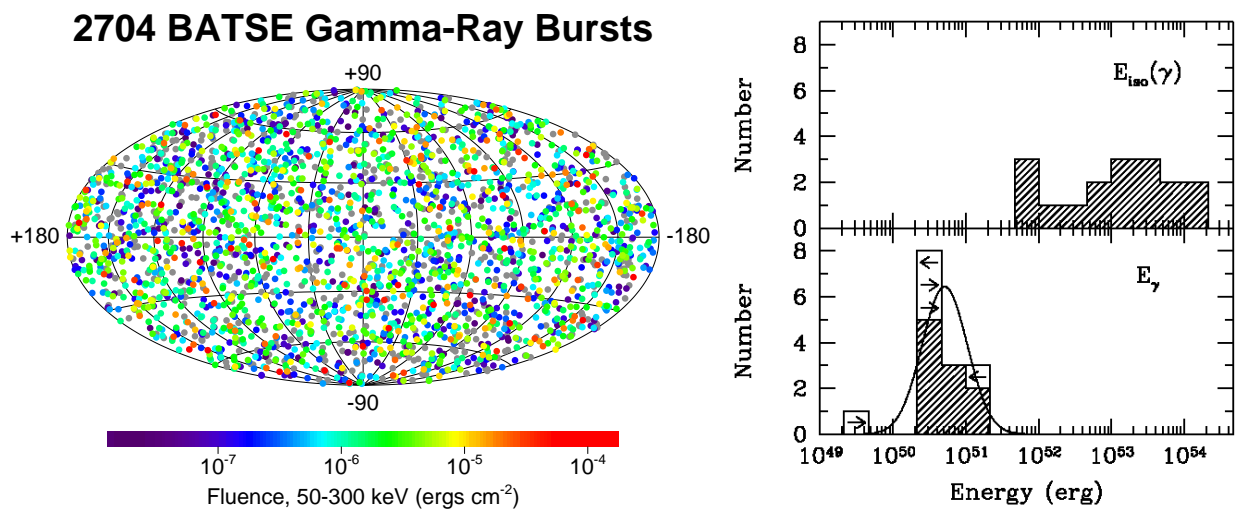


Figure 11.6.: Left: Sky distribution of GRBs detected by BATSE in Galactic coordinates. Right: The distribution of the apparent isotropic γ -ray burst energy of GRBs with known redshifts (top) versus the geometry-corrected energy for those GRBs whose afterglows exhibit the signature of a non-isotropic outflow (bottom). The mean isotropic equivalent energy $\langle E_{iso}(\gamma) \rangle$ for 17 GRBs is 110×10^{51} erg with a $1\text{-}\sigma$ spreading of a multiplicative factor of 6.2. The value of $\langle \log E_{\gamma} \rangle$ is 50.71 ± 0.10 (1σ) or equivalently, the mean geometry-corrected energy $\langle E_{\gamma} \rangle$ for 15 GRBs is 0.5×10^{51} erg. The standard deviation in $\log E_{\gamma}$ is $0.31_{-0.06}^{+0.09}$, or a $1\text{-}\sigma$ spread corresponding to a multiplicative factor of 2.0; from Ref. [9]

speed of light and the motion of the Earth in its orbit around the Sun. Assume e.g. to observe a star at the moment when it is right in the zenith. Since the Earth moves, you have to point the telescope a bit “ahead” and thus the position of stars changes in the course of one year.

To obtain the relativistically correct form for the aberration formula, we rewrite first the Lorentz transformations for x and t in differential form,

$$dt = \gamma(dt' + v/c^2 dx') \quad (11.15)$$

$$dx = \gamma(dx' + v dt'), \quad (11.16)$$

$$dy = dy', \quad dz = dz'. \quad (11.17)$$

Then we obtain the transformation law for velocities \mathbf{u} as

$$u_{\parallel} = \frac{dx_{\parallel}}{dt} = \frac{u'_{\parallel} + v}{1 + vu'_{\parallel}/c^2} \quad (11.18)$$

$$u_{\perp} = \frac{dx_{\perp}}{dt} = \frac{u'_{\perp}}{\gamma(1 + vu'_{\parallel}/c^2)}. \quad (11.19)$$

The so-called aberration formula connects the angle between the velocities \mathbf{u} and \mathbf{u}' in the two frames,

$$\tan \vartheta = \frac{u_{\perp}}{u_{\parallel}} = \frac{u' \sin \vartheta'}{\gamma(u' \cos \vartheta' + v)}. \quad (11.20)$$

The most interesting case is the aberration of light. We set $\vartheta' = \pi/2$, i.e. we ask how light emitted into one half-sphere appears in a different inertial system. With $u = u' = c$ it follows then

$$\tan \vartheta = \frac{c}{\gamma v} \quad (11.21)$$

or $\vartheta \approx 1/\gamma$ for $v \rightarrow c$. Thus a fast moving source emits photons mainly in a cone of opening angle $\vartheta \approx 1/\gamma$ around its forward direction.

The presence of beaming and in particular the value of the Gamma factor be observationally tested by the effect of “jet breaking”, cf. with Fig. 11.7.

Photon escape The threshold energy for pair production $\gamma\gamma \rightarrow e^+e^-$ can be derived from the condition that the e^+e^- pair is created at rest, or

$$(p_a + p_b)^2 \geq (2m_e c^2)^2 \quad (11.22)$$

if p_a and p_b denote the four-momentum of the two photons. Squaring the LHS, it follows with ϑ as the angle between the three-momenta of the two photons

$$(p_a + p_b)^2 = 2\varepsilon_a \varepsilon_b (1 - \cos \vartheta) \geq (2m_e c^2)^2 \quad (11.23)$$

The minimal energy is obtained for a head-on collision, $\varepsilon_a \varepsilon_b = (m_e c^2)^2$. In contrast, collinear photons of arbitrarily high energy cannot produce a e^+e^- pair.

We are now in the position to understand how high-energy photons can escape from the relativistic fireball of a GRB. The three-momenta of such photons measured by an observer at rest are contained within an angle $\vartheta \simeq 1/\Gamma$. If we choose Γ sufficiently high, the photons are

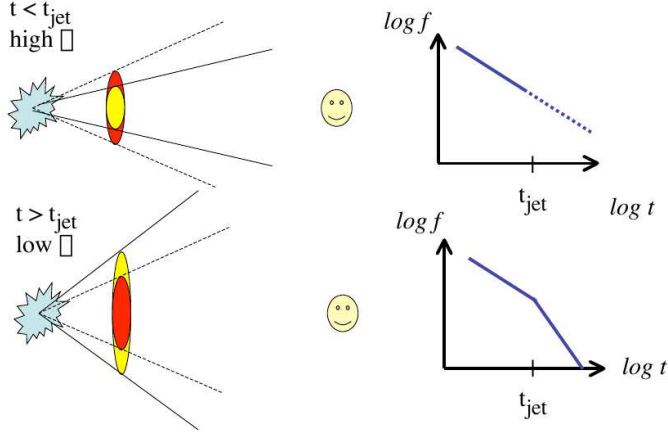


Figure 11.7.: Jet breaking

below the pair-creation threshold. Using $1 - \cos \vartheta \simeq \vartheta^2/2 = 1/2\Gamma^2$ for $\Gamma \gg 1$, this condition becomes

$$\Gamma^2 \geq \frac{\varepsilon_a \varepsilon_b}{(2m_e c^2)^2}. \quad (11.24)$$

If we require that 10 GeV photons can escape from the fireball, then we obtain as lower limit for the gamma factor

$$\Gamma \gtrsim 100 \left(\frac{\varepsilon_a}{\text{MeV}} \right)^{1/2} \left(\frac{\varepsilon_b}{10 \text{ GeV}} \right)^{1/2}. \quad (11.25)$$

Source size Additionally, our causality constraint on the source size has to be modified. Let us assume that a shell moving radially outwards emits at $t_{\text{em},1}$ and $t_{\text{em},2}$ two light signals which are at $t_{\text{obs},1}$ and $t_{\text{obs},2}$ measured by an observer at an angle ϑ . Then

$$c(t_{\text{obs},2} - t_{\text{obs},1}) - c(t_{\text{em},2} - t_{\text{em},1}) = v(t_{\text{em},2} - t_{\text{em},1}) \cos \vartheta \quad (11.26)$$

Solving for $\Delta t_{\text{obs}} = t_{\text{obs},2} - t_{\text{obs},1}$ gives

$$\Delta t_{\text{obs}} = (1 - \beta \cos \vartheta) \Delta t_{\text{em}}. \quad (11.27)$$

For $\beta \rightarrow 1$ and $\vartheta \simeq 0$, it follows $\Delta t_{\text{obs}} \simeq \Delta t_{\text{em}}/(2\Gamma^2)$. Thus the source size is $R \lesssim 2\Gamma^2 c \delta t_{\text{var}}$, i.e. a factor $2\Gamma^2$ larger than our naive estimate.

Interpretation A cartoon illustrating current models for short and long GRBs is shown in Fig. 11.8. Short duration GRBs are the result of the coalescence of a binary system, consisting most likely of two neutron stars. As discussed in 8.5, such events lead to gravitational wave signal. Moreover, they were suggested as sites of r -process nucleosynthesis. These ideas were confirmed by the observation of GW 170817 followed by GRB 170817A.

Long duration GRBs which make up about 2/3 of all GRBs are associated with supernova events in extremely massive stars (“hypernovae”). The observation of GRB 180720B by H.E.S.S. confirmed that the gamma-ray emission extends at least up to TeV energies.

In both types of GRBs, two collimated highly relativistic ($\Gamma = 100$ –1000) outflows form an expanding fireball with temperatures around MeV (i.e. a plasma consisting of photons

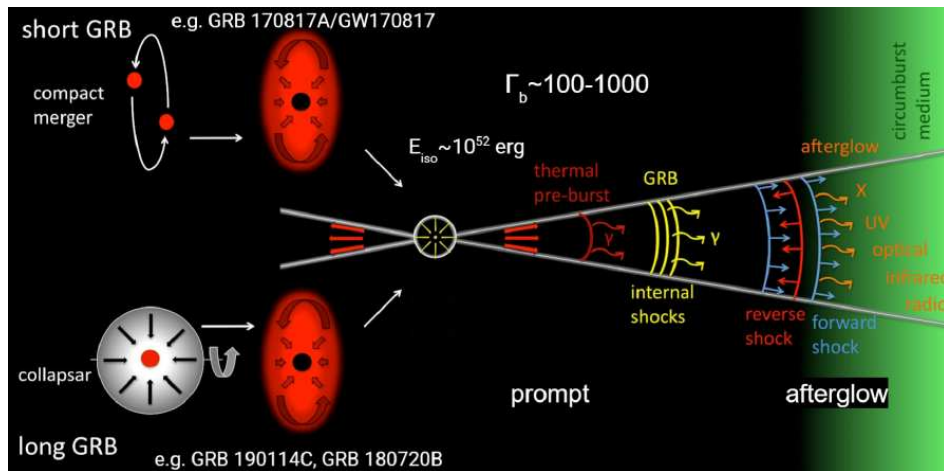


Figure 11.8.: Schematic time evolution of a GRB.

and e^+e^- pairs). As the fireball expands, it cools. Shocks form, when layers with different velocities overtake, and when the external ISM is rammed up. These shocks are crucial for the transformation of part of the thermal energy into high-energy particles, as we will see in the next chapter.

12. Cosmic rays and acceleration

We discuss Fermi first- and seconder acceleration as two of the most popular approaches to explain the presence of high-energy electrons and proton around sources like SNR, GRBs and AGNs.

12.1. Acceleration of cosmic rays

12.1.1. Bell's approach

Average energy gain We consider a cosmic ray with initial energy E_1 “scattering” elastically on a magnetic cloud that moves with velocity $V \ll c$. We want to derive the energy gain $\xi \equiv (E_2 - E_1)/E_1$ per scattering. The variables (E_1, ϑ_1) and (E_2, ϑ_2) are shown in Fig. 12.1, which we label with a prime in the cloud system and without a prime in the lab system.

With a first Lorentz transformation between the lab and cloud system we connect the variables characterizing the cosmic ray entering the cloud,

$$E'_1 = \gamma E_1 (1 - \beta \cos \vartheta_1) \quad \text{where} \quad \beta = V/c \quad \text{and} \quad \gamma = 1/\sqrt{1 - \beta^2}, \quad (12.1)$$

and with a second Lorentz transformation the exit variables,

$$E_2 = \gamma E'_2 (1 + \beta \cos \vartheta'_2). \quad (12.2)$$

Since the scattering off magnetic irregularities is collisionless and the cloud is very massive, energy is conserved, $E'_2 = E'_1$. Hence we can eliminate E'_2 and obtain as relative energy gain

$$\xi = \frac{E_2 - E_1}{E_1} = \frac{1 - \beta \cos \vartheta_1 + \beta \cos \vartheta'_2 - \beta^2 \cos \vartheta_1 \cos \vartheta'_2}{1 - \beta^2} - 1. \quad (12.3)$$

To proceed, we need the average values of $\cos \vartheta_1$ and $\cos \vartheta'_2$. Since the cosmic ray scatters off magnetic irregularities many times in the cloud, its exit direction is randomized, $\langle \cos \vartheta'_2 \rangle = 0$. The collision rate of the cosmic ray with the cloud is proportional to their relative velocity v_{rel} . We will derive the definition of v_{rel} valid for relativistic particles in the next chapter. In the case at hand, the use of the non-relativistic $v_{\text{rel}} = (v - V \cos \vartheta_1) = c(1 - \beta \cos \vartheta_1)$ gives the correct result also in the limit $v \rightarrow c$. Thus the collision rate is

$$\frac{dn}{d\Omega_1} \propto (1 - \beta \cos \vartheta_1). \quad (12.4)$$

We obtain $\langle \cos \vartheta_1 \rangle$ averaging $\cos \vartheta_1$ weighted by $dn/d\Omega_1$ over all angles,

$$\langle \cos \vartheta_1 \rangle = \int \cos \vartheta_1 \frac{dn}{d\Omega_1} d\Omega_1 / \int \frac{dn}{d\Omega_1} d\Omega_1 = -\frac{\beta}{3}. \quad (12.5)$$

Plugging $\langle \cos \vartheta'_2 \rangle = 0$ and $\langle \cos \vartheta_1 \rangle = -\beta/3$ into Eq. (12.3) and taking into account that $\beta \ll 1$ gives as average gain

$$\langle \xi \rangle = \frac{1 + \beta^2/3}{1 - \beta^2} - 1 \simeq \frac{4}{3} \beta^2. \quad (12.6)$$

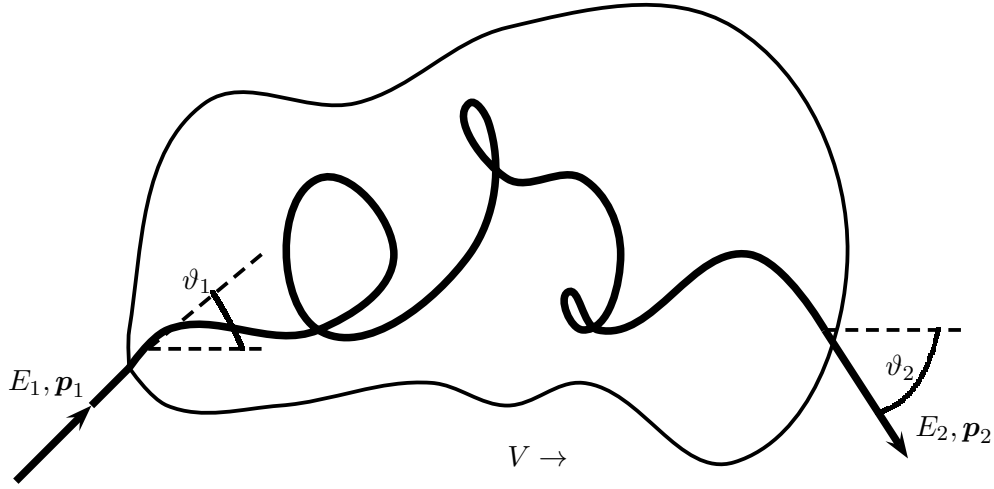


Figure 12.1.: A cosmic ray “scattering” elastically at a magnetic cloud moving with velocity V .

Thus $\langle \xi \rangle \propto \beta^2 > 0$ and we have shown that on average a cosmic ray gains energy scattering on “magnetic clouds” with an ordered bulk velocity V . The energy gain per scattering is however only of second order in the small parameter β , and acceleration is therefore rather inefficient. Moreover, one can show that the resulting energy spectrum would depend strongly on the cloud parameters, making thereby the observed feature-less power spectrum of cosmic rays difficult to understand. Acceleration at shocks that we consider next avoids both disadvantages.

We consider again a cosmic ray with initial energy E_1 “scattering” at magnetic irregularities that are now separated by a planar shock moving with velocity v_s . The only change to the previous discussion are the resulting different angular averages. The (normalized) crossing rate is given by the projection of an isotropic flux on the planar shock,

$$\frac{dn}{d \cos \vartheta_1} = \begin{cases} 2 \cos \vartheta_1 & \cos \vartheta_1 < 0 \\ 0 & \cos \vartheta_1 > 0 \end{cases} . \quad (12.7)$$

while the crossing rate $dn/d \cos \vartheta_2$ is non-zero for $\cos \vartheta_2 > 0$. Thus $\langle \cos \vartheta_1 \rangle = -\frac{2}{3}$ and $\langle \cos \vartheta_2 \rangle = \frac{2}{3}$ and hence

$$\langle \xi \rangle \approx \frac{4}{3} \beta = \frac{4}{3} \frac{v_1 - v_2}{c} . \quad (12.8)$$

The average gain $\langle \xi \rangle$ is now linear in β and justifies the name “first-order” Fermi or diffusive shock acceleration.

Energy spectrum produced by Fermi acceleration The energy E_n of a cosmic ray after n acceleration cycles is

$$E_n = E_0(1 + \xi)^n \quad (12.9)$$

and the number of cycles needed to reach E_n is thus

$$n = \frac{\ln(E_n/E_0)}{\ln(1 + \xi)} . \quad (12.10)$$

If the escape probability p_{esc} per encounter is constant, then the probability to stay in the acceleration region after n encounters is $(1 - p_{\text{esc}})^n$. We obtain the fraction f of particles with energy $> E_n$ as

$$f(> E) = \sum_{m=n}^{\infty} (1 - p_{\text{esc}})^m = \frac{(1 - p_{\text{esc}})^n}{p_{\text{esc}}} \propto \frac{1}{p_{\text{esc}}} \left(\frac{E}{E_0} \right)^{\gamma}, \quad (12.11)$$

where

$$\gamma = \ln \left(\frac{1}{1 - p_{\text{esc}}} \right) / \ln(1 + \xi) \approx p_{\text{esc}} / \xi \quad (12.12)$$

with $\xi \ll 1$ and $p_{\text{esc}} \ll 1$. Hence, both first and second order Fermi acceleration produces a power-law energy spectrum.

The maximal energy achievable by a specific source is determined by several factors. First, the finite life-time limits the number of cycles n and thus E_n . Second, the escape probability is energy dependent and increases generally for increasing energy. Third, energy losses like synchrotron radiation increase with energy and balance at a certain point the energy gain.

Exponent γ for shock acceleration Since we know already that $\xi \approx \frac{4}{3}\beta = \frac{4}{3}\frac{v_1 - v_2}{c}$, we have to determine only the escape probability p_{esc} in order to estimate the exponent $\gamma \approx p_{\text{esc}} / \xi$ of the integral spectrum produced by shock acceleration. The particle flux \mathcal{F} through an infinite, planar shock front is (cf. Eq.(2.23))

$$\mathcal{F}(E) = \pi I(E) = \frac{cn(E)}{4}, \quad (12.13)$$

assuming $v_s \ll c$ and an efficient isotropization of cosmic rays up-stream.

In the shock rest frame, there is a particle flow $\mathcal{F}_{\text{esc}}(E) = v_2 n(E)$ downstream away from the shock front that will be lost for the acceleration process. Thus the escape probability p_{esc} as the ratio of the loss and the crossing flux is

$$p_{\text{esc}} = \frac{\mathcal{F}_{\text{esc}}}{\mathcal{F}} = \frac{v_2 n}{cn/4} = \frac{4v_2}{c} \quad (12.14)$$

and the spectral index of the integral energy spectrum follows as

$$\gamma \approx p_{\text{esc}} / \xi \approx \frac{3}{v_1/v_2 - 1}. \quad (12.15)$$

Typical values for the sound speed in the interstellar medium around a SNR are $c_1 \sim 10$ km/s, while the shock velocities are $v_1 \sim 10^4$ km/s. Thus the Mach number $\mathcal{M} = v_1/c_1 \gg 1$ and we can use the result $v_1 = 4v_2$ in the strong shock limit. The exponent predicted by Fermi acceleration at non-relativistic shock is therefore independent of the shock parameters and agrees with the value needed to explain the spectrum of Galactic cosmic rays. These are the two main reasons for the popularity of shock acceleration.

12.1.2. ***Fluid approach***

While in Bell's approach we considered CRs as individual particles, we can view CRs also as a fluid. Then we replace the random scattering on magnetic clouds or irregularities by a

diffusion process. Hence the acceleration process is described by a diffusion equation (2.39) for the phase-space density $f(\mathbf{x}, \mathbf{p})$ of cosmic rays, adding advection terms,

$$\frac{\partial f}{\partial t} + \mathbf{u} \cdot \nabla f = -\nabla \cdot \mathbf{j}_x + \frac{\partial j_p}{\partial p} \quad (12.16)$$

$$= \nabla \cdot D \nabla f + \frac{1}{3} \nabla \cdot \mathbf{u} p \frac{\partial f}{\partial p}. \quad (12.17)$$

The LHS corresponds to the convective derivative \mathcal{D} applied to $f(x, p)$. The first term on the RHS corresponds to $D\Delta f$, after inserting Fick's law (2.38) and assuming then a uniform, isotropic diffusion constant D . The second term on the RHS accounts for the momentum change due to the expansion or compression of a fluid element. We have already seen an example for the importance of adiabatic cooling in section 11.2. The precise form of this term can be derived from

$$\frac{\partial f}{\partial t} = \frac{\partial f}{\partial p} \frac{\partial p}{\partial t} \quad (12.18)$$

with

$$\frac{dE}{dt} = -\frac{1}{3} \frac{E}{V} \frac{dV}{dt} = \frac{1}{3} E \nabla \cdot \mathbf{u} \quad (12.19)$$

and assuming the ultrarelativistic limit, $E \simeq p$.

We consider a one-dimensional shocked flow in the shock rest frame as shown in the lower panel of Fig. 7.4. If the shock is located at $x = 0$, then the flow speed is

$$u(x) = \begin{cases} u_1 & \text{for } x < 0, \\ u_2 & \text{for } x > 0, \end{cases} \quad (12.20)$$

with u_1 as the upstream and $u_2 < u_1$ the downstream speed. For simplicity, we assume that the diffusion coefficient is constant, but may have different constant values upstream and downstream of the shock,

$$D(x) = \begin{cases} D_1 & \text{for } x < 0, \\ D_2 & \text{for } x > 0. \end{cases} \quad (12.21)$$

For instance, the magnetic field may be enhanced by the shock, leading to an increased diffusion coefficient downstream.

Then the diffusion equation with advection becomes in the 1d limit

$$\frac{\partial f(x, p)}{\partial t} + u(x) \frac{\partial f(x, p)}{\partial x} = D(x) \frac{\partial^2 f(x, p)}{\partial x^2}, \quad (12.22)$$

where $f(x, p)$ is the particle distribution function. In a steady state, this equation simplifies to

$$u(x) \frac{\partial f(x, p)}{\partial x} = D(x) \frac{\partial^2 f(x, p)}{\partial x^2}. \quad (12.23)$$

The general solution of (12.23) is

$$f(x, p) = \begin{cases} A(p) \exp(u_0 x / D_0) + B(p) & \text{for } x < 0, \\ C(p) \exp(u_2 x / D_2) + E(p) & \text{for } x > 0, \end{cases} \quad (12.24)$$

as can be checked by substituting.

Next we seek for the special solution which obeys the boundary conditions we want to impose. First, we assume for simplicity that the particles far upstream from the shock have a unique momentum, i.e. we approximate the distribution function of non-accelerated particles as

$$\lim_{x \rightarrow -\infty} f(x, p) = f_0(p) = \frac{f_0}{p_0} \delta(p - p_0) \quad (12.25)$$

Moreover, we require that the distribution function of outgoing particles is bounded from above, $f(x, p) < \infty$ for all x . Next we impose the continuity of the particle density and of the particle flux at the discontinuity/shock $x = 0$,

$$\lim_{x \rightarrow 0^-} f(x, p) = \lim_{x \rightarrow 0^+} f(x, p) \quad (12.26)$$

$$\lim_{x \rightarrow 0^-} \left(-D_0 \frac{\partial f(x, p)}{\partial x} - \frac{p}{3} \frac{\partial f(x, p)}{\partial p} \right) = \lim_{x \rightarrow 0^+} \left(-D_2 \frac{\partial f(x, p)}{\partial x} - \frac{p}{3} \frac{\partial f(x, p)}{\partial p} \right) \quad (12.27)$$

The first equation expresses the requirement of continuity of the particle density, and the second of particle flux. Boundary conditions require $B = f_0$ and $C = 0$.

Now we can use the conditions at $x = 0$, where the density continuity equation constrains A and E as

$$A(p) + f_0(p) = E(p) \quad (12.28)$$

We rewrite the flux continuity condition as

$$D_0 \lim_{x \rightarrow 0^-} \left(-D_0 \frac{\partial f(x, p)}{\partial x} \right) - \lim_{x \rightarrow 0^+} \left(-D_2 \frac{\partial f(x, p)}{\partial x} \right) = -\frac{p}{3} \frac{\partial f(0, p)}{\partial p} \quad (12.29)$$

Let us finally state the assumptions used in our derivation: For simplicity, we assume that the diffusion coefficient does not depend on the momentum the diffusion particles. A generalisation of our result is done in exercise X. Moreover, we have assumed that the diffusion being isotropic in the plasma frame. This assumption breaks down for fast, relativistic shock: If the shock is fast enough, it catches the particle up-stream before isotropization is complete.

12.1.3. Other acceleration mechanisms

Direct acceleration of particles by pulsars Recall the rotating dipole model for a pulsar:

The energy of a rotating sphere is $E = I\omega^2/2$ and the energy change is

$$\dot{E} = I\omega\dot{\omega}. \quad (12.30)$$

The rotational kinetic energy of the Crab nebula, the remnant of a SN observed by Chinese astronomers in 1054, is $E = \frac{1}{2}I\omega^2 \approx 3 \times 10^{49}$ erg with $I = aMR^2$ and $a \approx 2/5$ for a homogeneous sphere; its energy-loss per time is the time-derivative $\dot{E} = I\omega\dot{\omega} \approx 7 \times 10^{38}$ erg/s, with $I = 1.5 \times 10^{45}$ g cm² and $\dot{\omega} = 4 \times 10^{-4}$ yr⁻¹ ω .

If the energy is lost as electromagnetic dipole radiation, then

$$\dot{E} = -\frac{B^2 R^6 \omega^4 \sin^2 \alpha}{6c^3} \quad (12.31)$$

where α denotes the angle between rotation and dipole axis, and we obtain an estimate for Crab's magnetic field, $B \approx 7 \times 10^{12}$ G for $\sin \alpha = 1$. Thus pulsars have indeed extremely strong magnetic fields that, if they are fast rotating, may accelerate particles to high energies.

The light-cylinder around a pulsar is the surface at $R_c = c/\omega$. If the magnetic field lines would rotate rigidly with the pulsar, then the linear velocity reaches the speed of light, $v = c$, at R_c .

If the magnetosphere is filled sufficiently with plasma, the electric conductivity $\sigma \rightarrow \infty$, and Ohm's law $J = \sigma(E + vB/c)$ implies

$$\mathbf{E} = -\mathbf{v} \times \mathbf{B}/c, \quad (12.32)$$

where $\mathbf{v} = \boldsymbol{\omega} \times \mathbf{r}$.

For a magnetic dipole field pointing along $\vartheta = 0$,

$$\mathbf{B}(r) = \frac{B_0 R^3}{r^3} (2\mathbf{e}_r \cos \vartheta + \mathbf{e}_\vartheta \sin \vartheta), \quad (12.33)$$

the potential difference between the polar cap and infinity follows as

$$\Delta\phi = \int \mathbf{E} \cdot d\mathbf{s} = -\frac{1}{c} \int \mathbf{v} \times \mathbf{B} \cdot d\mathbf{s} = \frac{B_0 R^2 \omega}{c} \sin^2 \vartheta. \quad (12.34)$$

Open field lines that extend beyond the light cylinder c/ω start near the polar cap, within the cone $\vartheta_0 \sim \sqrt{\omega R/c}$. Inserting ϑ_0 into Eq. (12.34) we obtain as maximal acceleration energy achievable by a pulsar

$$E_{\max} \approx \frac{Z B_0 R^2 \omega \sin^2 \vartheta_0}{c} \approx \frac{Z B_0 R^3 \omega^2}{c^2} \approx 8 \times 10^{20} \text{ eV} \frac{Z B}{10^{13} \text{ G}} \left(\frac{\Omega}{3000 \text{ s}^{-1}} \right)^2. \quad (12.35)$$

Thus a young, fast rotating pulsar appears to be a very good particle accelerator. The main problems are that in realistic models the potential difference $\Delta\phi$ that can be used for particle acceleration is much smaller and the extreme energy losses due to, e.g. curvature radiation. The magnetosphere of a pulsar may be also filled by $\gamma \rightarrow e^+e^-$ with a plasma. Finally, pulsars as main source of UHECRs would predict a strong anisotropy of the UHECR intensity, because neutron stars are concentrated in the Galactic plane.

12.2. *** Sources of cosmic rays ***

Basic observations The presence of an ionizing radiation at the Earth's surface was already recognized by Coulomb in 1785 [6]. More than a century later, Hess showed conclusively that the ionisation rate increases with altitude, suggesting that it has a cosmic origin [12]. By the 1930s, the observations of the geomagnetic latitude effect by Clay [5] and coincidence measurements using two Geiger-Müller counters by Bothe and Kohlhörster [4] demonstrated that this ionizing radiation consists mainly of charged particles, coined later "cosmic rays". In the 1940s, measurements using cloud chambers and photographic plates carried by balloons into the stratosphere showed that cosmic rays (CRs) consist mainly of relativistic protons, with an admixture of heavier nuclei [19].

The existence of extensive air showers triggered by high-energy CRs was established by Kohlhörster, Auger, and their collaborators in the 1930s [14, 2]. After the second world war, large detector arrays were installed to measure these extensive air showers, establishing a power law $dN/dE \propto 1/E^\alpha$ for the energy spectrum of CRs with $\alpha \simeq 2.7$. At the energy

$E \simeq 4 \text{ PeV}$, a hardening of the spectral index to $\alpha \simeq 3.1$ dubbed the CR knee was discovered by Kulikov and Khristiansen in the data of the MSU experiment in 1958 [15]. In the following years, the M.I.T. group deployed at the Volcano Ranch an array of scintillation counters covering an area of 12 km^2 which recorded in 1962 an air shower with energy around 10^{20} eV [16]. At present, the two largest arrays observing CRs are the Pierre Auger Observatory (PAO) located in Argentina covering an area of 3000 km^2 and the Telescope Array (TA) in the USA covering 900 km^2 . Both are hybrid experiments combining surface detectors to measure air showers on the ground and fluorescence detectors which can follow the longitudinal development of the showers in the atmosphere.

A summary of CR intensity measurements is shown in the left panel of Fig. 1. The (particle) intensity $I(E)$ is defined as the number N of particles with energy E crossing a unit area per unit time and unit solid angle and is thus connected to the (differential) number density of CRs with velocity v as $n(E) = \frac{4\pi}{v} I(E)$. If the intensity $I(E)$ is isotropic, the flux $F(E)$ through a planar detector is simply $F(E) = \pi I(E)$. In such figures, the particle intensity $I(E)$ is often multiplied by a power α of the energy E such that $E^\alpha I(E)$ becomes approximately flat, making thereby structures in $I(E)$ more visible. In the flux of CR nuclei, which is the dominating contribution to the total CR flux, additional to the CR knee another break at $\simeq 3 \times 10^{18} \text{ eV}$ called the ankle and a cut-off like feature around 10^{20} eV are visible. Below $\simeq 20 \text{ GeV}$, the CR spectrum is suppressed because the magnetic field embedded within the Solar wind plasma prevents that charged low-energy particles enter the Solar system. The second most-prominent species in the CR flux are electrons which flux is reduced by a factor of order 100 relative to the one of nuclei. The fluxes of their antiparticles, antiprotons and positrons, are of comparable magnitude and suppressed by two orders of magnitude relative to electrons.

In the left panel of Fig. 1, the intensities $I_j(E) \propto dN_j/dE$ are multiplied with E^2 which implies that the area $\int dE E I_j(E)$ is proportional to the energy density contained in particles of type j . Thus the energy carried by neutrinos (indicated by the magenta band) and by the extragalactic gamma-ray background (EGRB) (green) is of the same order. A sizeable part of both the diffuse neutrino and gamma-ray flux could be produced by extragalactic protons, if a large fraction of these protons interacts in their sources.

Figure 1 contains also for the energies of the knee and ankle the number of particles crossing a detector of a given size per year. Since the maximal area of a balloon or satellite experiment is of the order of a few square meter, the energy 10^{14} eV marks the end of direct detection experiments. These experiments have typically the ability to measure the charge of individual CRs and thus the fluxes of individual CR nuclei are relatively well-known up to this energy. At higher energies, the CR flux drops to a level which prohibits to collect them with high enough statistics using detectors of few m^2 size. However, at these energies, the extensive showers of secondary particles initiated by CR primaries interacting in the atmosphere start to reach the ground. Detecting Cherenkov and fluorescence light of such showers in the atmosphere, as well as the secondary particles on the ground allows one to reconstruct the energy and arrival direction of the primary CR rather precisely. The determination of the primary mass has been, however, a challenging problem for these indirect measurements, although considerable progress has been made in the last 15 years.

Cosmic rays are measured locally, with the two Voyager satellites as the most distant experiments from Earth as the only exceptions. While these two satellites have started to probe the conditions outside the heliosphere, photons and neutrino observations provide in addition directional information about CRs and the physical processes taking place along the

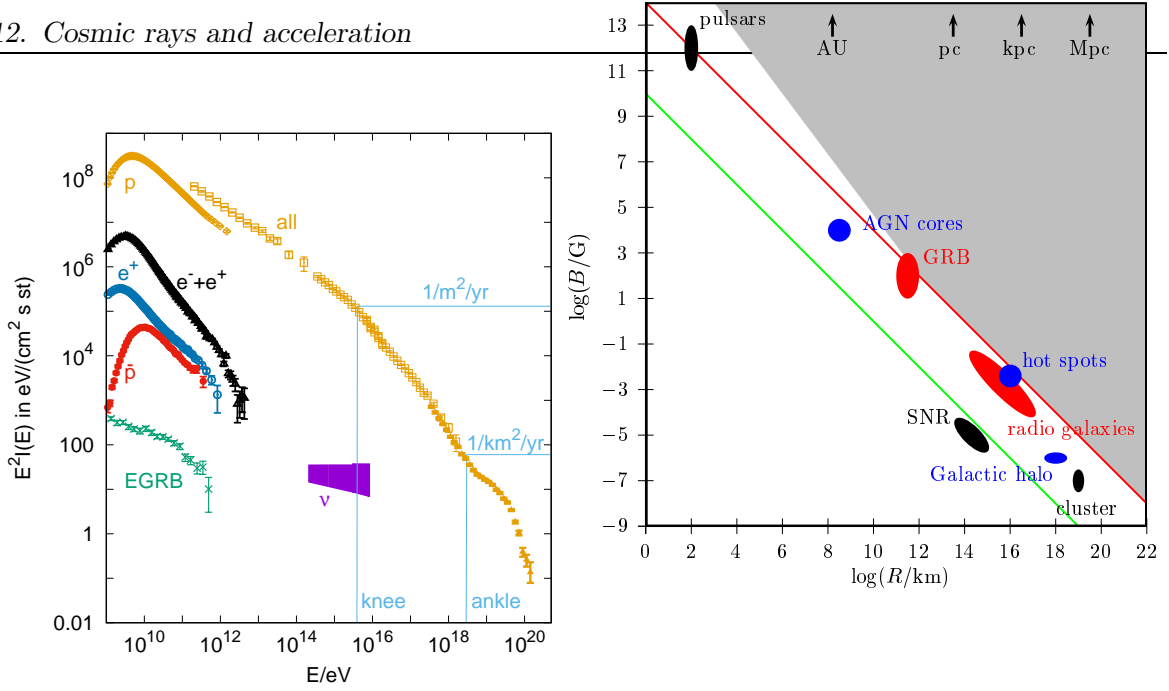


Figure 12.2.: *Left panel:* Summary of intensity measurements $E^2 I(E)$ of CR nuclei and protons (orange), electrons plus positrons (black), positrons (blue), antiprotons (red), neutrinos (magenta) and diffuse photons (green). *Right panel:* Magnetic field strength B versus size R of various suggested CR sources; adapted from Refs. [13, 18].

observed line-of-sight. Connecting these and the local measurements to the physics occurring in CR sources requires an accurate modelling of CR transport. Since the turbulent component of the Galactic magnetic field (GMF) scatters efficiently CRs, they perform a random walk and escape only slowly from the Galaxy. Before they escape, they cross many times the Galactic disk producing secondary CRs in hadronic interactions with gas. Additionally, CRs accumulate a grammage in their source region which typically has an increased density compared to the average density in the Galactic disk. As a result of these interactions, the abundance of elements which are produced rarely in big-bang and stellar nucleosynthesis like the lithium-beryllium-boron group or titanium is strongly enhanced in CRs, cf. with Fig. 12.3. The production of these secondaries provides an important handle to constrain the parameters of a given propagation and source model.

Requirement on sources

Energy argument favoring supernova remnants (SNR) The luminosity L_{CR} of Galactic cosmic ray sources has to fit the observed energy density $\rho_{\text{CR}} \sim 1 \text{ eV}/\text{cm}^3$ of cosmic rays, taking into account their residence time $\tau_{\text{esc}} \sim 6 \times 10^6 \text{ yr}$ in the Galactic disk. With $V_D = \pi R^2 h \sim 4 \times 10^{66} \text{ cm}^3$ for $R = 15 \text{ kpc}$ and $h = 200 \text{ pc}$ as volume of the Galactic disc, the required luminosity is $L_{\text{CR}} = V_D \rho_{\text{CR}} / \tau_{\text{esc}} \sim 5 \times 10^{40} \text{ erg/s}$.

In a successful core-collapse supernova (SN) around $10 M_{\odot}$ are ejected with $v \sim 5 \times 10^8 \text{ cm/s}$. Assuming $1/(30 \text{ yr})$ as SN rate in the Milky Way, the average output in kinetic energy of Galactic SNe is $L_{\text{SN,kin}} \sim 3 \times 10^{42} \text{ erg/s}$. Hence, if the remnants of SNe can accelerate particle with efficiency $O(0.01)$, they could explain all galactic cosmic rays as it was suggested first

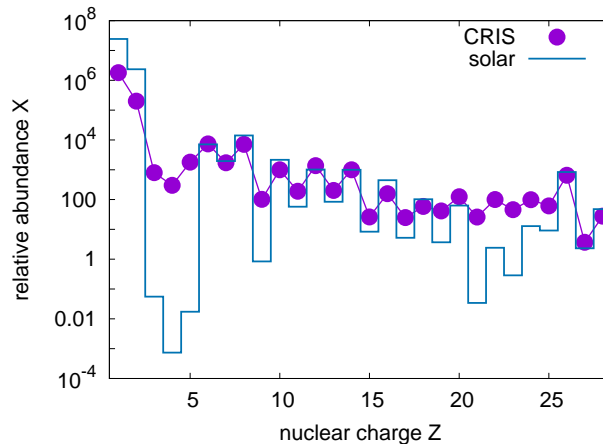


Figure 12.3.: Relative abundances X normalised to $X(\text{Si}) = 1000$ for the proto-sun (solar system abundances) from Ref. [17] shown as boxes versus the abundances in CRs measured by BESS [20] and CRIS [7, 10].

by Ginzburg and Syrovatskii in the early 1960s.

Hillas argument The Larmor orbit $R_L = E/(ZeB)$ of accelerated particles has to fit inside the accelerator of size R_s , $R_L = E/(ZeB) \leq R_s$. For known magnetic fields and source sizes, one can constrain thus the maximal achievable energy as $E_{\text{max}} = \Gamma ZeBR_s$, as it is done in Fig. 12.2 for a compilation of potential cosmic ray sources. The Lorentz factor Γ introduced in E_{max} accounts for a possible relativistic bulk motion of the source and is probably only for gamma ray bursts a significant correction. In Fig. 12.2, a so-called “Hillas plot,” sources able to accelerate protons to $E > 10^{21}$ eV should lie above the solid red line, while sources above the green line can accelerate iron up to 10^{20} eV. Few candidate sources for acceleration to $E = 10^{21}$ eV seem to be compatible with Hillas’ argument.

On one hand, this constraint looks like a solid upper limit, because energy losses are neglected, the maximal acceleration time is finite and no accelerator is 100% efficient. On the other hand, nonlinear processes may lead to an amplification of magnetic fields inside the source. In general, sources neither too small (minimizing energy losses) nor too big (avoiding too long acceleration times) are favored.

Blandford argument The acceleration of a proton to the energy $E = 10^{20}$ eV by regular electromagnetic fields requires the potential difference $U = 10^{20}$ V. What is the minimal power P dissipated by such an accelerator? In order to use the basic equation $P = UI = U^2/R$ known from high-school physics, we have to know the appropriate value of the resistance R . Since the acceleration region is in most cases nearly empty, we use $R \sim 1000 \Omega$ (lead by the “impedance of the vacuum”, $R = 4\pi k_0/c = 1/(\epsilon_0 c) \approx 377 \Omega$). Hence a source able to produce protons with $E = 10^{20}$ eV by regular acceleration in electromagnetic fields has the minimal luminosity [3]

$$L = U^2/R \gtrsim 10^{37} \text{ W} = 10^{44} \text{ erg/s.} \quad (12.36)$$

This can be transformed into an upper limit on the density n_s of ultrahigh energy cosmic rays (UHECR) sources, since the observed UHECR intensity fixes the required emissivity \mathcal{L} ,

i.e. the energy input per volume and time, as $\mathcal{L} \sim 3 \times 10^{46} \text{erg}/(\text{Mpc}^3 \text{yr})$. Hence, the density of UHECR sources able to accelerate protons to $E = 10^{20} \text{eV}$ should be smaller than $n_s = \mathcal{L}/L \sim 10^{-5}/\text{Mpc}^3$, if the acceleration is by regular electromagnetic fields. For comparison, the density of normal galaxies is $n_s \approx 10^{-2}/\text{Mpc}^3$, while the most common type of active galactic nuclei in the nearby Universe, Seyfert galaxies, has the density $n_s \approx (1 - 5) \times 10^{-5}/\text{Mpc}^3$ within redshift $z \lesssim 0.02$.

Sources

12.2.1. Galactic cosmic rays

13. Non-thermal radiation

13.1. Electrodynamical processes

generalities: wave eq, Green function, far-field, multipole exp, Lamor dipole formula

13.1.1. Synchrotron radiation

Cyclotron radiation An electron in a homogeneous magnetic field of strength B moves on a Larmor orbit with radius $r_L = v_{\perp} mc / (eB)$. Because of its acceleration, the electron emits electromagnetic radiation. For typical magnetic field strengths found in galaxies, $B \sim \mu\text{G}$, and relativistic electrons, the emitted radiation is in the radio range.

We start by considering non-relativistic electrons. Then the Lorentz force is

$$\mathbf{F}_L = -\frac{e}{c} \mathbf{v} \times \mathbf{B} = m\mathbf{a}. \quad (13.1)$$

Hence the motion parallel to \mathbf{B} is force-free ($\mathbf{v} \times \mathbf{v} = 0$), while the acceleration in the plane perpendicular to \mathbf{B} is constant, $a_r = (e/m)v_{\perp} B$. Thus the electron moves along a helix.

Equating the Lorentz and the centripetal force,

$$(e/c)v_{\perp} B = \frac{mv_{\perp}^2}{r}, \quad (13.2)$$

and introducing the angular frequency $\omega = 2\pi\nu = v_{\perp}/r$, the cyclotron frequency ω_0 follows as

$$\omega_0 = \frac{eB}{mc} \quad \text{or} \quad \nu_0/\text{Mhz} = 2.8B/\text{G}. \quad (13.3)$$

As long as electrons are non-relativistic, i.e. their total energy is dominated by their rest energy mc^2 , they emit cyclotron radiation with the frequency ν_0 independent of their velocity.

Synchrotron radiation For a relativistic electron, we have to replace $m\mathbf{a}$ by $\gamma m\mathbf{a}$ and thus the cyclotron frequency becomes $\omega_c = \frac{eB}{\gamma mc} = \frac{eB}{E/c}$. However, there are two additional effects. First, the radiation is beamed and emitted in a small cone of opening angle $\Delta\vartheta \approx 1/\gamma$. Second, there is a time-dilation between the frame of the electron and the observer,

$$\frac{dt}{d\tau} = 1 - \beta \cos(\Delta\vartheta) \simeq 1 - \beta + \beta(\Delta\vartheta)^2/2 \simeq 1/2\gamma^2. \quad (13.4)$$

As a consequence, all frequencies from ω_0 to $2\gamma^2\omega_0$ are emitted, although most energy goes into the frequency range around $\omega_{\text{cr}} = (3/2)\gamma^2\omega_0$.

Example 13.1: Determine the Larmor radius r_L , its orbital period P , the opening angle ϑ and the frequency ν_{cr} in which the radiation is mainly emitted, for an electron with $\gamma = 10^4$ in a magnetic field with strength typical for galaxies, $B = 3\mu\text{G}$.

The Larmor radius is $r_L = 6.0 \times 10^{12}\text{cm}$, the orbital period with $P = 1/\nu = \gamma/\nu_0 = 20\text{min}$, the

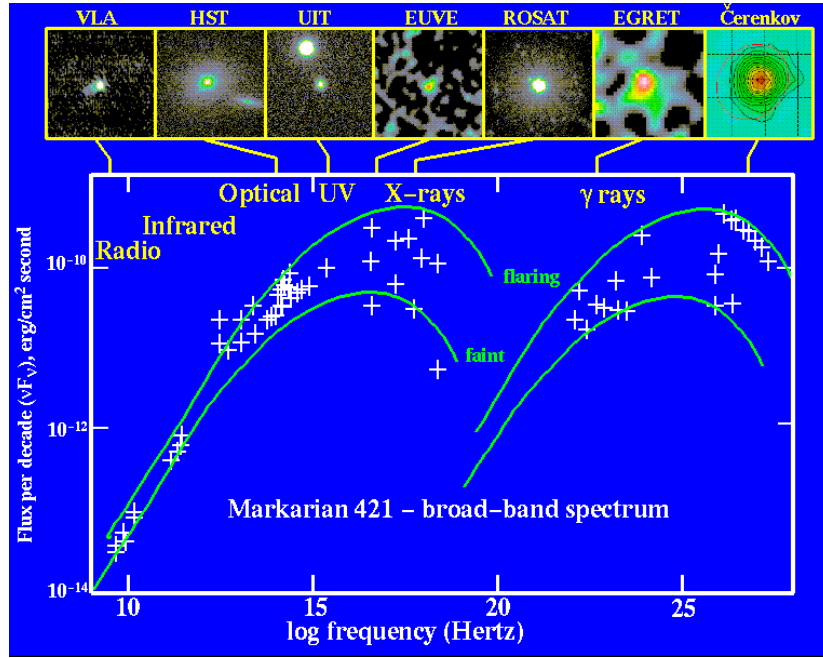


Figure 13.1.: The emitted flux $\nu\mathcal{F}$ from the BL Lacartae Markarian 421 as function of frequency ν , in a quiet (lower line) and a flaring state (upper line).

opening angle $\vartheta = 0.005^\circ$ and the frequency $\nu_{\text{cr}} = 890\text{Mhz}$.

We now use that the power $P = -dE/dt$ is Lorentz-invariant. Thus we can evaluate P employing the non-relativistic Larmor formula in a frame where the electron velocity is small,

$$P = \frac{2}{3} \frac{e^2 a^2}{c^3} = \frac{2e^2}{3c^3} (\gamma\omega_0 v \sin \alpha)^2. \quad (13.5)$$

Since we used the correct relativistic acceleration, $a = \gamma\omega_0 v \sin \alpha$, this expression is valid in any frame.

Next we want to rewrite this formula in a way which allows an easier interpretation of its ingredients. First, we insert $\omega_0 = eB/(mc)$ and introduce $\beta = v/c$,

$$P = \frac{2e^2}{3c} (\beta\gamma \sin \alpha)^2 \left(\frac{eB}{mc} \right)^2. \quad (13.6)$$

Then we note that B^2 can be interpreted as the energy density, $u_B = B^2/(8\pi)$, of the magnetic field. Thus we should be able to express the synchrotron power as

$$P = \frac{\text{volume}}{\text{time}} u_B = \text{area } c u_B. \quad (13.7)$$

The only area relevant for a classical electron is either the squared classical electron radius r_0 or, equivalently, the Thomson cross section $\sigma_{\text{Th}} = 8\pi r_0^2/3$ with $r_0 = e^2/(mc^2)$. Using the latter results in

$$P_{\text{cl}} = 2 \sigma_{\text{Th}} c (\beta\gamma \sin \alpha)^2 u_B. \quad (13.8)$$

This expression suggests that we can interpret synchrotron emission as the scattering process of an electron on the virtual photons constituting a classical magnetic field.

In the second variation of this formula, we want to exhibit more clearly that the power is invariant. In general, the synchrotron power is a function of m , \mathbf{p} and \mathbf{B} , or $P = P(m, \mathbf{p}, \mathbf{B})$. Out of these three quantities, only the electron mass m is invariant. Thus we should be able to express the synchrotron power as $P = f(\mathbf{p}, \mathbf{B})m^2$, where the function f has to be Lorentz invariant too. If we factor out $(mc^2)^2/\hbar$ instead of m^2 , the function f has to be in addition dimensionless. Using also $e^2 = \hbar c\alpha$, it follows

$$P_{\text{cl}} = \frac{2}{3} \alpha \left(\frac{p_{\perp}}{mc} \frac{e\hbar B}{m^2 c^3} \right)^2 \frac{m^2 c^4}{\hbar}. \quad (13.9)$$

Since α and $p_{\perp}/(mc)$ are dimensionless, the second factor in the parenthesis has to be dimensionless too. Thus the combination $m^2 c^3/(q\hbar)$ is a magnetic field strength characteristic for a particle with mass m and electric charge q . It is called the critical magnetic field and its numerical value for an electron is $B_{\text{cr}} = m_e^2 c^3/(e\hbar) = 4.41 \times 10^{13}$ G. Since B_{cr} contains c and \hbar , we expect that both relativistic and quantum effects become important for $B \gtrsim B_{\text{cr}}$.

This guess is confirmed solving the Schrödinger (or better Dirac) equation for an electron in an homogenous magnetic field: The electron momentum perpendicular to \mathbf{B} is quantised in Landau levels, $p_{\perp}^2 = 2NeB$. Thus the critical magnetic field is the field strength, when the energy difference between the first and second Landau level equals half the electron rest energy.

Finally, we use that the parenthesis has to be a dimensionless Lorentz scalar constructed out of p^{μ} and $F^{\mu\nu}$. The only possible choice is the so-called dynamical field parameter,

$$\chi = \frac{\hbar e}{m^2 c^3} (eF^{\mu\nu} p_{\mu})^2 = \frac{p_{\perp}}{mc} \frac{\hbar e B}{m^2 c^3} = \frac{p_{\perp}}{mc} \frac{B}{B_{\text{cr}}}, \quad (13.10)$$

where we inserted for $F^{\mu\nu}$ a uniform magnetic field B in the second step. Thus we can express the classical synchrotron power as

$$P_{\text{cl}} = \frac{2}{3} \alpha \chi^2 \frac{m^2 c^4}{\hbar}. \quad (13.11)$$

We can now convert our previous argument, that the classical approximation breaks down for $B \gtrsim B_{\text{cr}}$, into a Lorentz-invariant statement: For a non-relativistic electron, $B \gtrsim B_{\text{cr}}$ agrees with $\chi \gtrsim 1$. The latter equation is however invariant, and applies therefore also for a relativistic electron. An interpolation formula valid both in the classical Thomson and the quantum regime given by [?] is

$$\frac{dE}{dt} \simeq \frac{\chi^2}{[1 + 4.8(1 + \chi) \ln(1 + 1.7\chi) + 3.44\chi^2]^{2/3}} \frac{m_e^2 c^4}{\hbar}. \quad (13.12)$$

As expected, deviations from the classical formula become significant around $\chi \sim 1$, cf. the right panel of Fig. 13.2.

We state without calculation the result for the differential synchrotron power $P(\nu)$. Expressed via the ratio $x = \nu/\nu_{\text{cr}}$, it is given by

$$P(x) = \frac{\sqrt{3}e^3 B \sin \alpha}{2\pi m c^2} F(x) \quad \text{with} \quad F(x) = x \int_x^{\infty} dy K_{5/3}(y). \quad (13.13)$$

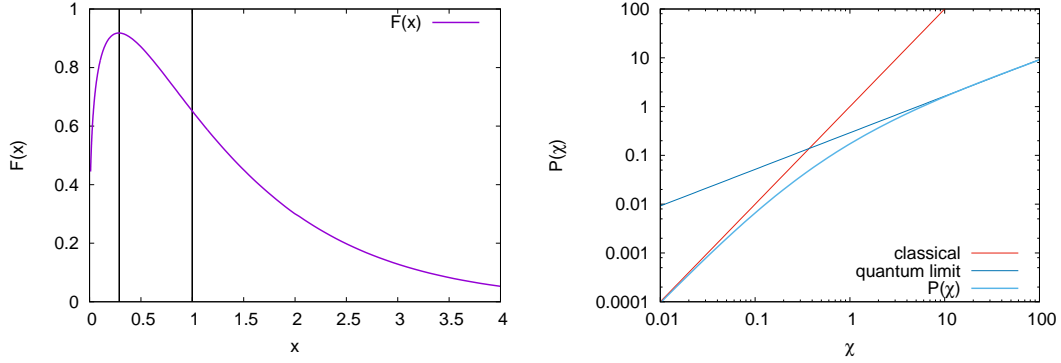


Figure 13.2.: Left: Differential synchrotron power $P(x)$ as function of $x = \nu/\nu_{\text{cr}}$. Right: Exact synchrotron power $P(\chi)$ as function of χ compared to the classical and quantum limit.

As shown in the left panel of Fig. 13.2, this function peaks at $x \simeq 0.29$, while half of the radiation is emitted below $x = 1$, and half above.

The energy loss per time is $\beta = dE/dt = -P \propto m^{-4}$ and hence is most severe for the lightest charged particle, the electron. The typical length-scale l_{syn} of synchrotron losses

$$l_{\text{syn}} = \left(\frac{1}{E} \frac{dE}{dt} \right)^{-1} = \frac{3}{2\alpha m} \frac{1}{\gamma} \left(\frac{B_{\text{cr}}}{B} \right)^2. \quad (13.14)$$

For electrons with $E = 10^{15}$ eV in the Galactic disc, $B \sim 3\mu\text{G}$, we have $l_{\text{syn}} \sim 100$ pc. Thus one of the reasons why we have not discussed electrons as a major component of cosmic rays is that their energy losses are too severe. On the other side, synchrotron radiation of relativistic electrons is in the radio range and explains the strong radio emission of many AGNs: Synchrotron radiation peaks at $0.29\omega_c$ with

$$\omega_c = \frac{3\gamma^2 B}{2B_{\text{cr}}} m. \quad (13.15)$$

For $B \sim 0.1$ G close to a source and $\gamma = 10^9$, the peak of synchrotron radiation is at $10^{-10} m_e \sim 100$ GHz. Synchrotron radiation is the explanation of the first peak visible in Fig. 15.4, showing the observed spectrum from a Blazar.

Remark 13.1: Curvature radiation: The results for synchrotron radiation for an electron following an helix with radius $r = R_L$ can be applied to the case of a general trajectory with local curvature radius R_C . Replacing the magnetic field strength using $R_C = R_L = E/(eB)$, the dynamical field parameter becomes for curvature radiation

$$\chi = \frac{E^2}{m^3 R_c} \quad (13.16)$$

An important example for this emission mechanism are electrons travelling along the curved magnetic field lines of a pulsar.

Synchrotron self-absorption For typical electron slopes $\alpha = [2 : 3]$, the slope of the synchrotron spectrum in the range $\beta = [-1 : -1/2]$. Thus the synchrotron intensity overshoots for $\nu \rightarrow 0$ the intensity of a blackbody, $I_\nu = B_\nu \propto T\nu^2$.

The resolution to this puzzle is the fact that, as for $\nu \rightarrow 0$ the density of synchrotron photons increases, the inverse process of synchrotron absorption becomes more and more important and can be not neglected anymore.

For a stationary source, synchrotron absorption and emission are in equilibrium, and the energy is equally shared between electrons and photons, $E_e = E_\gamma$, or

$$\gamma m_e c^2 = \frac{3}{2} kT(\nu). \quad (13.17)$$

Since the electrons are not in thermal equilibrium—we assume that they follow a power-law not a Maxwell distribution—the temperature of the synchrotron photons is energy-dependent. With $\gamma \sim (\nu/\nu_{\text{cr}})^{1/2}$, it follows

$$T(\nu) \propto \nu^{1/2}. \quad (13.18)$$

Thus the intensity of synchrotron radiation at low frequencies is $I_\nu \propto T(\nu)\nu^2 \propto \nu^{5/2}$. In this regime, the source is optically thick. In most cases, deviations from the $\nu^{5/2}$ behavior are important, e.g., because of the finite size of a source: The observed spectrum is a mixture of the optically thick interior and the optically thin “atmosphere” of the source.

13.1.2. Compton scattering

Thomson scattering Using the same line of argument as for synchrotron, one can show that electrons moving through a bath of real background photons lose in the classical limit energy as

$$P_{\text{cl}} = 2 \sigma_{\text{Th}} c (\beta \gamma \sin \alpha)^2 u_{\text{rad}}. \quad (13.19)$$

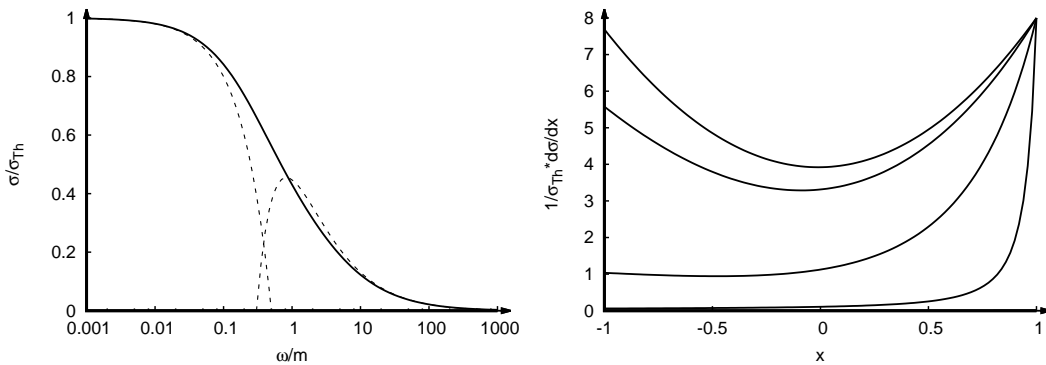


Figure 13.3.: Left: The total cross-section $\sigma/\sigma_{\text{Th}}$ as function of $\tilde{\omega}$ together with the classical and ultra-relativistic limits given in Eq. (??). Right: The normalised differential cross-section $\sigma_{\text{Th}}^{-1} d\sigma/dx$ as a function of $x = \cos \vartheta$ for $\tilde{\omega} = 0.01, 0.1, 1, 10$ (from top down).

Inverse Compton scattering The usual text book set-up for Compton scattering assumes an energetic photon hitting an electron at rest, transferring part of its energy to the electron. In an astrophysical environments, the opposite situation is realized more often: A fast electron hits a low-energy photon and transfers a large fraction of its energy to the photon. (“Inverse Compton scattering”). Thus charged electron are accelerated by electromagnetic fields, emit synchrotron radiation in the radio range as well as high-energy photons via inverse Compton scattering. An example where this two different components of the electromagnetic radiation are visible is shown in Fig. 15.4.

The cross section for Compton scattering $e^- + \gamma \rightarrow e^- + \gamma$ is with $\sigma_{\text{Th}} = 8\pi\alpha^2/(3m_e^2)$

$$\sigma = \sigma_{\text{Th}} (1 - s/m^2 + \dots) \quad \text{for } s/m^2 \ll 1 \quad (13.20)$$

$$\sigma = \frac{3m^2}{4s} \sigma_{\text{Th}} \left(\ln s/m^2 + \frac{1}{2} + \dots \right) \quad \text{for } s/m^2 \gg 1 \quad (13.21)$$

i.e. Compton scattering is suppressed for $s \gg m^2$.

While in the classical Compton experiment an energetic photon hits an electron at rest and transfers part of its energy, in astrophysics “Inverse Compton scattering” is more important: A fast electron hitting a low-energy photon transfers a large fraction y of its energy to the photon,

$$y \approx 1/\ln(s/m_e^2). \quad (13.22)$$

This is the explanation of the second peak visible in Fig. 15.4, showing the observed spectrum from a blazar.

There are three main choices for the source of background photons used in ICS:

- CMB photons are an unavoidable target, with fixed properties. Thus this contribution can be reliably calculated, but may be usually too small.
- The synchrotron photons generated by the high-energy electrons may serve also as target for ICS. There is a thight correlation of the two contributions, depending on the source parameters: the ratio of the energy in the synchrotron and ICS bumps is given by $u_{\text{syn}}/u_{\text{rad}}$.
- Finally, one can use external photons: UV photons from the accretion disk, IR photons from dust emission, X-ray photons, etc. Clearly, such models allow for a much larger variation in the background spectrum, and thus also of the ICS photon bump.

Pair production The pair-production cross section $\sigma_{\text{pair}}(s)$ is given by

$$\sigma_{\text{pair}}(s) = \frac{3}{4} \sigma_{\text{Th}} \frac{m_e^2}{s} \left[(3 - \beta^4) \ln \frac{1 + \beta}{1 - \beta} - 2\beta(2 - \beta^2) \right], \quad (13.23)$$

with $\sigma_{\text{Th}} = 8\pi\alpha^2/(3m_e^2)$ as Thomson cross section and $\beta = \sqrt{1 - 4m_e^2/s}$.

Electrons emit in the Thomson regime mainly soft photons, cf. Eq. (??).

13.2. Hadronic processes

Finally, we consider strong interactions. The largest contribution to the proton-proton cross section should result from the exchange of the lightest, strongly interacting particle, the pion.

hadron	valence quarks	hadron	valence quarks
p	uud	Λ	uds
n	udd	K^+	$u\bar{s}$
π^+	$u\bar{d}$	K^0	$d\bar{s}$
π^0	$(u\bar{u} + d\bar{d})/\sqrt{2}$		

Table 13.1.: Valence quark content of hadrons

Integrating gives

$$\sigma \sim \frac{g_\pi^4}{(4\pi)^2} \int_{-s}^0 \frac{dt}{(t - m_\pi^2)^2} = \alpha_\pi^2 \frac{s}{m_\pi^2(s - m_\pi^2)} \rightarrow \frac{\alpha_\pi^2}{m_\pi^2} \approx 20\alpha_s^2 \text{ mbarn} \quad (13.24)$$

compared to the measured value $\sigma \approx 50 \text{ mbarn}$. Hence the proton-pion coupling $\alpha_\pi = g_\pi^2/(4\pi)$ is of order one and perturbation theory for strong interactions seems to make no sense. However, coupling constants are—despite the name—in generally not constant but depend on the scale Q^2 probed. In the case of strong interactions, the coupling becomes smaller for large Q^2 , a phenomenon called “asymptotic freedom.” As a consequence, perturbation theory can be used in QCD¹, however only in a restricted kinematical range, $Q^2 \gtrsim \text{few} \times \text{GeV}^2$. Unfortunately, for cosmic ray interactions most important is the regime of small momentum-transfer that is not (yet) accessible to predictions from first principles and requires therefore the use of phenomenological models.

Quark model and hadronization For $q \gtrsim 1/m_p$, the scattering amplitude for e.g. electron-proton scattering should reflect the proton size 10^{-13} cm . However, a form factor typical for scattering on point-like particles was found experimentally. This led to the parton model: Protons (as all hadrons) consist of point-like constituents, quarks and gluons. The valence quark content of some hadrons is given in Tab. 13.1. At high momentum transfer, a probe scatters on partons independently (“spectator model”). Hence, the parton model predicts e.g. for the ratio of pion-proton and proton-proton cross sections

$$\frac{\sigma_{\pi p}}{\sigma_{pp}} = \frac{2}{3}, \quad (13.25)$$

in good agreement with experiment.

Which kind of hadrons are mainly produced in the process $e^+e^- \rightarrow q\bar{q} \rightarrow \text{hadrons}$? Mainly mesons ($q\bar{q}$) with only $\sim 5\%$ of nucleons (qqq), because it is easier to combine two quarks into a colorless, light meson than three quarks into a colorless, rather heavy baryon. Out of the mesons, 90% are pions while the remaining ones are mainly kaons. While 1/3 of pions are neutral ones and produce photons, the other 2/3 are charged and produce neutrinos. Hence photon and neutrino fluxes produced by hadronization are closely connected.

Neutral pion decay $\pi^0 \rightarrow 2\gamma$ In the rest system of the π^0 , the two photons are emitted back-to-back, $\mathbf{p}_1 = -\mathbf{p}_2$ and $E_1 = E_2 = m_\pi/2$. How are the photon energies distributed, if the pion was moving with velocity v ?

¹Quantum chromo-dynamics is the fundamental theory describing strong interactions

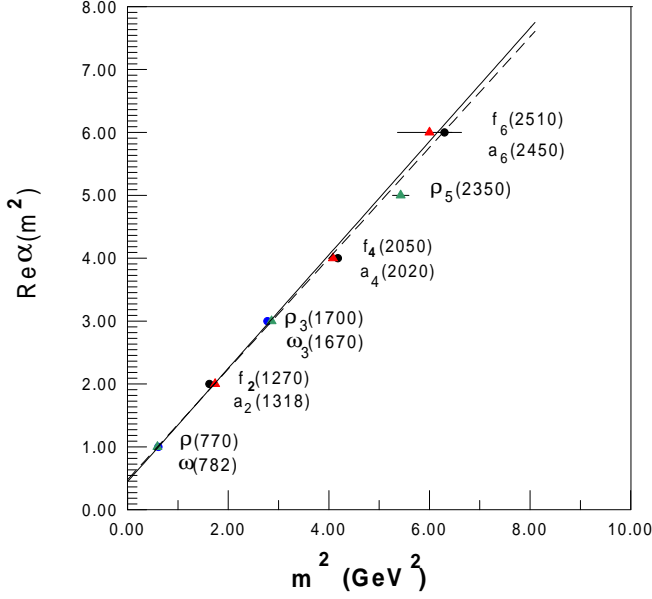


Figure 13.4.: Chew-Frautschi plot, i.e. the spin against the squared mass, for the trajectories of the ω , ρ , f_2 , and a_2 mesons, from Ref. [?].

Let us use the Lorentz transformation between energies in the rest and the lab system. In the lab system,

$$E = \gamma(E' + \beta p' \cos \vartheta) \quad (13.26)$$

where ϑ is the angle between the velocity β of the pion and the emitted photon. The maximal/minimal values of E follow directly as $E = \gamma(E' \pm \beta p')$ for $\cos \vartheta = \pm 1$, i.e. if the photons are emitted parallel and anti-parallel to the direction of flight of the pion.

Inserting $E' = p' = m_\pi/2$ and the definition of γ gives

$$E_{\min}^{\max} = \frac{1}{2} (\gamma m_\pi \pm \beta \gamma m_\pi) = \frac{m_\pi}{2} \sqrt{\frac{1 \pm \beta}{1 \mp \beta}}. \quad (13.27)$$

Thus $E_{\max} \rightarrow E_\pi = \gamma m_\pi$ and $E_{\min} \rightarrow 0$ in the ultra-relativistic limit $\beta \rightarrow 1$.

What is the distribution of the emitted photons? Since the pion is a scalar particle, the photon distribution is isotropic in the lab system,

$$dN = \frac{1}{4\pi} d\Omega = \frac{1}{2} d|\cos \vartheta|. \quad (13.28)$$

Using (13.26), one can express dE as $\gamma \beta p' d|\cos \vartheta|$ and thus

$$dN = \frac{1}{4\pi} d\Omega = \frac{dE}{2\gamma p'}. \quad (13.29)$$

Hence $dN/dE = \text{const.}$, and the photon spectrum produced by a pion beam with uniform velocity is a box between E_{\min} and E_{\max} from Eq. (13.27). Taking the log of the extremal energies, we obtain

$$\ln(E_{\min}^{\max}) = \ln(m_\pi/2) \pm \frac{1}{2} \ln \left(\frac{1 + \beta}{1 - \beta} \right). \quad (13.30)$$

Thus the boxes are symmetric with respect to $m_\pi/2$, if we use $\log(E)$ as x coordinate.

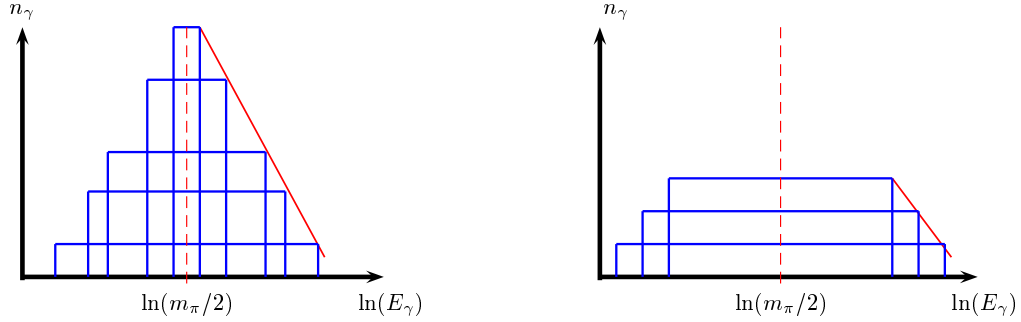


Figure 13.5.: The photon spectrum $n_\gamma = dN/dE_\gamma$ produced in π^0 decays as function of $\ln(E_\gamma)$ for Ap (left panel) and for A_γ (right panel) interaction: the total spectrum is the envelope (red line) of the boxes produced by pions with fixed energy.

Photon spectrum from “many pion decays” Consider now the photon spectrum not from a single pion, but from a beam of pions with arbitrary energy spectrum. Each photon spectrum from a single decay is as we saw a box centered at $m_\pi/2$. Hence also the total photon spectrum from pions with an arbitrary energy distribution is symmetric with respect to $m_\pi/2$.

Connection to the proton spectrum Finally, we want to connect the observed photons to the energy spectrum of the parent protons. The differential number of pions produced in p interactions with gas with density n after the distance l is

$$\frac{dN_\pi}{dE} = nl \int_E^\infty dE' \frac{d\sigma_{ki}(E', E)}{dE} \frac{dN_p}{dE'}. \quad (13.31)$$

Here, $d\sigma_{ki}(E', E)/dE$ is the differential cross section to produce pions with energy E by a proton with energy E' .

We can proceed analytically, if we assume that *i*) the proton spectrum is a power law, $dN_p/dE = KE^{-\alpha}$, (*i*) the cross section is not energy dependent, and (*ii*) the differential cross section scales: In this case, the cross section does not depend separately on both E and E' , but only on the ratio $z = E/E'$,

$$f(z) = \frac{1}{\sigma} \frac{d\sigma}{dz} = \frac{E'}{\sigma} \frac{d\sigma(E', E)}{dE}. \quad (13.32)$$

The second and third conditions hold to a reasonable degree in hadronic interaction at high-energies, while we saw that CR acceleration leads to power laws. Using these assumptions, we can write first $dN/dE' = KE'^{-\alpha} = Kz^\alpha E^{-\alpha}$. Inserting this and the scaling relation, we obtain

$$\frac{dN_\pi}{dE} = nl\sigma KE^{-\alpha} \int_0^1 dz z^{\alpha-1} f(z) = Z(\alpha)nl\sigma \frac{dN_p}{dE}. \quad (13.33)$$

As a result of our assumption of a scale-invariant cross section, the meson spectra follow the slope of the parent CRs. Even allowing for realistic scaling violations, the slopes differ typically only by $\Delta\alpha \simeq 0.1$.

The integral defines the spectrally averaged energy loss fraction

$$Z(\alpha) = \int_0^1 dz z^{\alpha-1} f(z), \quad (13.34)$$

which contains all the particle physics. The Z -factor weights the energy loss z properly not only with the normalised cross section $f(z)$ but also with the spectral shape $N(E) \propto E^{-\alpha}$. For a steeply falling spectra, $\alpha > 1$, the region $z \rightarrow 1$ gives the dominating contribution to the integral defining $Z(\alpha)$. This illustrates that for the modeling of hadronic interactions in astroparticle physics the knowledge of cross sections in the “forward” region $z \rightarrow 1$ is crucial.

Charged pion decay any process involving hadronization, i.e. the formation of colorless hadrons out of quarks and gluons, leads mainly to the production of pions. Isospin symmetry fixes then the ratio of charged and neutral pions. For instance, close to the threshold, the two possible channels of photo-meson production, $p + \gamma \rightarrow p + \pi^0$ and $p + \gamma \rightarrow n + \pi^+$ have a ratio that is close to 2:1. While the π^0 decay produces two photons, the final state of the second channel contains after the decays $n \rightarrow p + e^- + \nu_e$ and $\pi^+ \rightarrow \mu^+ + \nu_\mu \rightarrow e^+ + \nu_e + \bar{\nu}_\mu + \nu_e$ two electrons and four neutrinos. Clearly, the production of neutrinos is thus intimately tied to the one of photons and electrons, and both depend in turn on the flux of primary cosmic rays.

13.A. ***Reaction rates and cross sections***

Reaction rate Up-to-now, we have considered the reaction rates of non-relativistic particles, as e.g. the rate of nuclear fusion processes in the Sun. Such rates depends on the relative velocity $v_{\text{rel}} = |\mathbf{v}_1 - \mathbf{v}_2|$ of the two incoming particles, i.e. the difference between two three-velocities. Such a quantity has no natural place in a relativistic theory—defining the reaction rate of relativistic particle requires therefore to find a valid relativistic extension of v_{rel} . Such a generalisation is not unique and there two different extensions used: One, the Møller velocity $v_{\text{Møll}}$ is mainly used by particle physicists in the definition of the differential cross section; the other one, simply called the relative velocity v_{rel} by astrophysicists is mainly used to calculate reaction rates.

In order to find such a definition, we consider the interaction of two particles in the rest-frame of either particle 1 or 2. For simplicity, we consider two uniform beams. They may produce n final-state particles. The total number of such scatterings is

$$dN \propto v_{\text{Møll}} n_1 n_2 dV dt \quad (13.35)$$

where n_i is the density of particle type $i = 1, 2$. The Møller velocity $v_{\text{Møll}}$ is a quantity which coincides in the rest-frame of particle 1 or 2 with $|\mathbf{v}_2|$ and $|\mathbf{v}_1|$, respectively. The proportionality constant in (13.35) has the dimension of an area and is called cross-section σ . We define in the rest-system of either particle 1 or 2

$$dN = \sigma v_{\text{Møll}} n_1 n_2 dV dt, \quad (13.36)$$

while we set in an arbitrary frame

$$dN = A n_1 n_2 dV dt. \quad (13.37)$$

We determine now A . Since both dN and $dV dt = d^4x$ are Lorentz-invariant, the expression $A n_1 n_2$ has to be Lorentz-invariant too. The densities transform as

$$n_i = n_{i,0} \gamma = n_{i,0} \frac{E_i}{m_i}, \quad (13.38)$$

and thus the expression

$$A \frac{E_1 E_2}{p_1 \cdot p_2} \quad (13.39)$$

is also Lorentz-invariant. In the rest-frame of particle 1, it becomes

$$A \frac{E_1 E_2}{E_1 E_2 - \mathbf{p}_1 \mathbf{p}_2} = A = \sigma v_{\text{Møll}}. \quad (13.40)$$

Thus we found that A in an arbitrary frame is given by

$$A = \sigma v_{\text{Møll}} \frac{p_1 \cdot p_2}{E_1 E_2}. \quad (13.41)$$

The reaction rate, i.e. the invariant number of reactions $1 + 2 \rightarrow$ all per volume and time follows as

$$R = \frac{dN}{dV dt} = n_1 n_2 A = n_1 n_2 \sigma v_{\text{Møll}} \frac{p_1 \cdot p_2}{E_1 E_2} = n_1 n_2 \sigma v_{\text{rel}}. \quad (13.42)$$

Here, we introduced in the last step the relativistic generalisation of the relative velocity,

$$v_{\text{rel}} \equiv v_{\text{Møll}} \frac{p_1 \cdot p_2}{E_1 E_2}. \quad (13.43)$$

We still have to determine $v_{\text{Møll}}$. In the rest-frame 1, we have

$$p_1 \cdot p_2 = m_1 E_2 = m_1 \frac{m_2}{\sqrt{1 - v_{\text{Møll}}^2}}. \quad (13.44)$$

Thus the Møller velocity is given in general by

$$v_{\text{Møll}} = \sqrt{1 - \frac{m_1^2 m_2^2}{(p_1 \cdot p_2)^2}}. \quad (13.45)$$

Since this expression is Lorentz-invariant, we see that the notion of the Møller velocity as a velocity is misleading. For the relativ velocity, we obtain finally

$$v_{\text{rel}} = \frac{\sqrt{(p_1 \cdot p_2)^2 - m_1^2 m_2^2}}{E_1 E_2}. \quad (13.46)$$

Thus the relative velocity transforms inversely to $n_1 n_2$, such that the rate (13.42) is invariant as required. If one of the two initial particles is massless (or ultrarelativistic) and the other one has the velocity β , then $v_{\text{rel}} = 1 - \beta \cos \vartheta$.

As an example, we consider the pair-production process $\gamma\gamma \rightarrow e^+e^-$. The interaction rate $R_\gamma(E)$ of a single photon with energy E can be connected to the pair-production cross section $\sigma_{\text{pair}}(s)$ and the spectral density of isotropic background photons $n_\gamma(\varepsilon)$ as

$$R_\gamma(E) = \frac{dN}{dt} = \frac{1}{2} \int_0^\infty d\varepsilon' n_\gamma(\varepsilon') \int_{-1}^1 d\mu (1 - \mu) \sigma_{\text{pair}}(s) \Theta(s - s_{\text{min}}). \quad (13.47)$$

Here, $\mu \equiv \cos \vartheta$ and thus the factor $1 - \mu$ corresponds to the relative velocity v_{rel} of the photons. The pair-production cross section $\sigma_{\text{pair}}(s)$ is a function of the squared center-of-mass energy $s = 2E\varepsilon\mu$, and the integration $d\mu/2$ averages σ_{pair} over all possible scattering angles. Note that an anisotropic photons background can be accounted for by using $n_\gamma(\varepsilon, \vartheta, \phi)$ and replacing the average $d\mu/2$ by an integration $d\Omega = d\mu d\phi$.

Cross section Finally, we comment on the connection to the differential cross section and the S -matrix calculated in QFT. Splitting the scattering operator S into a diagonal part and the transition operator T , $S = 1 + iT$ and taking matrix elements, we obtain

$$S_{fi} = \delta_{fi} + iT_{fi} = \delta_{fi} + (2\pi)^4 \delta^{(4)}(P_i - P_f) i\mathcal{M}_{fi}, \quad (13.48)$$

where we factored out a delta function expressing four-momentum conservation in the second step. Squaring the scattering amplitude S_{fi} for $i \neq f$ using $(2\pi)^4 \delta^{(4)}(0) = VT$ gives as the differential transition probability into a n particle-final state

$$dW_{fi} = (2\pi)^4 \delta^{(4)}(P_i - P_f) VT |\mathcal{M}_{fi}|^2 \prod_{f=1}^n \frac{V d^3 p_f}{(2\pi)^3}. \quad (13.49)$$

In addition, we introduce the flux factor I defined as

$$I \equiv v_{\text{Mol}} p_1 \cdot p_2 = \sqrt{(p_1 \cdot p_2)^2 - m_1^2 m_2^2}. \quad (13.50)$$

Inserting then (13.41) for A together with the definition of I into (13.37), we obtain

$$dN = \sigma \frac{I}{E_1 E_2 V} (n_1 V) (n_2 dV) dt. \quad (13.51)$$

Here, we regrouped the terms to make clear that after integration the total number N of scattering events is proportional to the number $N_1 = n_1 V$ and $N_2 = \int n_2 dV$ of particles of type 1 and 2, respectively. The number N of scattering events per time and per particles 1 and 2 is, however, simply the transition probability per time,

$$\frac{dW_{fi}}{T} = \frac{dN}{N_1 N_2 T} = d\sigma \frac{I}{E_1 E_2 V}. \quad (13.52)$$

Inserting the expression (13.49) for dW_{fi} , we find for the differential cross section

$$d\sigma = \frac{E_1 E_2 V^2}{I} (2\pi)^4 \delta^{(4)}(P_i - P_f) |\mathcal{M}_{fi}|^2 \prod_{f=1}^n \frac{V d^3 p_f}{(2\pi)^3}. \quad (13.53)$$

Changing from the normalised matrix element \mathcal{M} to the Feynman amplitude \mathcal{A} via

$$\mathcal{M}_{fi} = \prod_{i=1}^n (2E_i V)^{-1/2} \prod_{f=1}^m (2E_f V)^{-1/2} \mathcal{A}_{fi} \quad (13.54)$$

introduces a factor $(2E_1 V)^{-1} (2E_2 V)^{-1}$ for the initial state and $\prod_f (2E_f V)^{-1}$ for the final state. Thus the arbitrary normalisation volume V cancels and we obtain

$$d\sigma = \frac{1}{4I} (2\pi)^4 \delta^{(4)}(P_i - P_f) |\mathcal{A}_{fi}|^2 \prod_{f=1}^n \frac{d^3 p_f}{2E_f (2\pi)^3} = \frac{1}{4I} |\mathcal{A}_{fi}|^2 d\Phi^{(n)} \quad (13.55)$$

with the final-state phase space $d\Phi^{(n)}$. The three pieces composing the differential cross-section, the flux factor I , the Feynman amplitude \mathcal{A} and the final-state phase space $d\Phi^{(n)}$, are each Lorentz-invariant. Integrating the differential cross section $d\sigma$ over the final-state phase space, one obtains the total cross section σ which enters the rates (13.42) and (13.47).

14. *** Milky Way and normal galaxies ***

Are nebula as e.g. Andromeda galactic objects as globular clusters? Or is our galaxy just one of many in the Universe?

Ernst Julius Öpik estimated 1922 the distance to Andromeda as follows: The rotation velocity at the edge of Andromeda was known from Doppler measurements. Expressing then the radius R of Andromeda as $R = \vartheta d$, where d is its distance and ϑ the angular diameter, in the virial theorem, he obtained

$$\frac{GM}{(\vartheta d)^2} = \frac{v^2}{\vartheta d}. \quad (14.1)$$

The luminosity L and the observed flux \mathcal{F} are connected by $\mathcal{F} = L/4\pi d^2$. Öpik did not know L , but he assumed that M/L is quite universal. Thus he used $M/L \simeq 3M_{\odot}/L_{\odot}$ determined as average value for stars in the solar neighborhood also for Andromeda. Inserting $d^2 = L/4\pi\mathcal{F}$ on the LHS of Eq. (14.1) gives then

$$d \approx \frac{v^2 \vartheta L}{4\pi \mathcal{F} GM} \simeq 450 \text{ kpc}. \quad (14.2)$$

This distance is much larger than the size of the galactic stellar disc. Edwin Hubble measured 1924 the distance to three spiral nebula including Andromeda by observing Cepheids, confirming that these are extragalactic objects.

14.1. Milky Way

In visible light we see an accumulation of stars as a band across the sky. In the infrared or far-infrared the structure of the Milky Way consisting of a disk and a bulge starts to be revealed. The Milkyway is an example for a spiral galaxy; it can be subdivided into (cf. also Fig. 14.2):

- The galactic bulge with a radius of 3 kpc around the center of the galaxy. It is composed both of old (pop II) and young (pop I) stars.
- The galactic disk with a radius of 20 kpc and a thickness 300 pc contains also both pop I and pop II stars together with gas and dust. The disk appears not uniform, but has probably four spiral arms and a central bar. The reason why the arms of spiral galaxies are so prominent is that the brightest stars are found in the spiral arms. Spiral arms are the major regions of star formation in spiral galaxies and this is where most of the major nebulae are found.
- The galactic halo with a radius of 25 kpc includes globular clusters (consisting only of old stars (population II))
- A dark halo with an extension of order 100 kpc contains 80%-95% of the mass of the galaxy (dark matter).

The number of stars in the Milky Way is $\sim 10^{11}$, while its total mass is estimated to be $10^{12}M_{\odot}$.

14.1.1. Evolution of star cluster

Rms and escape velocity from the virial theorem: The total kinetic energy of cluster with mass $M = Nm$ is

$$\langle E_{\text{kin}} \rangle = \frac{1}{2}M\langle v^2 \rangle \quad (14.3)$$

where $v_{\text{rms}} \equiv \langle v^2 \rangle^{1/2}$ is the root mean square (rms) velocity. Applying the virial theorem and using $\langle E_{\text{pot}} \rangle = 3GM^2/5D$, it follows

$$\langle v^2 \rangle = \frac{3GM}{5D}. \quad (14.4)$$

Example: Find the typical rms velocity of stars in a spherical cluster with size $D = 5$ pc that consists of 10^6 stars with average mass $m = 0.5M_{\odot}$.

$$\langle v^2 \rangle = \frac{3GM}{5D} = 2.5 \times 10^{12} \text{cm}^2/\text{s}^2 \quad (14.5)$$

or $v_{\text{rms}} \approx 16 \text{km/s}$. This value can be compared with observations; if the observed velocities are significantly higher, the cluster cannot be gravitationally bound or its total mass has to be higher.

Crossing time: The crossing time t_{cr} is the typical time required for a star in the cluster to travel the characteristic size D of the cluster (typically taken to be the half-mass radius). Thus, $t_{\text{cr}} \sim D/v$ or $t_{\text{cr}} \sim 3 \times 10^5$ yr for the values of our example.

Relaxation time: The relaxation time t_{rel} is the typical time in which the star's velocity changed an amount comparable to its original velocity by gravitational encounters. Thus one might think of it as the time-scale after which the velocity distribution of stars bound in a cluster has reached an equilibrium distribution by the exchange energy and momentum with each other. But since part of the stars will have velocities $v > v_{\text{esc}}$ and escape, the velocity distribution of a cluster is not stationary: High-velocity stars escape, the cluster contracts and its core is heated-up.

The depth τ for collisions of stars with each-other is

$$\tau = \sigma nl = \sigma nvt, \quad (14.6)$$

when n denotes the density of stars and $l = vt$ the path traveled by a single star. Let us call the relaxation time t_{rel} the time for which $\tau = 1$. Thus $t_{\text{rel}} = 1/(\sigma nv)$.

What should we use for R (as function of v) in $\sigma = \pi R^2$? Stars are certainly gravitationally interacting with each other, if they are bound to each other. Therefore we can estimate the effective interaction range R from $T = V$, $mv^2/2 = Gm^2/R$ or $R = 2Gm/v^2$. Then

$$t_{\text{rel}} = \frac{1}{\pi R^2 nv} = \frac{v^3}{4\pi n(Gm)^2}. \quad (14.7)$$

Inserting $1/n = (m/M)(4\pi/3)D^3$ (with $M = Nm$ as total mass of the cluster) gives

$$t_{\text{rel}} = \frac{v^3 D^3}{3G^2 m M}. \quad (14.8)$$

If the cluster is dynamically relaxed and the virial theorem applies, then $v^2 = 3GM/(D5)$ and thus

$$t_{\text{rel}} = \frac{D}{v} \frac{M}{m} \frac{v^4 D^2}{3G^2 M^2} \sim \frac{ND}{v} = N t_{\text{cross}}. \quad (14.9)$$

Note that $t_{\text{rel}} \gg t_{\text{cross}}$, in striking contrast to an ordinary gas

We should take into account how much momentum per collision is exchanged: In a collision at small impact parameter b the momentum transfer is larger than in one at large b . Moreover, one cannot treat relaxation just as a two-body process, because of the infinite range of the gravitational force. Formalizing this, the relaxation time given by Eq. (14.9) becomes reduced by a logarithmic term, $\approx 12 \ln(N/2)$, or

$$t_{\text{rel}} \approx 0.1 t_{\text{cross}} \frac{N}{\ln(N)}. \quad (14.10)$$

Thus, $t_{\text{rel}} \sim 2 \times 10^9$ yr for the values of our example.

Evaporation time: The evaporation time for a cluster is the time required for the cluster to dissolve through the gradual loss of stars that gain sufficient velocity through encounters to escape its gravitational potential.

Assuming an isolated cluster with negligible stellar evolution, the evaporation time t_{ev} can be estimated by assuming that a constant fraction α of the stars in the cluster is evaporated every relaxation time. Thus, the rate of loss is $dN/dt = -\alpha N/t_{\text{rel}} = -N/t_{\text{ev}}$. The value of α can be determined by noting that the escape speed v_{esc} at a point x is related to the gravitational potential $E_{\text{pot}}(x)$ at that point by $v_{\text{esc}}^2 = -2E_{\text{pot}}(x)$. (The total energy of a particle able to escape gas to be equal or larger than zero, i.e. $T + V \geq 0$ or $v_{\text{esc}}^2 \geq 2GM/R$.) If the system is virialized (as we would expect after a relaxation time), then also $\langle v^2 \rangle = 3GM/(5R)$.

Thus, stars with speeds above twice the RMS speed will evaporate. Assuming a Maxwellian distribution of speeds, the fraction of stars with $v > 2v_{\text{rms}}$ is $\alpha = 7.4 \times 10^{-3}$. Therefore, the evaporation time is

$$t_{\text{ev}} = \frac{t_{\text{rel}}}{\alpha} \approx 136 t_{\text{rel}}. \quad (14.11)$$

Stellar evolution and tidal interactions with the galaxy tend to shorten the evaporation time. Using a typical t_{rel} for a globular cluster, we see that $t_{\text{ev}} \sim 10^{10}$ yr, which is comparable to the observed age of globular clusters.

Dynamical friction What happens when a test body of mass M moves through a background of matter? Our test body will attract matter towards his position, creating a high-density “wake” trailing with him. The energy transferred to the surrounding material has to be supplied by the kinetic energy of our test body. As a result, a force F know as gravitational drag or dynamical friction acts on M .

We can obtain an understanding of this effect using just dimensional analysis. Since the force F can depend only on GM , v and ρ , the unique combination with the dimension of a force is (cf. Exercise 13.1)

$$F \approx C \frac{\rho(GM)^2}{v^2}, \quad (14.12)$$

where C is a dimensionless constant. This constant has to be determined from numerical simulations and varies between 10–100.

Inserting the density distribution appropriate for a dark matter halo, $\rho = v^2/(4\pi r^2 G)$, the force acting on a star cluster of mass M moving around a galaxy is

$$F \approx C \frac{GM^2}{4\pi r^2}. \quad (14.13)$$

The angular momentum of the cluster is $J = Mvr$. Since F acts tangentially to the orbit (assumed to be circular), the torque $\boldsymbol{\tau} = d\mathbf{J}/dt = \mathbf{r} \times \mathbf{F}$ is simply

$$\frac{dJ}{dt} = -rF. \quad (14.14)$$

Using $v(r) = \text{const.}$ motivated by the observed rotation curves, we obtain

$$Mv \frac{dr}{dt} = -C \frac{GM^2}{4\pi r}. \quad (14.15)$$

Separating the variables and integrating from the initial distance R until zero gives the lifetime τ of a cluster moving through background matter with density ρ ,

$$\int_R^0 dr r = -\frac{CGM}{4\pi v} \int_0^\tau dt \quad (14.16)$$

or

$$\tau = \frac{2\pi v R^2}{CGM}. \quad (14.17)$$

Example: i) The age of the oldest globular cluster in the Milky Way is $t = 13$ Gyr. Estimate with $C = 76$, $M = 5 \times 10^6 M_\odot$ and $v = 220$ km/s the maximal distance from which globular clusters could have been spiraled into the center of the galaxy.

ii) The large Magellanic Cloud (LMC), which has $M = 2 \times 10^{10} M_\odot$, orbits the Milky Way at a distance of 51 kpc. Assuming that the Milky Way's dark matter halo and flat rotation curve extends out to the LMC, estimate how much time it will take for the LMC to spiral into the Milky Way ($C = 23$).

For both questions we can use Eq. (14.38). Solution to i) is $R = 4$ kpc and to ii) $\tau = 1.7$ Gyr. Thus inside 4 kpc there should be no globular clusters, because they spiraled already into the center of the Milky Way and were dissolved, while the LMC has still some time to go...

Isothermal sphere In an isothermal sphere, the temperature does not depend on the radius. Thus the density distribution $\rho(r)$ depends only on the gravitational potential $\phi(r)$. With $\rho(r) \propto \exp(-E/kT)$, the density is

$$\rho(r) = \rho_0 \exp\{-\beta[\phi(r) - \phi_0]\}. \quad (14.18)$$

The connection between the mass density and the gravitational potential is given by the Poisson equation,

$$\Delta\phi = 4\pi G\rho_0 \exp\{-\beta[\phi(r) - \phi_0]\} \quad (14.19)$$

We introduce a dimensionless radius $x = r/L_0$ with the help of the Jeans length,

$$L_0 = (4\pi G\rho_0\beta)^{-1/2} \quad (14.20)$$

Setting also

$$y = \beta(\phi - \phi_0) \quad (14.21)$$

and assuming spherical symmetry, we can transform the Poisson equation (14.19) into an ordinary differential equation for $y(x)$,

$$\frac{1}{r^2} \frac{d}{dr} \left(r^2 \frac{d\phi}{dr} \right) = 4\pi G\rho(r) \quad \rightarrow \quad \frac{1}{x^2} \frac{d}{dx} \left(x^2 \frac{dy}{dx} \right) = e^{-y}. \quad (14.22)$$

Thus we see that i) the Lane-Emden equation is a special case of the Poisson equation and ii) an isothermal sphere corresponds to a polytropic EoS with $n \rightarrow \infty$. From the solution $y = 2 \ln x$, we obtain immediately

$$\rho(r) = \rho_0 e^{-y} = \rho_0 \left(\frac{L_0}{r} \right)^2. \quad (14.23)$$

This solution is rather pathological: The density diverges for small r , while the integrated mass $M(r)$ diverges for $r \rightarrow \infty$. Although the solution is thus unphysical, it is as a limiting case very useful. First, we note that $\rho(r) \propto r^{-2}$ gives rotation curves $v(r) \propto \text{const.}$ as observed in galaxies. Second, a real physical system has a finite size, connected e.g. to the distance between neighbors, while physical processes like annihilations or degeneracy pressure become important for large ρ . Thus the isothermal sphere is a useful description for intermediate distances.

Last but not least, the solution is important since it is an attractor. To see the exact meaning of this statement we rewrite the differential equation in a form similar to the equation of motion for a dynamical system. Changing variables to $q = \ln(x)$, we obtain

$$\frac{1}{x^2} \frac{d}{dx} \left(x^2 \frac{dy}{dx} \right) = e^{-3q} \frac{d}{dq} \left(e^q \frac{dy}{dq} \right) = e^{-y} \quad (14.24)$$

and setting $z = 2q - y$

$$\frac{d^2 z}{dq^2} + \frac{dz}{dq} = -(e^z - 2) = -\frac{\partial V}{\partial z}. \quad (14.25)$$

We can now give all three terms of this equation a simple interpretation, if we interpret z as the coordinate of a one-dimensional dynamical system and q as time: acceleration \ddot{z} , friction \dot{z} and potential energy $V = e^z - 2z$. Hence the system (alas the density distribution $\rho(r)$) will move towards the minimum of the potential V , slowed by the friction term. But the minimum of V at $z = \ln 2$ or $y = 2q - z = 2 \ln x + \text{const.}$ corresponds to the isothermal sphere.

Thus we found the important result that a self-gravitating system will evolve towards the density distribution (14.23) of an isothermal system, if degeneracy pressure or energy production play no important role. Such systems are for instance objects dominated by dark matter (galaxies, dark matter clumps inside galaxies) and stellar clusters.

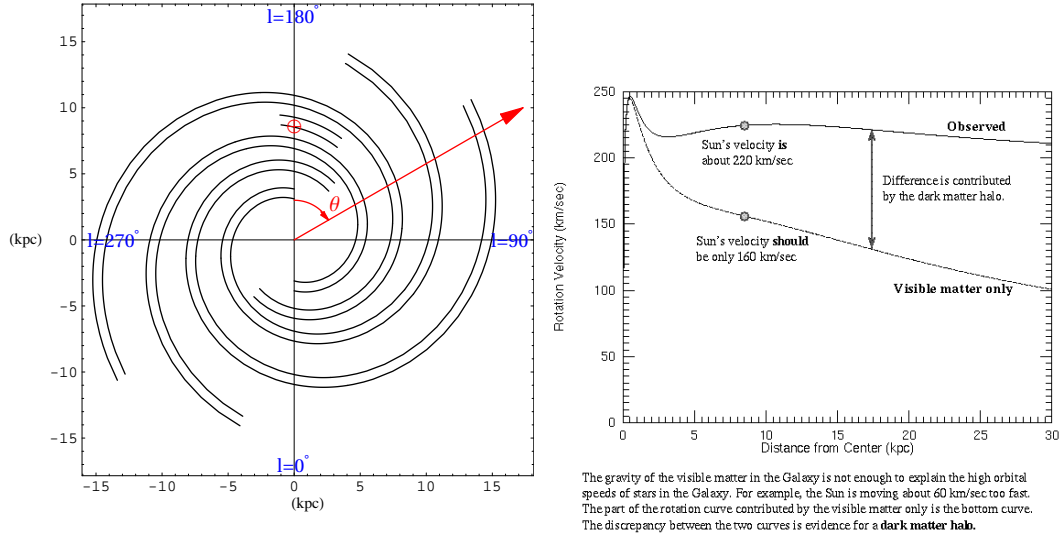


Figure 14.1.: Left: Schematic view of the spiral structure of the Milky Way; the position of the Sun is marked by a red dot. Right: Rotation curve of the Milky Way.

14.1.2. Rotation curve of the Milkyway

In the disk of the Milky Way, stars and other matter is rotating around the center in a regular pattern, as revealed by Doppler effects. In the galactic halo and the galactic bulge, the motion is largely random.

Determination of the rotation curve For simplicity, we assume a spherical mass distribution and use again the enclosed mass $M(r)$. For circular orbits, $GM(r)m/r^2 = mv^2(r)/r$, or

$$M(r) = \frac{rv^2(r)}{G}. \quad (14.26)$$

Measurements of $v(r)$ are mainly done using the 21cm line of gas clouds as tracer. For orbits inside the Sun's orbit, the radial velocity is largest, when the distance along the line-of-sight to the Galactic center is minimal: Hence the maximal Doppler shift along one line-of-sight determines $v(r)$ at this minimal distance r_{\min} .

If the visible stars dominate the mass distribution of the Milky Way, then we expect for small r inside the bulge, $M(r) \propto r^3$ and thus $v(r) \propto r$. Outside the disc, for $r \gtrsim 20$ kpc, $M(r) = \text{const.}$ and gas clouds should follow Keplerian orbits with $v(r) \propto 1/r^{1/2}$.

Figure 14.1 compares the observed rotation curve with the one obtained theoretically from the observed distribution $M(r)$ of visible matter as stars and gas. The discrepancy indicates that a large fraction, around 90%, of the mass in the Milky Way is non-visible. What $\rho(r)$ corresponds to $v(r) = \text{const.}$? We have $v^2(r) = GM(r)/r = \text{const.} \propto \rho r^2$ or $\rho \propto 1/r^2$. Thus each radial shell of thickness dr contains the same amount of dark matter, $dM \propto \rho(r)r^2 dr \propto \text{const.}$ (This makes the definition of the "size" or edge of the DM halo somewhat arbitrary.) We shall discuss what could be the explanation for this unseen matter later, in Sec. 14.2.2.

Rotation and the spiral structure The rotation of stars around the center of the Milky Way is differential: The observed constant rotation velocity, $v(r) \approx \text{const.}$, means that the rotation

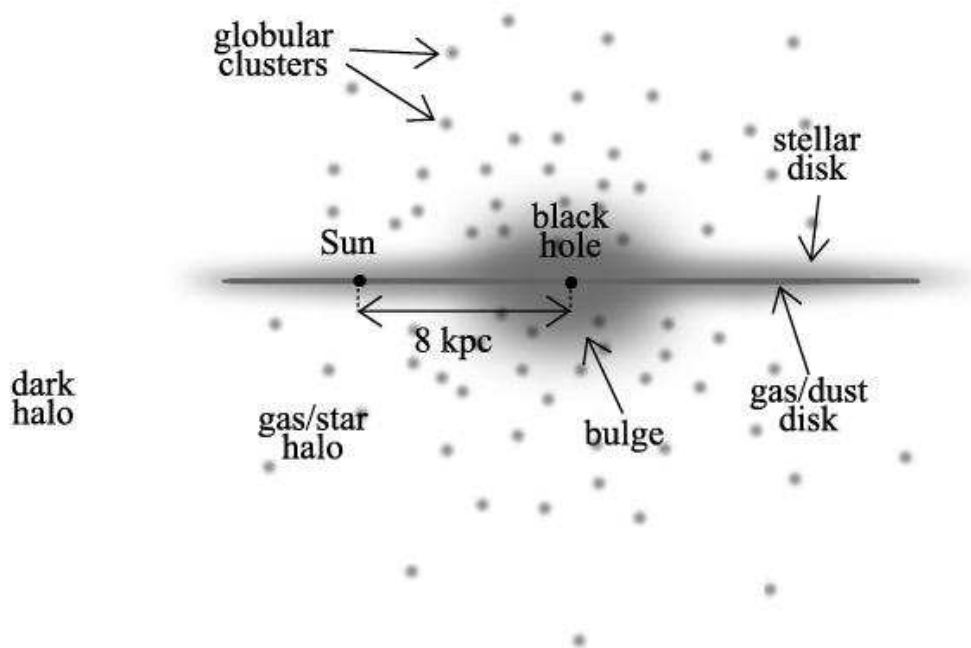


Figure 14.2.: Schematic picture of the Milky Way with a nuclear bulge in the center, a gas and dust disc of height $h = 300$ pc. The whole visible galaxy is immersed in a dark matter halo.

Figure 14.3.: Winding-up of the spiral arms due to differential rotation.

period increases linearly with the distance to the Galactic center, $P \propto r$. Thus the spiral arms should wind up as shown schematically in Fig. 14.3. For instance, the rotation period of the Sun around the Galactic center is 2×10^8 yr, so the Sun completed 20 turns around the Milky Way. How does the observed spiral pattern survives?

The wind-up picture assumes that the spiral arms are a denser region of stars. However, we noted already that spiral arms are instead the major regions of star formation in spiral galaxies. Star formation is triggered by gravitational perturbations, in particular during encounters with neighbor galaxies, which compress interstellar matter. The velocity with which these density perturbations travel has a priori nothing to do with the rotation velocity of individual stars.

Remark 14.1: . The density waves first concern interstellar matter, which is compressed, forms diffuse nebulae which become star-forming regions, and later form (open) clusters and associations of young stars, the most luminous and conspicuous of which are massive, hot, blue and short-lived. Therefore, we see the most current density wave in the reddish H II regions, the elder next in the blueish clouds and associations of hot young stars, the next in age are characterized by type II (and Ib, Ic) supernova remnants and a bit older, less hot and blue open clusters. They can also be traced by the stars of the hotter spectral types, O, B, and A. The stars which are even older have dissipated into a more diffuse background; this includes intermediate population I stars, older star clusters and

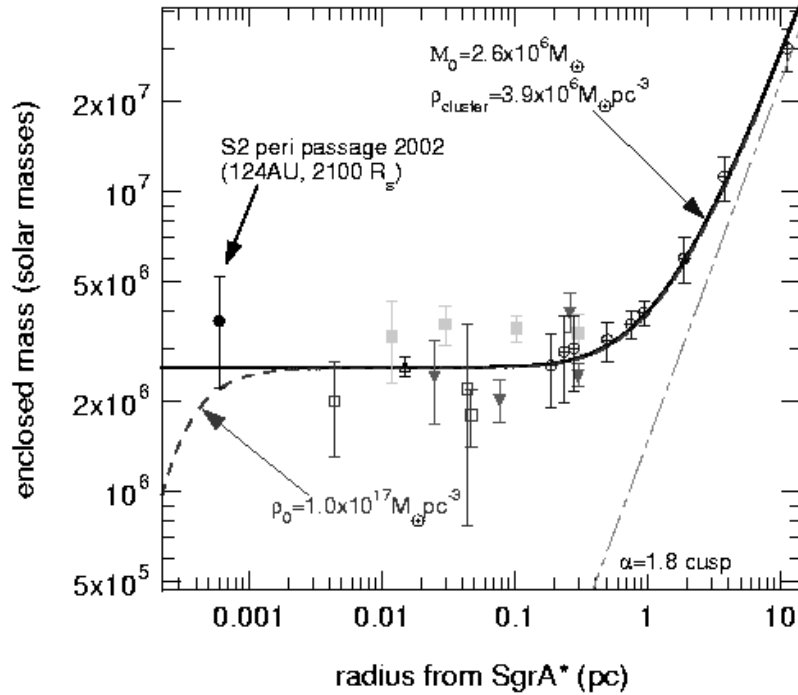


Figure 14.4.: Enclosed mass as function of the distance to Sgr A (an object at the galactic center); the dashed-dotted line gives for comparison the enclosed mass for a DM halo with $\rho(r) \propto r^{-\alpha}$ and $\alpha = 1.8$.

the younger representatives of the planetary nebulae.

14.1.3. Black hole at the Galactic center

Supermassive black holes (SMBH) with masses up to $10^{10} M_{\odot}$ are supposed to be in the center of most galaxies, and that includes our own galaxy, the Milky Way. One way to show the existence of a SMBH is to deduce first the enclosed mass from rotation curves around the supposed BH. Then one has to show that no object with such a mass has a sufficient long lifetime.

Observationally, it is crucial to observe stars as close as possible to the BH. The large amount of dust in the Galactic bulge requires excellent IR observations. In spring 2002, a star was passing with $v = 5000$ km/s at 17 light hours distance – or 3AU – the point of closest approach to the black hole. One could determine a unique Keplerian orbit (highly elliptical (eccentricity 0.87), semimajor axis of 5.5 light days, a period of 15.2 years and an inclination of 46 degrees). Kepler's 3rd law gives as enclosed mass $M(r) = (3.7 \pm 1.5) \times 10^6 M_{\odot}$, cf. Fig. 14.4. It is not possible to explain this result with a dense cluster of dark astrophysical objects because such a cluster would have the extremely short lifetime of at most a few hundred thousand years.

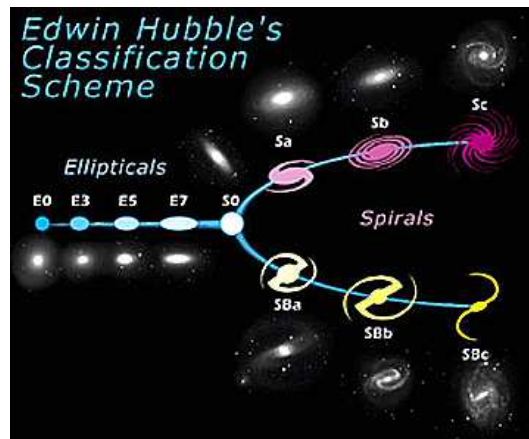


Figure 14.5.: Hubble's classification scheme for galaxies.

14.2. Normal Galaxies

The total energy emitted by a normal galaxies is the sum of the emission from each of the stars found in the galaxy. Thus the emission is roughly thermal and mainly in the infrared, visible and ultraviolet bands.

14.2.1. Hubble sequence

Spiral galaxies are two-dimensional objects, with or without bar. They make up 2/3 of all bright galaxies. They contain gas and dust; young and old stars. The stars move regularly in the disc. The surface luminosity of spiral galaxies decreases exponentially for large radii, $L(r) = L_0 \exp(-r/r_0)$ with $r_0 \sim 5$ kpc.

Elliptical galaxies have a three-dimensional, elliptical appearance. Most common are dwarf elliptical galaxies, with sizes of only a few kpc. But there exist also giant elliptical galaxies with an extension up to 100 kpc. Their low gas content ($< 1\%$) excludes the idea of an evolution from elliptical to spiral galaxies by flattening.

Elliptical galaxies contain no young stars. Stars are moving randomly. Their surface luminosity decreases as $L(r) = L_0 \exp(-r/r_0)^{1/4}$ with a large variation of r_0 .

S0 and irregular galaxies are the remaining ones.

Demography/Schechters....

14.2.2. Dark matter in galaxies

Flat rotation curves as far as luminous matter extends are found in practically all galaxies. Hence, as for the Milky way, $v(r) = \text{const.}$ corresponds to $\rho \propto 1/r^2$, compared to an exponential fall-off of luminous matter.

What are potential explanations for this discrepancy?

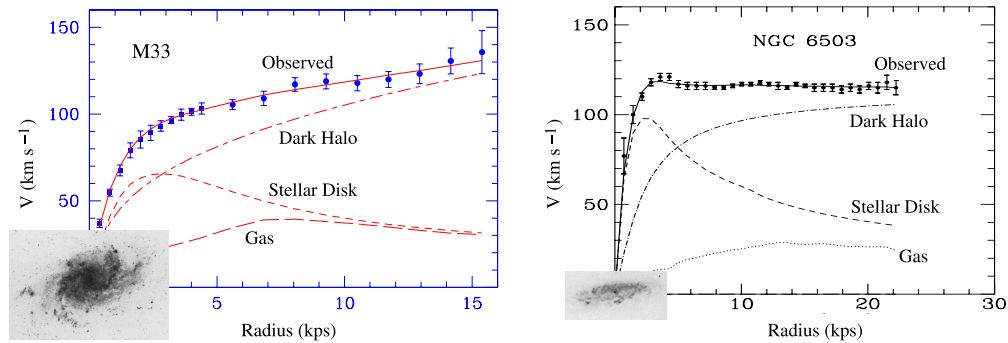


Figure 14.6.: Rotation curves of two galaxies, superimposed are optical images.

- Dust and gas clouds are seen by their blocking effect on light or in radio. Their contribution to the mass density has been accounted for. Moreover, big bang nucleosynthesis limits the fraction baryonic matter **expl.?** can contribute to the total mass of the universe as we will see later in Sec. ??.
- Most of the mass contained in galaxies could consist of non-luminous objects, so-called MAssive Compact Halo Object (MACHOs) like brown dwarfs, Jupiter-like objects, or black holes. This possibility can be tested by microlensing, i.e. the occasional amplification of light from extragalactic stars by the gravitational lens effect. Searches for microlensing towards the Large Magellanic Cloud exclude MACHOs as main component of dark matter in the Milky Way.
- The missing matter is composed of a new stable, neutral particle: “dark matter.”
- Gravity has to be modified.

Microlensing of MACHOs In microlensing experiments that have tried to detect dark matter in the form of MACHOs (black holes, brown dwarfs,...) one observed stars of the LMC. If a MACHO with speed $v \approx 220$ km/s moves through the line-of-sight of a monitored star, its light-curve is magnified temporally. If v is the perpendicular velocity of the source, see Fig. 14.8

$$\beta(t) = \left[\beta_0^2 + \frac{v^2}{D_{ol}^2} (t - t_0)^2 \right]^{1/2} \quad (14.27)$$

with β_0 and t_0 as the lensing angle and time at closest approach, The magnification $a(t)$ is symmetric around t_0 and its shape can be determined inserting typical values for D_{ol} , the MACHO mass.

Pacienxky proposed the following method to search for MACHOs: The Large Magellanic Cloud (LMC) contains xx stars at a distance $l = 50$ kpc that allows telescopes to resolve the stars. If the DM halo of the Milky Way consists of MACHOs, then from time to time the Earth, a MACHO and a star in the LMC will be aligned, resulting in a microlensing event.

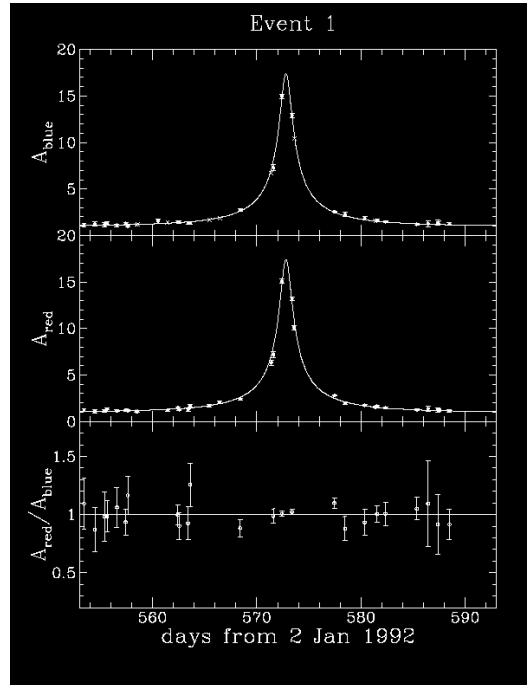
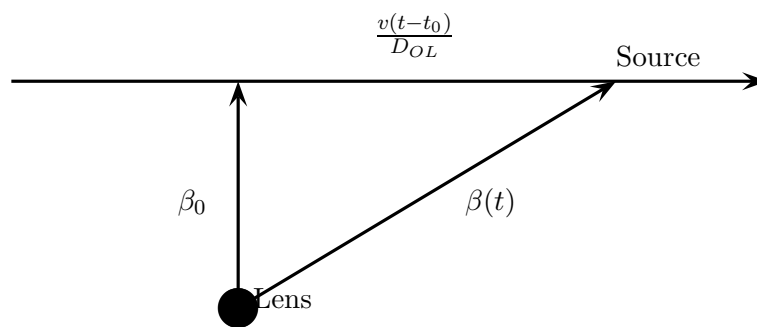


Figure 14.7.: A potential MACHO microlensing event.

Figure 14.8.: The lensing angle $\beta(t)$ for a motion along a straight line.

Let us now estimate if this proposal is feasible. The number density n of MACHO objects with mass m is

$$n \sim \frac{M_{\text{gal}}}{\frac{4}{3}\pi R_{\text{gal}} m} \quad (14.28)$$

If we define the lensing cross section σ as the area within the amplification factor is larger than $a = 1.34$, then

$$\sigma = \pi(\vartheta_E D_{OL})^2 \quad (14.29)$$

Analogous to the optical depth, we define the lensing depth towards the LMC as

$$\tau = n\sigma l \sim \frac{Gm}{lc^2} \sim \left(\frac{v_{\odot}}{c}\right)^3 \sim 10^{-6} \quad (14.30)$$

which is independent of the MACHO mass m . Here, we used the virial theorem, $v(r) \sim GM/r$, and the observation $v(r) \sim \text{const.}$ The small lensing depth $\tau \sim 10^{-6}$ implies that the light curve of millions of stars has to be monitored at the same time.

The typical rise-time of the light-curve is $T = 2\vartheta_E D_{OL}/v$. If we use $v = 220 \text{ km/s}$, then $T \sim 6$ months for $m = M_{\odot}$, while $T \sim 6$ days for $m = 10^{-3} M_{\odot}$.

Modification of gravity (MOND) Newton's laws have been tested successfully within the solar system with typical accelerations $a_{\oplus} = v_{\oplus}^2/d_{\oplus} \approx (30 \text{ km/s})^2/(1 \text{ AU}) \approx 0.6 \text{ cm/s}^2$, but could be wrong for the very small accelerations $a \sim a_0 = v_{\oplus}^2/d_{\oplus} \approx (220 \text{ km/s})^2/(8.5 \text{ kpc}) \approx 2 \times 10^{-8} \text{ cm/s}^2$ that are relevant for the dynamics of galaxies. Flat rotation curves of galaxies without the need for dark matter can be achieved by introducing a function μ in Newton's law,

$$m\mu(a/a_0)\mathbf{a} = \mathbf{F} \quad (14.31)$$

with $\mu(x) \rightarrow 1$ for $x \rightarrow \infty$ and $\mu(x) \rightarrow x$ for $x \rightarrow 0$. Choosing $a_0 \sim 10^{-8} \text{ cm/s}^2$, all Newtonian standard results and observations are reproduced. Alternatively, Newtonian gravity could be modified,

$$\mu(g/a_0)\mathbf{g} = \mathbf{g}_N. \quad (14.32)$$

As long as gravity is the only force relevant for the dynamics, the two alternatives cannot be distinguished. MOND describes a large amount of data successful and also a relativistic generalization of MOND is possible. However, MOND fits many cosmological observations (that we shall discuss later) worse than the hypothesis that a large fraction of the mass of the universe is in form of a new dark matter particle.

Example: Show that the modified law of inertia, Eq. (14.31), leads to flat rotation curves without dark matter.

Equating gravitational and centripetal forces in the regime $\mu(x) \rightarrow x$ for $a \ll a_0$, i.e. $F = ma^2/a_0$, gives

$$\frac{v^4}{r^2 a_0} = \frac{GM(r)}{r^2}$$

or

$$v^4 = a_0 GM(r) \stackrel{!}{=} \text{const.}$$

Hence a constant rotation velocity is obtained, if $M(r)$ does not increase with r , i.e. without the need for dark matter.

Neutrinos as DM and dwarf galaxies If the mass of galaxies consists indeed mainly of an elementary particle different to protons, then our only candidate for the dark matter particle we know already are neutrinos. As neutrino oscillations show, they are massive and they are most likely stable even on time-scales much larger than the age of the universe. However, we can use an argument similar to the one we used to derive the degeneracy pressure of fermions to exclude this possibility. Since neutrinos are fermions, they cannot be packed arbitrarily dense. Together with the upper mass limit $m_\nu < 3 \text{ eV} \approx 6 \times 10^{-6} m_e$ from beta-decay experiments, the Pauli principle excludes neutrinos as main component of dark matter in galaxies.

Example: Neutrinos as dark matter.

Consider cold neutrinos with arbitrary mass m as explanation for dark matter in spiral and dwarf galaxies. (Use $M \sim 10^{11} M_\odot$ and $R = 50 \text{ kpc}$ for spiral and $M \sim 10^7 M_\odot$ and $R = 0.1 \text{ kpc}$ for dwarf galaxies.) Derive a lower limit for the neutrino mass m using that neutrinos are fermions. (Hint: connect the escape velocity from the galaxy with the maximal momentum of a degenerate Fermi gas.) A neutrino bound to a galaxy has energy $E = GMm/R + mv^2/2 \leq 0$, hence its momentum should be smaller than $p_{\text{esc}} = mv_{\text{esc}} = \sqrt{2GM/R}$. On the other hand, the number N of possible neutrino states inside the volume $V = 4\pi R^3/3$ up to p_{esc} can be estimated with Heisenberg's uncertainty principle: In one dimension $\Delta x p_x / \hbar \gtrsim 1$ and thus

$$N \approx (1/\hbar^3) \int d^3x d^3p = \frac{4\pi}{3} R^3 \frac{4\pi}{3} (p_{\text{esc}}/\hbar)^3.$$

Since the Pauli principle forbids that 2 fermions occupy the same state, N is equal to the maximal number of neutrinos in the galaxy. The total mass in neutrinos follows as

$$M = Nm \leq \left(\frac{4\pi}{3}\right)^2 m^4 (2GM/R/\hbar^2)^{3/2}$$

or neglecting numerical factors

$$m \gtrsim (G^3 R^3 M / \hbar^6)^{-1/8}.$$

For typical spiral galaxies, $m \gtrsim 10 \text{ eV}$, while for typical dwarf galaxies $m \gtrsim 500 \text{ eV}$. The current experimental upper limit is $m \lesssim \text{few eV}$ and excludes therefore neutrinos as main component of DM.

14.2.3. Tully-Fisher relation

An empirical relation published 1977 between the luminosity of a spiral galaxies and the width of its spectral lines, especially the 21cm line. Since $M \propto v^2$ and there is red- and blue-shifting on opposite sides, such a relation is expected. The detailed form has to derived empirically, since it depends on the distributions $v(r)$ and $L(r)$. Uses then the distance modulus to find distance from luminosity and apparent magnitude.

14.2.4. Galactic evolution

Galaxies are not isolated objects that are well-separated from each other. Instead they are bound together forming larger clusters, collide with each other and may merge. We discuss just one example for what might happen to a smaller body moving in the dark matter cloud of a larger one. For a concrete realization one can think at a dwarf galaxy like the Magellanic clouds orbiting around the Milky Way.

Dynamical friction What happens when a test body of mass M moves through a background of matter? Our test body will attract matter towards his position, creating a high-density “wake” trailing with him. The energy transferred to the surrounding material has to be supplied by the kinetic energy of our test body. As a result, a force F know as gravitational drag or dynamical friction acts on M .

We can obtain an understanding of this effect using just dimensional analysis. Since the force F can depend only on GM , v and ρ , the unique combination with the dimension of a force is (cf. Exercise 13.1)

$$F \approx C \frac{\rho(GM)^2}{v^2}, \quad (14.33)$$

where C is a dimensionless constant. This constant has to be determined from numerical simulations and varies between 10–100.

Inserting the density distribution appropriate for a dark matter halo, $\rho = v^2/(4\pi r^2 G)$, the force acting on a star cluster of mass M moving around a galaxy is

$$F \approx C \frac{GM^2}{4\pi r^2}. \quad (14.34)$$

The angular momentum of the cluster is $J = Mvr$. Since F acts tangentially to the orbit (assumed to be circular), the torque $\boldsymbol{\tau} = d\mathbf{J}/dt = \mathbf{r} \times \mathbf{F}$ is simply

$$\frac{dJ}{dt} = -rF. \quad (14.35)$$

Using $v(r) = \text{const.}$ motivated by the observed rotation curves, we obtain

$$Mv \frac{dr}{dt} = -C \frac{GM^2}{4\pi r}. \quad (14.36)$$

Separating the variables and integrating from the initial distance R until zero gives the lifetime τ of a cluster moving through background matter with density ρ ,

$$\int_R^0 dr r = -\frac{CGM}{4\pi v} \int_0^\tau dt \quad (14.37)$$

or

$$\tau = \frac{2\pi v R^2}{CGM}. \quad (14.38)$$

Example: i) The age of the oldest globular cluster in the Milky Way is $t = 13$ Gyr. Estimate with $C = 76$, $M = 5 \times 10^6 M_\odot$ and $v = 220$ km/s the maximal distance from which globular clusters could have been spiraled into the center of the galaxy.

ii) The large Magellanic Cloud (LMC), which has $M = 2 \times 10^{10} M_\odot$, orbits the Milky Way at a distance of 51 kpc. Assuming that the Milky Way’s dark matter halo and flat rotation curve extends out to the LMC, estimate how much time it will take for the LMC to spiral into the Milky Way ($C = 23$).

For both questions we can use Eq. (14.38). Solution to i) is $R = 4$ kpc and to ii) $\tau = 1.7$ Gyr. Thus inside 4 kpc there should be no globular clusters, because they spiraled already into the center of the Milky Way and were dissolved, while the LMC has still some time to go...

15. Active galaxies

An active galaxy can be defined as any galaxy satisfying one of the following four criteria:

- a compact nucleus emits with $L \gg L_{\text{star}}$
- a compact nucleus with non-stellar continuum emission
- strong emission lines with ratios atypical for stars
- temporal variations

The core of an active galaxy is called active galactic nucleus or AGN.

15.1. ***Mini cosmology – redshift and distances***

Active galaxies are often at cosmological distances, implying that deviations from static Euclidean space become important: redshift, Hubble parameter, luminosity distance, comoving density.

15.2. Observations and zoology

Radio galaxies Radio galaxies emit typically 10^6 times more energy in the radio range than normal galaxies. The main emission mechanism is synchrotron radiation of electrons. The radio emission comes mainly from two *radio lobes* separated by distances up to the order of 10 Mpc, cf. Fig. 15.1. Additionally, there is a weaker radio source in center of the galaxy. Radio galaxies appear in the visible light as giant elliptical galaxies.

The lobes are caused by the interaction of a jet of high energy particles and the intergalactic medium: The medium slows down the jet, material is dragged along with the jet, while higher velocity particle are coming from behind. Thus a shocks forms and creates a "Hot Spot," which is the site of most intense emission, see Fig. 15.1.

We can estimate the activity period of AGNs using Cygnus A, the first extragalactic radio source detected, as an example. Its two radio lobes are separated by 140 kpc; their kinetic energy is around 10^{60} erg, while the radio luminosity is $L \simeq 5 \times 10^{44}$ erg/s. Thus the life-time follows as $\tau \simeq E_{\text{lobe}}/L_{\text{radio}} \simeq 65$ Myr. In general, the activity periods of AGNs are of order 10–100 Myr.

Quasars Quasi-stellar objects were discovered in late 1963, when a star-like object with $m = 13$ was identified with a strong radio source. Emission line as Balmer lines, but displaced by $\Delta\lambda/\lambda = 0.15$ were found. If interpreted as redshift due to expansion of Universe, quasars are at "cosmological distance." For the particular case of the quasi-stellar objects found 1963, the distance is 640 Mpc. This requires enormous luminosities: The distance modulus is

$$m - M = 5 \log(d/10pc) = 39 \tag{15.1}$$

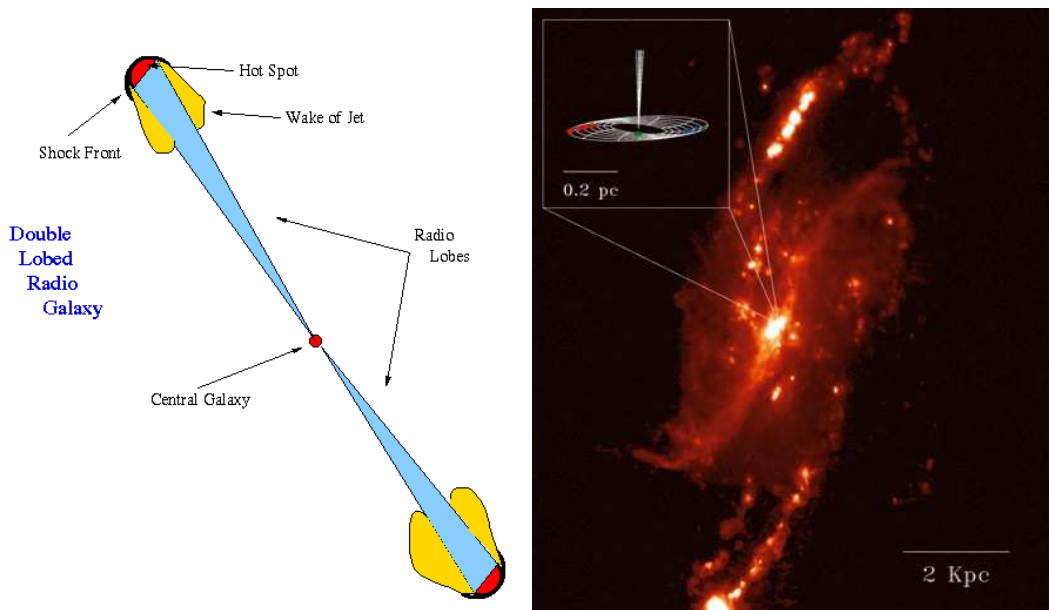


Figure 15.1.: Left:Schematic picture of a radio galaxy. Right: NGC4258

of $M = -26$. For comparison, the absolute magnitude of the Sun is 5, a difference of 31 corresponds to a brightness ratio of 10^{12} . In the radio, the source emits even stronger.

Seyfert galaxies In 1943, Carl Seyfert noticed that certain nearby spiral galaxies have very bright, pinpoint nuclei. The spectra of these galaxies show very strong, often broad, emission lines. The brightness of the cores of Seyfert galaxies fluctuates: The light from the central nucleus varies in less than a year, which implies that the emitting region must be less than one light year across. They do not have radio lobes. Most are powerful sources of infrared radiation. In addition, some emit intensely in the radio, X ray, and gamma ray regimes. Approximately 2% of all spiral galaxies are Seyfert galaxies.

Seyfert galaxies are divided into two classes, based upon the widths of their spectral emission features. Seyfert 1 galaxies have hydrogen emission features with very large widths, indicating that the gas in the galaxy's central regions is moving with velocities of several thousand km/sec (Seyfert 1 galaxies show velocities up to almost $0.1c$). Seyfert 2 galaxies have much narrower emission features implying much lower velocities (note that the Seyfert 1 in Fig. 15.2 shows narrow features as well).

BL Lacertae Main characteristics of BL Lacertae is their fast variability, with night-to-night variations of 10-30%, or a factor 100 within weeks if the source flares. Their spectra show no emission lines, and their appearance in the optical is point-like.

Superluminal motion For relatively nearby AGNs, one can resolve spatially structures close to their nucleus (e.g. 2 spots with stronger emission moving along the jet of a radio galaxy). One finds often that their apparent relative velocity is superluminal, what can be explained as follows:

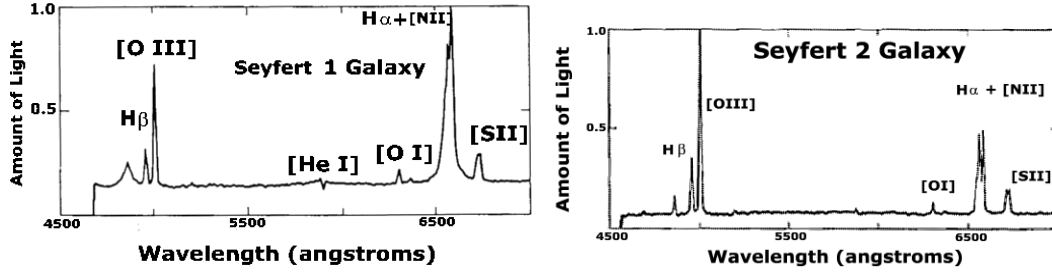


Figure 15.2.: The spectra of Seyfert 1 (left) and Seyfert 2 (right) galaxies.

Consider a source moving with velocity v from A to B towards an observer. Denote the difference in radial distance to the observer by x_{\parallel} , the perpendicular one by x_{\perp} . Then a light signal from B needs x_{\parallel}/c less time than a signal from A . Thus, the apparent time for the object to travel from A to B the distance r is

$$t_{\text{app}} = \frac{r}{v} - \frac{x_{\parallel}}{c} = \frac{r}{v} - \frac{r}{c} \cos \vartheta = \frac{r}{v} (1 - \beta \cos \vartheta), \quad (15.2)$$

where r is the distance between A and B . The apparent velocity across the sky is then

$$v_{\text{app}} = \frac{x_{\perp}}{t_{\text{app}}} = \frac{r \sin \vartheta}{\frac{r}{v} (1 - \beta \cos \vartheta)} = \frac{v \sin \vartheta}{1 - \beta \cos \vartheta}. \quad (15.3)$$

For $v \ll c$, we obtain the expected result $v_{\text{app}} \approx v \sin \vartheta$, while for $\beta \rightarrow 1$ the apparent velocity can exceed the speed of light. We determine the maximal value of the apparent velocity by first deriving the maximum of v_{app} as function of ϑ ,

$$\frac{dv_{\text{app}}}{d\vartheta} \propto \cos \vartheta_0 (1 - \beta \cos \vartheta_0) - \beta \sin^2 \vartheta_0 = 0 \quad (15.4)$$

or $\cos \vartheta_0 = \beta$. Inserting the latter condition into Eq. (15.3) gives then

$$\left(\frac{v_{\text{app}}}{v} \right)_{\text{max}} = \frac{1}{(1 - \beta^2)^{1/2}} = \gamma. \quad (15.5)$$

Hence the apparent velocity is maximally increased by the Lorentz factor γ of the source towards the direction $\cos \vartheta = \beta$.

15.3. Nucleus of active galaxies

In Fig. 15.3, we show how in a simplistic picture the various AGN types may be unified. We start by sketching the key elements of this picture.

SMBH At the center of the active nuclei a supermassive black hole (SMBH) resides. It is typically rotating and thus described by the Kerr metric. It is fully described by two parameters, the mass and the angular momentum. A key question is to explain the fast growth of SMBHs such that they can explain the observation of quasars up to redshift $z \sim 9$. If their seeds are $\sim 20M_{\odot}$ BHs formed in the SN explosion of the first generation of stars

(“pop III stars”), and their growth is mainly by accretion, then the accretion rate has to be at super-Eddington rate.

Blandford-Znajek mechanism:

Penrose showed that one can extract the rotation energy of a Kerr BH. Blandford and Znajek applied this idea to a Kerr BH immersed in magnetic field. The basic mechanism can be understood by an analogy with a unipolar conductor: Using cylindrical coordinates, a magnetic field $\mathbf{B} = B\mathbf{e}_z$ along the rotation axis leads to the Lorentz force $\mathbf{F} = q\mathbf{v} \times \mathbf{B} = q\omega\rho B\mathbf{e}_\rho$ acting on the electrons in the rotating conductor. The force induces the voltage

$$U = \frac{1}{q} \int_0^\rho d\mathbf{s} \cdot \mathbf{F} = \frac{1}{2}\omega\rho^2 B \quad (15.6)$$

Introducing the magnetic flux $\phi_B = \int d\mathbf{A} \cdot \mathbf{B} = \pi\rho^2 B$, we can write the voltage as $U = \omega\phi_B/(2\pi)$. We can extract the power

$$P = \frac{U^2}{R} = \frac{\omega^2\phi_B^2}{4\pi^2 R}, \quad (15.7)$$

if we wire the unipolar conductor into a circuit.

How this can be applied to a rotating BH? Imagine to drop positive and negative charges on the opposite sides of a BH. For an observer at infinity, the charges cross only for $t \rightarrow \infty$ the horizon. They contribute to a kind of charge surface density and, since the BH is rotating, to a current. The horizon of a Kerr BH can be viewed therefore as a membrane with definite electric properties; in particular, we can attribute the resistance R to the BH horizon. Finally, the wire is replaced in this astrophysical setting by e^+e^- pairs initiated by synchrotron photons. With $R \simeq 377\Omega$ appropriate for a Kerr BH, $\rho \sim GM/c^2$ and $a \in [0 : 1]$ as dimensionless parameter characterising the angular momentum of the BH, it follows

$$U = 10^{20}\text{V} \frac{B}{10^4\text{G}} \frac{M}{10^9 M_\odot} a \quad (15.8)$$

and

$$P = 10^{45}\text{erg/s} \left(\frac{B}{10^4\text{G}}\right)^2 \left(\frac{M}{10^9 M_\odot}\right)^2 a^2. \quad (15.9)$$

The voltage is sufficient to accelerate protons to the highest observed energies; power.

Thus the SMBH in the nucleus of an active galaxy may convert the rotational energy gained from the infalling material into a high-power outflow of relativistic particles.

Growth of BHs:

The accretion rate is limited by radiation pressure,

$$L = \xi \dot{M}c^2 < L_{\text{Edd}} = \frac{4\pi cGM}{\kappa}$$

Setting $L = L_{\text{Edd}}$, it is $\dot{M}/M = \text{const}$ and thus the BH mass grows exponentially, $M = M_0 \exp(\tau)$ with time-scale

$$\tau = \frac{M}{\dot{M}} \simeq 4.5 \times 10^7 \text{yr} \frac{\xi}{0.1} \frac{L_{\text{Edd}}}{L}$$

The number N of e-foldings during the age of the universe is thus $N = \tau/t_0 \simeq 280$, and the existence of SMBH seems unproblematic. However, their presence in early galaxies at redshift $z = 10$ (when $t = 0.5\text{Gyr}$ and thus $N = 10$) is problematic.

Accretion disks The temperature profile discussed in sec. 8.2 is a useful approximation for a realistic accretion disk of an AGN, if its accretion rate is high, $\dot{M} \sim \dot{M}_{\text{Edd}}$. For lower rates, the structure of the disk can change considerably. For SMB with mass of order $10^8 M_{\odot}$, one expect a bump in the UV caused by the thermal emission of the accretion disk.

Broad-line region consists of high-density ($n \sim 10^{10}/\text{cm}^3$) clouds at a distance 0.1–1 pc from the SMBH. They fill around $\lesssim 10\%$ of the area. The clouds emit emission lines. The Dopler shift due to their Keplerian speed which is around 3000km/s allows to estimate the mass of the SMBH and explains the large line-widths of the lines. If the line-width of an individual cloud is caused by thermal motion, $\delta v \sim c_s \sim 10\text{km/s}$, then a large number of clouds is needed to fill the observed line profiles.

The emission is in the X-ray range, extending the UV bump of the accretion disk.

Dust torus The non-observation of the broad-line emission region if the AGN is seen from the side requires the existence of an obscuring region. This is often modeled as torus of dust extending on scales of 1–100 pc.

Narrow-line region

Hot corona–outflows–jets

Unified picture The fast variability and the large energy output point to accretion on SMBH as main energy source of the AGN activity. We observe different types of AGN due to their time evolution (e.g. from Quasars to Seyfert), different angles of view and different stages: i) active vs. quiet due to changes in dm/dt caused by “natural” fluctuations or mergers of host galaxies; ii) change of the relative angular momentum of accretion disk and SMBH leads to change in efficiency η and jet activity. The main division between radio loud or radio quiet AGN is believed to be caused by the strength of magnetic fields near the SMBH. A cartoon sketching the different types of AGN is shown in Fig. ??.

Electromagnetic spectrum The energy spectrum observed from blazars, i.e. AGN which jets are pointing towards us, covers all the electromagnetic spectrum from radio frequencies up to TeV energies. It is characterized by two bumps, cf. Fig. 15.4, one peaking between the IR and the X-ray band, another one at gamma-ray energies. The first peak can be explained as synchrotron radiation from relativistic electron, while the second one is presumably due to inverse Compton scattering – between the same electrons and either soft photons or synchrotron photons.

Although sources like blazars should accelerate not only electrons but also protons, synchrotron radiation and inverse Compton scattering of electrons are sufficient to explain in most cases the observed spectra. There are only few exceptions where an additional photon component from pion decay at the highest energies might be needed.

Time variability The high-energy part of the spectrum varies on scales of months to days. In general, the emission from the broad-line region lags behind. The time-delays allows one to determine the distance r of this region to the nuclei, cf. with Fig. ??: For an observer at

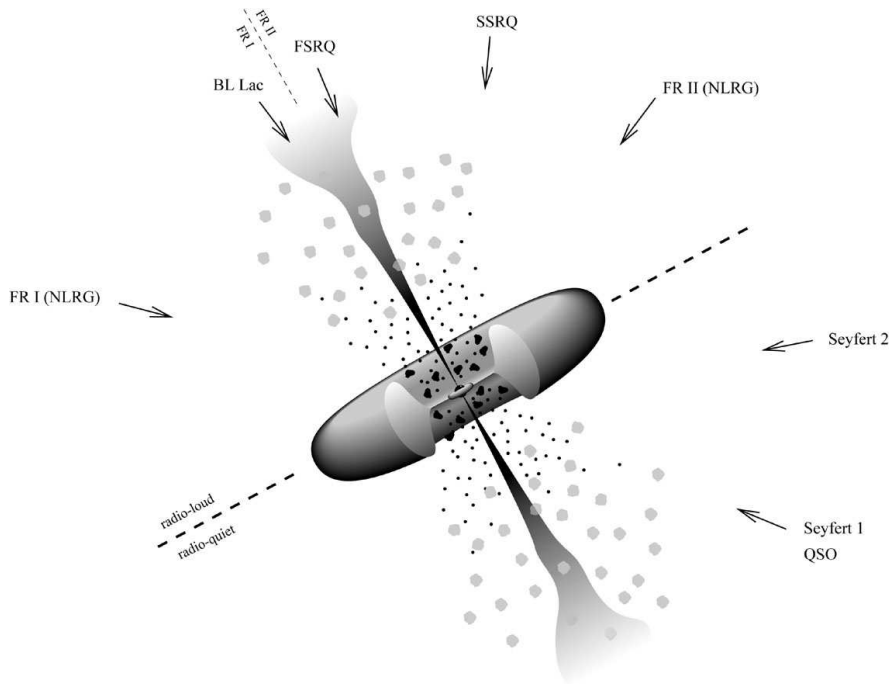


Figure 15.3.: The unified picture for AGN explains the large AGN variety mainly as differences in the viewing angle relative to the jet axis.

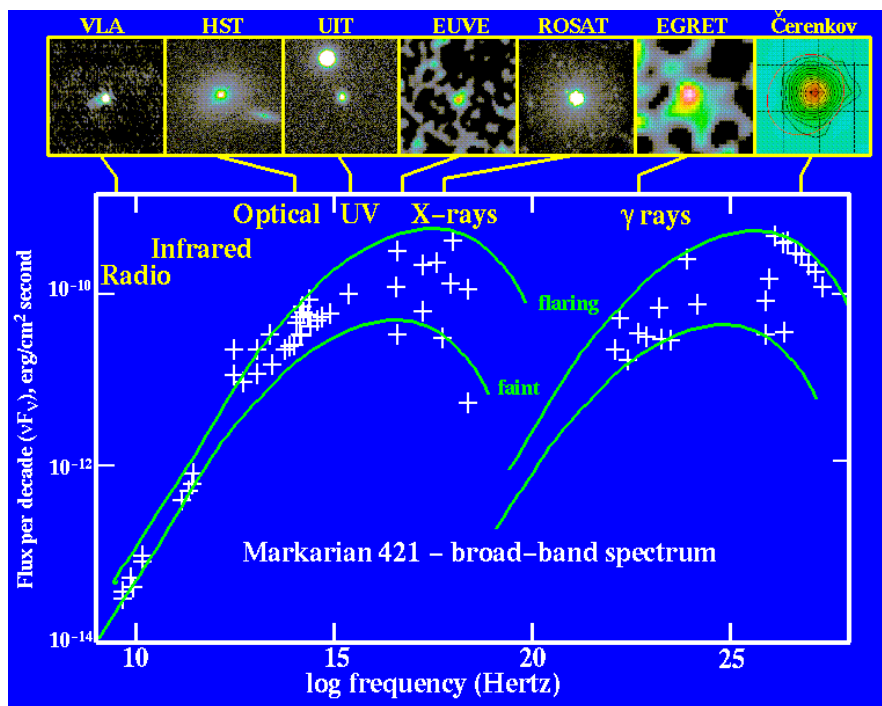


Figure 15.4.: Spectrum from the blazar Markarian 421 in a flaring and a quiet state [?].

infinity, the surface of constant time-delay τ forms a parabola, and $\tau = (1 + \cos \vartheta)r/c$. Moreover, a sharp rise will be spread out over the time interval $[0, 2r/c]$. From these observations one deduces $r = 0.1\text{--}1$ pc. Assuming then Keplerian orbits, one can estimate the mass of the SMBH. Since $v \propto 1/\sqrt{r} \propto 1/\sqrt{\tau}$, time-delays and line-widths are correlated.

Acceleration sites Various potential acceleration sites exist in a AGN: magnetic fields close to the SMBH could accelerate particles via the Blandford-Zjenak mechanism. A standing accretion shock can lead to diffusive shock acceleration. In both cases significant secondary production due to scattering on background photons or gas are expected. On much larger scales, internal shocks in the jet or its termination shock can lead to diffusive shock acceleration. In addition, plasma processes like reconnection may accelerate particles. In the jet, secondary production should be suppressed, since densities are much smaller.

15.4. Diffuse spectra of high-energy particles

We can approximate the emission of high-energy particles by discrete sources by the smooth injection rate $\dot{Q} = dN/(dEdVdt)$. The injection rate \dot{Q} is the product of the density n_s of sources and the injected energy spectrum $dN_i/(dEdt)$ of particles per time of individual sources.

In a static, uniform universe, the observed differential number density at the present time t_0 is then

$$n(\mathbf{x}, t) = \int_{t_*}^{t_0} dt \dot{Q}, \quad (15.10)$$

if particles are neither absorbed or lose energy. For an eternal universe, we obtain ‘‘Olber’s paradox’’: $n \rightarrow \infty$ for $t_* \rightarrow \infty$.

Next we want to include that the universe is expanding, starting from a ‘‘big bang.’’ The scale factor $a(t)$ describes how distances between (unbound) objects change with time. This applies in particular for the wave-length of a free particle. Thus the energy of a photon changes as

$$\frac{a_0}{a} = \frac{E}{E_0} \equiv 1 + z, \quad (15.11)$$

where the last relation defines the redshift z . It is convenient to use redshift as integration variable, using the redshift-time relation

$$\frac{dz}{dt} = -\frac{a_0}{a^2} \frac{da}{dt} = -(1+z)H(z) \quad (15.12)$$

with $H(z) = \dot{a}/a$ as the time-dependent Hubble parameter. While the redshift z of a source is directly observable via the change of known emission or absorption lines, the corresponding emission time depends on the cosmological model. Similarly, the Hubble parameter is given by

$$H(z) = H_0 \sqrt{\Omega_\Lambda + \Omega_m(1+z)^3 + \Omega_{\text{rad}}(1+z)^4} \quad (15.13)$$

for a universe with the fractions Ω_Λ , Ω_m and Ω_{rad} of dark energy, matter and radiation at the present epoch, respectively. If we integrate the redshift-time relation using 0.7, 0.3 and 0 for the fractions, we find $t/t_0 \simeq 0.5$ already at $z \simeq 0.6$. Thus if there is no strong source evolution, the low-redshift universe $z \lesssim 1$ dominates. This is even more the case if absorption

and/or energy losses are important, as in the case of photons with energies above ~ 10 TeV or UHECRs. On the other hand, star formation peaks at $z \sim 1.5$, and thus redshifts up to 2–3 may be important for processes involving SNe, GRBs, ... Next we rewrite (15.10) as

$$n(E) = \int_0^{t_0} dt \dot{Q}(E(t), t) = \int_0^\infty \frac{dz}{(1+z)} \frac{\dot{Q}((1+z)E, z)}{H_0 \sqrt{\Omega_\Lambda + \Omega_m(1+z)^3}} \quad (15.14)$$

Here, the argument of Q takes into account that a particle observed with energy E was generated with the energy $E_g = (1+z)E$. Moreover, in the injection rate $\dot{Q}(E, z) = n_s dN/(dEdt)$ the source density is the comoving density, i.e. we divide the number of sources not by the physical volume dV but by $dV(1+z)^3$ such that n_s is constant without source evolution. This is enough to write down to obtain the (particle) intensity or the diffuse flux of extragalactic neutrinos,

$$I_\nu(E) = \frac{c}{4\pi} n_\nu(E) = \int_0^\infty \frac{dz}{(1+z)} \frac{\dot{Q}_\nu((1+z)E, z)}{H_0 \sqrt{\Omega_\Lambda + \Omega_m(1+z)^3}}. \quad (15.15)$$

The next simplest case are protons. They can interact with CMB photons, $p + \gamma \rightarrow p + e^+ + e^-$ and, at even higher energies, $p + \gamma \rightarrow p + \pi^0$ or $p + \gamma \rightarrow n + \pi^+$. Since baryon number is conserved, we can treat this reactions however as a (continuous) energy loss $b(E, t) = -dE/dt$. We can treat synchrotron losses of electrons similarly. First we recall the conservation law in the case of current in coordinate space,

$$\frac{\partial n}{\partial t} + \nabla \cdot \left(\frac{d\mathbf{x}}{dt} n \right) = 0. \quad (15.16)$$

The energy loss $b(E, t) = -dE/dt$ in energy space (E, t) correspond to the current $\mathbf{u} = d\mathbf{x}/dt$ in coordinate space (\mathbf{x}, t) . Thus

$$\frac{\partial n(E)}{\partial t} - \frac{\partial}{\partial E} (b(E)n(E)) = \dot{Q}. \quad (15.17)$$

If the losses can be described by a simple analytical expression, as e.g. in the case of synchrotron losses $b \propto E^2$, the equation can be solved analytically.

loss length

Cascade limit The general concept of electromagnetic cascades discussed in Sec. ?? has several important applications. Firstly, we can use it to derive a simple bound on the HE neutrino flux. Using the branching ratio 2:1 for $p + \gamma \rightarrow p + \pi^0$ and $p + \gamma \rightarrow n + \pi^+$, the approximation that the four leptons produced in muon decay share equally the energy as well as the fact that in neutron decay almost all energy is taken by the proton, the ratio of energy transferred to neutrinos and the electromagnetic channel follows as 1:3, $u_\nu = 3u_\gamma$. In pp interactions, the ratio is 1:2.

The energy in the electromagnetic channel is bounded by the observed extragalactic gamma-ray background, $u_\gamma < u_{\text{EGRB}} \simeq 2 \times 10^{-7} \text{eV/cm}^3$. If we assume that $I_\nu(E_\nu) = AE_\nu^{-2}$, then

$$u_\nu = \frac{4\pi}{c} \int_{E_{\min}}^{E_{\max}} dE E I_\nu(E) = \frac{4\pi}{c} A \ln(E_{\max}/E_{\min}) = \frac{4\pi}{c} E^2 I_\nu(E) \ln(E_{\max}/E_{\min}) \leq u_{\text{EGRB}}. \quad (15.18)$$

This gives the bound

$$E_\nu^2 I_\nu(E_\nu) \leq \frac{c}{4\pi} \frac{u_{\text{EGRB}}}{\ln(E_{\text{max}}/E_{\text{min}})} \simeq 40 \text{ eV cm}^{-2} \text{ s}^{-1} \text{ sr}^{-1} \quad (15.19)$$

using $\ln(10^5) \simeq 11$. Interestingly, the neutrino flux shown in the left panel of Fig. 12.2 is somewhat above this limit—despite the fact that several other contributions (e.g. unresolved sources) contribute to u_{EGRB} .

Electromagnetic cascades may happen also inside many sources. Since the Thomson cross section is a factor 3000 larger than the cross section for photo-meson production, $\sigma_{\text{Th}}/\sigma_{p\gamma} \sim 3000$, sources where photo-meson reactions are relevant are likely optically thick. To be specific, let us assume that the source of opacity are UV photons, $\varepsilon_\gamma \sim 10 \text{ eV}$, as it is the case for many AGNs. Hence the critical energy for pair production is reduced to $E_{\text{cr}} \sim 25 \text{ GeV}$ compared to $E_{\text{cr}} \sim 400 \text{ TeV}$ for cascades on CMB photons. Thus the picture of the escaping photon radiation is as follows:

- Photons with $E \gg E_{\text{cr}}$ escape from the source only from an outer layer of such a thickness l that the interaction depth $\tau_{\gamma\gamma} = l\sigma_{\gamma\gamma}n_\gamma$ for pair-production is small, $\tau_{\gamma\gamma} \sim 1$.
- The source is bright in the $\sim 10 - 100 \text{ GeV}$ range, where the last generation of photons generated in the cascade can escape.
- Electrons with energy below E_{cr} continue to scatter in the source in the Thomson regime, producing photons in the X-ray range with average energy

$$E_\gamma = \frac{4}{3} \frac{\varepsilon_\gamma E_e^2}{m_e^2} \sim 100 \text{ eV} - 0.1 \text{ MeV} \quad (15.20)$$

for $E_e = 1 \text{ GeV}$ and 25 GeV , respectively.

16. Dark matter

16.1. Thermal relic particles

16.1.1. Freeze-out of thermal relic particles

When the number density n_X of a particle species X is not changed by interactions, then it is diluted just by the expansion of space, $n_X \propto R^{-3}$. It is convenient to account for this trivial expansion effect by dividing n_X through the entropy density $s \propto R^{-3}$, i.e. to use the quantity $Y = n/s$. We first consider again the equilibrium distribution Y_{eq} for $\mu_X = 0$,

$$Y_{\text{eq}} = \frac{n_X}{s} = \begin{cases} \frac{45}{2\pi^4} \left(\frac{\pi}{8}\right)^{1/2} \frac{g_X}{g_{*S}} x^{3/2} \exp(-x) = 0.145 \frac{g_X}{g_{*S}} x^{3/2} \exp(-x) & \text{for } x \gg 3, \\ \frac{45\zeta(3)}{2\pi^4} \frac{\varepsilon g_X}{g_{*S}} = 0.278 \frac{\varepsilon g_X}{g_{*S}} & \text{for } x \ll 3 \end{cases} \quad (16.1)$$

where $x = T/m$ and $g_{\text{eff}} = 3/4$ ($g_{\text{eff}} = 1$) for fermions (bosons). If the particle X is in chemical equilibrium, its abundance is determined for $T \gg m$ by its contribution to the total number of degrees of freedom of the plasma, while Y_{eq} is exponentially suppressed for $T \ll m$ (assuming $\mu_X = 0$). In an expanding universe, one may expect that the reaction rate Γ for processes like $\gamma\gamma \leftrightarrow \bar{X}X$ drops below the expansion rate H mainly for two reasons: i) Cross sections may depend on energy as, e.g., weak processes $\sigma \propto s \propto T^2$ for $s \lesssim m_W^2$, ii) the density n_X decreases at least as $n \propto T^3$. Around the freeze-out time x_f , the true abundance Y starts to deviate from the equilibrium abundance Y_{eq} and becomes constant, $Y(x) \approx Y_{\text{eq}}(x_f)$ for $x \gtrsim x_f$. This behavior is illustrated in Fig. 16.2.

Boltzmann equation When the number $N = nV$ of a particle species is not changed by interactions, then the expansion of the Universe dilutes their number density as $n \propto R^{-3}$. The corresponding change in time is connected with the expansion rate of the universe, the Hubble parameter $H = \dot{R}/R$, as

$$\frac{dn}{dt} = \frac{dn}{dR} \frac{dR}{dt} = -3n \frac{\dot{R}}{R} = -3Hn. \quad (16.2)$$

Additionally, there might be production and annihilation processes. While the annihilation rate $\beta n^2 = \langle \sigma_{\text{ann}} v \rangle n^2$ has to be proportional to n^2 , we allow for an arbitrary function as production rate ψ ,

$$\frac{dn}{dt} = -3Hn - \beta n^2 + \psi. \quad (16.3)$$

In a static Universe, $dn/dt = 0$ defines equilibrium distributions n_{eq} . Detailed balance requires that the number of X particles produced in reactions like $e^+e^- \rightarrow \bar{X}X$ is in equilibrium equal

Figure 16.1.: Illustration of the freeze-out process.

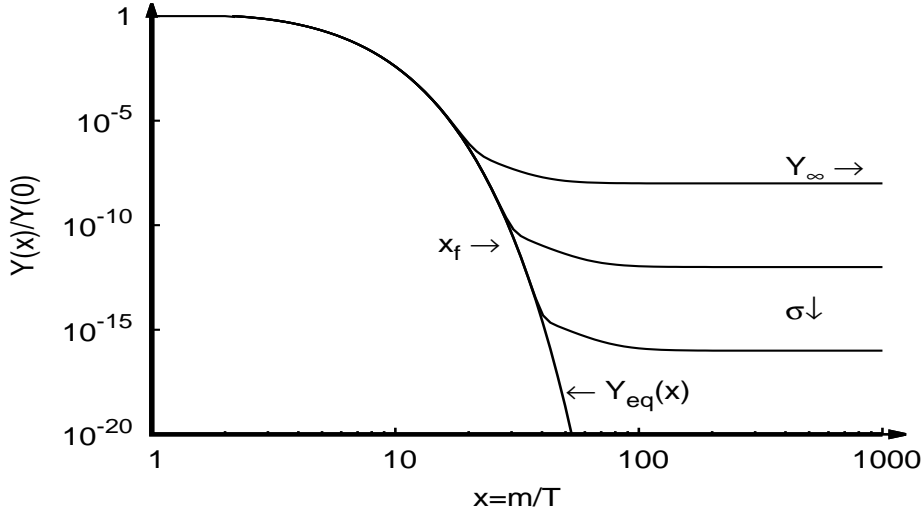


Figure 16.2.: Illustration of the freeze-out process. The quantity $Y = n_X/s$ is n_X divided by the entropy density $s \propto R^{-3}$ to scale out the trivial effect of expansion.

to the number that is destroyed in $\bar{X}X \rightarrow e^+e^-$, or $\beta n_{\text{eq}}^2 = \psi$. Thus we can replace ψ by βn_{eq}^2 and obtain

$$\frac{dn}{dt} = -3Hn - \langle \sigma_{\text{ann}} v \rangle (n^2 - n_{\text{eq}}^2). \quad (16.4)$$

This equation together with the initial condition $n \simeq n_{\text{eq}}$ for $T \rightarrow \infty$ determines $n(t)$ for a given annihilation cross section σ_{ann} . Changing to the new variables $Y(x)$ one obtains

$$\frac{dY}{dx} = -\frac{x}{H} \langle \sigma_{\text{ann}} v \rangle (Y^2 - Y_{\text{eq}}^2) \quad (16.5)$$

or

$$\frac{x}{Y_{\text{eq}}} \frac{dY}{dx} = -\frac{\Gamma_A}{H} \left[\left(\frac{Y}{Y_{\text{eq}}} \right)^2 - 1 \right] \quad (16.6)$$

with $\Gamma_A = n_{\text{eq}} \langle \sigma_{\text{ann}} v \rangle$. This expression illustrates nicely our intuitive ‘‘Gamov criterion’’: The relative change of Y is controlled by the factor Γ_A/H times the deviation from equilibrium. For the discussion of approximate solutions to this equation, it is convenient to distinguish different dark matter particles according to their freeze-out temperature: Hot dark matter (HDM) with $x_f \ll 3$, cold dark matter (CDM) with $x_f \gg 3$ and the intermediate case of warm dark matter with $x_f \sim 3$. The evolution of $Y = n_X/s$ is shown schematically in Fig. 16.2: As the universe expands and cools down, n_X decreases at least as R^{-3} . Therefore, the annihilation rate $\propto n^2$ quenches and the abundance ‘‘freezes-out.’’ The reaction rates are not longer sufficient to keep the particle in equilibrium and the ratio n_X/s stays constant.

Remark 16.1: Unitarity bounds each partial-wave l of the thermally averaged annihilation cross section as $\langle \sigma_{\text{ann}} v \rangle^{(l)} \leq \text{const.}/(vm^2)$. Requiring $\Omega < 0.3$ leads to $m < (20\text{--}50)$ TeV. This bounds the mass of any stable particle that was once in thermal equilibrium.

For the discussion of approximate solutions to this equation, it is convenient to distinguish according to the freeze-out temperature: hot dark matter (HDM) with $x_f \ll 3$, cold dark matter (CDM) with $x_f \gg 3$ and the intermediate case of warm dark matter with $x_f \sim 3$.

16.1.2. Hot dark matter

For $x_f \ll 3$, freeze-out occurs when the particle is still relativistic and Y_{eq} is not changing with time. The asymptotic value of Y , $Y(x \rightarrow \infty) \equiv Y_\infty$, is just the equilibrium value at freeze-out,

$$Y_\infty = Y_{\text{eq}}(x_f) = 0.278 \frac{g_{\text{eff}}}{g_{*S}}, \quad (16.7)$$

where the only temperature-dependence is contained in g_{*S} . The number density today is then

$$n_0 = s_0 Y_\infty = 2970 Y_\infty \text{cm}^{-3} = 825 \frac{g_{\text{eff}}}{g_{*S}} \text{cm}^{-3}. \quad (16.8)$$

The numerical value of s_0 used will be discussed in the next paragraph. Although a HDM particle was relativistic at freeze-out, it is today non-relativistic if its mass m is $m \gg 3\text{K} \approx 0.2\text{meV}$. In this case its energy density is simply $\rho_0 = m s_0 Y_\infty$ and its abundance $\Omega h^2 = \rho_0 / \rho_{\text{cr}}$ or

$$\Omega h^2 = 7.8 \times 10^{-2} \frac{m}{\text{eV}} \frac{g_{\text{eff}}}{g_{*S}}. \quad (16.9)$$

Hence HDM particles heavier than $O(100\text{eV})$ overclose the universe.

16.1.3. Cold dark matter

Abundance of CDM For CDM with $x_f \ll 3$, freeze-out occurs when the particles are already non-relativistic and Y_{eq} is exponentially changing with time. Thus the main problem is to find x_f , for late times we use again $Y(x \rightarrow \infty) \equiv Y_\infty \approx Y(x_f)$, i.e. the equilibrium value at freeze-out. We parametrize the temperature-dependence of cross section as $\langle \sigma_{\text{ann}} \rangle = \sigma_0 (T/m)^n = \sigma_0 / x^n$. For simplicity, we consider only the most relevant case for CDM, $n = 0$ or s-wave annihilation. Then the Gamov criterion becomes with $H = 1.66\sqrt{g_*} T^2 / M_{\text{Pl}}$ and $\Gamma_A = n_{\text{eq}} \langle \sigma_{\text{ann}} v \rangle$,

$$g \left(\frac{m T_f}{2\pi} \right)^{3/2} \exp(-m/T_f) \sigma_0 = 1.66\sqrt{g_*} \frac{T_f^2}{M_{\text{Pl}}} \quad (16.10)$$

or

$$x_f^{-1/2} \exp(x_f) = 0.038 \frac{g}{\sqrt{g_*}} M_{\text{Pl}} m \sigma_0 \equiv C. \quad (16.11)$$

To obtain an approximate solution, we neglect first in

$$\ln C = -\frac{1}{2} \ln x_f + x_f \quad (16.12)$$

the slowly varying term $\ln x_f$. Inserting next $x_f \approx \ln C$ into the $\ln x_f$ term of Eq. (16.12) to improve the approximation gives then

$$x_f = \ln C + \frac{1}{2} \ln(\ln C). \quad (16.13)$$

The relic abundance for CDM follows from $n(x_f) = 1.66\sqrt{g_*} T_f^2 / (\sigma_0 M_{\text{Pl}})$ and $n_0 = n(x_f) [R(x_f)/R_0]^3 = n(x_f) [g_{*,f}/g_{*,0}] [T_0/T(x_f)]^3$ as

$$\rho_0 = m n_0 \approx 10 \frac{x_f T_0^3}{\sqrt{g_{*,f}} \sigma_0 M_{\text{Pl}}} \quad (16.14)$$

or

$$\Omega_X h^2 = \frac{mn_0}{\rho_{\text{cr}}} \approx \frac{4 \times 10^{-39} \text{cm}^2}{\sigma_0} x_f \quad (16.15)$$

Thus the abundance of a CDM particle is inverse proportionally to its annihilation cross section, since a more strongly interacting particle stays longer in equilibrium. Note that the abundance depends only logarithmically on the mass m via Eq. (16.13) and implicitly via $g_{*,f}$ on the freeze-out temperature T_f . Typical values of x_f found numerically for weakly interacting massive particles (WIMPs) are $x_f \sim 20$. Partial-wave unitarity bounds $\sigma_{\text{ann}} \leq c/m^2$. Requiring $\Omega < 0.3$ leads to $m < 20 - 50$ TeV. This bounds the mass of any stable particle that was once in thermal equilibrium.

Baryon abundance from freeze-out:

We can calculate the expected baryon abundance for a zero chemical potential using the formulas derived above. Nucleon interact via pions; their annihilation cross section can be approximated as $\langle \sigma v \rangle \approx m_\pi^{-2}$. With $C \approx 2 \times 10^{19}$, it follows $x_f \approx 44$, $T_f \sim 22$ MeV and $Y_\infty = 7 \times 10^{-20}$. The observed baryon abundance is much larger and can be not explained as a usual freeze-out process.

Cold dark matter candidates

A particle suitable as CDM candidate should interact according Eq. (16.15) with $\sigma \sim 10^{-37} \text{cm}^2$. It is surprising that the numerical values of T_0 and M_{Pl} conspire in Eq. (16.15) to lead to numerical value of σ_0 typical for weak interactions. Cold dark matter particles with masses around the weak scale and interaction strengths around the weak scale were dubbed “WIMP”. An obvious candidate was a heavy neutrino, $m_\nu \sim 10$ GeV, excluded early by direct DM searches, neutrino mass limits, and accelerator searches. Presently, the candidate with most supporters is the lightest supersymmetric particle (LSP). Depending on the details of the theory, it could be a neutralino (most favorable for detection) or other options. The mass range open of thermal CDM particles is rather narrow: If it is too light, it becomes a warm or hot dark matter particle. If it is too heavy, it overcloses the universe. There exists however also the possibility that DM was never in thermal equilibrium. Two examples are the axion (a particle proposed to solve the CP problem of QCD) and superheavy particle (generically produced at the end of inflation). An overview of different CDM candidates is given in Fig. 16.3.

16.1.4. WIMP detection

Direct detection

Recoil energy The Sun moves with $v = 220$ km/s around the galactic center. We can consider therefore a WIMP scattering on a nucleus of a detector non-relativistically. We evaluate the cms energy squared first in the lab frame with $p_N^\mu = (m_N, \mathbf{0})$. Thus

$$s = (p_N + p_X)^2 = m_N^2 + m_X^2 + 2m_N E = (m_N + m_X)^2 + 2m_N E_{\text{kin}} \quad (16.16)$$

where we introduced the non-relativistic kinetic energy of the WIMP, $E_{\text{kin}} = E - m_X c^2 \simeq m_X v^2/2$. Next we compare

$$\sqrt{s} = (m_N + m_X) \left[1 + \frac{m_N E_{\text{kin}}}{(m_N + m_X)^2} - \dots \right] \quad (16.17)$$

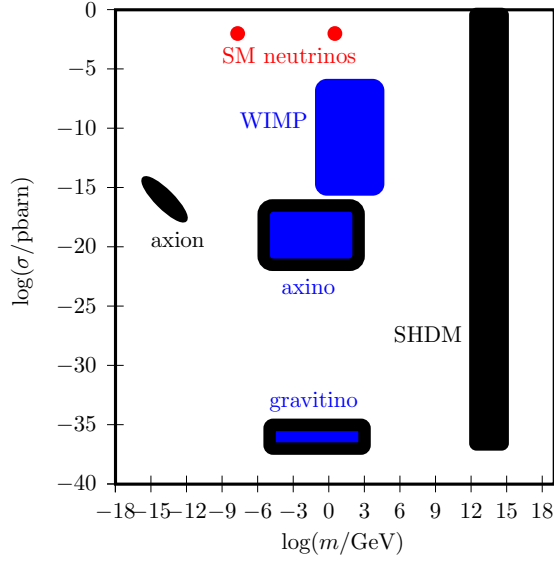


Figure 16.3.: Particles proposed as DM particle with $\Omega \sim 1$, the expected size of their cross section and their mass.

with the corresponding expression in the cm frame,

$$\sqrt{s} = m_N + \frac{p^2}{2m_N} + \dots + m_X + \frac{p^2}{2m_X} + \dots \simeq (m_N + m_X) \left[1 + \frac{p^2}{2m_N m_X} \right]. \quad (16.18)$$

The cms momentum follows as

$$p^2 = \frac{2\mu^2 E_{\text{kin}}}{m_X} = \mu^2 v^2, \quad (16.19)$$

where we introduced also the reduced mass $\mu = m_N m_X / (m_N + m_X)$. In the lab-frame, the scattering is isotropic and the recoil momentum of the nucleus varies as

$$E_{\text{rec}}(\vartheta) = \frac{p^2}{2m_N} (1 - \cos \vartheta) = \frac{\mu^2 v^2}{2m_N} (1 - \cos \vartheta). \quad (16.20)$$

The recoil energy is maximal when the WIMP is scattered backwards,

$$E_{\text{rec}}^{\text{max}} = \frac{\mu^2 v^2}{m_N} = \begin{cases} m_N v^2 & \text{for } m_x \gg m_N, \\ \frac{m_x^2}{m_N} v^2 & \text{for } m_x \ll m_N. \end{cases} \quad (16.21)$$

Hence the recoil energy becomes independent of the WIMP mass in the limit $m_X \gg m_N$. With $v \sim 10^{-3}$, is it of the order 10 keV. Using heavy nuclei as xenon with $A \simeq 130$ increases the recoil energy, and the cross section which scales $\sigma \propto A^2$ as long as the WIMP scatters coherently on the nucleus (i.e. the wave-length of the WIMP is large compared to the size of the nucleus). In the opposite limit, the recoil energy drops very fast, making the detection of recoils of light WIMPs challenging.

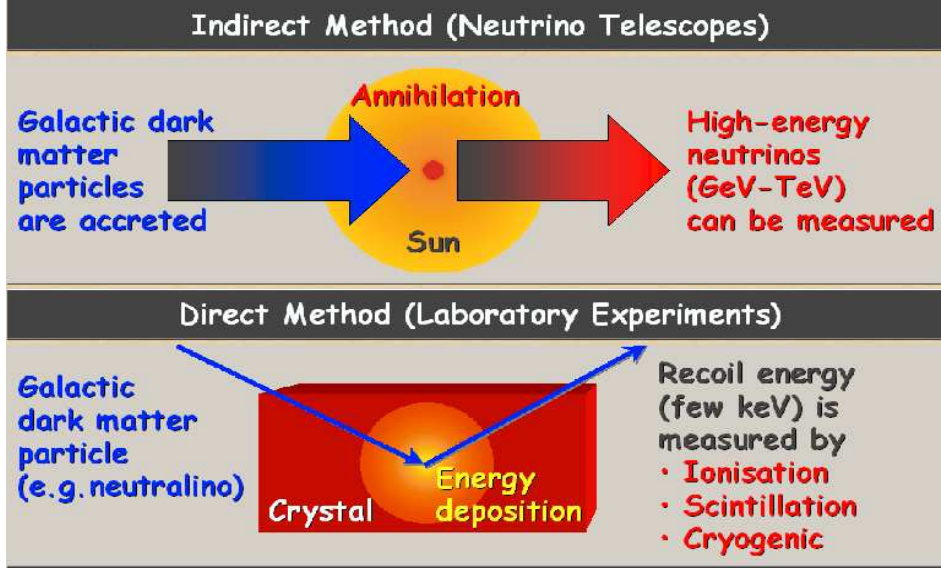


Figure 16.4.: Methods to detected WIMPs

Event rate The local density of DM is estimated as $\rho \approx 0.3 \text{ GeV/cm}^3$. The flux F follows as $\phi = \rho/m_X v/4$ and the scattering rate per target as $R = \sigma F$. Typical event rates per ton detector and day are 0.1.

Main problem is the elimination of background (natural radioactivity in the detector, cosmic rays) and establishing a clear experimental signature of WIMPs. The latter can be an annual modulation of the event rate, the direction of the recoil momentum, differences how the energy is transferred (different ratio of ionisation/scintillation, ...).

Indirect detection of WIMPS

The average density of DM in the Galaxy is strongly increased compared to the extragalactic space, $n_{\text{MW}}/n_{\text{ex}} \sim 10^5$. Therefore the annihilation rate of DM can become appreciable inside the Milky Way, and in particular, in objects where DM is even stronger accumulated.

DM distribution and clumps Typical results from N -body simulations are for the smooth DM mass density profile ρ_{sm}

$$\rho_{\text{sm}}(r) = \rho_{\odot} \left(\frac{r_{\odot}}{r} \right) \left(\frac{r_{\odot} + a}{r + a} \right)^2, \quad (16.22)$$

with $\rho_{\odot} = 0.3 \text{ GeV/cm}^3$ as the dark matter density at the solar distance from the GC, and $a = 45 \text{ kpc}$ as the characteristic scale where the slope changes from r^{-3} to r^{-1} (“Navarro-Frenk-White profile”). At small radii $r \lesssim 1 \text{ kpc}$, the missing resolution of N -body simulations, the influence of baryonic matter and of the galactic SMBH make a reliable estimate of the DM density difficult. According the model of hierarchical structure formation, the first objects to form are the smallest structures. For the case of neutralino DM, 10^{15} Earth-mass dark-matter haloes about as large as the Solar System might be in the Milky Way. The annihilation signal is dominated by smaller clumps that have a denser core and may be at small distance.

Accumulation of WIMPs in Sun or Earth Neutralinos scattering on matter in the Sun or Earth lose energy, part becomes gravitationally bound. They continue to lose energy and sink down to the center where they annihilate.

Photons, neutrinos and antiprotons from DM The secondaries of a DM annihilation will be the stable particle of the SM, i.e. photons, neutrinos, electrons and protons. For the latter two, only the anti-particles may provide some useful information. The differential flux of the final state i at the Earth from DM annihilation is

$$I_{\text{sm}}(E, \psi) = \frac{dN_i}{dE} \frac{\langle \sigma v \rangle}{2m_X^2} \int_{\text{l.o.s.}} ds \frac{\rho_{\text{sm}}^2[r(s, \psi)]}{4\pi}, \quad (16.23)$$

where $r(s, \psi) = (r_\odot^2 + s^2 - 2r_\odot s \cos \psi)^{1/2}$, ψ is the angle between the direction in the sky and the galactic center (GC), $r_\odot \approx 8.0 \text{ kpc}$ is the solar distance from the GC, and s the distance from the Sun along the line-of-sight (l.o.s.). In terms of galactic latitude b and longitude l , one has $\cos \psi = \cos b \cos l$. The energy spectrum dN_i/dE and $\langle \sigma v \rangle$ can be calculated only for a specific model calculated.

16.2. Axion-like particles

Axion-like particles (ALP) are defined by having a two-photon vertex,

$$\mathcal{L} = -\frac{1}{4} \frac{c_a}{f_a} a F_{\mu\nu} \tilde{F}^{\mu\nu} = \frac{c_a}{f_a} a \mathbf{E} \cdot \mathbf{B}. \quad (16.24)$$

One of the two photons can be virtual, either from the Coulomb field of a nucleus or a magnetic field, the other one a real one. Thus axions could be created via photon scattering on a nucleus in the Sun, and then back-convert traversing a magnetic field. Moreover, this vertex leads to axion-photon oscillations in the presence of an external magnetic field.

Axions are a special case of an ALP that solves the strong CP problem. As a consequence, they have in addition a coupling to gluons, with the same structure as (16.24), and mix with pions. This relates their mass and couplings as

$$m_a f_a \simeq m_\pi f_\pi. \quad (16.25)$$

Thus lighter axions are more weakly interacting and light axions were never in thermal equilibrium. They are produced instead as a “classical condensate”, with very little momentum and behave therefore as cold dark matter.

16.3. Primordial black holes

Primordial black holes (PBH) in the mass range $10^{-4} - 0.1 M_\odot$ have been searched for by microlensing, cf. section 9.5. Light PBH with mass $\lesssim 10^{-14} \text{ g}$ evaporate at the present epoch or earlier. They contribute e.g. to the diffuse extragalactic gamma-ray background around tens of MeV.

A selection of limits on PBHs is shown in Fig. 16.5.

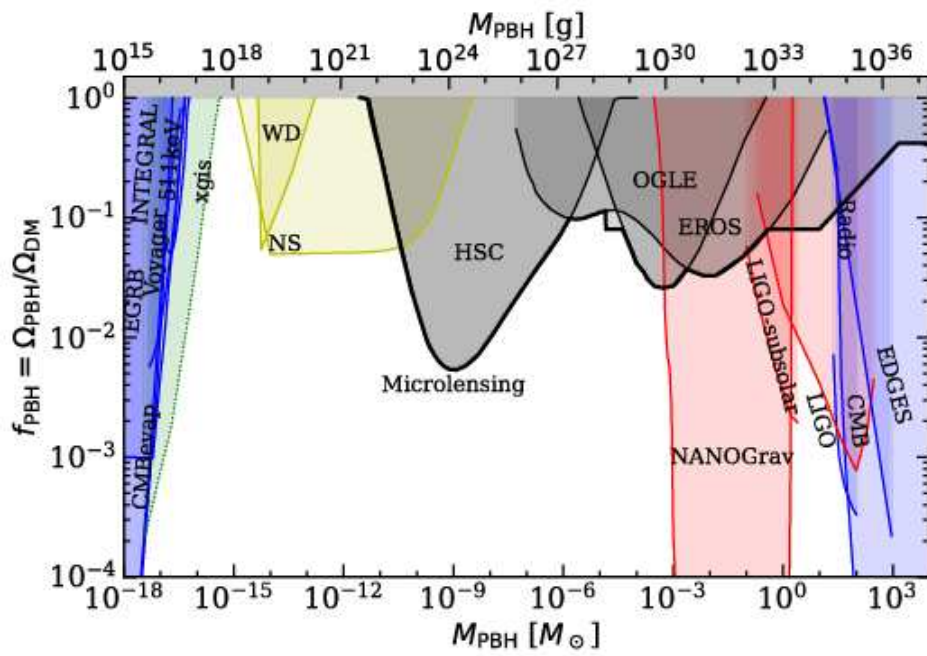


Figure 16.5.: Constraints on the fraction of the dark matter consisting of PBHs as a function of their mass.

A. Some formulae

A.1. Mathematical formulae

The following integrals frequently appear in the context of calculations involving particle reactions in thermal media, where ζ refers to the Riemann zeta function.

Table A.1.: Thermal integrals.

	Maxwell–Boltzmann	Fermi–Dirac	Bose–Einstein
	$\int_0^\infty \frac{x^n dx}{e^x}$	$\int_0^\infty \frac{x^n dx}{e^x+1}$	$\int_0^\infty \frac{x^n dx}{e^x-1}$
$n = 2$	2	$\frac{3}{2}\zeta_3 \simeq 1.8031$	$2\zeta_3 \simeq 2.40411$
$n = 3$	6	$\frac{7\pi^4}{120} \simeq 5.6822$	$\frac{\pi^4}{15} \simeq 6.4939$

A.2. Abbreviations:

B	Kirchoff-Planck function
E	energy of a single object
\mathcal{F}	energy flux $dE/(dAdt)$
F	energy fluence dE/dA
I_ν	(spectral) intensity of energy $I_\nu = dE/(d\nu dt dA_\perp d\Omega)$
J	(spectral) intensity of particles $J = dN/(dE dt dA_\perp d\Omega)$
J	angular momentum $J = mrv$
κ	opacity (cross section per mass)
L	luminosity, emitted energy per time
m	mass (of a single object), apparent magnitude
M	mass of a system of objects, absolute magnitude
Φ	gravitational potential $-GM/r$
p	momentum
P	pressure
\mathcal{R}	gas constant per mass $\mathcal{R} = k/m_H$
ρ	mass density $\rho = dm/dV$
σ	cross section
T	temperature
u	energy density, specific energy, fluid velocity
U	energy of a system of objects

A.3. Physical constants and measurements

Gravitational constant	$G = 6.674 \times 10^{-11} \text{ m}^3 \text{ kg}^{-1} \text{ s}^{-2} = 6.674 \times 10^{-8} \text{ cm}^3 \text{ g}^{-1} \text{ s}^{-2}$
Planck's constant	$\hbar = h/(2\pi) = 1.055 \times 10^{-27} \text{ erg s}$
velocity of light	$c = 2.998 \times 10^8 \text{ m/s} = 2.998 \times 10^{10} \text{ cm/s}$
Boltzmann constant	$k = 1.381 \times 10^{-23} \text{ J/K} = 1.38 \times 10^{-16} \text{ erg/K}$
electron mass	$m_e = 9.109 \times 10^{-28} \text{ g} = 0.5110 \text{ MeV}/c^2$
proton mass	$m_p = 1.673 \times 10^{-24} \text{ g} = 938.3 \text{ MeV}/c^2$
Fine-structure constant	$\alpha = e^2/(\hbar c) \approx 1/137.0$
Fermi's constant	$G_F/(\hbar c)^3 = 1.166 \times 10^{-5} \text{ GeV}^{-2}$
Ideal gas constant	$\mathcal{R} = k/m_H \simeq 8.314 \times 10^7 \text{ erg s}^{-1} \text{ K}^{-1}$
Stefan-Boltzmann constant	$\sigma = (2\pi^5 k^4)/(15c^2 h^3) \approx 5.670 \times 10^{-5} \text{ erg s}^{-1} \text{ cm}^{-2} \text{ K}^{-4}$
Radiation constant	$a = 4\sigma/c \approx 7.566 \times 10^{-15} \text{ erg cm}^{-3} \text{ K}^{-4}$
Rydberg constant	$R_\infty = 1.10 \times 10^5 \text{ cm}^{-1}$
Thomson cross-section	$\sigma_T = 8\pi\alpha_{\text{em}}^2/(3m_e^2) = 6.652 \times 10^{-25} \text{ cm}^2$

A.4. Astronomical constants and measurements

Astronomical Unit	$\text{AU} = 1.496 \times 10^{13} \text{ cm}$
Parsec	$\text{pc} = 3.086 \times 10^{18} \text{ cm} = 3.261 \text{ ly}$
Tropical year	$\text{yr} = 31\,556\,925.2 \text{ s} \approx \pi \times 10^7 \text{ s}$
Solar radius	$R_\odot = 6.960 \times 10^{10} \text{ cm}$
Solar mass	$M_\odot = 1.998 \times 10^{33} \text{ g}$
Solar luminosity	$L_\odot = 3.84 \times 10^{33} \text{ erg/s}$
Solar apparent visual magnitude	$m = -26.76$
Earth equatorial radius	$R_\oplus = 6.378 \times 10^8 \text{ cm}$
Earth mass	$M_\oplus = 5.972 \times 10^{27} \text{ g}$
Age of the universe	$t_0 = (13.7 \pm 0.2) \text{ Gyr}$
present Hubble parameter	$H_0 = 73 \text{ km}/(\text{s Mpc}) = 100 h \text{ km}/(\text{s Mpc})$
present CMB temperature	$T = 2.725 \text{ K}$
present baryon density	$n_b = (2.5 \pm 0.1) \times 10^{-7} \text{ cm}^3$
	$\Omega_b = \rho_b/\rho_{\text{cr}} = 0.0223/h^2 \approx 0.0425$
dark matter abundance	$\Omega_{\text{DM}} = \Omega_m - \Omega_b = 0.105/h^2 \approx 0.20$

A.5. Other useful quantities

cross section	$1 \text{ mbarn} = 10^{-27} \text{ cm}^2$
flux conversion	$L = 3.02 \times 10^{28} \text{ W} \times 10^{-0.4M}$

A.6. Properties of main-sequence stars

The spectral class, absolute visual magnitude M_V color index B-V, effective surface temperature radius T , lifetime on the main sequence, and the fraction of the spectral class out of all stars is given in the following table:

A. Some formulae

SK	M_V	B-V	T_e/K	R/R_\odot	M/M_\odot	lifetime/yr	fraction
O5	-6	-0.45	35000	13.4	60	$< 10^6$	10^{-5}
B0	-3.7	-0.31	21000	6.7	17.5	3×10^6	10^{-3}
B5	-0.9	-0.17	13500	3.2	5.9		
A0	0.7	0.0	9700	2.2	2.9	4×10^8	0.01
A5	2.0	0.16	8100	1.8	2.0		
F0	2.8	0.30	7200	1.4	1.6	4×10^9	0.02
F5	3.8	0.45	6500	1.2	1.4		
G0	4.6	0.57	6000	1.06	1.05	1×10^{10}	7%
G5	5.2	0.70	5400		0.96		
K0	6.0		4700	0.93	0.79	6×10^{10}	15%
K5	7.4	1.11	4000	0.80	0.67		
M0	8.9	1.39	3300	0.63	0.51	$> 10^{11}$	75%
M5	12.0	1.61	2600	0.29	0.21		

Bibliography

- [1] Philip J. Armitage. Lecture notes on accretion disk physics. 1 2022.
- [2] P. Auger, P. Maze, and Th. Grivet-Meyer. Grandes gerbes cosmiques atmosphériques contenant des corpuscules ultra-pénétrants. *Comptes Rendus de l'Académie des Sciences*, 206:1721, 1938.
- [3] R. D. Blandford. Acceleration of ultrahigh-energy cosmic rays. *Phys. Scripta*, T85:191–194, 2000.
- [4] Walther Bothe and Werner Kolhörster. Das Wesen der Höhenstrahlung. *Z. Phys.*, 56:751–777, 1929.
- [5] Jakob Clay. Penetrating Radiation. *Proc. Kon. Akademie (Amsterdam)*, 30(9-10):1115–1127, 1927.
- [6] Charles Augustine de Coulomb. Troisième Mémoire sur l'Electricité et le Magnétisme. *Histoire de l'Académie Royale des Sciences*, pages 612–638, 1785.
- [7] Georgia A. de Nolfo et al. Observations of the Li, Be, and B isotopes and constraints on cosmic-ray propagation. *Adv. Space Res.*, 38:1558–1564, 2006.
- [8] Dillon R. Foight, Tolga Güver, Feryal Özel, and Patrick O. Slane. Probing X-Ray Absorption and Optical Extinction in the Interstellar Medium Using Chandra Observations of Supernova Remnants. *Astrophys. J.*, 826(1):66, July 2016.
- [9] Dale A. Frail et al. Beaming in gamma-ray bursts: Evidence for a standard energy reservoir. *Astrophys. J. Lett.*, 562:L55, 2001.
- [10] J. S. George, K. A. Lave, M. E. Wiedenbeck, W. R. Binns, A. C. Cummings, A. J. Davis, G. A. de Nolfo, P. L. Hink, M. H. Israel, R. A. Leske, R. A. Mewaldt, L. M. Scott, E. C. Stone, T. T. von Rosenvinge, and N. E. Yanasak. Elemental Composition and Energy Spectra of Galactic Cosmic Rays During Solar Cycle 23. *Astrophys. J.*, 698:1666–1681, June 2009.
- [11] Karl D. Gordon, Geoffrey C. Clayton, K. A. Misselt, Arlo U. Landolt, and Michael J. Wolff. A quantitative comparison of SMC, LMC, and Milky Way UV to NIR extinction curves. *Astrophys. J.*, 594:279–293, 2003.
- [12] Victor F. Hess. Über Beobachtungen der durchdringenden Strahlung bei sieben Freiballonfahrten. *Phys. Z.*, 13:1084–1091, 1912.
- [13] M. Kachelrieß. Lecture notes on high energy cosmic rays. 2008.
- [14] W. Kolhörster, I. Matthes, and E. Weber. Gekoppelte Höhenstrahlen. *Naturwissenschaften*, 26:576–576, September 1938.

- [15] G. V. Kulikov and G. B. Khristiansen. On the Size Spectrum of Extensive Air Showers. *J. Exp. Theor. Phys.*, 35:8, 1958.
- [16] John Linsley. Evidence for a primary cosmic-ray particle with energy 10^{20} eV. *Phys. Rev. Lett.*, 10:146–148, 1963.
- [17] K. Lodders. Solar System Abundances and Condensation Temperatures of the Elements. *Astrophys. J.* , 591:1220–1247, July 2003.
- [18] Kseniya V. Ptitsyna and Sergei V. Troitsky. Physical conditions in potential sources of ultra-high-energy cosmic rays. I. Updated Hillas plot and radiation-loss constraints. *Phys. Usp.*, 53:691–701, 2010.
- [19] Marcel Schein, William P. Jesse, and E. O. Wollan. The Nature of the Primary Cosmic Radiation and the Origin of the Mesotron. *Phys. Rev.*, 59:615, 1941.
- [20] J. Z. Wang, E. S. Seo, K. Anraku, M. Fujikawa, M. Imori, T. Maeno, N. Matsui, H. Matsunaga, M. Motoki, S. Orito, T. Saeki, T. Sanuki, I. Ueda, K. Yoshimura, Y. Makida, J. Suzuki, K. Tanaka, A. Yamamoto, T. Yoshida, T. Mitsui, H. Matsumoto, M. Nozaki, M. Sasaki, J. Mitchell, A. Moiseev, J. Ormes, R. Streitmatter, J. Nishimura, Y. Yajima, and T. Yamagami. Measurement of Cosmic-Ray Hydrogen and Helium and Their Isotopic Composition with the BESS Experiment. *Astrophys. J.* , 564:244–259, January 2002.

Index

- aberration
 - relativistic, 126
- accretion disk, 86, 99
- adiabatic expansion, 28
- adiabatic exponent, 28
- adiabatic index, 29
- amplitude
 - transition, 152
- beaming, 126
- black hole, 107
 - entropy, 109
 - merger, 92
 - supermassive, 160
 - temperature, 109
- blackbody radiation
 - cosmic, *see* cosmic microwave background
- Blandford-Znajek mechanism, 170
- Boltzmann distribution, 20
- Boltzmann equation, 176
- Bondi accretion, 85

- chirp mass, 92
- CNO-cycle, 54
- compression ratio, 75
- convection, 31–33, 36
- cross section, 13
- cyclotron radiation, 141

- dark matter, 161
 - cold, 177
 - hot, 177
- diffusion equation, 18
- Doppler factor, 126
- dynamical friction, 155, 166

- Eddington luminosity, 35, 86
- Eddington model, 36
- eddy, 76

- Einstein angle, 102
- emission coefficient, 13
- energy-momentum tensor, *see* stress tensor
- entropy
 - black hole, 109
 - ideal gas, 109
 - photon gas, 109
- equilibrium
 - kinetic, 9, 20
- equivalence principle, 95
- Euler formulation, 71

- field parameter
 - dynamical, 143
- flux factor, 152
- frequency, angular, 141
- frequency, cyclotron, 141

- galaxies
 - active, 167
 - evolution, 165
 - radio, 167
 - Seyfert, 168
- gamma-ray bursts, 125
- Gamov peak, 53
- gas constant, 22
- Gravitational lensing, 100
- gravitational radiation, 89, 105

- Hawking radiation, 110
- Hertzsprung-Russel diagram, 35
- holographic principle, 110

- Jeans instability, 73

- Kramer’s law, 17

- Lagrangian formulation, 71
- Lagrangian points, 88
- Lane-Emden equation, 38
- last stable orbit, 99

- lens equation, 101
- Møller velocity, 150
- Mach number, 71
- MACHO, 162
- magnetic field
 - critical, 143
- main sequence stars, 35
- mass number, 22
- Maxwell-Boltzmann distribution, 23
- mean atomic weight, 22
- MOND, 164

- neutrino
 - dark matter, 165
 - oscillations, 55
- nucleosynthesis
 - r-process, 59
 - s-process, 59

- Olber's paradox, 173
- opacity, 16
 - Rosseland, 31
- optical depth, 13

- perihelion procession, 100
- polytrope, 28, 33
- pp-chains, 54
- pressure integral, 21
- principle of equivalence, 96

- radiation pressure, 23
- random walk, 17
- Rankine-Hugoniot conditions, 74
- relaxation time, 154
- Reynolds number, 78
- Rosseland opacity, 31

- Saha equation, 20
- Schwarzschild criterion, 32
- Schwarzschild metric, 98
- Schwarzschild radius, 107
- Sedov-Taylor solution, 124
- self-similar, 124
- shock, 74
- singularity, 108
- S -matrix, 152
- superluminal motion, 168

- supernova remnants, 123
- synchrotron radiation, 141

- turbulence, 76–80

- virial theorem, 27